IMPROVED THROAT INSERTS
FOR
ABLATIVE THRUST CHAMBERS

by

D. N. Crump, H. H. Henderson, and K. J. Smith

prepared for

NATIONAL AERONAUTICS AND SPACE ADMINISTRATION

TRW INC.

FINAL REPORT

IMPROVED THROAT INSERTS FOR ABLATIVE THRUST CHAMBERS

by

D. N. Crump, H. H. Henderson, and K. J. Smith

prepared for

NATIONAL AERONAUTICS AND SPACE ADMINISTRATION

September 1967

TRW

Improved Throat Inserts for Ablative Thrust Chambers

by

D. N. Crump, H. H. Henderson, and K. J. Smith

ABSTRACT

Information contained in this report summarizes work performed on a NASA LeRC program aimed at achieving greater durability for throat inserts in highly oxidizing environments. Discussions are presented on materials oxidation performance and developments in overcoming thermal shock characteristics of oxide and carbide materials through both material composite development and unique design constructions. Design construction for four unique concepts and the performance they achieve in a N_2O_4-50% UDMH 50% N_2H_4 environment at 100 psi pressure are presented. Notable successes include exposure times in excess of 1250 seconds in uncooled pulsed and sustained burst (300 seconds) tests with zero throat erosion in combination hard throat ablative chamber constructions.

TABLE OF CONTENTS

LIST OF ILLUSTRATIONS

x

LIST OF TABLES

SUMMARY

This is the final report covering all work performed by TRW under contract NAS 3-6280 for the NASA Lewis Research Center. The period of performance of the contract was from July 1964 to May 1966.

The objective of the program was to provide improvements in the capabilities of throat insert materials and ablative chamber designs to meet the more severe conditions imposed by the increasing requirements of present as well as future systems. To attain this objective, TRW conducted detailed studies of existing and improved materials and design concepts for use in liquid propellant rocket thrust chambers. The developed designs provided improvements over existing systems in reduced erosion rates, greater resistance to severe chemical environments, ability to withstand high temperature for extended durations, capability to perform successfully when subjected to engine duty cycles of varying duration, increased resistance to thermal shock, and better methods for insert retention.

The program was divided into three major work tasks that were completed consecutively. The three major tasks were:

Task I   - Preliminary Design, Analyses & Evaluation

Task II - Final Design

Task III - Fabrication & Test Evaluation

Six units, as based on four designs, were fabricated and tested. The four designs consisted of similar chamber and exit sections with the throat insert consisting of:

1) Reinforced oxide - A composite mixture of tungsten-rhenium reinforcing wires in a matrix of partially stabilized zirconia.

2) Refractory Laminate - A layered assembly of zirconia and pyrolytic graphite disks.

3) Prestressed - A pure tantalum carbide throat insert prestressed at assembly to reduce OD tensile stresses under test.

4) Graded carbide - A graded structure consisting of an inner layer of hafnium carbide and three outer layers of tantalum carbide with an increasing quantity of graphite.

Two reinforced oxide units were fabricated. One insert contained five volume percent reinforcing wire and the second, seven volume percent. The five volume percent unit was tested for a sustained 310 second burst, cooled to ambient and examined; pulse fired for five 20 second pulses with cool down for fifteen minutes between pulses, and refired for a second sustained 300 second burst. Dimensional change in the throat was negligible. Disassembly of the unit showed a capability for further testing. The seven volume percent unit was tested for a duty cycle comprising a 180 second burst, cool to ambient; a 300 second pulse followed by five 20 second pulses, a 300 second burst, and a 373 second burst for a total of 1253 seconds. No dimensional loss occurred.

Two refractory laminate constructions were tested. The first of these employed alternate zirconia-PG washers. A sustained pulse of 214 seconds was applied at which time a dimensional loss in the throat was noted and the test

1

terminated. It was determined that the PG washers had oxidized at a greater rate than anticipated, permitting the exposed zirconia disks to fracture. The second unit consisted entirely of zirconia disks. This unit was tested for a sustained 300 second burst with no throat dimensional loss. In both the PG and no PG cases, the oxide disks cracked radially.

The prestressed unit was tested for a total of 225 seconds in two tests with a cool to ambient between tests. No cracking of the insert occurred during either pulse. The carbide insert oxidation rate was higher than anticipated however, resulting in major dimensional loss in the throat for the second test.

The layered carbide insert failed during the initial pulse and was terminated at 38 seconds. Examinations revealed evidence of both oxidation and thermal shock failure.

In support of the design, material property evaluations and reactivity comparisons between $H_2 + O_2$ and $N_2O_4 + 50\%$ UDMH - 50% N_2H_4 propellant systems were made. These studies indicated that a more severe reactivity problem exists with the N_2O_4 system. Materials ranking in order of oxidation resistance were: oxide, carbide, tungsten, graphite, intermetallics and plastics. Thermal shock resistance was almost in reverse order as determined by laboratory screening tests. Property evaluations of thermal expansion, modulus, and conductivity were made for those materials having insufficient design knowledge.

Processing studies incorporating both phosphate bonding and pressing and sintering of the zirconia plus tungsten-rhenium wire were made. The useable range of fiber volume percent appears to be from 3 to 10 percent. Phosphate bonding resulted in lowering the useable temperature to about 3300°F.

Scale-up potential for both the refractory laminate and reinforced oxide approaches appears good. Predictability in performance by analysis was proven leading to high probability in a successfully performing larger size unit.

2

SECTION II

INTRODUCTION

In pursuit of the program's major objective - improved throat insert materials and design concepts for ablative thrust chambers - a number of significant accomplishments have been achieved. These accomplishments include the demonstration of stabilized throat dimension under both steady pulse durations in excess of 300 seconds and cyclic operation. Reactivity, oxidation threshold temperatures, and oxidation rates for various materials were determined. Design analysis methodology, material synthesis methods for increased oxidation resistance, and thermal shock resistance determinations were also verified.

A total of six units comprising four designs were fabricated for testing in an N_2O_4 + 50% UDMH -50% N_2H_4 environment at an O/F ratio of 2.0. The designs were based on the following criteria:

1) Chamber pressure - 100 psia

2) Throat inside diameter - 1.2 inches

3) Chamber inside diameter - 2.94 inches

4) Nominal nozzle exit diameter - 1.69 inches

5) Nominal convergent half angle - 25°F

6) Nominal divergent half angle - 15°

7) Nominal radius of curvature at throat - 1.2 inches

8) Nominal combustion temperature - 5500°F

9) Engine duty cycle - variable; both long and short pulses

The program was divided into three major work tasks that were completed consecutively. The three major tasks were:

Task I   - Preliminary Design, Analyses & Evaluation.

Task II   - Final Design

Task III - Fabrication and Test Evaluation

Task I constituted the initial design and analysis activity directed toward improvement in throat inserts for ablative chambers. It was comprised of two phases. The initial phase of the activity was related to establishing design and acceptability criteria for current designs and materials with respect to both gas side (hot) and insulative functions. To accomplish this, a thorough review of material performance history together with laboratory screening tests of candidate materials was performed. The materials screening tests included plasma-jet, thermal shock, and propellant gas specie reactivity tests. The general classes of materials included refractory metals, carbides, oxides, nitrides, intermetallics, and composites.

Concurrent with this activity, analyses were made for various design concepts to determine material thickness requirements for stress and heat transfer. These design studies also investigated methods of auxiliary cooling as a means of extending operating life.

At the conclusion of this phase, an ablative chamber design using a coated refractory throat (SIVB reaction control motor) was supplied by TRW and was tested in the actual environment to be imposed on units under this program.

3

The test results indicated a more severe environment existed than anticipated and necessitated a phase two definition incorporating more radical design concepts and materials selection.

Under Task II, detailed thermal and stress analyses were performed for four unique designs. These selected designs employed: a prestressed insert, a layered insert, a laminated throat construction and a composite insert material. Material process development was also initiated for the selected insert materials concurrent with the design analyses.

Task III was initiated by fabrication of one of each of the four selected designs. Following testing and post firing evaluation, one additional unit each of the laminated throat and composite insert was fabricated and tested.

TECHNICAL PROGRAM

A. TASK I - ANALYSIS, EVALUATION, AND PRELIMINARY DESIGN

The intent of Task I was to evolve potential concepts as candidates for the final designs and to evaluate materials most applicable for use as throat inserts in the NASA test environment. For the initial phase of Task I, currently available materials were reviewed in appropriate design concepts to establish the potential range of use. The concepts reviewed were:

Heat Sink Concept - The material behind the throat insert has a high thermal conductivity. The intent is to maintain a low throat surface temperature.

Heat Barrier Concept - A thermal insulating material is used behind the throat insert to reduce the heat flow to the structural support.

Radiative Concept - The materials are selected to cause heat transfer from the walls by radiation.

Auxiliary Cooled Concept - Primary cooling of the nozzle wall is accomplished by some external means.

Prestressed Concept - A thermal-shock sensitive material is preloaded in compression to reduce the imposed tensile stress.

Concurrently, the materials evaluation phase was started to select and better define potential throat insert materials. Included in the materials evaluation was a study to compare the severity of reaction with insert materials of the two candidate propellant systems $H_2 + O_2$ and 50/50 UDMH-Hydrazine + N_2O_4. The results, indicating that the combustion products of N_2O_4 + 50/50 resulted in the severest environment, were used in selecting N_2O_4 50/50 as the representative material screening test propellant system and the system to be used by NASA for test unit evaluation.

1. Preliminary Design Concepts

For the preliminary design effort, only the throat section was analyzed. Transient heat transfer analyses and thermal stress analyses were performed to eliminate or refine each configuration. It should be noted that the preliminary analyses considered a flight environment. That is, internal and external cooling was computed by radiation to space (near earth). The products of combustion of the storable bipropellants were used for each design. At the throat section, the convective heat transfer coefficient was based on a C* efficiency of 98 percent. The convective heat transfer coefficient was initially estimated to be approximately 40 percent of that predicted by Bartz's relation using adiabatic wall temperature. Based on this, the following gas properties were used:

Mixture Ratio (O/F)	=	1.2
Ratio of Specific Heats (γ)	=	1.3
Average Molecular Wt. (M)	=	22.1
Viscosity (μ)	=	0.167 lb_m Ft^{-1} Hr^{-1}
Average Flame Temp. (T_c)	=	5629°R

Chamber Pressure (P_c) = 100 psia

Heat Transfer Coefficient (h) = 314 BTU Ft^{-2} Hr^{-1} $°F^{-1}$

The most suitable materials for the throat section are graphite, coated refractory alloys, and ceramics. Monolithic graphite (JTA) will have minimal erosion when its surface temperature is maintained below 4000°F. Pyrolytic graphite has an erosion threshold temperature of 3800°F. The limiting temperature of the refractories is determined by the melting point of the oxidation resistant coating (3200°F).

a. Heat Sink Concept

In the operation of any rocket system, control of the surface temperature is all important in maintaining dimensional stability. In general, for a specified flame temperature, reduction in the nozzle wall-material surface temperature is realized by providing as rapid a heat transmission away from the backside as possible. To accomplish this, a material which readily absorbs heat (high diffusivity) is ideal as a "heat sink".

Materials which might be considered as heat sink types for this program include graphites, metals such as Na, K, Li, liquids and salts. Of these materials, the most feasible appear to be graphites and salts. The light-metals Na, K, and Li are extremely reactive and would lead to shielding problems. Liquids, while providing a good heat sink potential, are subject to high vapor pressure at elevated temperatures thereby leading to containment problems. With salts, a similar problem exists but to a far lesser degree.

Solid Phase Backup

A heat sink design utilizing a solid phase backup material for a molybdenum insert was evaluated. Figure 1 is a sketch of the design showing the insert, an ATJ graphite backup and an asbestos phenolic insulator. Figure 2 shows a plot of temperature versus time for three 100 second tests with 1800 second cool-down periods between tests. The computed temperatures indicate that the surface temperature of the moly insert is 3200°F at 80 seconds into the third 100 second test cycle. The asbestos phenolic is completely charred shortly after the completion of the second 100 second test.

A stress analysis was made to establish a thermal stress profile through the composite structure. The results are shown graphically on Figure 3. It may be seen that the moly insert is stressed in compression beyond the allowable for the insert temperature at 100 seconds. However, the OD is well within allowable limits for tension. Failure, other than local yielding of the ID surface would not be predicted.

A second solid phase, heat sink design was evaluated. The design was similar to that previously described with the exception that the asbestos phenolic was replaced with pyrolytic graphite. The "C" plane is oriented perpendicular to the nozzle centerline as shown on the sketch on Figure 4.

The result of a heat transfer computation is shown on Figure 5. The duty used was the same as that on the previous design which was a cycle of 100 second bursts with 1800 second cool down periods. The insert surface temperature was in excess of 3200°F at the end of the second burst. The gradient through the insert was similar to that indicated in the previous design. As a result, a stress analysis was not warranted.

6

SOLID PHASE BACKUP I

ASBESTOS PHENOLIC

ATJ

.40 MIN

1.20

.40

1.20 DIA

MOLYBDENUM

Figure 1

Figure 2

8
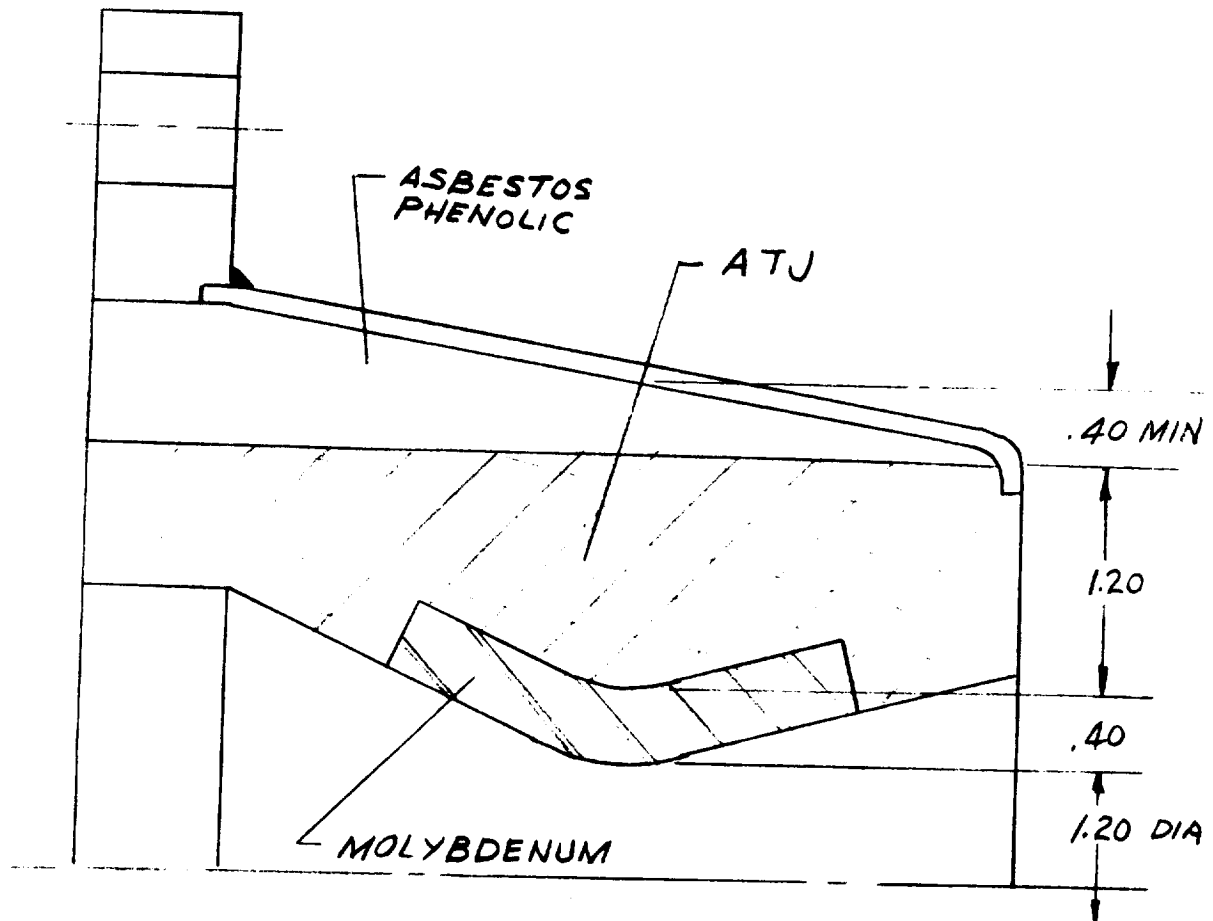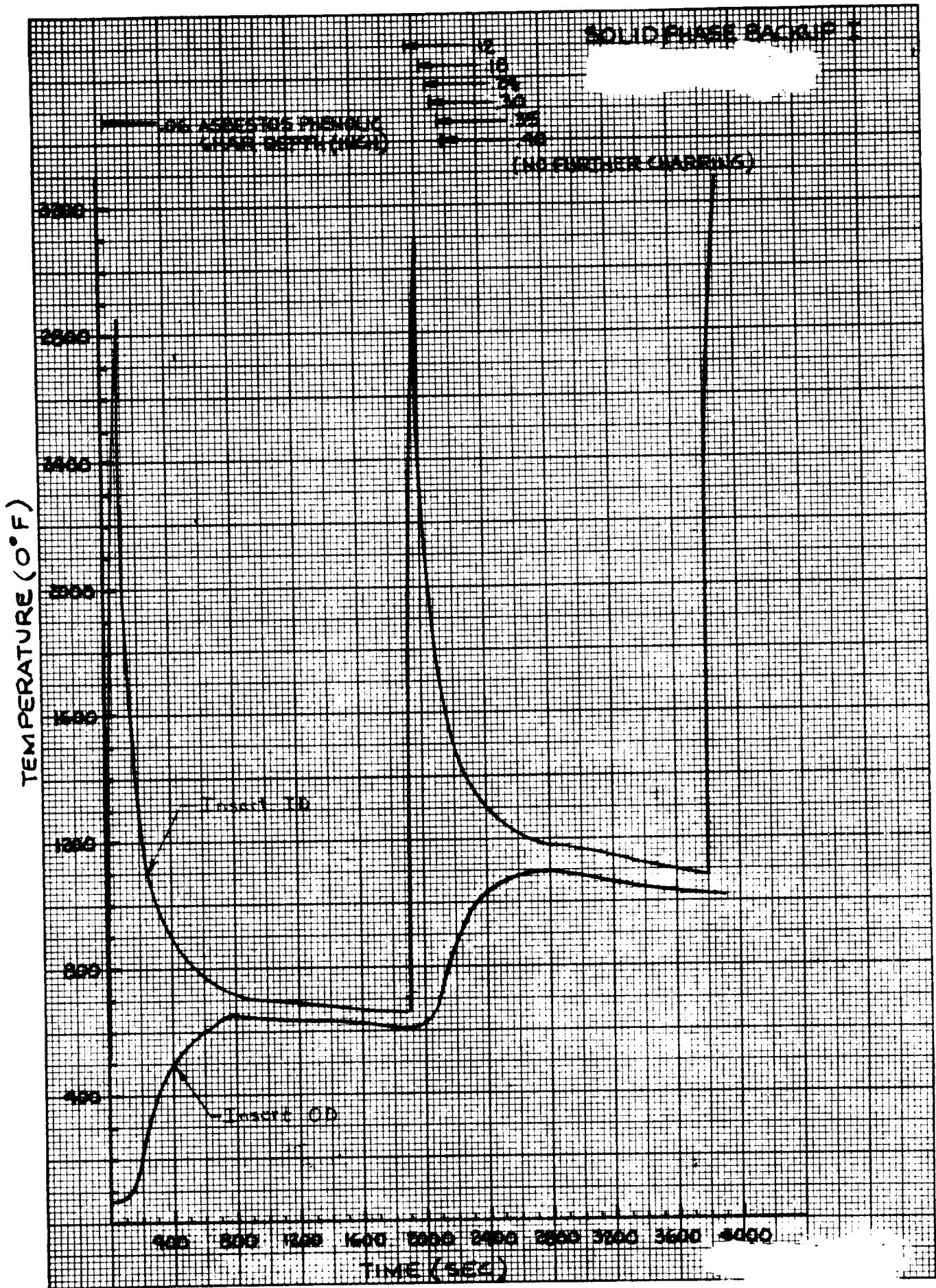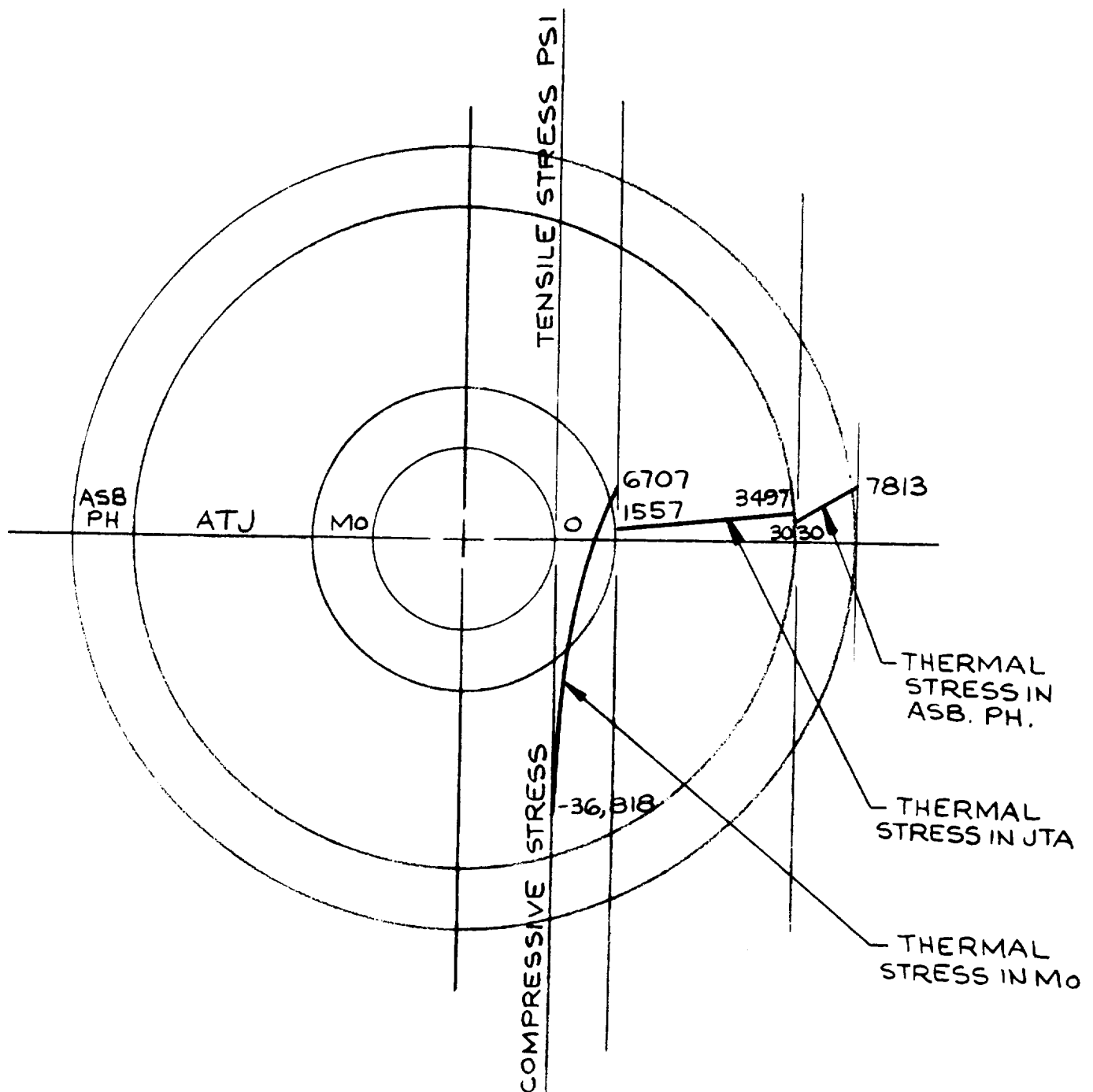
STRESS PROFILE FOR SOLID PHASE
BACKUP I. STRESSES ARE RESULT OF
TEMPERATURE GRADIENT AT END OF
100 SEC. PULSE

PYROLYTIC
GRAPHITE

ATJ

"C"

.40 MIN·

1.20

.40

MOLYBDENUM

1.20 DIA

SOLID PHASE BACKUP II

Moly ID

P6 OD

TEMP, °F

TIME, SECONDS

11

Figure 5
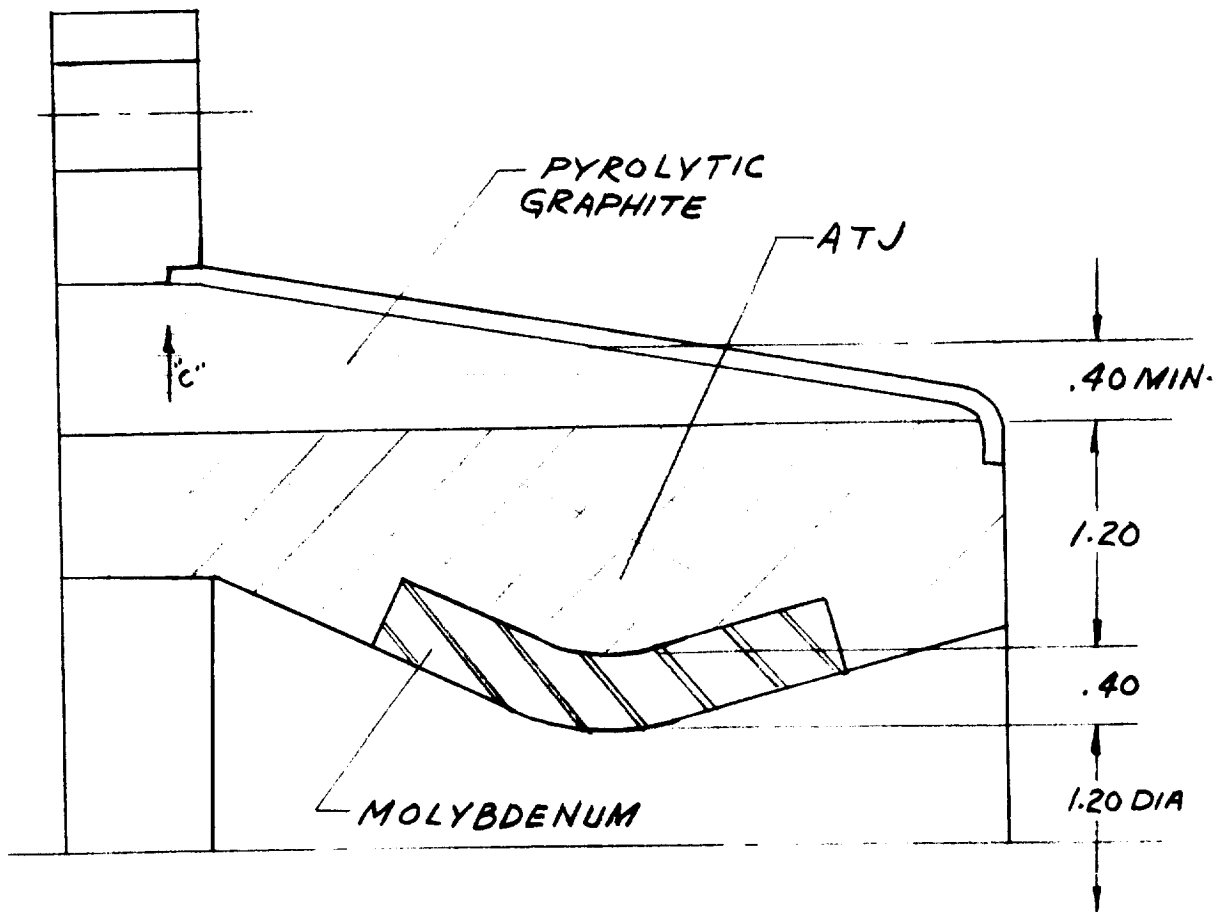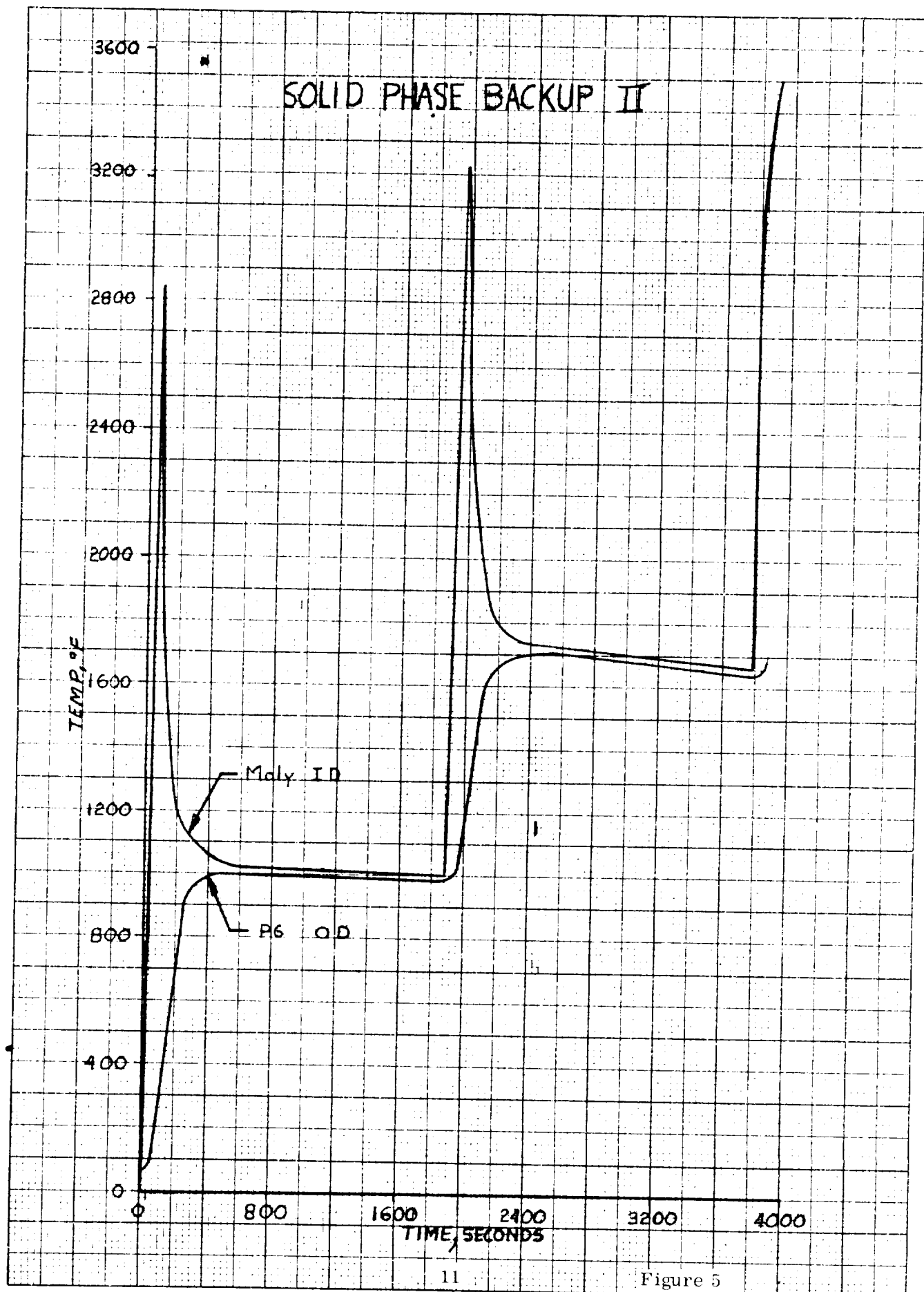
Reservoir Backup

A second design class evaluated under the heat sink category was the reservoir backup design. For this design molybdenum was selected as the throat insert material because of its high thermal conductivity. Ammonium chloride (NH_4Cl) salt was selected as the heat sink material because of its availability, storability, and low sublimation temperature (770°F). The design is shown on Figure 6.

The temperature at the molybdenum-salt interface was calculated to rise from the initial temperature of 70°F to 770°F, (the sublimation temperature of the salt) in three seconds. Therefore, the salt reservoir was assumed to remain at 770°F. In this case, the heat input to the salt reservoir would go toward vaporizing the salt, and the total salt required is a function of the duty cycle duration. The computer analysis results, given in Figure 7 show that the insert surface reaches 3200°F at approximately 15 seconds for a 100 second firing. After 100 seconds the surface temperature is $\approx$3600°F with intermittent 200 second cool down, the surface temperature is also $\approx$3600°F at the end of the second and third pulses which indicates that a quasi-steady state has been achieved. These results show that this design is not suitable for an extended duty cycle.

A stress analysis was not performed for this design because the high surface temperatures indicated that, for the materials used, the design was unsatisfactory.

b. Heat Barrier Concept

In defining the heat barrier concept, the premise that protection of the support structure from thermal penetration is of primary concern, was used. Thus, a material possessing high thermal resistance (low diffusivity) and high storage capacity (high specific heat/unit volume) would be used. The most common materials meeting this criteria are the reinforced phenolics. These materials are insulative, but possess a relatively large heat capacity through the heat of decomposition of the resin system.

In using these materials as insulators, care must be taken to assure structural integrity from two factors. First, the char layer formed by decomposition of the resin systems must be sound and possess a high crushing strength to carry the thermal expansion loads from the insert. Second, in no case should the temperature within the reinforced plastic be permitted to equal the melting temperature of the reinforcement or else rapid loss of insert retention will occur. Carbon cloth or graphite cloth reinforcements are not subject to this problem since they sublime at a temperature ($\sim$ 6700°F) higher than the flame temperature of the selected propellants ($\sim$ 5500°F). Silica or asbestos reinforcements are susceptible to this problem since their melting temperatures are approximately 3200°F.

Reinforced Phenolic Backup

In these design analyses, consideration has been given to the use of silica and graphite-cloth reinforcements. Each has its own advantages and disadvantages. Normally, the graphite cloth phenolic system provides a sounder char layer by virtue of the higher "breakdown" temperature of the reinforcement. However, it

SALT RESERVOIR

SILICA PHENOLIC

NH₄Cl SALT

1.25

.30

1.20 R.

1.20 DM.

MOLYBDENUM

SALT RESERVOIR

Figure 7
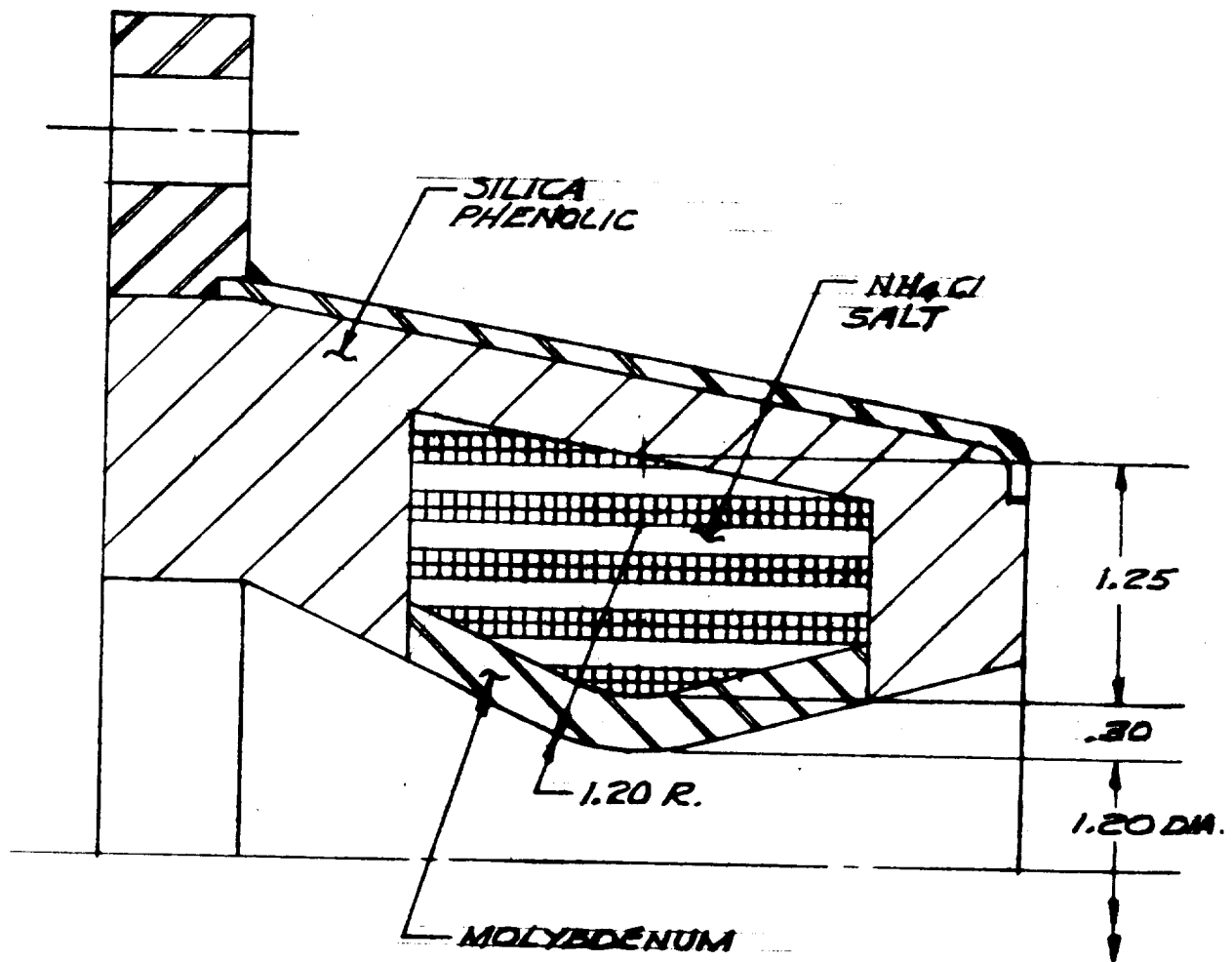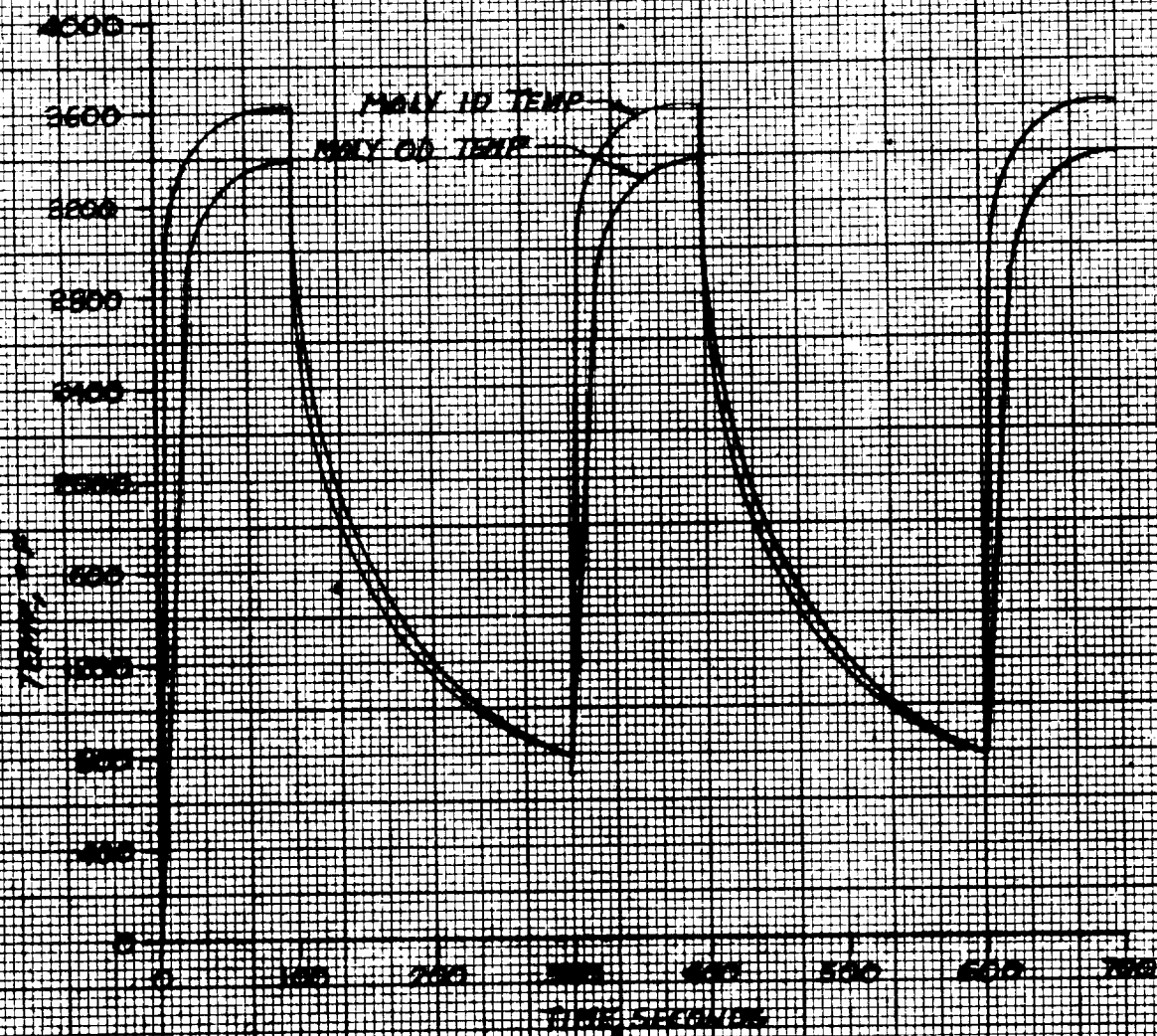
has one-half the insulative quality of the silica system. This latter material is a better structural material than graphite cloth in the virgin state. Selection then becomes a matter of carefully weighing all the considerations.

A sketch of the initial design is shown in Figure 8. As may be seen, the design is essentially a moly insert in a silica phenolic sleeve. An analysis was performed utilizing a duty cycle consisting of 100 second pulses and 1800 second cool-down periods. The time-temperature curve of Figure 9 shows the result of the analysis. The temperature at the ID of the insert is below the melting point of the moly for repetitive cycles. Charred silica phenolic will not carry loads until it has been compressed to about 18% of the char depth. The thermal expansion of the moly is less than 18% of char depth. Therefore, it is likely that the insert will not be rigidly held.

Hoop stress is negligible since the static pressure at the throat is only 57 psia. However, stresses due to the thermal gradient across the insert will be of prime consideration. The insert loses strength as the temperature increases. The tensile stress on the OD does not exceed the allowable, but the compressive stress on the ID is greater than the allowable yield strength at the temperature. The plastic yielding that will occur is considered acceptable.

The design was modified to replace 0.60 inch of the silica phenolic with graphite phenolic as shown in Figure 10. The design was subjected to the same thermal analysis used on the previous design and the result is shown in Figure 11. The surface heat-up is somewhat more rapid after the first cycle but the most important factor is that the graphite phenolic chars completely through during the initial seconds of the first cool-down period. The silica phenolic is completely charred through after approximately 200 seconds cool-down. Stress analyses were not performed on this design because of the rapid charring rate of the support material.

A third modification was made to the design where the throat insert was changed to JTA graphite. The graphite phenolic backup and the silica phenolic insulation were unchanged. The design sketch is shown on Figure 12. Figure 13 is a time-temperature plot for the imposed duty cycle. The indications are that this design would function satisfactorily. As may be seen in Figure 13, the silica phenolic has exceeded the char temperature of 800°F during the second cool-down phase. As a result of the complete charring of the graphite cloth, the JTA insert is unsupported. The stress analysis is then based on a thick cylinder with a temperature gradient. Using the maximum temperature differential across the JTA, as determined from the heat transfer analyses, ID and OD stresses are determined. Calculated stresses were 590 psi tension on the OD and 1085 psi compression on the ID. These are within allowable limits for JTA graphite. While the stresses were acceptable, it was indicated by the phenolic char that adjustments would be required to the insulation thickness.

Pyroid Insert

A unique material, Pyroid, which is basically pyrolytic graphite, can be fabricated with oriented planes of conductivity. The advantage of using this material is that "a-b" planes can be oriented to permit the insert to cool itself upstream of the throat by the rapid transfer of heat to a downstream region. The "c" planes are generally oriented to maintain the back side of the insert at a relatively low temperature. The design is shown in Figure 14, and as shown, several of the "a-b" conductive planes intersect with the ATJ graphite backup. However, the monolithic graphite will distribute the heat rapidly and prevent a local hot spot.
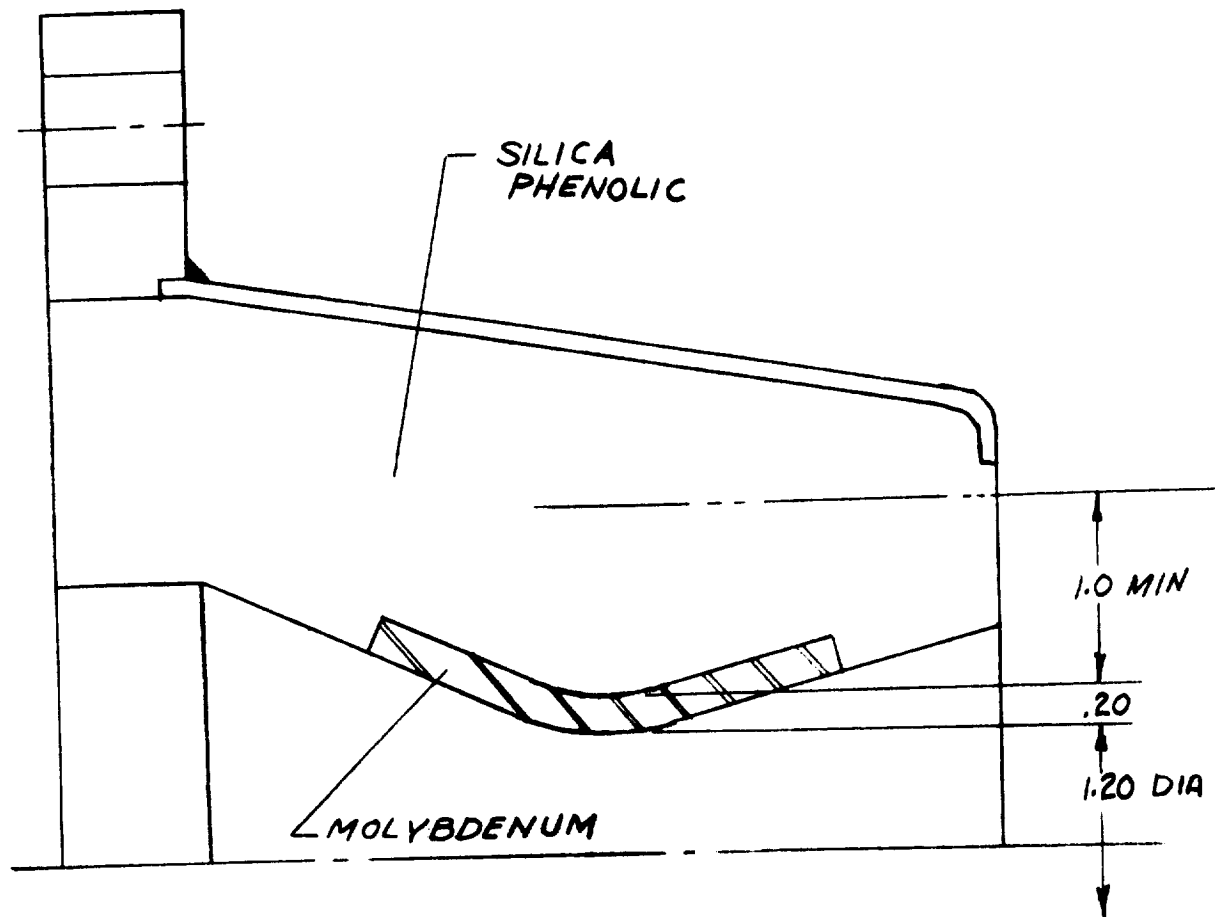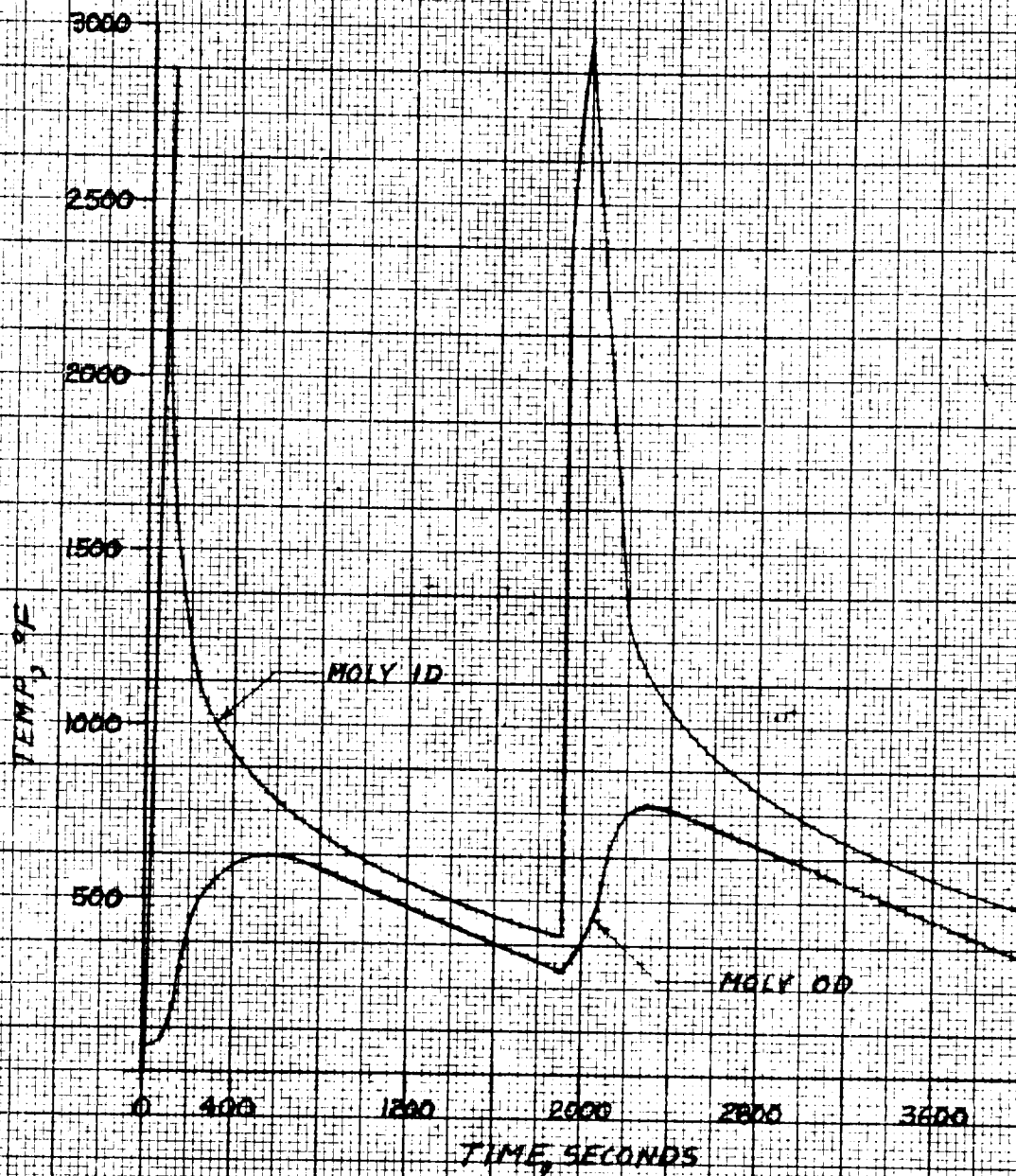
15

SILICA PHENOLIC

1.0 MIN

.20

1.20 DIA

MOLYBDENUM

Figure 8

REINFORCED PHENOLIC BACKUP I

TIME, SECONDS

17

Figure 9

Figure 10

REINFORCED PHENOLIC BACKUP II

TEMP, °F

TIME, SECONDS

Moly ID

Moly OD

19

Figure 11

SILICA PHENOLIC

GRAPHITE PHENOLIC

.80 MIN.

.60

.20

1.20 DIA.

1.20 R

JTA GRAPHITE

Figure 12

REINFORCED PHENOLIC BACKUP III

Figure 13

PYROID DESIGN

SILICA PHENOLIC

ATJ GRAPHITE

.50

.50

1.20 R.

1.20 DIA.

PYROID

Figure 14
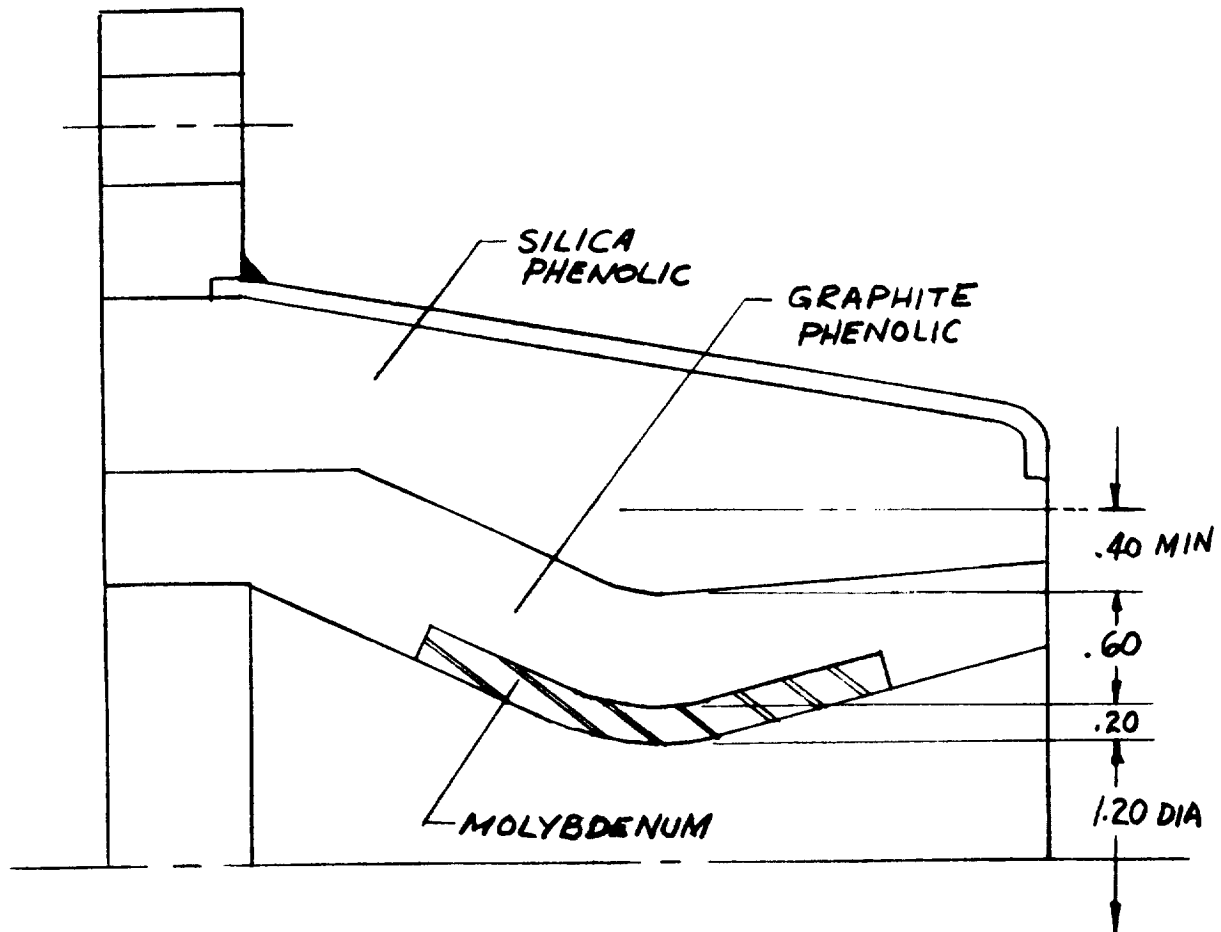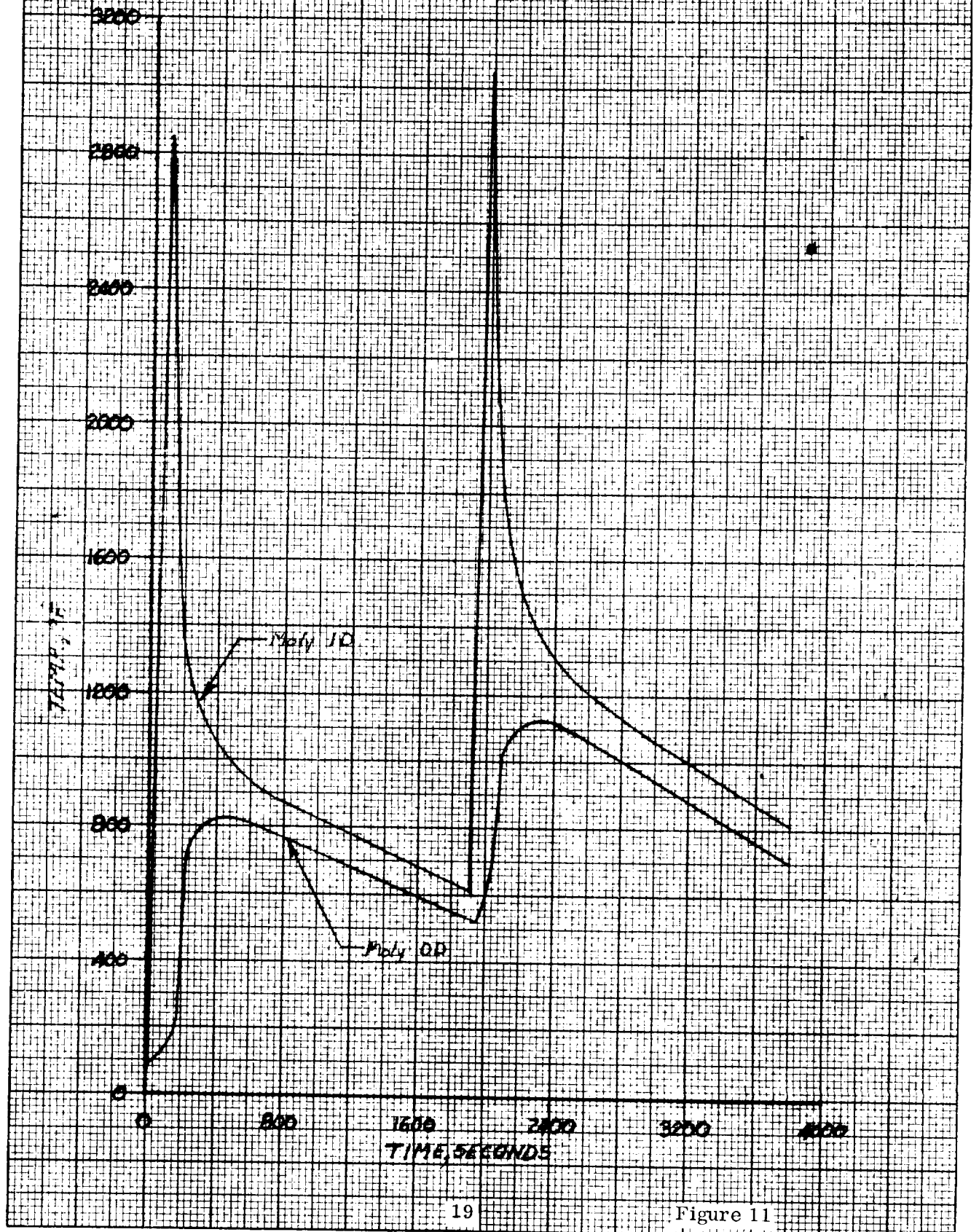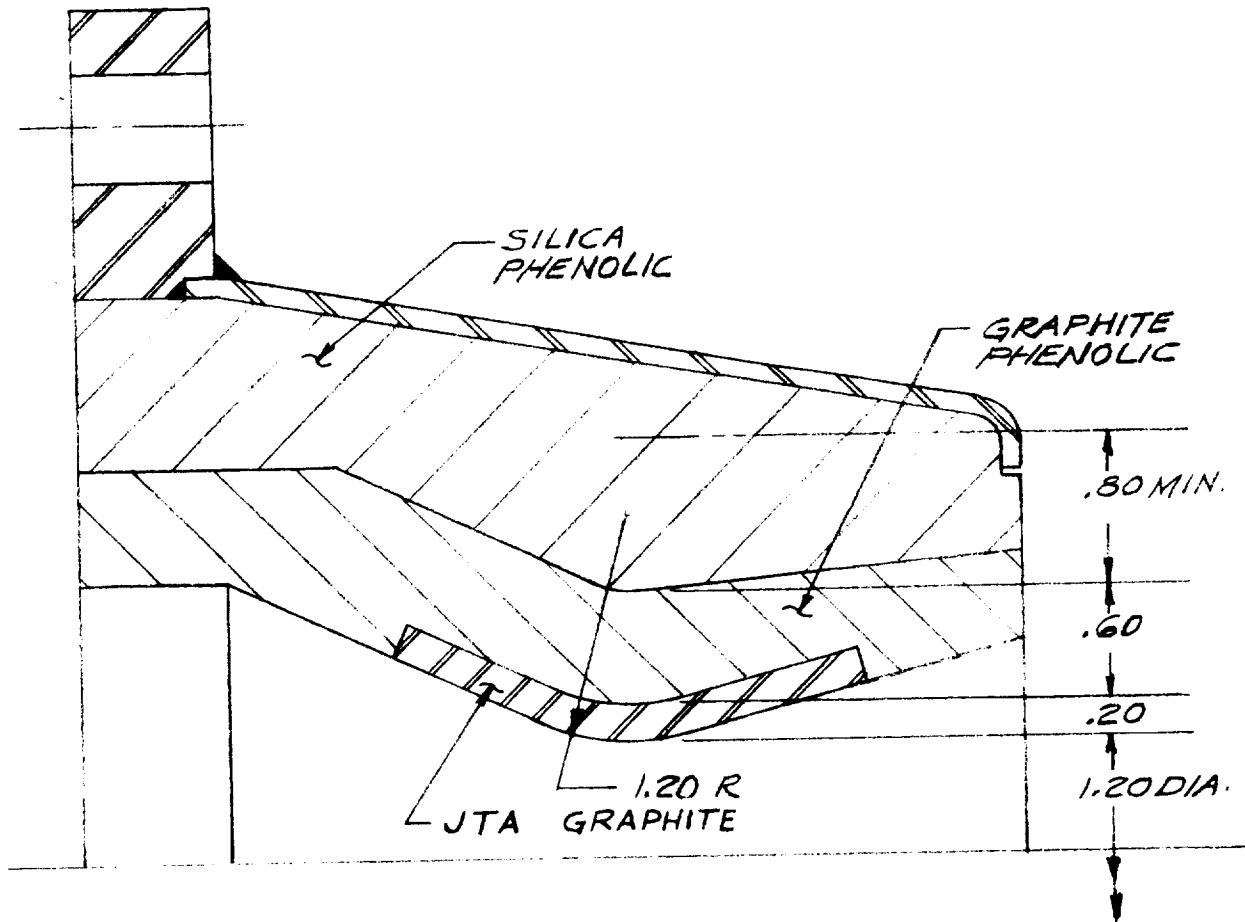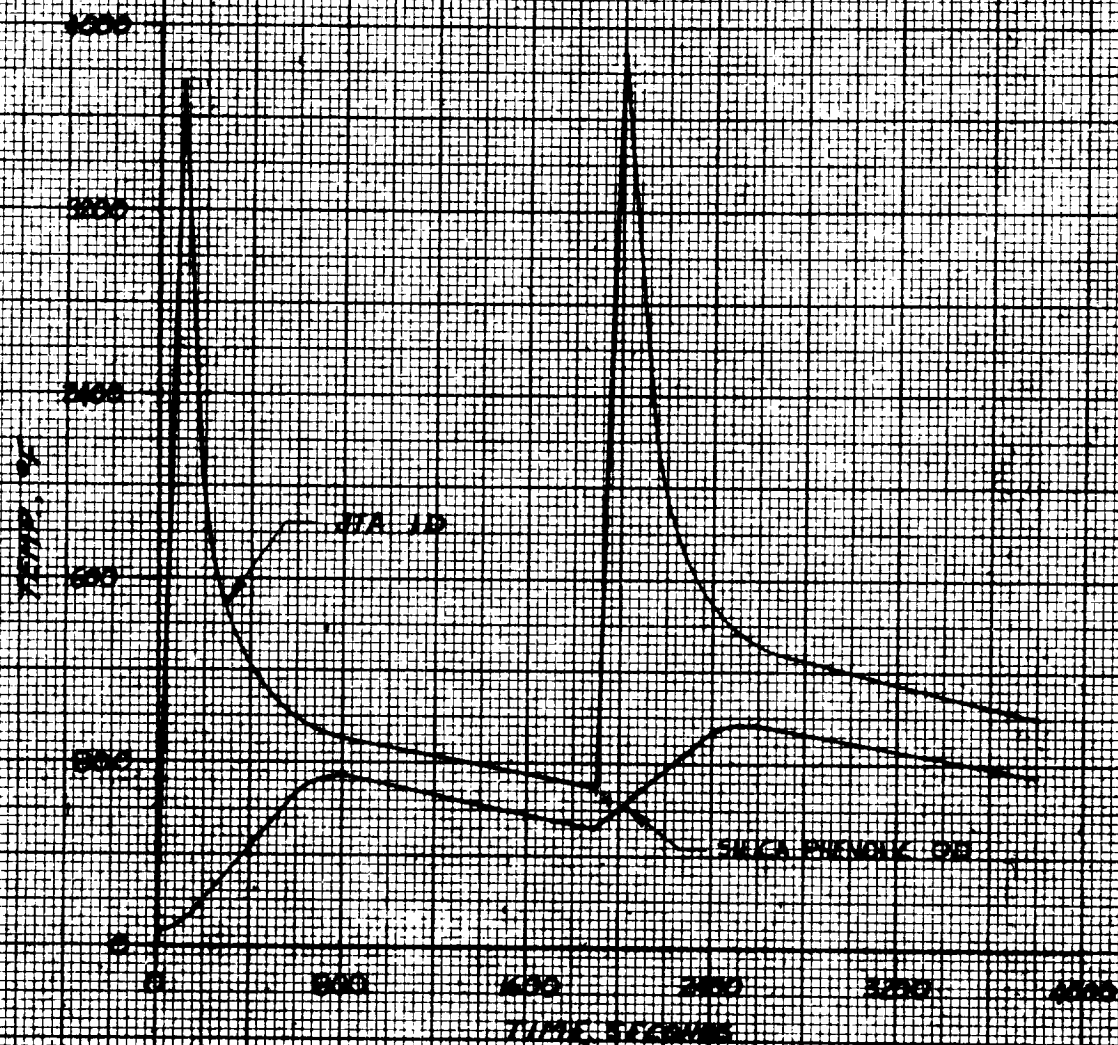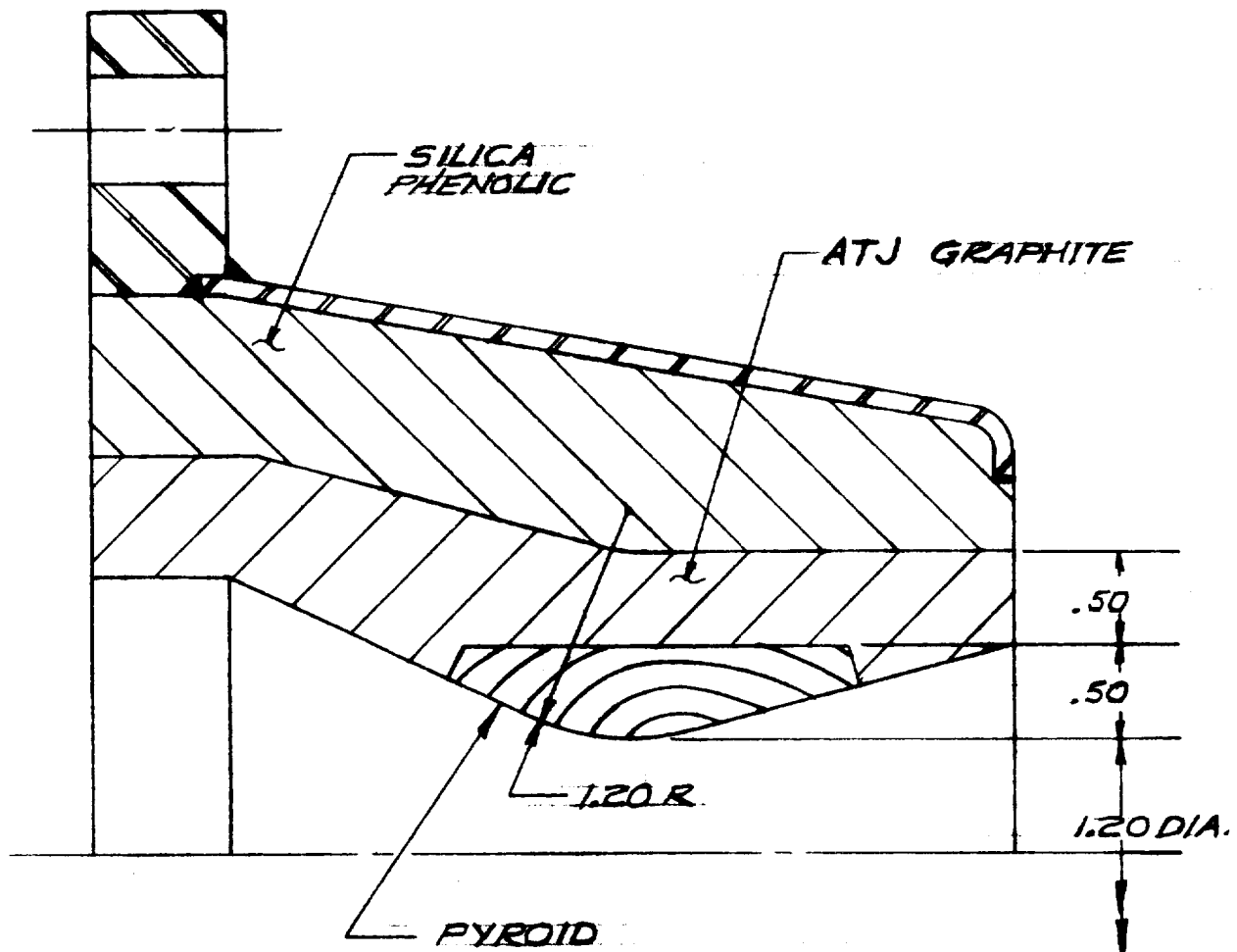
A detailed heat transfer investigation was not made because of the complexity a true solution requires. With reference to other designs, however, a logical determination of the expected temperatures can be made. The Pyroid material will behave in a manner akin to a mixture of the "washer type" PG design as noted later and the JTA graphite design (Reinforced Phenolic Backup III). The surface temperature will reach approximately 3400°F for long duration (100 second) pulses. The temperature of the ATJ-graphite silica phenolic interface will be approximately 1800°F. These temperatures are well within acceptable operating limits for the materials.

c. Radiation Cooled Concepts

The basic physical characteristics required for radiation cooled materials are high thermal diffusivity with low heat capacity. This permits rapid heat flow from the inner surface, T_{wi}, to the outer surface, T_{wo}, such that radiation to the ambient temperature, T_a, becomes an effective cooling process. Of the known materials, pyrolytic graphite is the most suitable.

In most instances involving radiation cooling, the inner surface (surface exposed to propellant gases) will be at higher temperatures than for other cooling methods because radiation is inefficient at low temperatures. Writing a simple heat balance and neglecting stored heat,

$$\text{heat in} = h\ (T_{aw} - T_{wi}) = \text{heat out} = \sigma\epsilon\ F\ (T_{wo}^4 - T_a^4).$$

where T_{aw}, T_{wi}, T_{wo}, and T_a are the adiabatic wall, inner surface, outer surface, and ambient temperatures respectively.

Assuming emissivity, ϵ, and view factor, F, are both equal to one,

$$T_{wi} = T_{aw} - \frac{\sigma\ (T_{wo}^4 - T_a^4)}{h}$$

The Boltzman constant, σ, has a value of $0.173 \times 10^{-8}\ \dfrac{\text{BTU}}{\text{Ft}^2 - \text{Hr} - °\text{R}^4}$

and the film coefficient, h, has a nominal value of approximately

$314\ \dfrac{\text{BTU}}{\text{Ft}^2 - \text{Hr} - °\text{R}}$ at the throat. Combining these terms,

$$T_{wi} \sim T_{aw} - 5.5 \times 10^{-12}\ (T_{wo}^4 - T_a^4)$$

It is evident that the inner wall will approach the adiabatic wall temperature, T_{aw}, for simple radiation cooled designs, especially for long duration firings when the heat capacity of the material has been saturated.

The major advantage to using radiative cooled designs is their simplicity in construction and in many cases, they are light in weight. As seen by the following design analyses, their duty cycle application must be restricted.

For the analyses of the radiation cooled concepts, convection was neglected, although the ambient radiation temperature was assumed to be 530°R. For space application this value is too high, although the correction is practically negligible for OD surface temperatures of 2000°F and higher. For atmospheric tests, The OD surface temperatures indicated are conservative because convection will be an appreciable heat transfer mode at the elevated temperatures indicated.

23

Pyrolytic Graphite Concepts

In all of the radiation cooled designs, pyrolytic graphite was oriented to provide for the rapid conduction of heat away from the ID surface to the OD surface. This was accomplished by using disks with the high conductivity planes perpendicular to the nozzle axis.

The initial design consisted of the pyrolytic graphite disks used as a backup to a molybdenum throat insert as shown in Figure 15.

A heat transfer analysis was performed on the design using a test duty cycle consisting of ten 20 second pulses with 1410 second cooldown periods between each pulse. This series was followed by a final 100 second burst. The results of the analysis, shown graphically on Figure 16, indicate that the design will survive the ten 20 second pulses but will exceed 3200°F after 40 seconds of the 100 second burst. This temperature was selected as the critical temperature at which erosion of the material will commence.

The design was modified by replacing the molybdenum insert with a JTA graphite insert as shown in Figure 17. The same duty cycle was imposed and used for the heat transfer analysis. The results, shown in Figure 18, indicate higher temperatures over the duration of the 20 second pulses but still within the temperature limits of the materials. As in the analysis of the previous design, the 100 second burst results in an excessive temperature on the ID surface.

Thermal stress values were determined by computer analysis for two conditions. They were for time t = 0.2 seconds when the temperature gradient of the JTA graphite was maximum and for t = 3.2 seconds when the temperature gradient across both rings was maximum. The resulting hoop stress profiles are shown in Figures 19 and 20. For each time interval, the inner surface of the JTA is loaded in compression. This results from the good backup support provided by the PG. Further stress analysis could be performed to obtain a better balance between tensile and compressive stresses.

A third design is shown in Figure 21 in which pyrolytic disks alone are used. For a duty cycle of ten 20 second pulses and 1410 second cooldown intervals, the resultant temperatures are shown on Figure 22. A long duration test will result in temperatures approaching 3800°F on the ID surface as shown in Figure 23. With a high ID surface temperature, surface regression may be a problem and further investigation would be warranted. Thermal stresses were analyzed for the maximum thermal gradient and were computed at 590 psi in compression at the ID and 340 psi in tension at the OD. Allowable stresses are greater than 10,000 psi which provides for a large margin of safety.

d. Auxiliary Cooled Concepts

The auxiliary cooled concepts presented herein are for transpiration and film cooling. In both of these concepts, an external coolant supply having a pressurizing source will be required. As with any outside cooling means, the most severe duty cycles are long duration pulses at high heat fluxes. These cycles require large storage capacity with large coolant flows.

Transpiration Cooled Concept

This design is illustrated in Figure 24. The analysis for this design is based upon work done on an Air Force contract and on company sponsored

PYROLYTIC GRAPHITE I
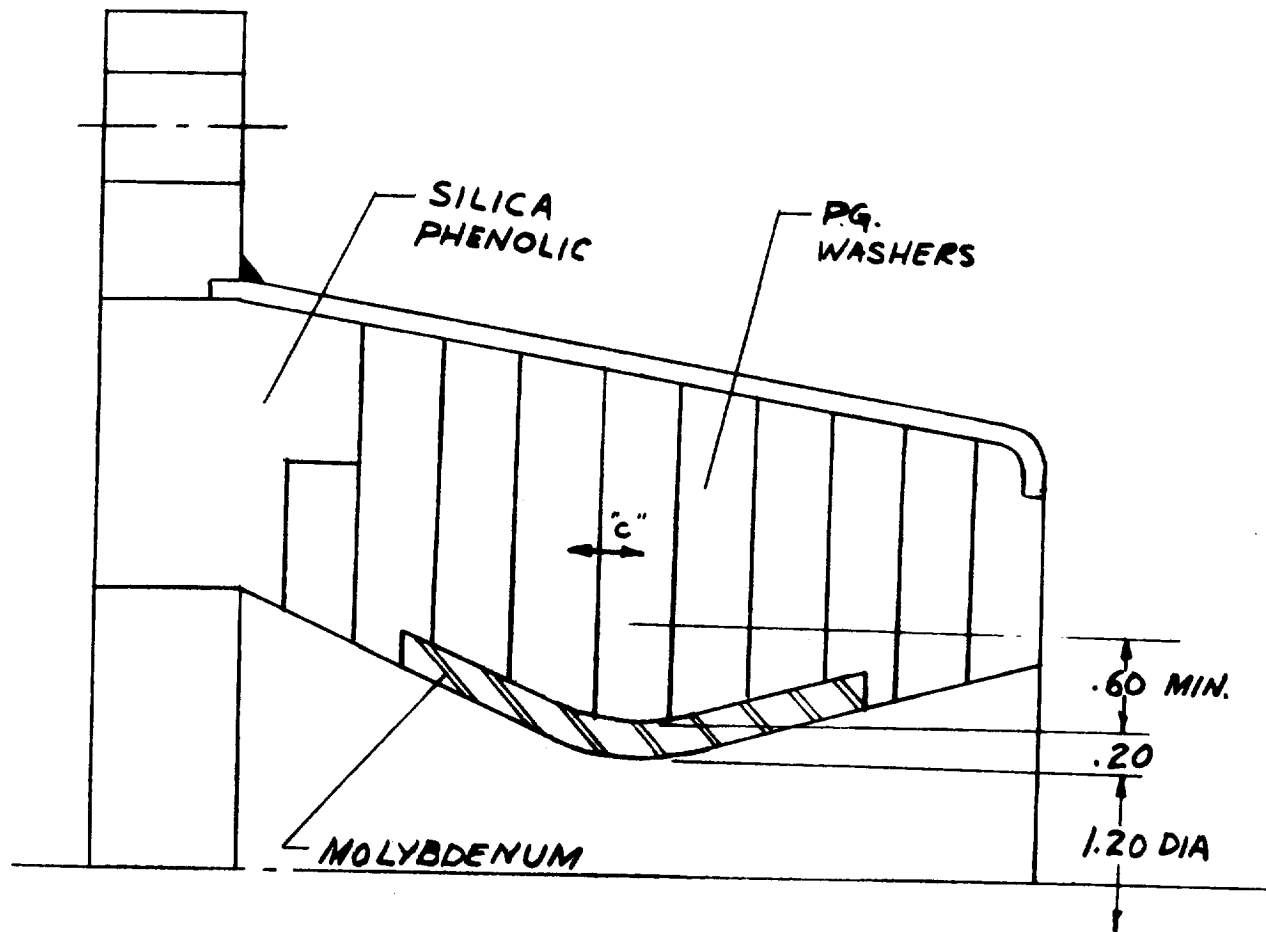
Figure 15

PYROLYTIC GRAPHITE 1

MOLY ID
1.56" x 1" OD
TEMP CURVES
COINCIDE

TEMPERATURE (°F)

TIME (SECONDS)

26   Figure 16

PYROLYTIC GRAPHITE II

SILICA PHENOLIC

P.G. WASHERS

.60 MIN.

.20

1.20 DIA

JTA GRAPHITE

PYROLITIC GRAPHITE II

Figure 18

28
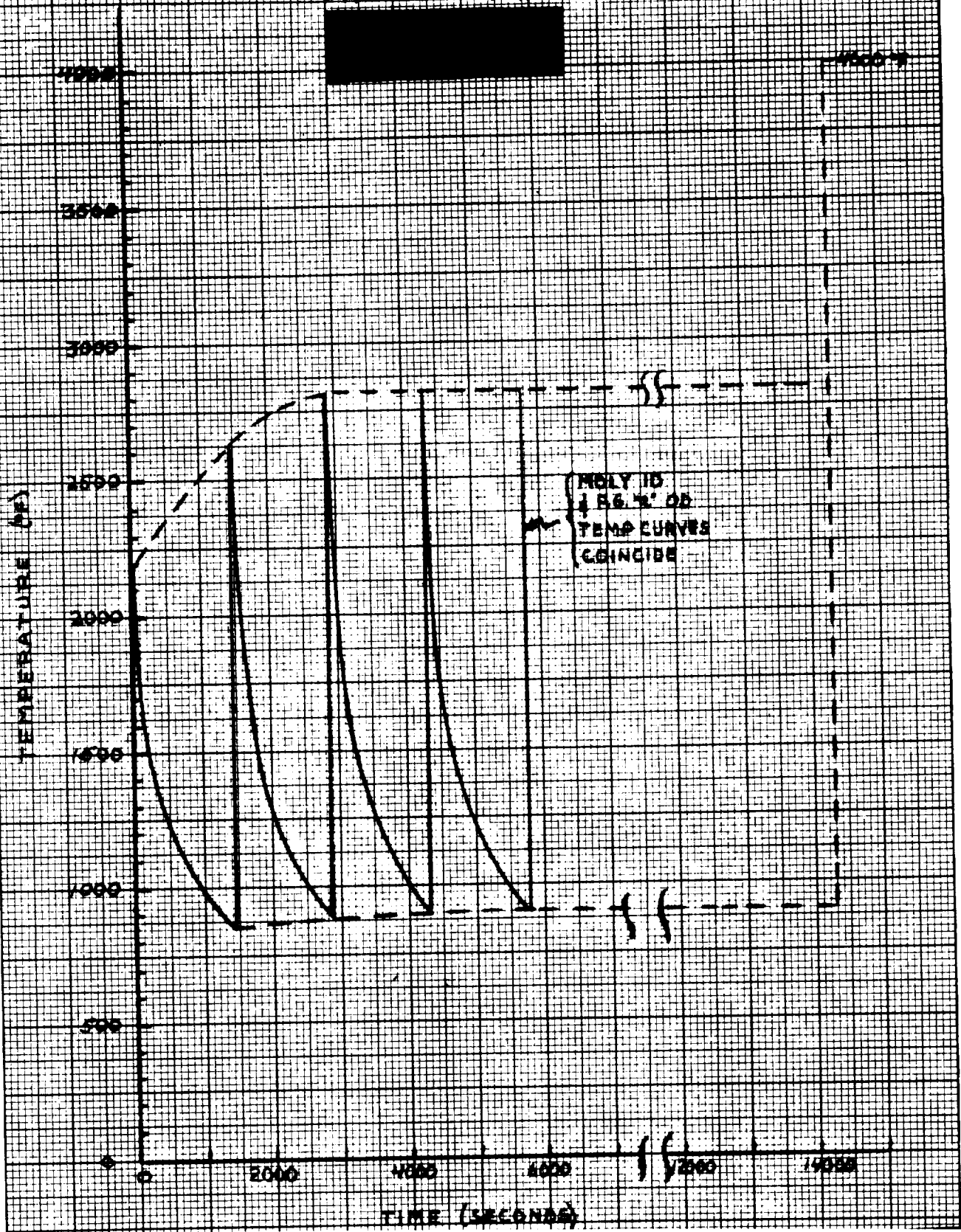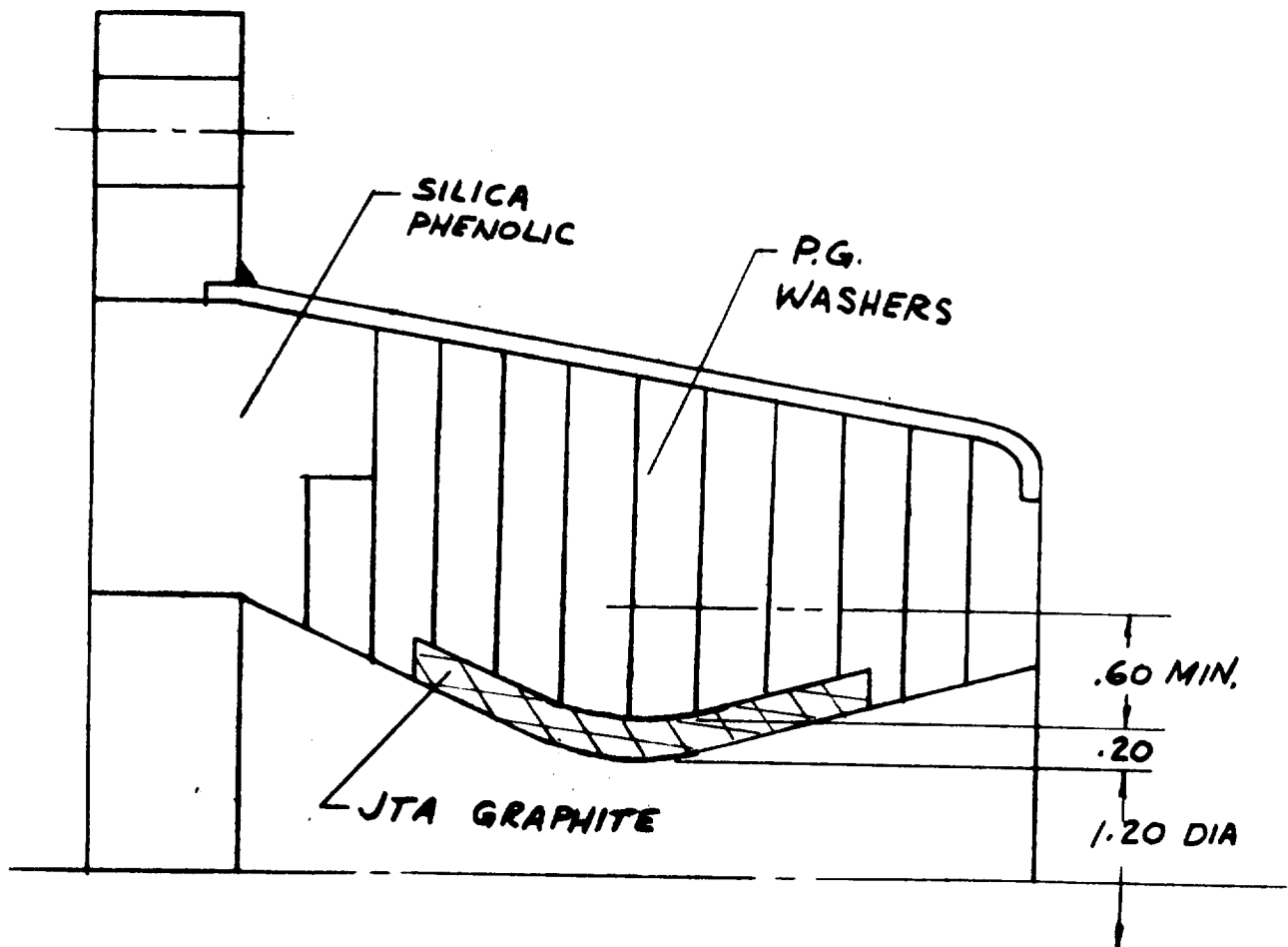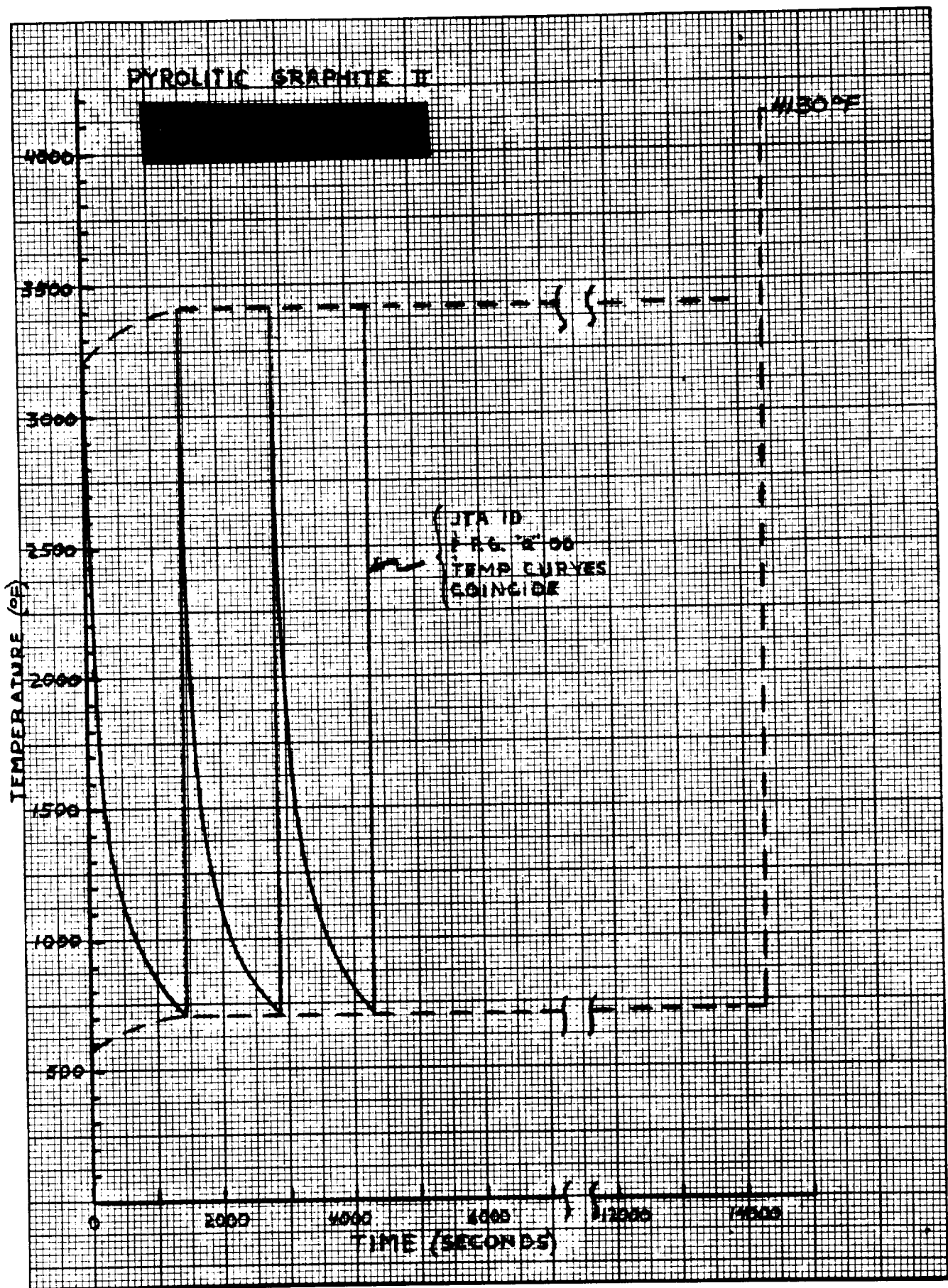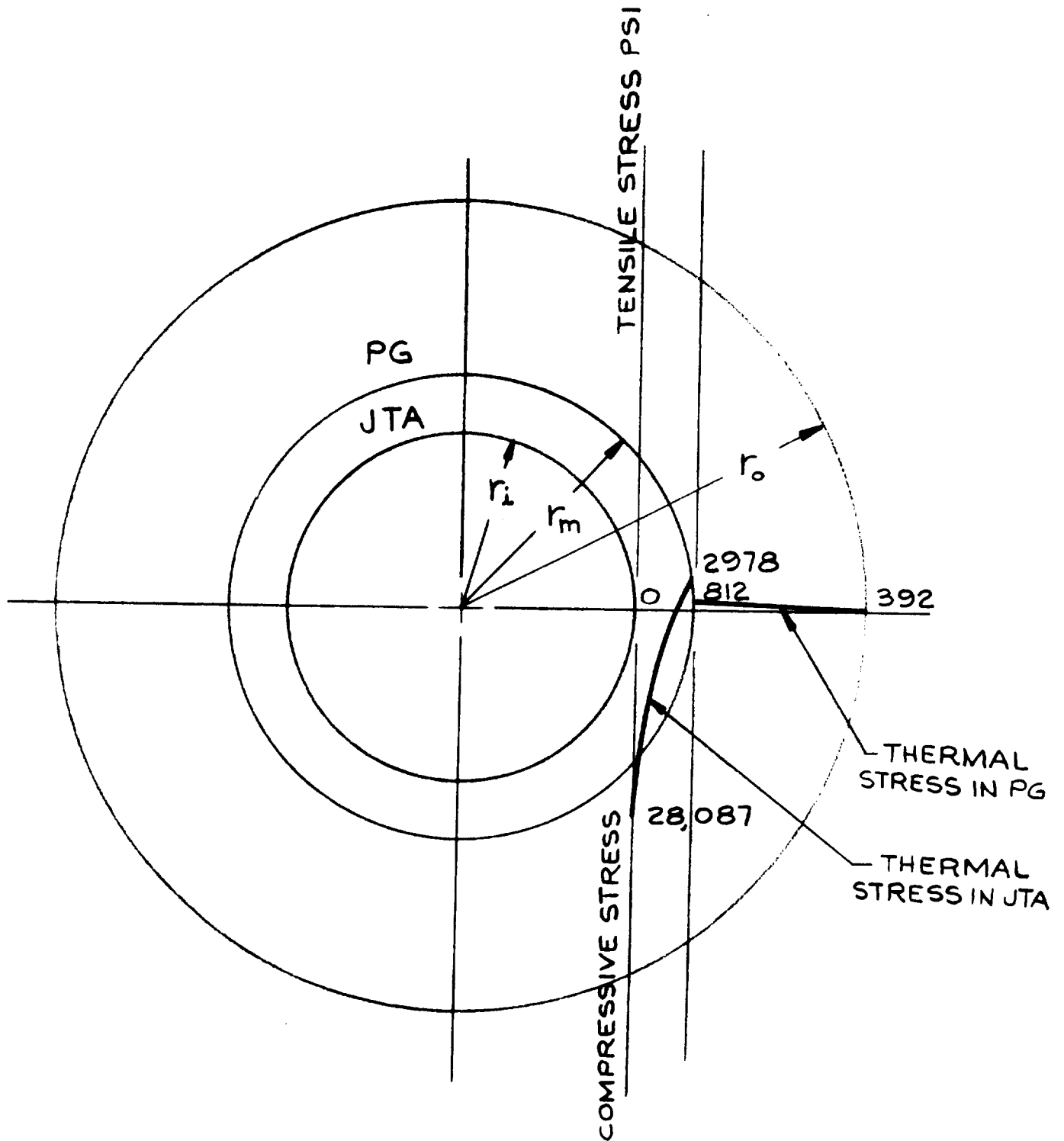
HOOP STRESS PROFILE - RADIATIVE
PYROLYTIC GRAPHITE II AT 0.2 SECONDS.
TEMPERATURE GRADIENT FROM
r_i TO r_m = 587° F.

29   Figure 19
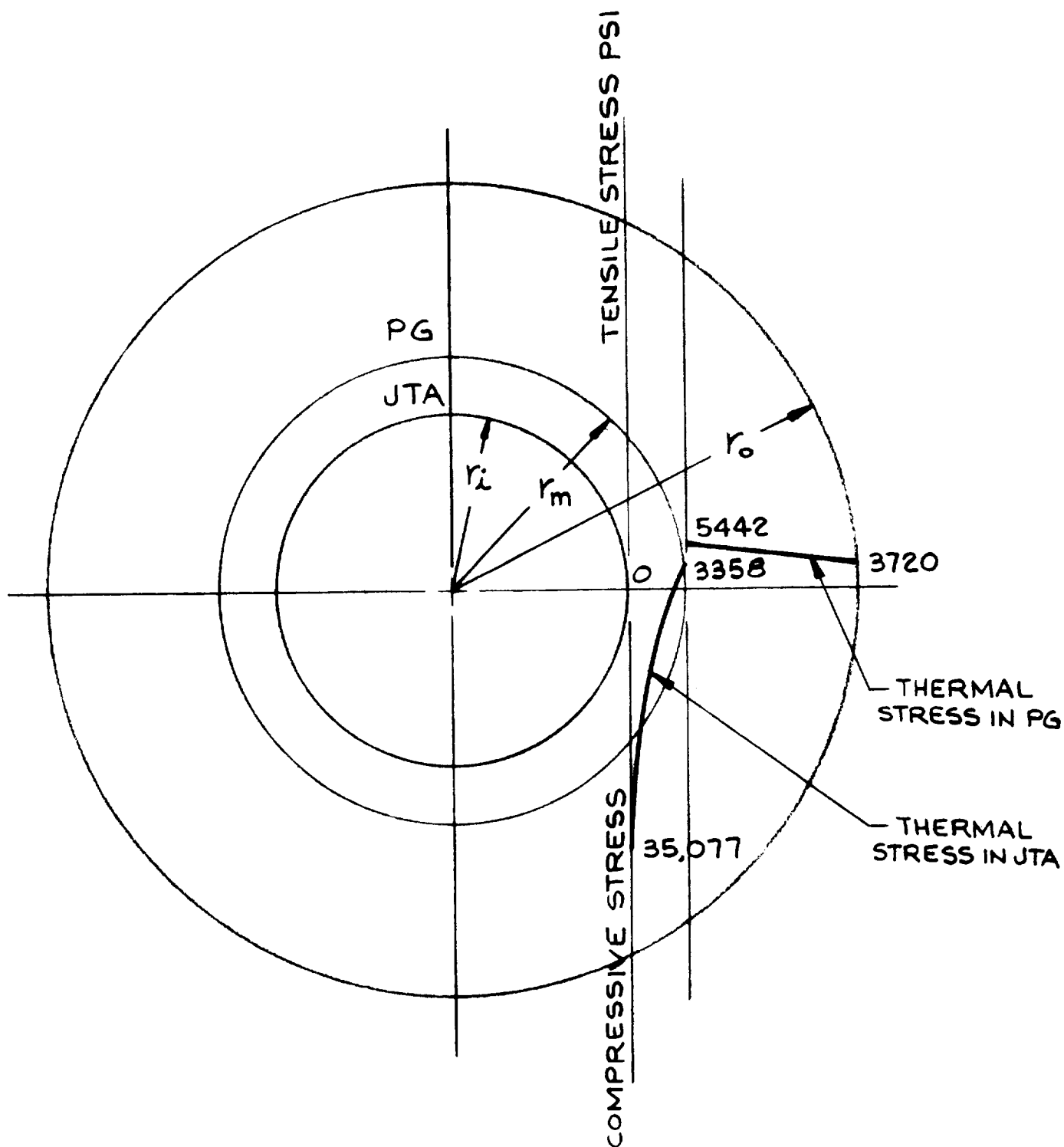
HOOP STRESS PROFILE - RADIATIVE
PYROLYTIC GRAPHITE II AT 3.2 SECONDS.
TEMPERATURE GRADIENT FROM
r_i TO r_o = 1124° F.

30   Figure 20

PYROLYTIC GRAPHITE III

SILICA
PHENOLIC

P.G.
WASHERS

'c'

.75 MIN

1.20 DIA.

Figure 21

Figure 22

PYROLYTIC GRAPHITE III

Figure 23

AUXILIARY COOLED I

SILICA PHENOLIC

NH₃ COOLANT

.75

.20

1.20 DIA.

POROUS MOLYBDENUM
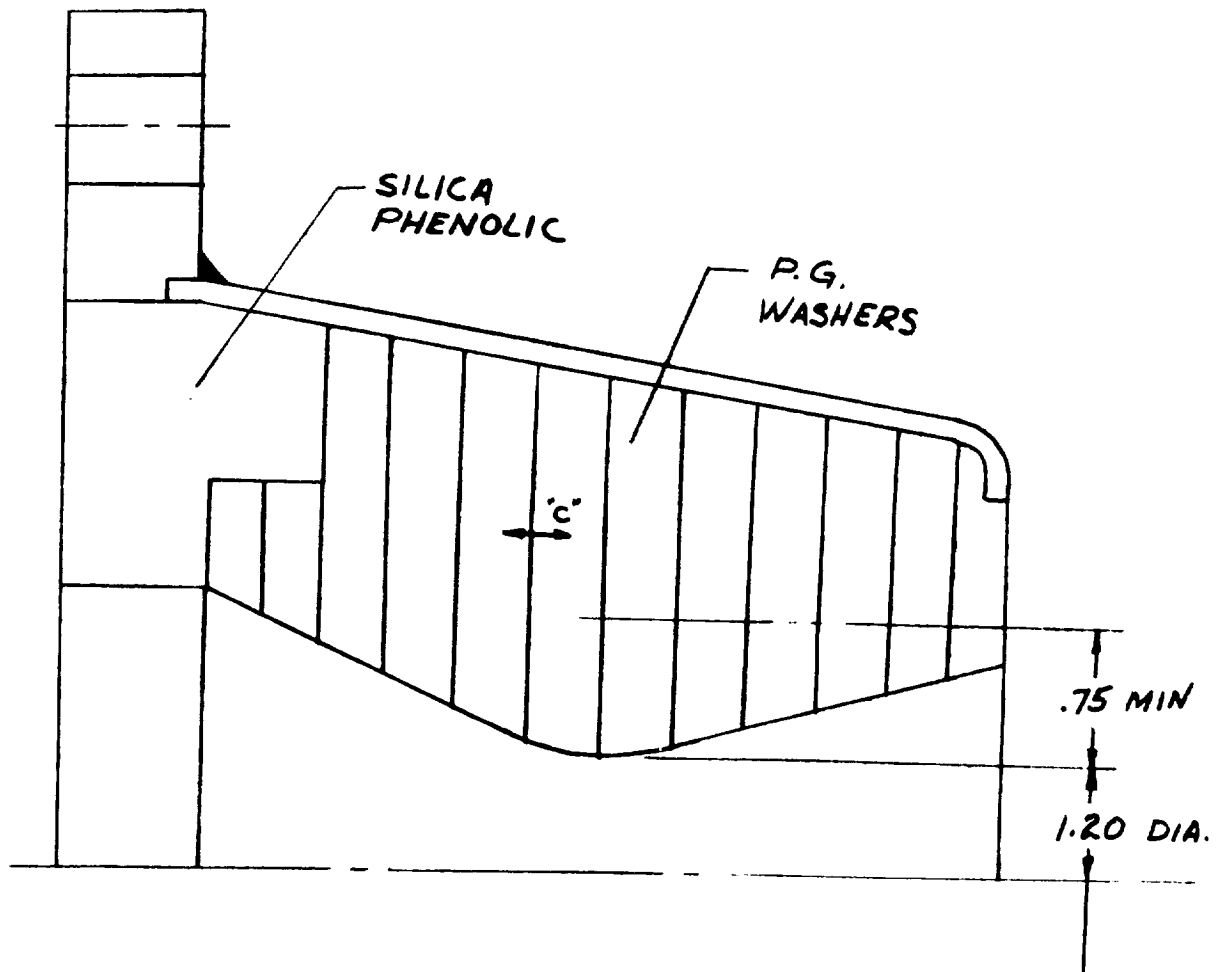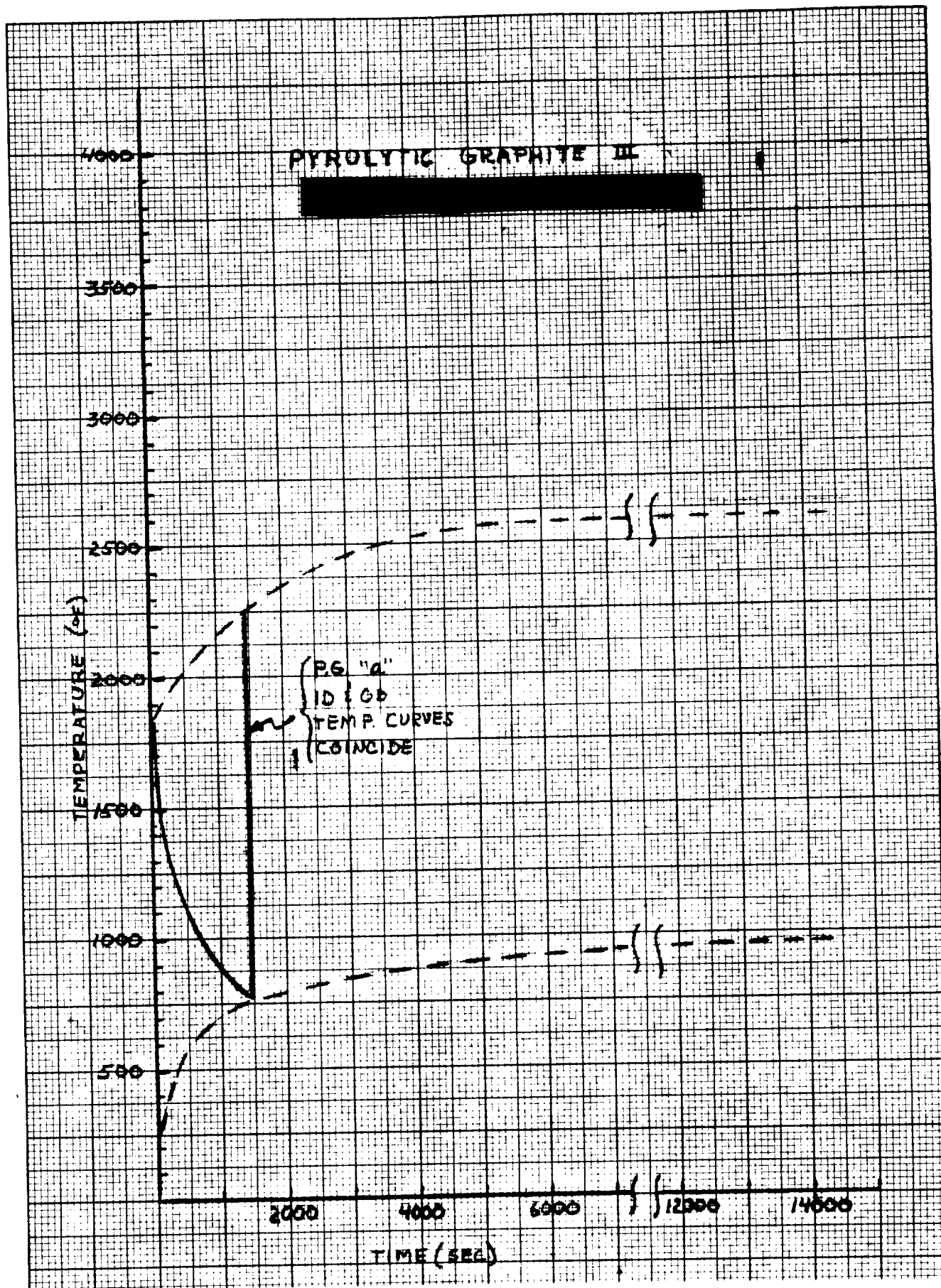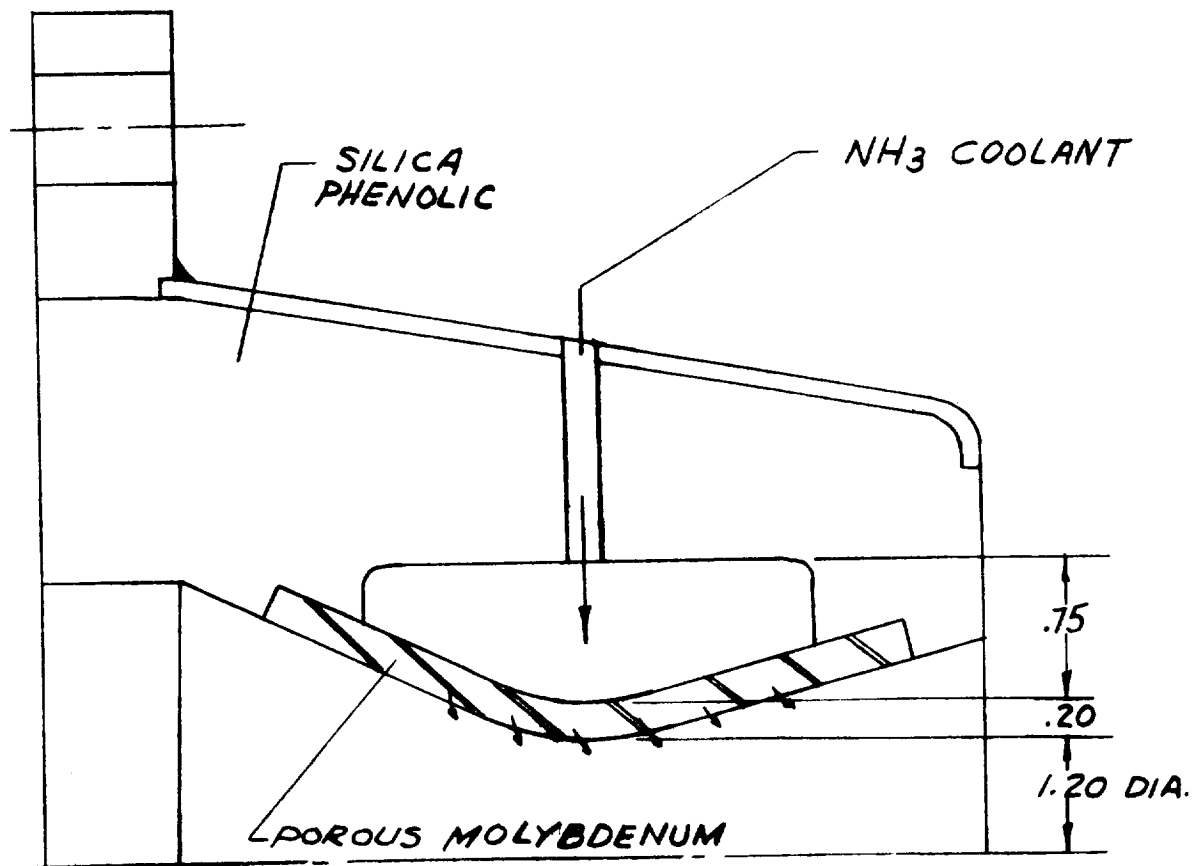
Figure 24

research. The temperature history during a 300 second pulse is plotted in Figure 25. The system uses a pressure differential of 200 psia to force 28 pounds per hour per foot of insert of NH_3 through the porous molybdenum.

The system reaches equilibrium conditions at the throat in 100 seconds. The porous moly ID temperature peaks at 3000°F, the OD at 2330. By selecting a higher flow rate, the surface temperature may be further decreased.

Thermal stresses in the porous insert were calculated for a temperature gradient of 825°F which occurs during the initial 15 seconds. Resulting stresses were 53,000 psi compression on the ID and 47,300 psi tension on the OD. In addition, an external pressure load was superimposed. The external pressure is necessary to provide gas flow inward through the porous insert. The net pressure gradient across the insert is 200 psi, and the resulting compressive hoop stress is 800 psi. Stresses in the insert are 53,800 psi compression on the ID surface and 46,500 psi tension on the OD.

The above net stresses are based on an elastic analysis and are higher than allowable. Optimization of the design with respect to the insert thickness is necessary. Because the above stresses were obtained by elastic analysis, an elastic-plastic study would be required to determine the stress level of the OD surface.

Film Cooled Concept

A sketch of this design is shown in Figure 26. In addition to conventional film cooling, the injectant serves as a diluent to the products of combustion. In order to reduce oxidation of the insert by the exhaust gases, the injectant acts as a barrier to the oxidizing components due to diffusion and chemical reaction. Thus the injectant gas should be a reducing agent, such as fuel, which is incapable of reacting with the wall, but which is readily oxidized by the free stream gas.

As the streams flow from the point of injection, they will tend to diffuse into each other. The amount of reacting gases passing into the injected film will be a function of the diffusion constants and concentrations of the system, as well as time (or distance downstream from the injection point). Possible chemical reactions between the injected fluid and free stream will also affect the concentration profile in the boundary layer.

In order to calculate the flow rate of the injected gas required to protect the nozzle wall from oxidation, a complete description of the system would be required including the chemical kinetics of the system, diffusion rates of the species, the behavior of the boundary layer as well as a large number of physical constants which are not generally available.

In order to arrive at useful results, some simplifying engineering assumptions must be made, combined with suitable tests and experiments. One possible simplifying assumption would be to have the mass flow rate of the injection gas large enough to chemically react with all of the oxidants in the free stream. This assumes that the oxidants will preferentially react with the injected gas rather than with the nozzle wall. However, this would be too conservative, as the mass blockage effect of the injected gas would be ignored. Also, if the amount of gas injected in the throat region is large enough to react chemically with all of the oxidants in the free stream, then the injected gases might just

AUXILIARY COOLED T

Figure 25

Figure 26
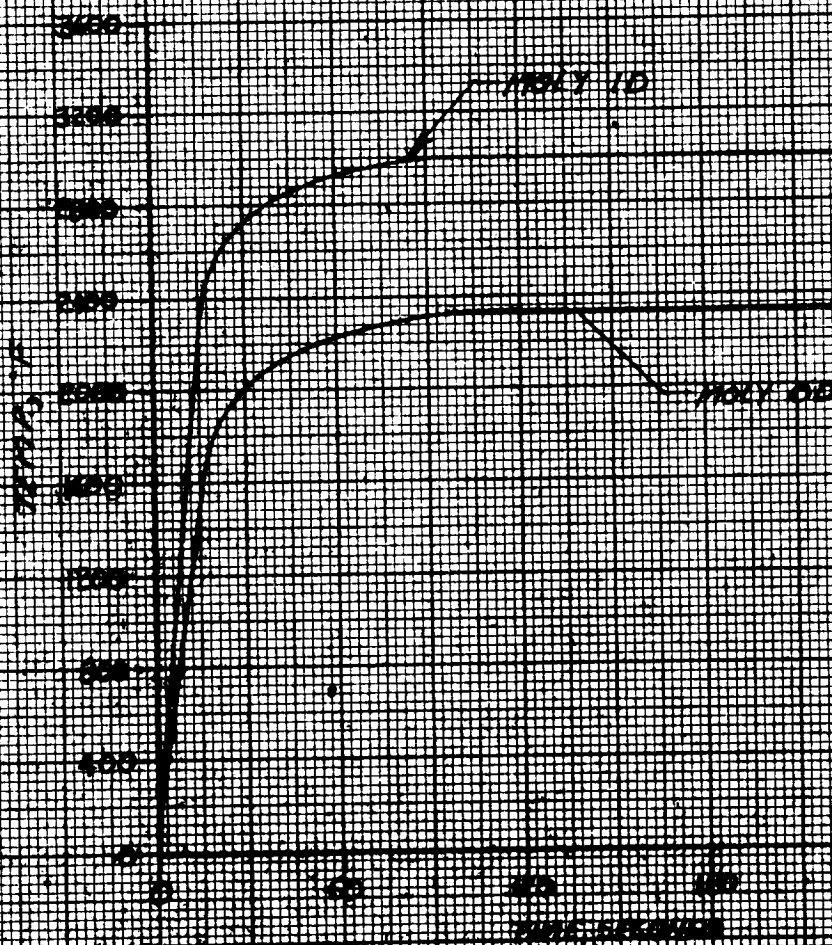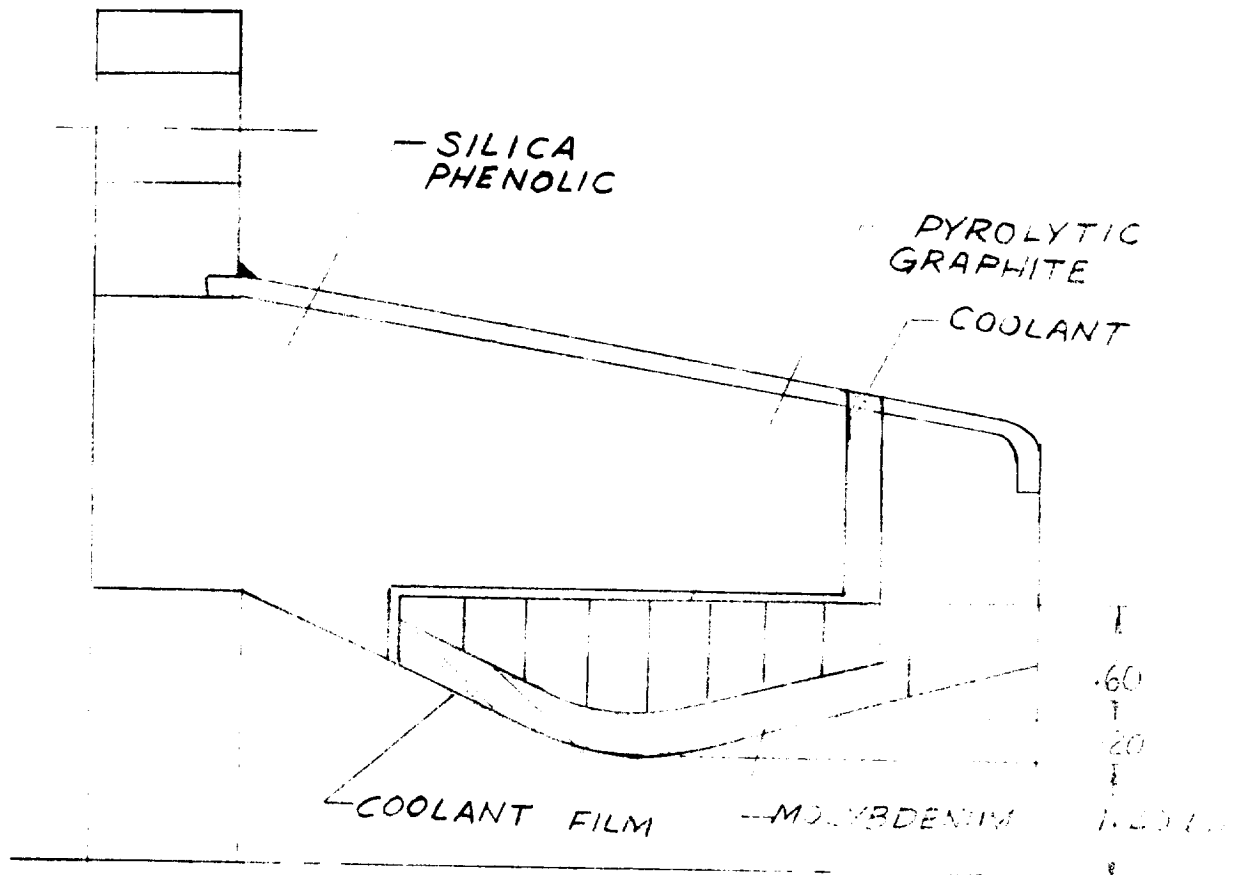
as well be injected with the rest of the fuel in the chamber, so that the reactions would occur where it would give the least decrease in performance. However, by doing this, the problem is not really solved, but circumvented, by altering the mixture ratio of the propellants so as to eliminate the oxidizing atmosphere.

A more realistic approach is required and can be based on previous analysis of chemical reactions and diffusion in compressible boundary layers. Most of this work has been confined to heat transfer where the injected fluid was considered to be a thermal barrier with diffusion effects of secondary importance. However, these analyses will serve as a good starting point, even though it is anticipated that the throat wall temperature will not be the controlling factor in the present case. To date, no concrete analysis has been completed which will allow accurate temperature predictions for the nozzle ID and OD surfaces. Examination of previous analyses, by comparison, would indicate temperature history similarity with regenerative type cooling methods but reduced by 10 to 20 per cent because of the shielding influence of the mass transfer within the boundary layer.

Prestressed Concept

In the prestressed concept, the insert is preloaded by an external metal hoop. The design intent is to restrict the development of tensile stresses in the insert to tolerable levels. Prestressing expands the list of candidate insert materials to include those that are brittle and weak in tension, but are desirable for their other properties. An example may be made of the ceramic oxides which possess a high level of oxidation resistance but are normally rejected as free standing inserts because of their extreme brittleness.

The prestressed concept lends itself to two design categories, both of which are discussed in a previous section. However, the unique qualities of the design concept set it apart from the specific categories. One of these is an insulative or heat-barrier design and the other is a conductive or radiative design.

Heat Barrier Design - Prestressed Insert

The heat barrier design provides an insulation of silica phenolic backing up the prestressing ring and insert as shown in Figure 27. Potential insert materials include zircon, zirconia, beryllium, and JTA graphite.

Figure 28 shows the result of a thermal analyses for ten twenty second pulses followed by a 100 second burst for a zircon insert. A 1410 second cool-down period was observed between each phase. The throat insert surface temperature goes just over 3000°F at the completion of the ten 20 second pulses while the additional 100 second burst causes a surface temperature of approximately 3500°F. Temperatures are well within the service range of zircon.

Table I gives the maximum thermal stress values as calculated at the specified times for the candidate materials. The difference between the imposed thermal stress and the material strength indicates the degree of prestressing to be applied to the insert.

38

PRESTRESSED INSERT

(Heat Barrier Design)

Ceramic

Prestressing Ring

JTA Graphite

0.40

0.25

Green Silica Phenolic
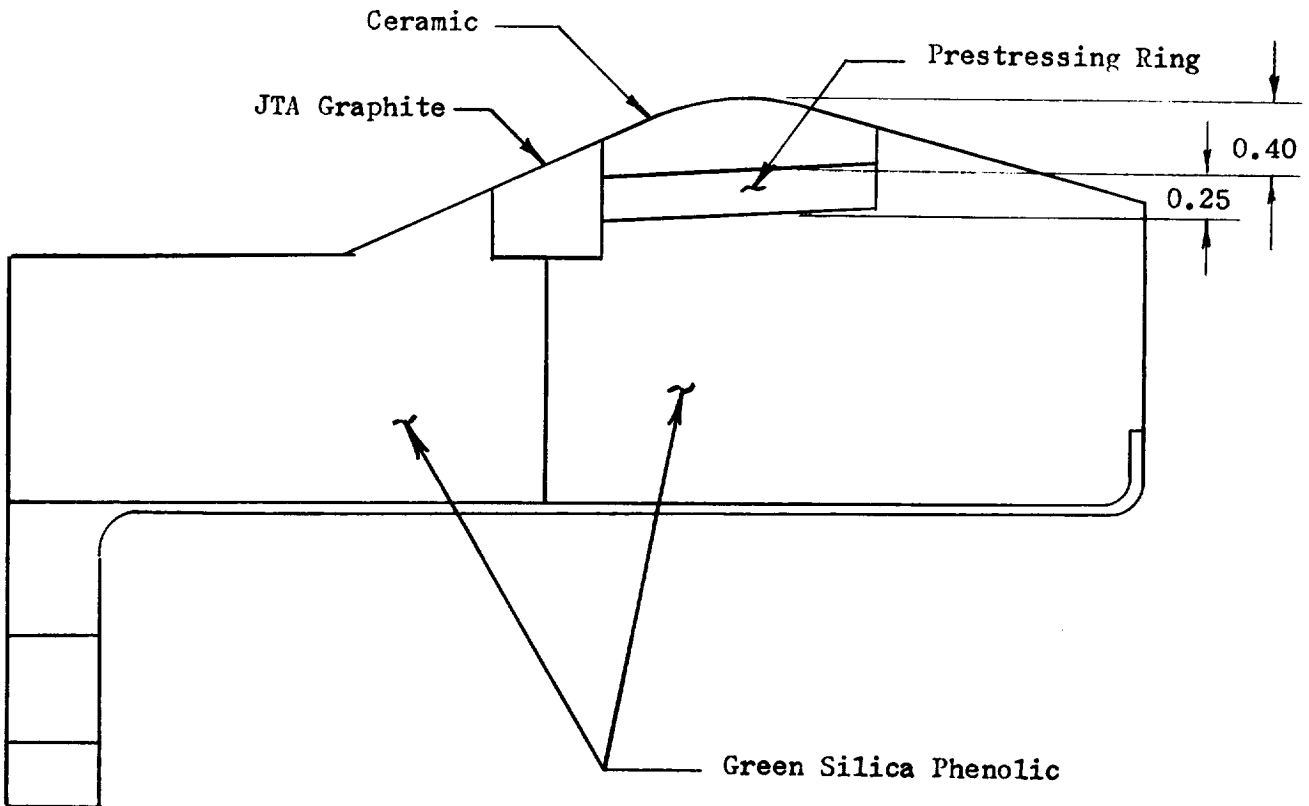
Figure 27

ZIRCON-PHENOLIC—TEMPERATURES AT THROAT (T_a), AT INTERFACES WITH PRESTRESSING RING (T_b AND T_c), AND AT OUTER SURFACE (T_d)

TEMPERATURE, DEG. F

TIME, SEC

NUMBER OF 20 SEC PULSES
(1400 SEC COOL-DOWNS NOT SHOWN)

T_a
T_b
T_c
T_d

40

Figure 28

THERMAL STRESSES IN INSERT WITH INSULATIVE BACKUP (PHENOLIC)
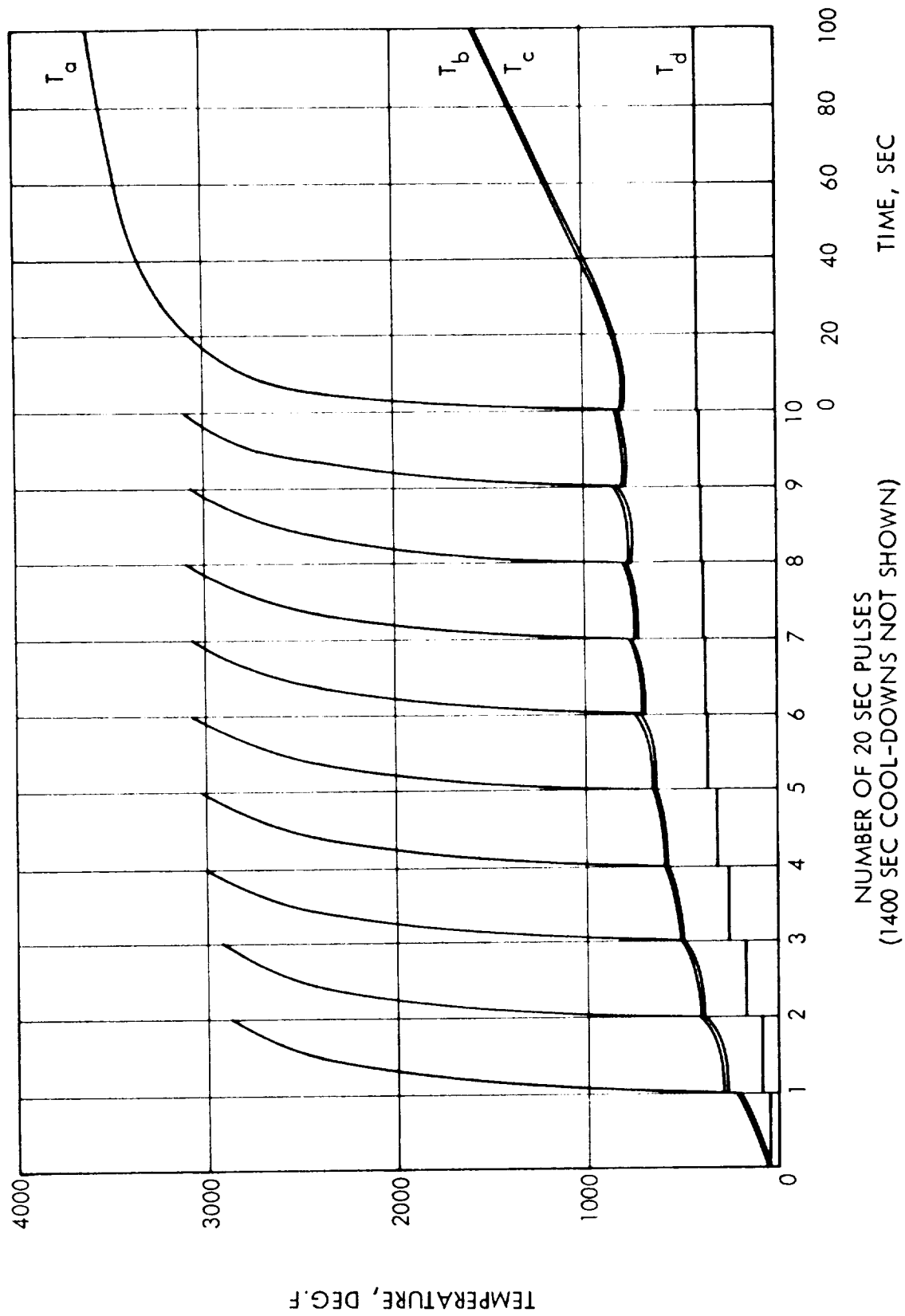
Material	Zircon		Zirconia		Beryllia		JTA Graphite	
Time, Sec.	20	14,300	20	14,300	20	14,300	20	14,300
Conditions at Nozzle Throat Surface								
Temp., F	2822	3619	3053	3631	1078	3080	1309	3195
Hoop Stress, ksi	-261.0	(1)	-307.9	-179.0	-61.3	(1)	-6.0	-4.1
Compr. Strength, ksi	nil	nil	nil	nil	69.0	nil	27.2 (2)	27.2 (2)
Axial Stress, ksi							-2.7	-2.4
Compr. Strength, ksi							34.0 (3)	34.0 (3)
Conditions at Insert Outside Surface								
Temp., F	220	1551	96	1491	784	2479	995	3013
Hoop Stress, ksi	+89.3	(1)	+107.0	+112.6	+25.5	(1)	+2.8	+2.2
Tensile Strength, ksi	11.5	8.9	21.0	16.6	15.2	nil	18.4 (4)	22.9 (4)
Axial Stress, ksi							+1.2	+1.3
Tensile Strength, ksi							8.8 (5)	12.0 (5)
Radial Displacement, mils.	2.8	8.0	4.9	14.0	3.2	15.1	3.2	9.9

1) No value of E at T_{max} (across insert)
2) Room Temperature values, with the grain
3) Room temperature values, across the grain
4) Flexural strength, with the grain
5) Flexural strength, across the grain

TABLE I

41

Radiative Design - Prestressed Insert

Geometry chosen for the preliminary design and analysis is illustrated in Figure 29, which is identical to that for the ablative backup with the exception that pyrolytic graphite is placed behind the prestressing hoop in place of phenolic. By orienting the "a - b" planes of the PG perpendicular to the nozzle axis, the thermal conductivity of the PG backup is made to be almost 100 times that of the phenolic backup.

Potential material candidates for the throat insert include zircon, zirconia, beryllia, JTA graphite, and silicon carbide. The silicon carbide material was used for the preliminary design analysis.

Figure 30 shows the results of the thermal analysis. The duty cycle is the same as used for the heat barrier-prestressed design. The maximum throat surface temperature of approximately 1600°F occurs at the completion of the 100 second burst. This is well below the temperature at which surface oxidation would become appreciable. The extremely low surface temperature results from the high conductivity of both the throat assembly and the pyrolytic graphite.

The thermal stresses are given in Table II for the JTA insert and the silicon carbide insert. The low thermal gradient is the primary cause of the low thermal stresses. These low stress values would indicate that the prestressing concept would be entirely feasible with a silicon carbide throat.

PRESTRESSED INSERT
(Radiative Design)

Ceramic

Prestressing Ring

JTA Graphite

0.40

0.25

Pyrolytic Graphite
(a-b plane radial)

Green Silica Phenolic
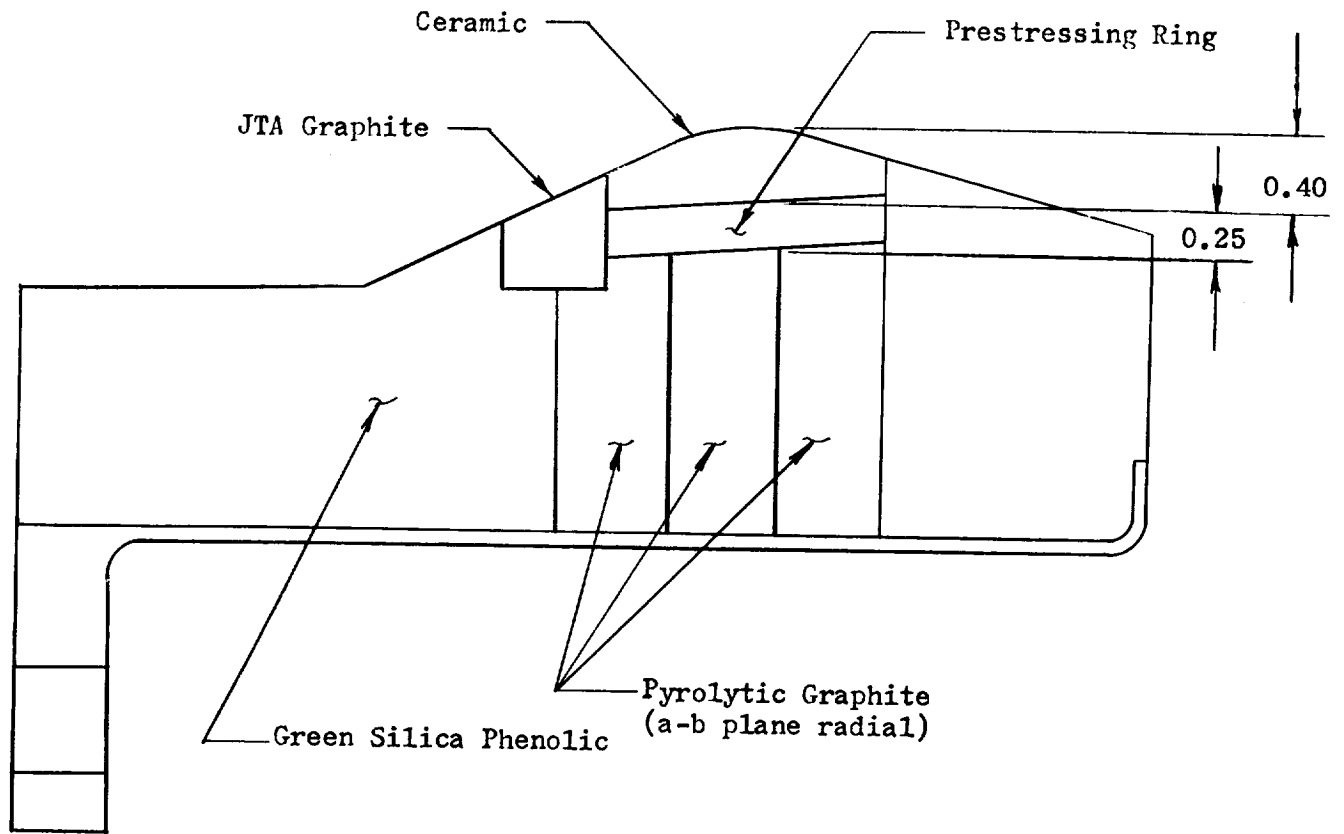
Figure 29

SILICON CARBIDE/PYROLYTIC GRAPHITE—TEMPERATURES AT THROAT(T_a), AT INTERFACES WITH PRESTRESSING RING
(T_b AND T_c), AND AT OUTER SURFACE (T_d)

Figure 30

44
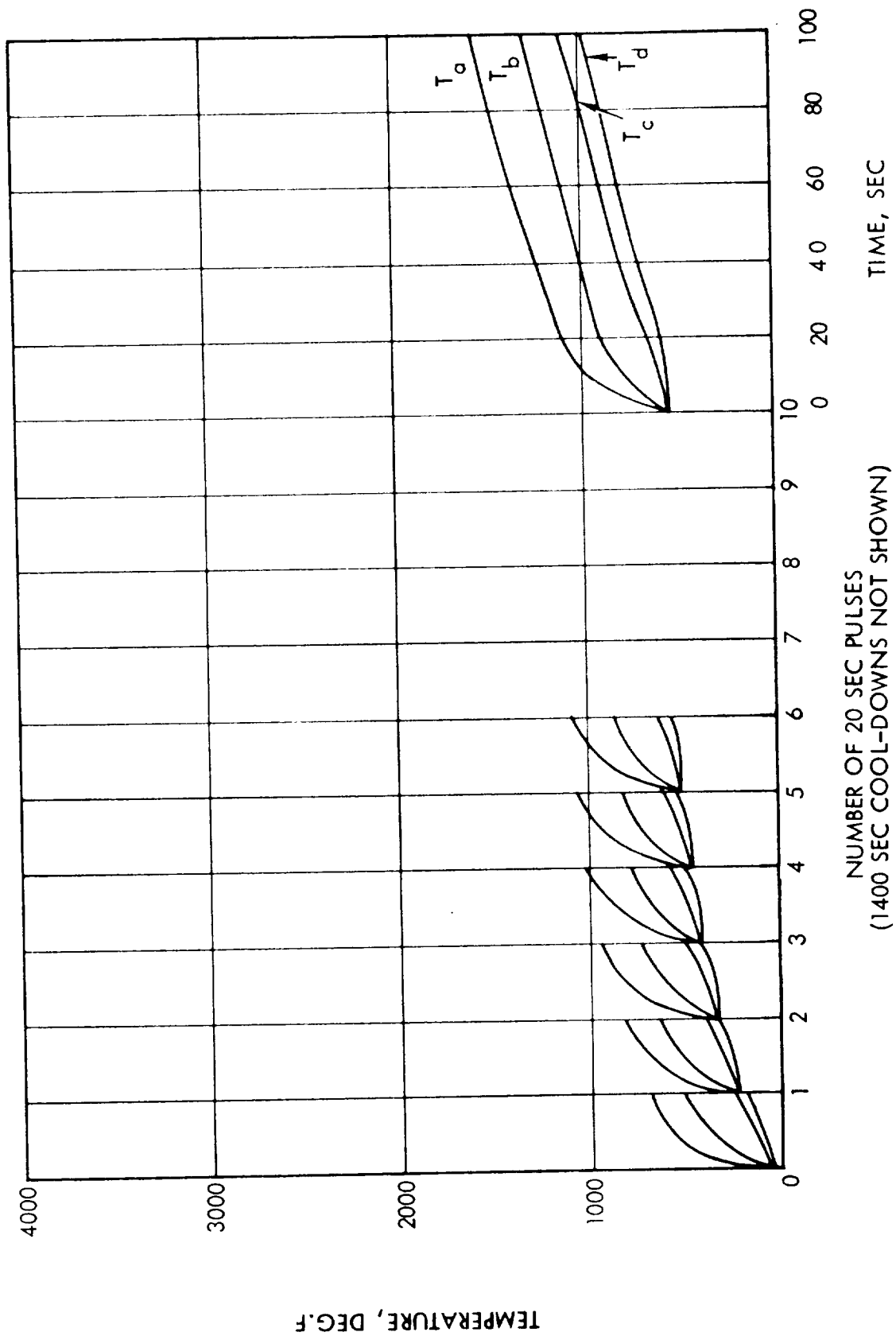
Material	JTA Graphite			Silicon Carbide	
Time, Sec.	20	14,240	14,300	20	14,300
Temp., F	879	1389	1648	700	1592
Hoop Stress, ksi	-6.2	-6.4	-6.3	-21.3	-36.3
Compr. Strength, ksi	27.2 (1)	27.2 (1)	27.2 (1)	150 (3)	150 (3)
Axial Stress, ksi	-2.8	-2.9	-2.9	Same as above	
Compr. Strength, ksi	34.0 (2)	34.0 (2)	34.0 (2)		
Temp., F	507	1004	1284	515	1294
Hoop Stress, ksi	+3.8	+4.5	+4.3	+13.7	+23.4
Tensile Strength, ksi	18.4 (4)	19.0 (4)	19.4 (4)	16-36 (4)	17-35 (4)
Axial Stress, ksi	+1.7	+2.0	+2.0	Same as above	
Tensile Strength, ksi	7.1-10.1 (4)	7.0-10.5 (4)	7.0-11.0 (4)		
Radial Displacement, mils.	3.1	3.4	4.4	1.4	3.9

Conditions at Nozzle Throat Inside Surface

Conditions at Nozzle Throat Outside Surface

1) Room temperature values, with the grain
2) Room temperature values, across the grain
3) Room temperature values
4) Flexural Strength values

TABLE II

THERMAL STRESSES IN INSERT WITH RADIATIVE BACKUP (PYROLYTIC GRAPHITE)

45

2. Environment Definition

In order to define accurately the test environment and, thus the design parameters, TRW provided, at the conclusion of Phase I of Task I, a coated refractory throat unit (similar to SIVB ACE reaction control motor) for testing by NASA Lewis on their evaluation stand. The data provided much insight into temperature and mixing characteristics for subsequent selection of concepts and completion of Phase I and for the final design portion of Phase II.

a. Environmental Test Unit

A throat insert and a portion of the combustion chamber from an SIVB attitude control engine were tested. The throat insert was unalloyed molybdenum coated with TRW's (Si-W) coating, while the portion of the combustion chamber tested was modified silica phenolic. A sketch of the unit is shown on Figure 31. Test firing was performed at an O/F ratio of 2.0 : 1 for a total of 48 seconds. The test firing was terminated at 48 seconds because of a gas leak through one of the monitoring thermocouple wells.

Visual examination of the interior of the combustion chamber, revealed very light charring. The maximum observed char depth was less than 0.400 inch and this maximum occurred near the top face of the throat insert. The average char depth along the combustion chamber was approximately 0.250 inch, while near the top of the Refrasil portion of the combustion chamber where the water cooled section was attached to the chamber, the char depth decreased to less than 0.100 inch. Most of the charring action occurred due to heat soak-back subsequent to the firing.

The throat insert had extensive areas of (Si-W) coating failure and severe deterioration of the molybdenum base metal. Failure of the protective (Si-W) coating allows fairly rapid loss of the molybdenum substrate by oxidation and vaporization of the molybdenum oxides thus formed. A picture of the post fired unit is given in Figure 32.

b. Environment Characteristics

Based on the results of this test, it was concluded that greater emphasis would be placed upon the effects of oxidation in order for acceptable insert performance in the test environment to be realized. The SIVB reaction control motor has been repeatedly steady pulse fired for periods in excess of 250 seconds without throat degradation in an identical propellant system and chamber pressure environment. This seemingly contradictory performance illustrates the necessity of fully recognizing the environment influences as affecting both the design concept and material selection.

The NASA Lewis test apparatus uses a water cooled chamber immediately ahead of the test chamber and extending for a length of about 4 inches upstream from the flange attachment point. The test injector is shown in Figure 33. The propellant supply is regulated to provide constant chamber pressure regardless of flow rate such that throat erosion can be directly associated with temperature and can be directly monitored.

TEST MODULE CONFIGURATION

Green Refrasil Phenolic
(45° Orientation)

Green Refrasil Phenolic
(45° Orientation)

$Zr O_2$ Reaction Barrier
(0.015 thick)

Unalloyed Moly

TRW W-Si-W Oxidation
Barrier

White Silica
(0° Orientation)
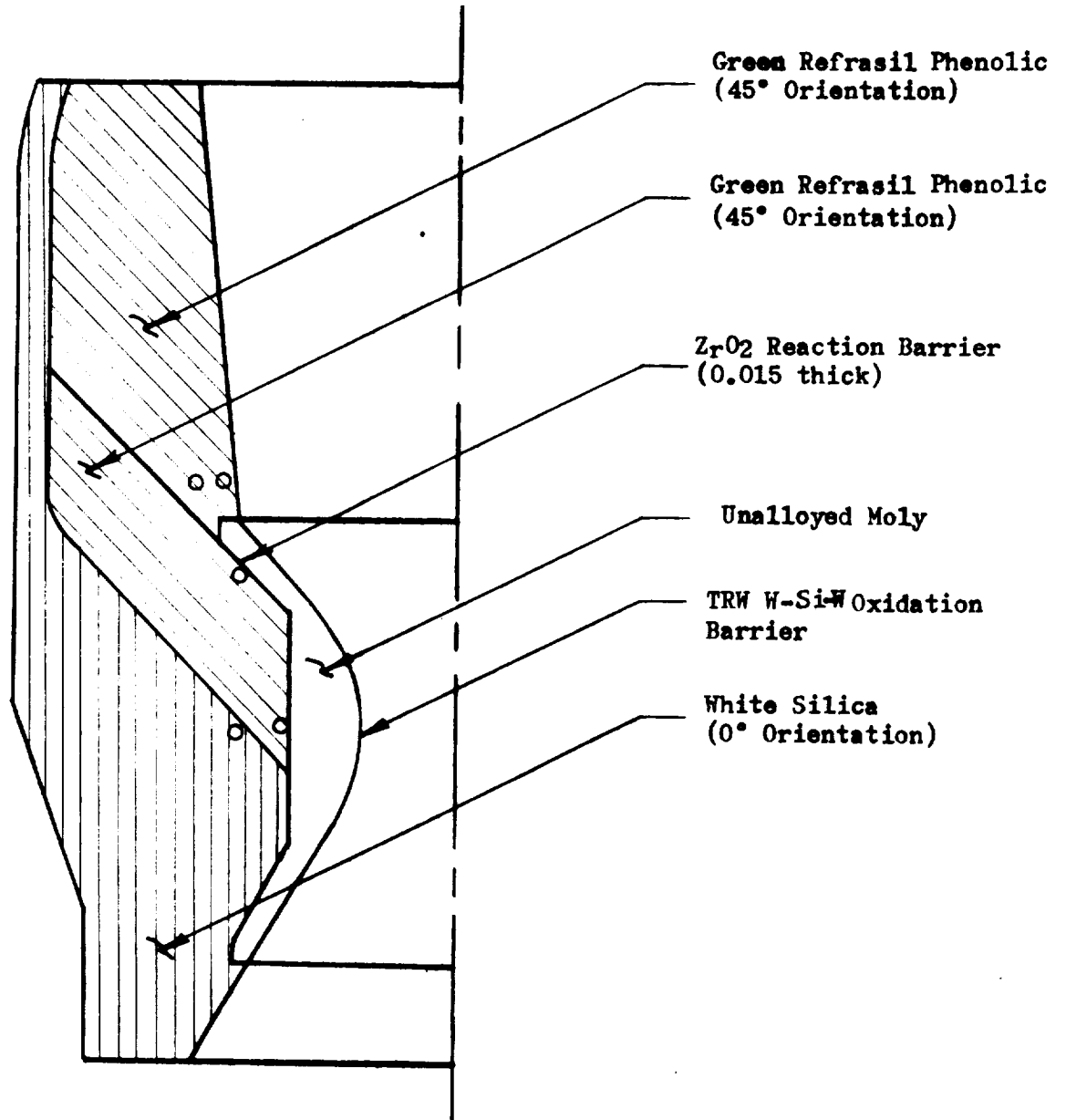
O - Thermocouple Location (7)

Figure 31

47
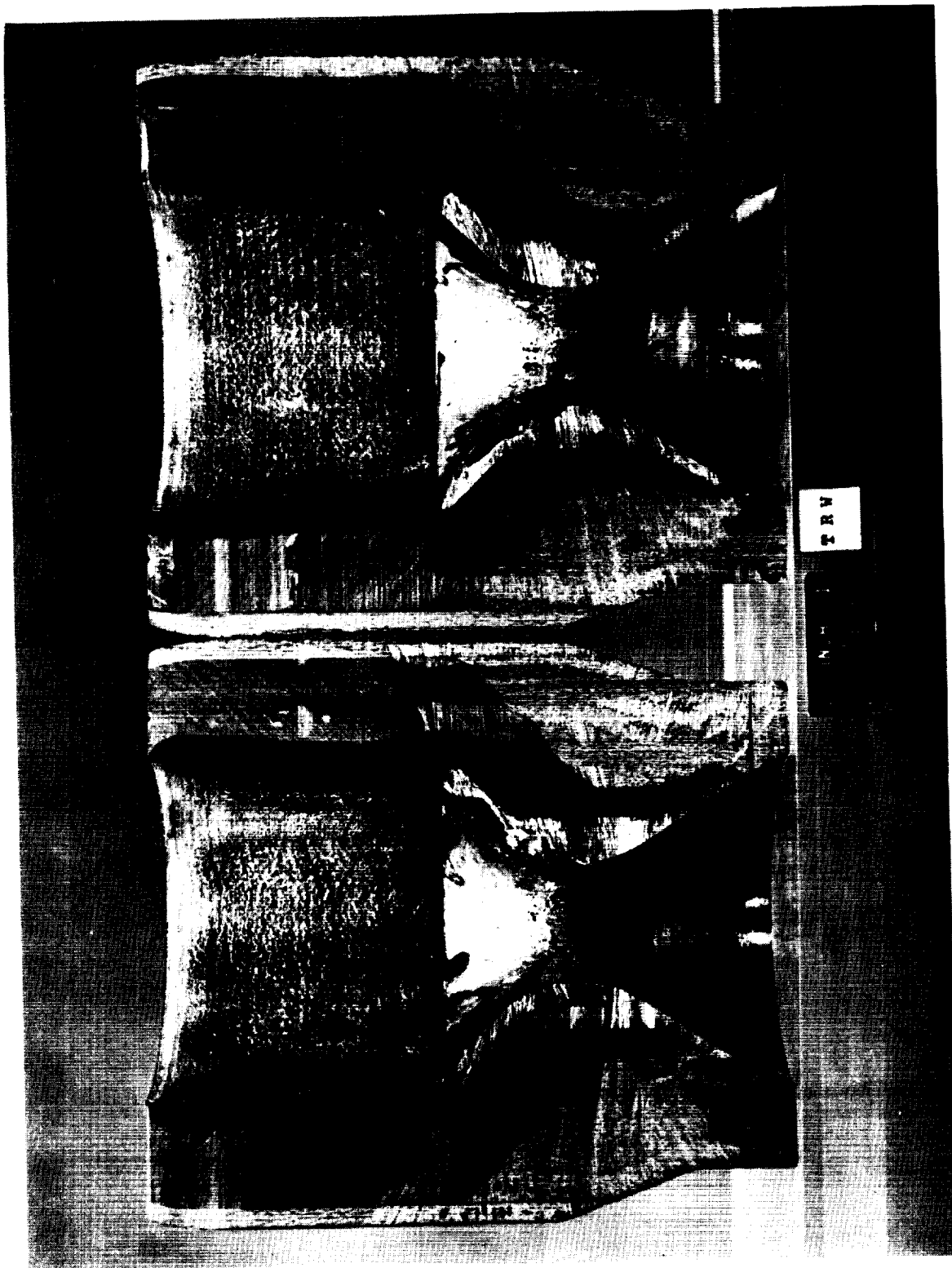
POST FIRED TEST MODULE

Figure 32

48

TEST INJECTOR

Figure 33

c. Reactivity Studies

In order to determine the relative oxidation resistance of candidate materials, a study was made to compare the severity of the oxidizing potential of the two candidate propellant combinations: $H_2 + O_2$, and 50/50 UDMH-Hydrazine + N_2O_4. The purpose of this study was to define the most severe propellant from an oxidation standpoint so that design and heat transfer analyses could concentrate on a single fuel system.

Tests were conducted by self-resistance heating 1/8-inch diameter rods of tungsten and exposing them to various CO/CO_2 and H_2/H_2O gas atmospheres for times between 75 and 120 seconds at gas flow rates of 5 cfh. The CO/CO_2 mixtures were obtained by using bottled gas and controlling the flow rate of the individual components, through a premixing chamber. The H_2/H_2O mixtures were obtained by bubbling H_2-gas through a water bath at 5 cfh before entering the reaction chamber. Both the pressure over the water and the temperature of the water could be controlled so that any ratio of H_2/H_2O could be obtained by adjusting these parameters.

The rate of decrease in specimen weight was used as the primary evaluation parameter. The influence of specimen temperature on the weight loss is shown in Figure 34, while the effects of gas ratio and chamber pressure are presented in Figures 35 and 36. In the case of the data in Figure 35, the relatively low weight loss obtained for the low H_2/H_2O ratios must be considered questionable due to problems in keeping the water vapor from condensing in the transfer system. Because of this problem the actual water vapor content in the chamber may have been less than the actual quantity measured in the generating system.

On the basis of the experimental data, attempts were made to predict the relative oxidizing severity of each of the propellant gases. The influence of temperature and oxidizer content were evaluated for the fuel conditions listed in Table III by using a simple law of mixtures in the multi-component gas systems and assuming: a) the temperature dependence of the gas reactivity is independent of the non-reactant to oxidizer ratio; b) the free oxidizer content increases the reactivity in direct proportion to the quantity present; and c) the material temperature is 1000°F less than the flame temperature. These assumptions along with the test data allowed a relative oxidation parameter (W) to be calculated for the O/F ratios produced by each fuel. The results, summarized in Table IV indicate that the $H_2 + O_2$ fuel produced the largest degree of oxidation primarily because the resulting material temperatures were as much as 500°F higher. If comparable flame temperatures and hence material temperatures were assumed, the relative reactivity of each of the fuels would be similar, with the 50/50 UDMH-Hydrazine + N_2O_4 appearing slightly more oxidizing for the majority of O/F ratios.

3. Preliminary Design

With the conditions of the test environment fully defined, the final phase of Task I was started. In general, it was necessary to upgrade all preliminary design concepts through the use of materials with higher temperature and oxidation resistance. The most applicable materials were primarily limited to the refractory carbides and the ceramics.

50
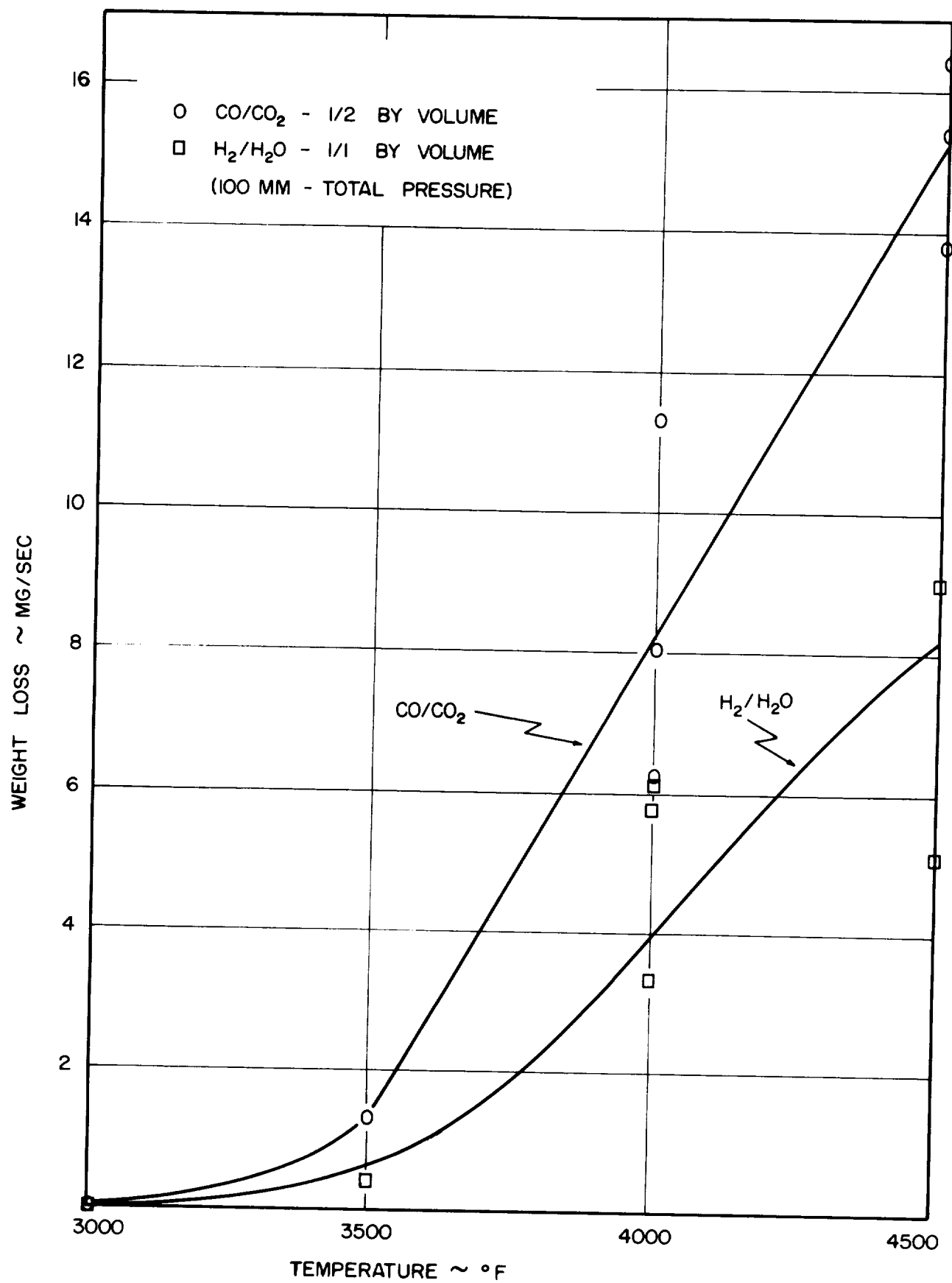
TEMPERATURE DEPENDENCE OF THE REACTIVITY OF VARIOUS
GAS MIXTURES WITH TUNGSTEN.

Figure 34

51
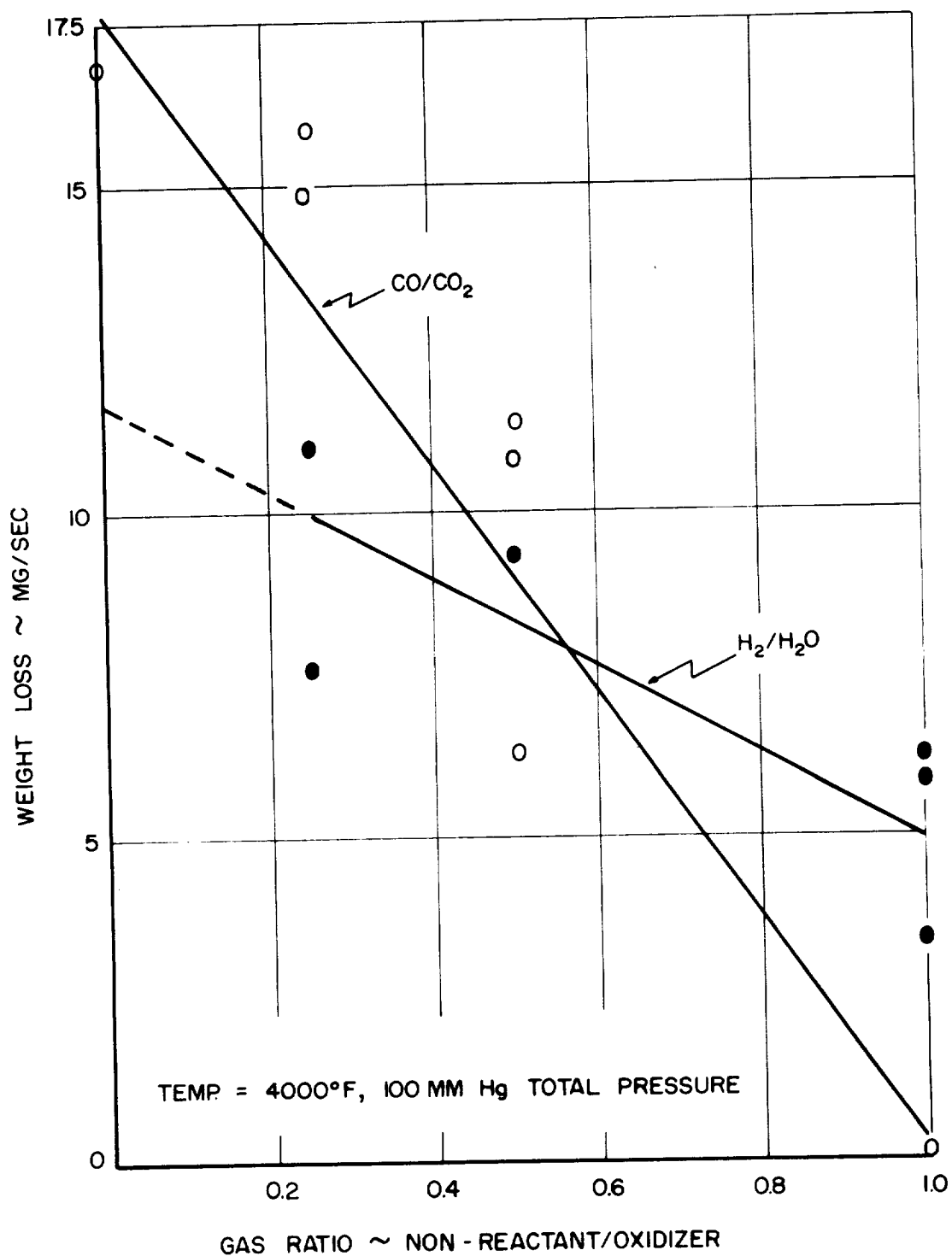
EFFECT OF VARIATION OF GAS MIXTURE ON THE REACTIVITY
OF TUNGSTEN.

52   **Figure 35**
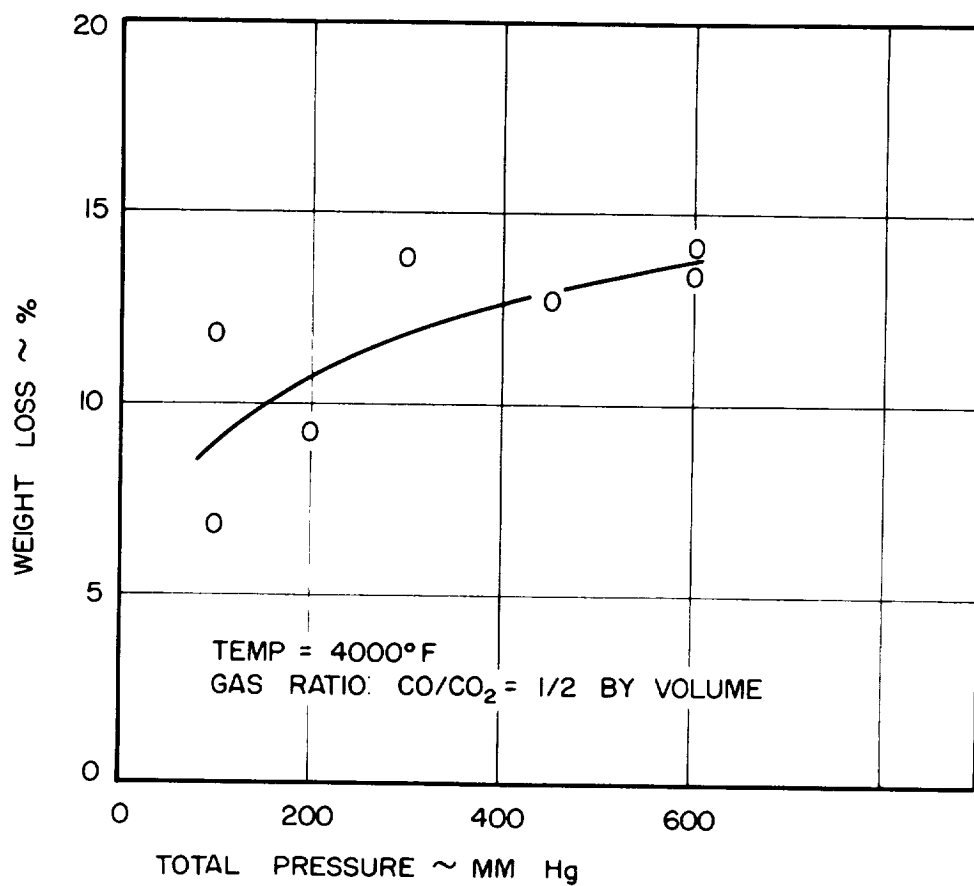
EFFECT OF TOTAL PRESSURE ON THE REACTIVITY OF A
CO/CO$_2$ GAS MIXTURE WITH TUNGSTEN.

Figure 36

TABLE III

COMPOSITION OF EXHAUST GASES FROM TWO LIQUID PROPELLANTS

50/50 - UDMH - Hydrazine - N_2O_4, P_c = 150 psia

O/F	T_c	H_2O	H_2/H_2O ratio	CO_2	CO/CO_2 ratio	N_2
By Wght.	°F	mol. frac.	mol. frac.	mol. frac.	mol. frac.	mol. frac.
2.2	5080	0.490	0.02	0.122	0.05	0.370
2	5090	0.453	0.125	0.103	0.27	0.360
1.8	5070	0.396	0.31	0.098	0.39	0.349
1.5	5030	0.302	0.75	0.098	0.42	0.331

"Propellant Performance and Gas Composition Hdbk," DCAS-TD R-62-2

Liquid H_2 and O_2, P_c = 150 psia

O/F	T_c	H_2O	H_2/H_2O ratio	O_2
By Wght.	°F	mol. frac.	mol. frac.	mol. frac.
4.8	5150	0.555	0.69	0.001
6.4	5520	0.638	0.35	0.011
8.0	5580	0.661	0.20	0.041
12.0	5360	0.628	0.07	0.168
16.0	5050	0.571	0.03	0.295

"Performance of Liquid Hydrogen and Liquid Oxygen as a Rocket Propellant," NASA Memo 5-21-59E.

TABLE IV

RELATIVE OXIDATION RATES FOR LIQUID PROPELLANTS OF VARIOUS O/F RATIOS

CALCULATED FROM LOW PRESSURE REACTIVITY TEST DATA

O/F	FLAME TEMP. °F	CALCULATED ΔW_{CO_2} (mg/sec)	N_{CO_2}	CALCULATED ΔW_{H_2O} (mg/sec)	N_{H_2O}	N_{O_2}	CALCULATED ΔW_{Total} (mg/sec)
Propellant:	50/50 UDMH - Hydrazine + H_2O_4						
2.2	5080	16.6	0.122	11.6	0.490	--	8.6
2	5090	12.8	0.103	10.9	0.453	--	7.1
1.8	5070	10.7	0.098	9.7	0.396	--	5.2
1.5	5030	10.2	0.098	6.7	0.302	--	3.8
Propellant:	Liquid H_2 + O_2						
4.8	5150	--	--	7.1	0.555	0.001	4.7
6.4	5520	--	--	9.4	0.638	0.01	8.2
8.0	5580	--	--	10.4	0.661	0.04	9.7
12.0	5360	--	--	11.3	0.628	0.17	9.2
16.0	5050	--	--	11.55	0.571	0.30	6.9

$$\Delta W_T = (N_{CO_2} \cdot \Delta W_{CO_2} + N_{H_2O} \cdot \Delta W_{H_2O}) \left(\frac{T}{T_0}\right)^3$$

T = Material surface temperature

T_0 = 4000°F, temperature at which W is calculated

N_{CO_2} = Mole fraction CO_2 in exhaust gas

N_{H_2O} = Mole fraction H_2O in exhaust gas

ΔW_{CO_2} = Weight loss due to given ratio of CO/CO_2 at 4000°F

ΔW_{H_2O} = Weight loss due to given ratio of H_2/H_2O at 4000°F

N_{O_2} = Mole fraction O_2 in exhaust gas

A series of 13 suggested designs were submitted based upon advanced concepts and materials. These 13 concepts were:

1. Reinforced zirconia insert backed by PG or reinforced plastic

2. Refractory laminate structure using PG and ZrO_2

3. Graded carbide backed up with PG or reinforced plastics

4. Prestressed carbide backed up with PG

5. Hypereutectic carbide backed up with PG or reinforced plastic

6. Hf-Ta Cladding on Ta backed up with PG or plastic

7. Auxiliary cooled forged tungsten

8. Film cooled carbide

9. PG wedges

10. Refractory foil

11. Filled honeycomb

12. Pre-pyrolyzed coated plastic

13. Metallic heat sink

From these candidates, four designs were selected for further evaluation.

The heat transfer and stress analyses on the preliminary designs were based on a minimum of materials property data. The materials that possessed melting points and oxidation resistance capable of withstanding the test environment were, in general, unproven materials with properties not completely defined. The intent of the initial analysis was to provide a guide post as to the feasibility of a design as based on the minimum available materials properties. The designs submitted did appear feasible; and as discussed in a subsequent section, required considerable development of new materials data. It will also be noted that the duty cycle used for the analyses changed from intermittent pulses to an extended burst of 300 seconds to maintain compatibility with overall program objectives.

a. Refractory Laminate Design

The refractory laminate insert design shown in Figure 37 consists of alternate discs of pyrolytic graphite and a refractory oxide. Two oxides were evaluated; thoria and zirconia. While thoria was recommended because of its higher melting temperature, atmospheric contamination problems dictated the use of zirconia.

Figure 37

57
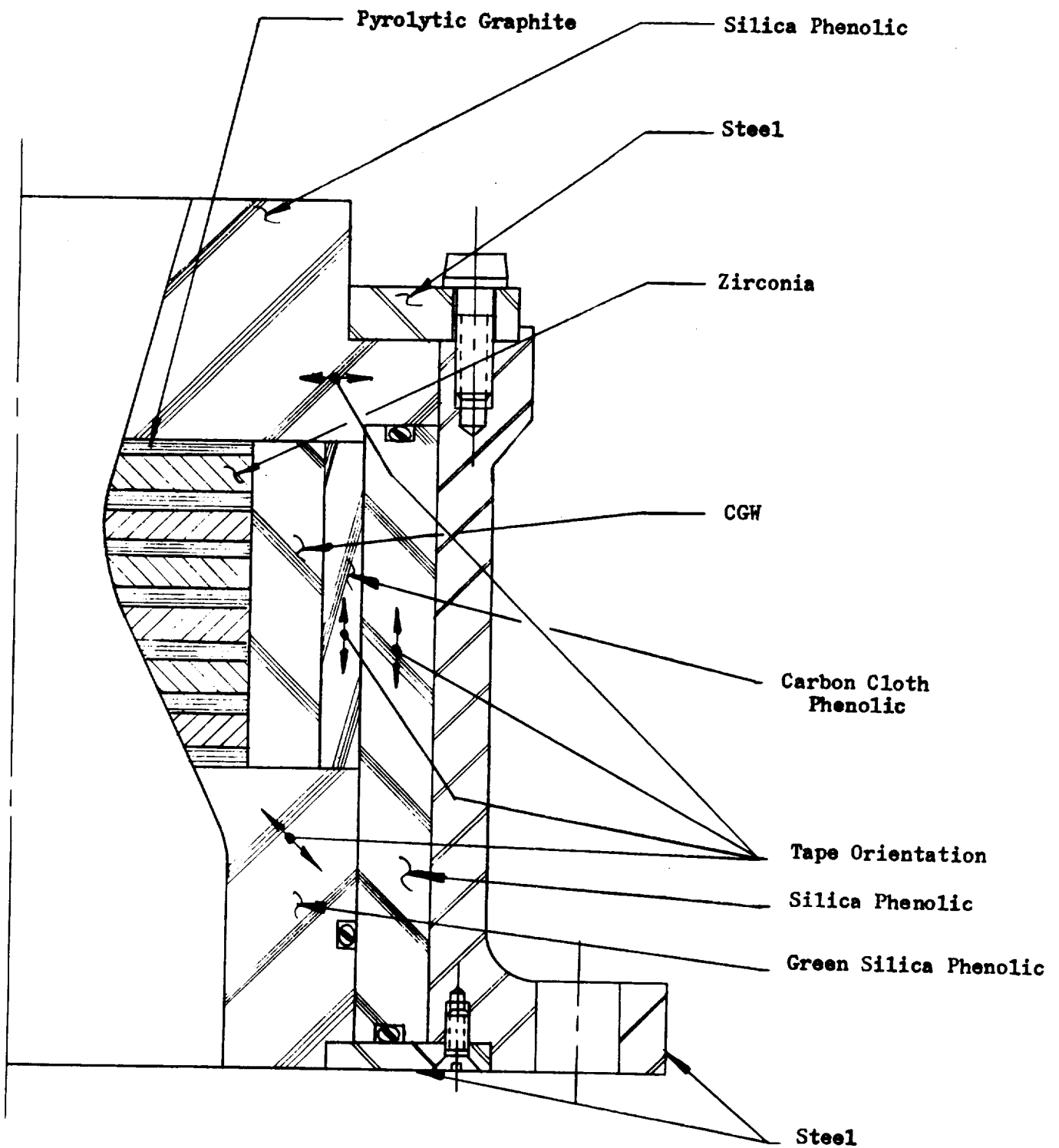
The refractory oxide will maintain dimensional characteristics of the insert under the environment action with the pyrolytic discs acting to provide retention. Cracking tendencies will be reduced by application of an initial compressive load. While it is probable that radial thermal cracking of the oxide discs will occur, the intent of the design is to prevent any movement or loss of the oxide discs by the compressive loads imposed by the pyrolytic graphite.

Figures 38 and 39 are the results of the heat transfer and stress analysis of the refractory laminate design. The data presented is applicable for both thoria and zirconia due to the similarity of properties. The stress level in the steel support structure is conservative. Design values and the computed stresses were made on the basis of a fully elastic material. It is known that the effect of charring of the plastic materials provides room for expansion through crushing of the char layer. This will reduce the steel stress levels markedly. An experienced estimate of the true stress value is one-half of the computed.

b. Reinforced Oxide Design

The reinforced oxide insert design (Figure 40) takes advantage of the high temperature and oxidation resistance of the refractory oxide materials without the accompanying thermal shock cracking problem. Through the use of reinforcing tungsten-rhenium wire, TRW has produced specimens exhibiting a high degree of resistance to thermal shock cracking. The reinforcing wire produces this resistance to thermal shock through a dual effect. It increases the thermal conductivity of the oxide and causes the strength properties to be increased by a significant degree.

The data presented in (Figure 41 and 42) indicate no adverse effects. While the stress imposed on the insert would normally be indicative of a problem area for a pure oxide insert, the increased thermal shock resistance and increased strength allow the reinforced insert to be used.

The data presented stands for both the zirconia and thoria reinforced inserts. The similarity of properties for these materials produced similar results in both the heat transfer and stress analysis. However, TRW recommends use of the thoria insert because of its higher melting temperature.

c. Graded Carbide Design

The carbides show excellent resistance to high temperature and possess good oxidation resistance potential; however, they are highly susceptible to thermal shock. Eutectic mixtures of carbides and graphite have less susceptibility to thermal shock but also show much greater oxidation because of the free graphite inclusion.

The graded (layered) carbide material combines the desirable properties of both types of materials (Figure 43). The first layer is pure carbide, chosen as either hafnium carbide or tantalum carbide for this application, and has excellent oxidation resistance at high temperatures. It is made 0.1 inch thick to diminish thermal shock susceptibility as much as possible. The remaining three layers contain increasing amounts of graphite in the radial direction. The carbide-graphite mixtures provide the following advantages:

REFRACTORY LAMINATE OXIDE AND PYROLYTIC WASHERS

Figure 38

59
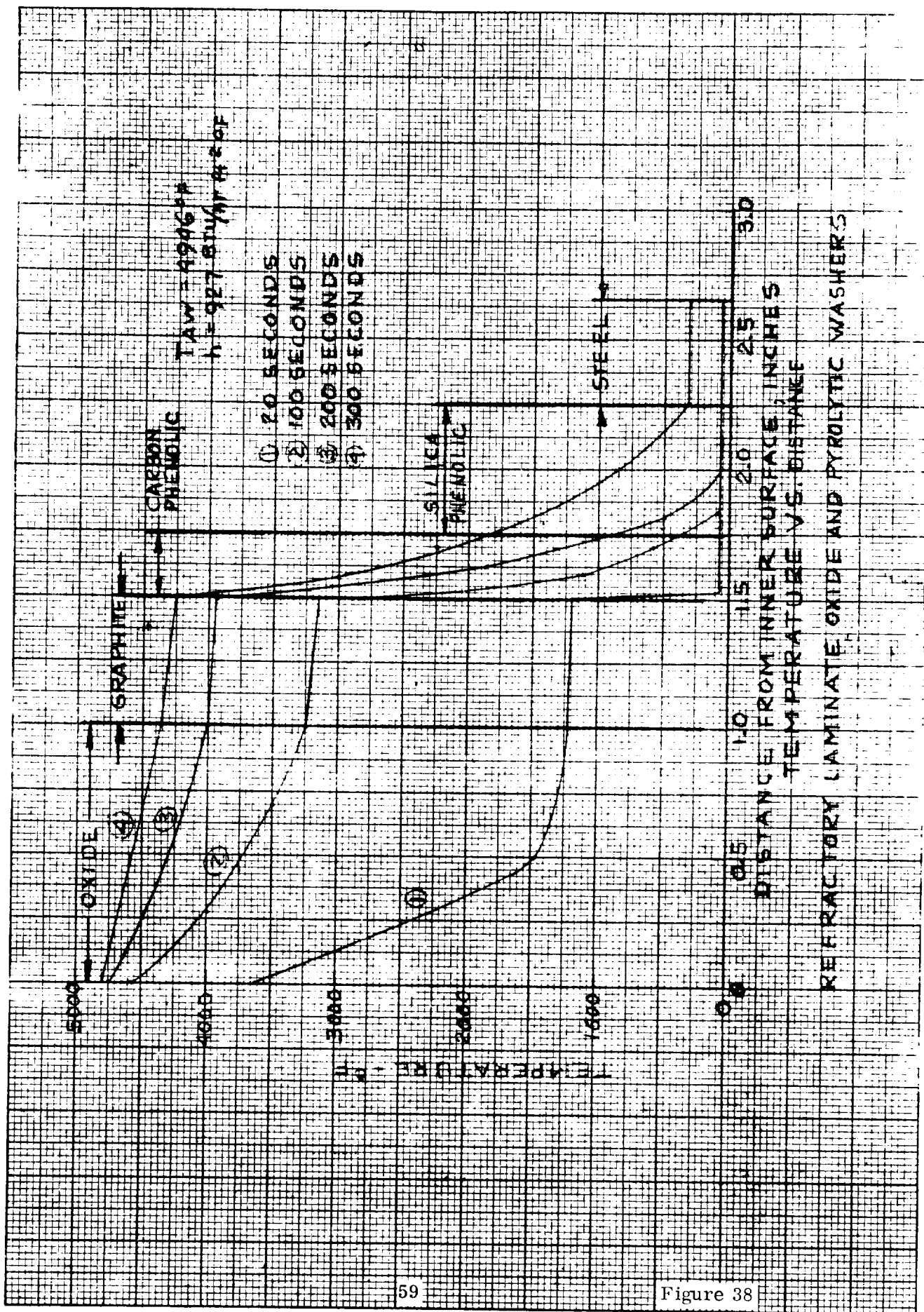
REFRACTORY LAMINATE
Stress Vs. Time

Axial Stress External Surface Oxide

Axial Stress Internal Surface Oxide

Hoop Stress External Surface Oxide

Hoop Stress Internal Surface Oxide

Stress - PSI (Compressive)

Time - Seconds

60

Figure 39

Tape Orientation

Steel

Reinforced Oxide

Silica Phenolic

Carbon Phenolic

CGW Graphite

Tape Orientation

Green Silica
Phenolic

Steel

Figure 40

Figure 41

62

REINFORCED OXIDE
Stress Vs Time

Axial Stress
External Surface
Oxide

Hoop Stress
External Surface
Oxide

Axial Stress
External Surface
Oxide

Hoop Stress
External Surface
Oxide

Stress (Psi)

Tension

Compression

Time, Seconds

63

Figure 42

H_fC

TaC + 10% G

TaC + 40% G

TaC + 70% G

Silica Phenolic

Steel

Tape Orientation

Silica Phenolic

Carbon Phenolic

Tape Orientation

Green Silica
Phenolic

Steel

Figure 43

1. The mixtures with greater amounts of graphite are less susceptible to thermal shock, allowing for a better resistance to thermal tensile stresses

2. The thermal expansion coefficient in the radial and axial directions remain the same or increase slightly in successive layers, allowing for uniform expansion and reduced stresses in the several layers.

Figures 44 and 45 show heat transfer and stress analyses made for this design.

Based on available data, the computed stress levels appear acceptable. Failure of the material was anticipated to result from failure to match precisely coefficients of expansion of the various layers.

d. Prestressed Design

Tantalum carbide was chosen for the insert (Figure 46), because of its high melting point, relative oxidation resistance and high thermal conductivity. The latter not only acts to reduce the throat surface temperature, but also to minimize ΔT across the insert. Hafnium carbide was ruled out because of its lower conductivity. Zirconium carbide was a close competitor. Oxide materials could not be used because of the extremely high pre-stress required. Thermal analyses showed negligible differences between ZrC and TaC. If the ZrO scale that presumable will form during firing adheres to the throat surface, ZrC would be a very desirable insert material. The thickness (0.200 inches) was made as small as could be fabricated readily. Temperature profiles are shown in Figure 47.

Major emphasis was placed on the selection of material and the thickness of the insulating annulus. Thickness had to be at least 0.20 inches, to fill the concave side of the insert. Carbon was selected to provide the conductivity required for the insert backup. Other characteristics required were low thermal expansion and low elastic modulus, so the thickness of the annulus was treated as a split, or segmented, ring with no hoop stresses acting.

Carbon, 0.25 inches thick, was chosen for the annulus after several trials, the results of which are given in Table V in terms of the design requirements. Results for carbon and pyrolytic graphite were compared on the basis of the ratio of thickness to conductivity, "t/k".

The recommended configuration, .25 inches carbon, is shown in the second column. Some worthwhile comparisons can be drawn between that case and the others. The throat temperature at 300 seconds could be reduced 300°F (from 3980°F to 3680°F) if t/k for the annulus were reduced to zero. The throat temperature would rise more than 450°F (to 4430°F or above) if t/k were made very large.

The maximum compressive stress at the throat of the insert is barely affected by t/k for the annulus. Apparently, this is because the maximum occurs so early in the firing (about one second) that the backup materials have little effect on the thermal gradient in the insert.

Tension at the back of the insert does increase sharply for t/k values less than that for the .25 inch carbon annulus, but it does not decrease much for greater t/k values. Pre-stressing effects were computed only for the .25 inch

Figure 44

GRADED CARBIDE
Stress Vs Time
(Hafnium Carbide Layer)
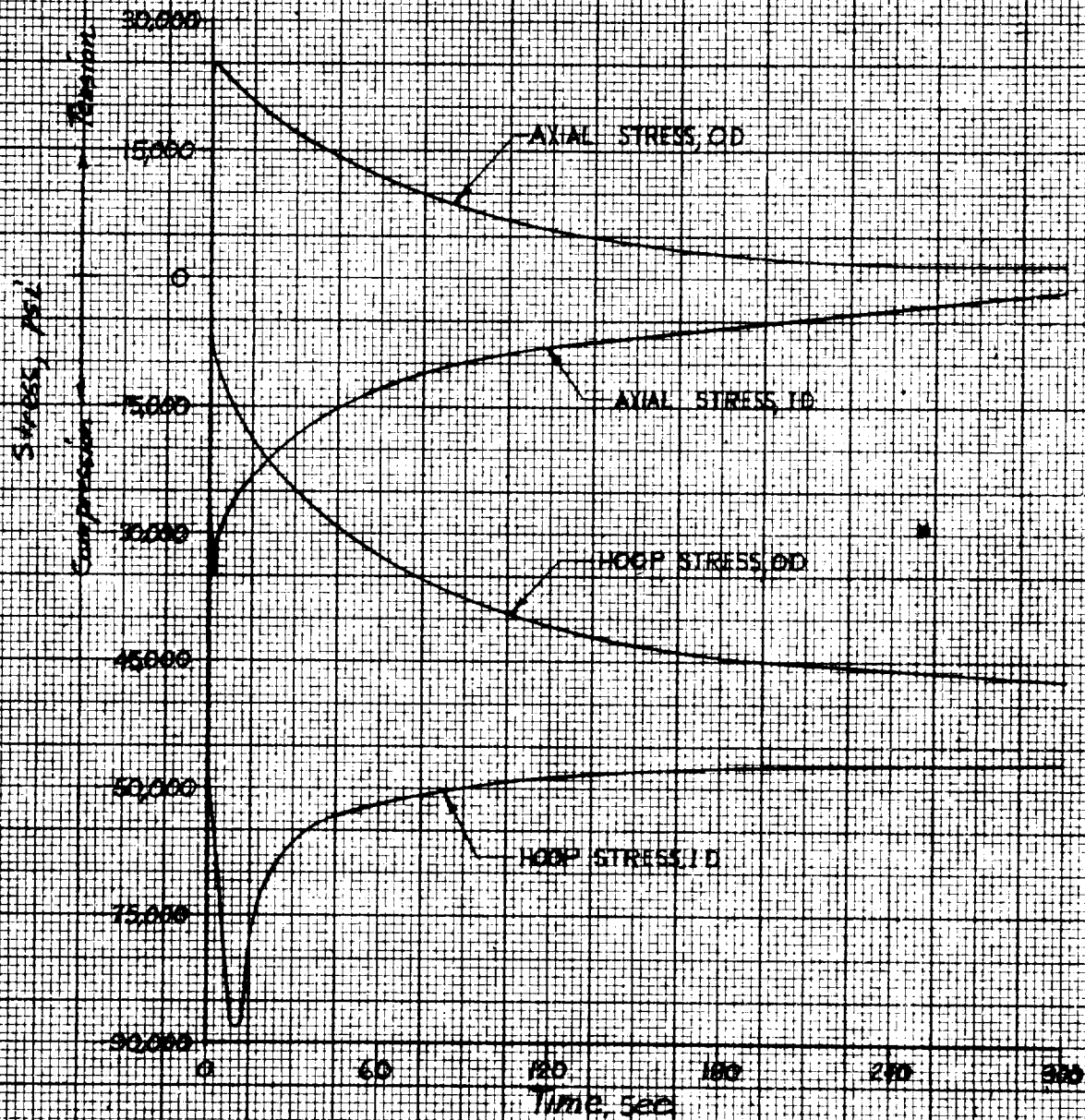
AXIAL STRESS OD

AXIAL STRESS ID

HOOP STRESS OD

HOOP STRESS ID

Figure 45

PRESTRESSED DESIGN

TaC

Carbon Brick

FS-85

Steel

Silica Phenolic

Tape Orientation

Pyrolytic Graphite

JTA Graphite

Silica Phenolic

Tape Orientation

Green Silica
Phenolic

Steel

Figure 46

RADIAL TEMPERATURE DISTRIBUTIONS AT VARIOUS TIMES

Figure 47
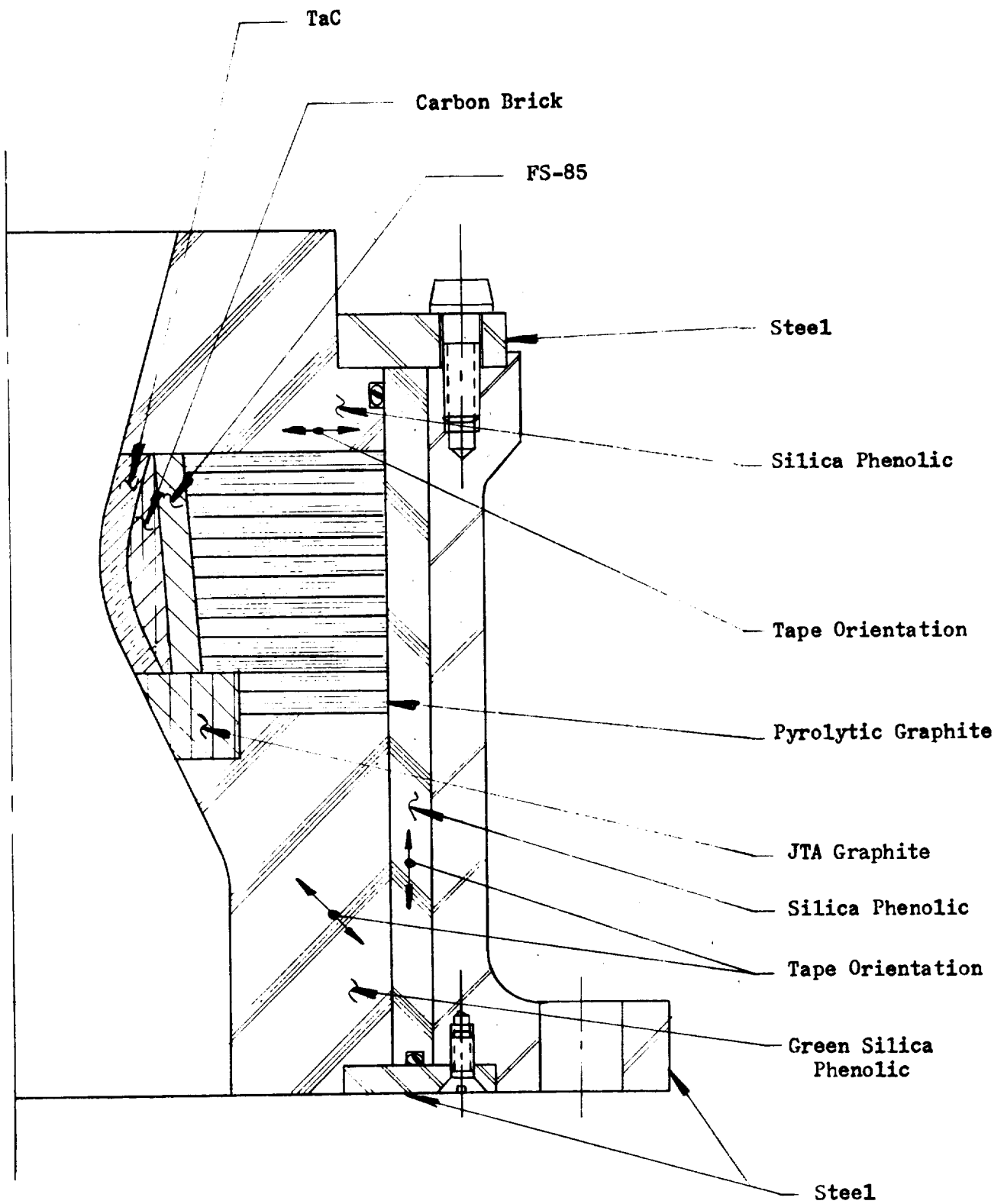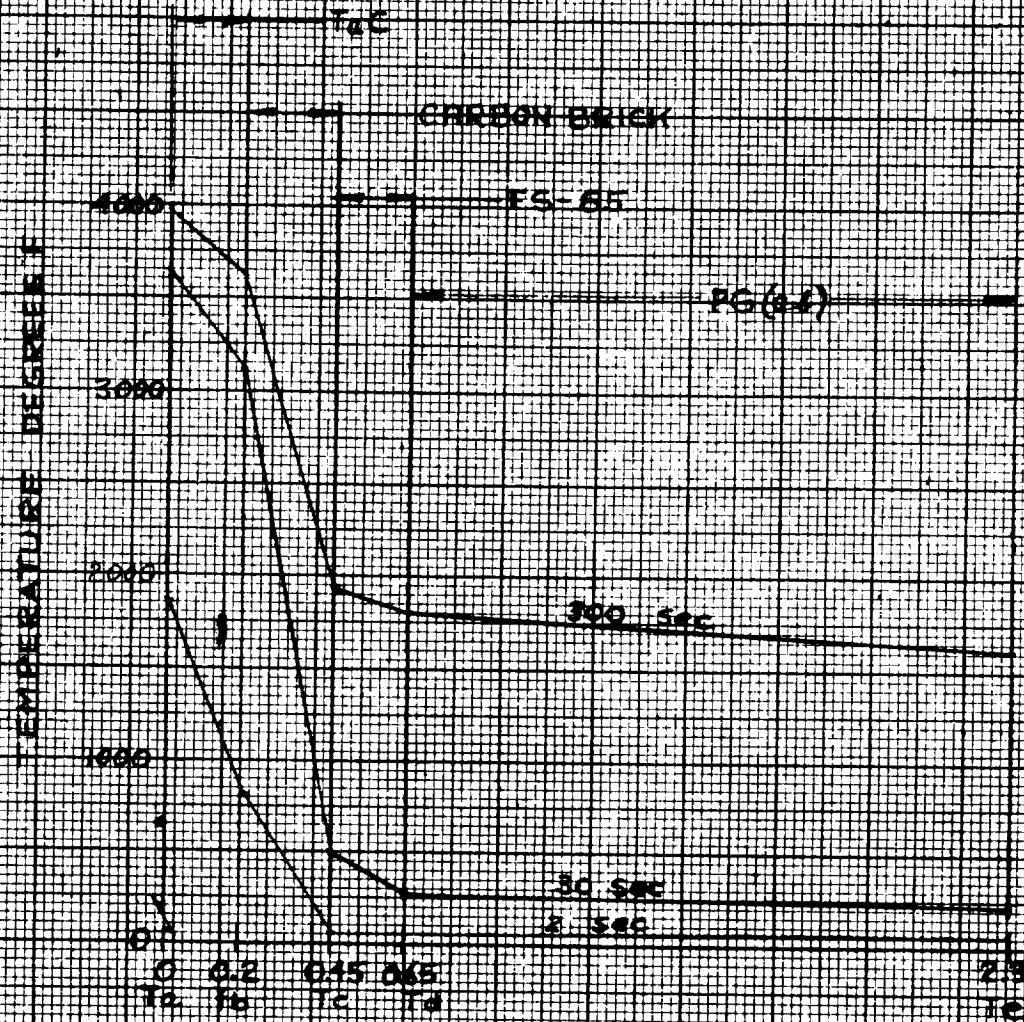
TABLE V

EFFECTS OF THICKNESS AND CONDUCTIVITY OF THE ANNULUS
ON CRITICAL STRESSES AND TEMPERATURES IN THE INSERT

Note: Insert is TaC, Prestressing Ring is FS-85, and Heat Sink is PG (a-b planes radial).

	Material		Carbon	Carbon	Pyrolytic Graphite
	Thickness, In.	0	.25	.50	.25
	t/k	0	.08	.17	.30
Throat Surface Temperature, deg. F	20 sec.	2530	3480	3550	3870
	100 sec.	3130	3810	4020	4380
	300 sec.	3680	3980	4140	4430
Compressive Stress at Throat Surface Thermal Only	Stress, ksi	162	158	162	156
	Time, sec.	.8	.6	.8	.8
Tensile Stress at Back Side of Insert, Thermal Only	Stress, ksi	112	70	62	63
	Time, sec.	5.0	3.0	2.0	2.0
Tensile Stress at Back Side of Insert, Thermal Plus Interference, ksi			39		
Maximum Interference	Mils	3.4	9.00	9.50	16.9
	Time, sec.	10	30	50	100
Temperature of Prestressing Ring at 300 seconds, deg. F			3170	1940	1500	830

carbon annulus, because the other cases had failed some other requirement. Temperature of the pre-stressing ring was tolerable from the strength standpoint except at the lowest value of t/k.

4. Materials evaluation

Knowledge of selected mechanical and physical properties of candidate materials is essential for the proper design of nozzle throat inserts for use at very high operating temperatures. Often the necessary properties are available from various sources, including published reports and company data sheets. However, some of the most promising candidate materials are relatively unexplored and some means must be provided to obtain the necessary properties. Some of the necessary properties can be estimated from known data on similar materials, but experimental measurements are required for other necessary properties to provide a more secure basis for design.

In order to provide the engineering data required for the candidate materials, the materials evaluation portion of Task I was divided into three phases. They were:

1) A literature and vendor survey to determine the availability and characteristics of candidate materials.

2) A screening program to select those materials with a high probability of successful performance under the test environment conditions.

3) The generation of physical and mechanical property data, where required, to permit a definitive design analysis.

The nature of the phases was such that they were conducted in a sequential order.

a. Literature and Vendor Survey

The survey was conducted to determine the availability and properties of materials that may have application as throat inserts. Relative material selection criteria were adopted to enable suitable choices based on grades of materials and possible duty cycles. The criteria are summarized as shown:

Property	Criterion	Possible Design Application
Melting Point	> 3000°F	Cooled Nozzle
Melting Point	> 3500°F	Pulsed duty cycle – No Cooling
Melting Point	> 4000°F	Continuous Firing – No Cooling
Oxidation Resistance	Greater than JTA Graphite as a starting baseline	All duty cycles

71

Property	Criterion	Possible Design Application
Thermal Shock Resistance	Superior to 80% dense porous tungsten (R* 30,000 BTU/ft-hr.	All duty cycles

*Where $R = K\ \sigma/E\ \alpha$ where

K = thermal conductivity, BTU-ft/ft^2- hr-°F

σ = flexural strength, psi

E = elastic modulus, psi

α = coefficient of thermal expansion, in/in/°F

A summary of the survey is given in Table VI. The properties of candidate materials are presented for the following classes; carbides, oxides, intermetallics and metalloids, and composites. Based on the results of the survey, the materials listed in Table VII were scheduled for screening tests.

b. Screening Tests

In order to perform satisfactorily, throat insert materials for ablative thrust chambers must be capable of surviving under conditions which involve thermal shock, high temperatures, and corrosive environments. Laboratory screening tests have been employed to aid in the selection from the candidate materials. These tests represent meaningful criteria since a significant degree of correlation has been established from past programs between actual firing behavior and laboratory test results.

Thermal shock, or the ability of a material to withstand a high thermal gradient over a short period of time, has never been adequately defined as related to a material physical property. In order to arrive at some preliminary relationship between a laboratory test and service use, TRW devised a thermal shock screening test.

For the thermal shock tests, heated 1 1/2 inch diameter by 1/4 inch thick discs were quenched into ice-brine, and the maximum temperature differences which could be sustained without cracking was used as a measure of thermal shock resistance. The apparatus is shown in Figure 48. Heating was accomplished in an inert atmosphere, and the specimens insulated so that cooling occurred only in a radial direction. Extensive tests conducted under these conditions have indicated that any material which failed due to thermal-shock with a temperature difference equal to or below 1900°F experienced severe thermal-shock cracking when used in liquid nozzle inserts fired under conditions comparable to those

72

PROPERTIES AND APPLICABILITY OF SELECTED CARBIDES (Room Temperature)

CARBIDE	MELTING POINT (°F)	ELASTIC MODULUS (10^6 psi)	BEND STRENGTH (10^3 psi)	LINEAR COEFFICIENT OF EXPANSION (10^{-6} in/in/°F)	THERMAL CONDUCTIVITY (BTU-ft/ft²-hr-°F)	THERMAL SHOCK RESISTANCE (R=$K\sigma$/Eα)	CONCLUSION
TaC	7010	41-76	40	3.6-3.7	13	2460	Fair oxidation resistance; not considered usable due to thermal shock sensitivity.
HfC	7030	51	--	2.4-3.6	4-8	--	Better oxidation resistance than TaC, comparable to that of W; not considered usable due to thermal shock sensitivity.
ZrC	5490-6460	59	20-50	3.7-4.2	20-25	3350	Not usable; thermal shock and oxidation.
SiC	3720-5707	40-70	14-39	2.9-3.3	35-100	10500	Best oxidation resistance below 3000°F; moderate thermal shock problem; limited by melting point of SiO2 which forms in an oxidizing environment.
B₄C	4440	42-65	50	2.6-3.9	18	5180	Not usable; thermal shock and oxidation.
TiC	5480-5880	45-60	75-175	4.1-5.1	13.2	7050	Not usable; thermal shock and oxidation.
CbC	6330	49	--	3.5	18	--	Marginal oxidation resistance; not usable due to thermal shock and oxidation susceptibility.

73

TABLE VI

PROPERTIES AND APPLICABILITY OF SELECTED OXIDES (Room Temperature)

OXIDE	MELTING POINT(°F)	ELASTIC MODULUS (10^6psi)	BEND STRENGTH (10^3psi)	LINEAR COEFFICIENT OF EXPANSION (10^{-6}in/in/°F)	THERMAL CONDUCTIVITY (BTU-ft/ft^2-hr-°F)	THERMAL SHOCK RESISTANCE (R= $K\sigma/E\alpha$)	CONCLUSION
BeO	4620	50-59	16-40	4.4-5.7	105-160	12000	All oxides limited by thermal shock. Possibly usable in prestressed nozzle insulative design.
MgO	5072	23	47	6.5-8	26	7300	"
ZrO$_2$(Stab.)	4710	21-26	20-26	4.4-6.6	12.8	2280	"
ThO$_2$	5970	35	10-15	4.5-5.5	8.5	1060	"
Zircon	4240-4620	32	10-30	2-5	2.5-5	332	"

74

TABLE VI Cont.

PROPERTIES AND APPLICABILITY OF SELECTED INTERMETALLICS AND METALLOIDS (Room Temperature)

MATERIAL	MELTING POINT (°F)	ELASTIC MODULUS (10^6 psi)	BEND STRENGTH (10^3 psi)	LINEAR COEFFICIENT OF EXPANSION (10^{-6} in/in°F)	THERMAL CONDUCTIVITY (BTU-ft/ft²-hr-°F)	THERMAL SHOCK RESISTANCE (R=Kσ/Eα)	CONCLUSION
TiB$_2$	5320	55-77	24-45	2.9-4.8	14	1930	Not usable; oxidation and thermal shock.
ZrB$_2$	5500	50	20-60	3.0-4.2	25	5950	Not usable; oxidation and thermal shock.
TaB$_2$	5610	37	--	2.8-3.2	10	--	Not usable; oxidation and thermal shock.
BN	4950	15	18	4.2	18	10300	Not usable; oxidation and marginal thermal shock.
TiN	5340	36	34	3.7-5.2	3-6	2750	Not usable; oxidation and thermal shock.
Ta$_2$Be$_{17}$	3610	45-55	30	7.5	15	1250	Not usable; oxidation and thermal shock.
ZrB$_2$-MoSi2	4000	65-72	--	3.3-5	18-22	--	Not usable; limited by melting point of SiO$_2$.

75

TABLE VI Cont.

PROPERTIES AND APPLICABILITY OF SELECTED COMPOSITE MATERIALS

COMPOSITE	NOMINAL COMPOSITIONS	MAXIMUM USE TEMPERATURE	THERMAL SHOCK RESISTANCE	OXIDATION RESISTANCE	CONCLUSION
Pyrolytic Graphite	Highly oriented Graphite	6600°F	Fair	Moderate	Recommended without evaluation for cooled structure design.
JT-0981	48-C, 35Zr, 17-Si	4000°F	Fair	Good	An improved JTA type graphite composite.
JT-0992	33-C, 12-Si, 55 Hf	----	----	----	An improved JTA type graphite composite.
MAP's Moldable X-4110-3	(90 SiC-10 Zrc) Coating on Graphite particles with organic binder.	----	----	----	Same category as JTA graphite composite.
Graded Carbide	CbC + Graphite TaC + Graphite	----	Marginal	Marginal	Expect improved thermal shock resistance over pure carbides.
Coated Molybdenum	Proprietary Coating on Mo	3500°F	Excellent	Excellent	Recommended without screening for insulative design.
Zirconia + Tungsten Screening	Phosphate-bonded Zirconia with 5 v/o Tungsten Screening	3000°F	Excellent	Fair	Not usable; temperature and oxidation limitation.
Titanium Boronitride	Mixture of TiN, TiB_2 and BN	4500°F	Marginal	Poor	Not usable; oxidation and thermal shock.
Phenolic Infiltrated ZrO_2 Foam	Phenolic Infiltrated ZrO_2 Foam	----	Marginal	Marginal	Not usable; foams presently available are not good enough to withstand induced stresses.

76

TABLE VI Cont.

TABLE VII

CANDIDATE MATERIALS SCHEDULED FOR SCREENING TESTS

Material	Supplier
Graded Carbide	Carborundum
X4110-3	Magnesium Aerospace Products
JT-0981	Union Carbide
JT-0992	Union Carbide
ZrO_2	Zircoa
ZrO_2 + W Reinforcement	TRW
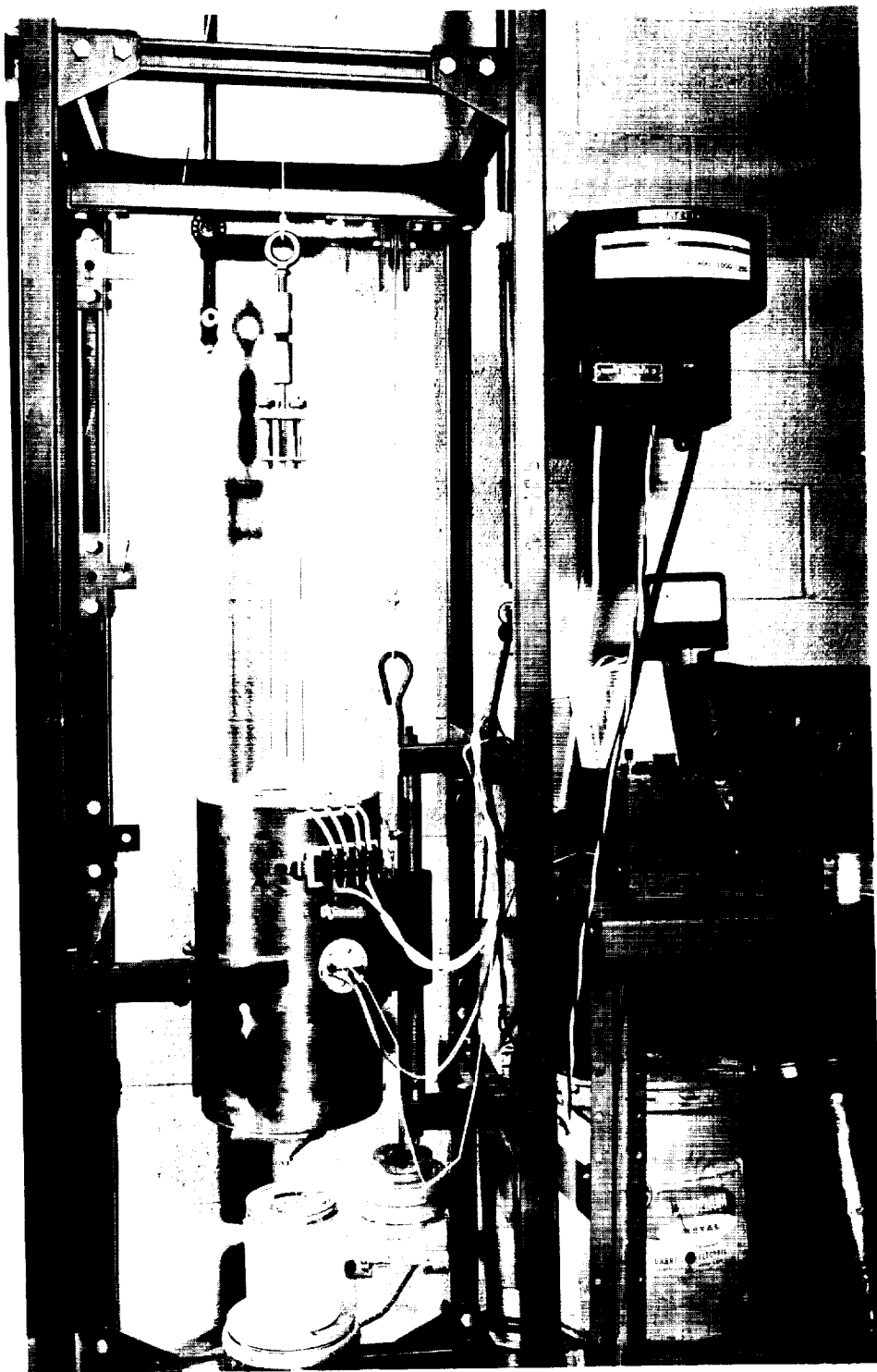
THERMAL SHOCK TEST APPAPATUS

Figure 48

to be used in this program. On this basis, materials which failed by thermal shock at a temperature difference less than 1900°F were not considered for subsequent insert fabrication.

The oxidation screening tests were performed in the apparatus illustrated in Figure 49. In cases where the material will conduct electrical current, the specimens were heated between two electrodes, and a gaseous reacting enviroment, consisting of $CO\text{-}CO_2$ or $H_2\text{-}H_2O$ of known ratios, was introduced into the chamber.

A different test, using the plasma jet, was also used to investigate the oxidation characteristics of candidate materials. In this test, non-conducting materials were also capable of being evaluated. A N_2-plasma arc with separate injection of oxygen on the downstream side of the plasma was employed. The test specimens were 2 x 2 x 1/2-inch blocks. The oxidation characteristics of JTA graphite composite materials were used as a standard. Materials which oxidized at a greater rate than JTA were not considered for subsequent nozzle fabrication.

c. Graded Carbides

Specimens of the graded TaC and CbC-graphite composites from Carborundun Company were tested for thermal shock resistance. As shown in Figure 50, the samples had a radial gradation in the composition with a 1/8" radius disc of pure carbide at the center, surrounded by a 1/4" wide ring of 70 v/o carbide, and finally encased in a 3/8" outside ring of 30 v/o carbide - 70 v/o graphite. This composition would simulate an actual nozzle containing carbide on the inner diameter graded to graphite on the outer diameter. The composite materials were prepared in a single hot-pressing operation as 1.5" diameter x 1.5" long slugs, and test discs 1.5" diameter x 0.25" thick were machined from these. When subjected to the stresses induced by a temperature difference of 1900°F in the thermal shock test, specimens of both materials developed radial cracks extending through the center, Figure 50. These cracks, however, did not result in complete specimen failure and could not be extended by hand flexure. This condition is slightly better behavior than that experienced by infiltrated 20% porous tungsten and, on this basis, the graded carbides were considered to be marginal for the current insert applications.

The discs of graded carbides were subjected to two different plasma jet tests. The results are shown in Figure 51. Initially, samples of both graded CbC and TaC-graphite were tested using an 80 N_2 - 20 O_2 plasma at 550 BTU/ft^2/ sec. heat pulse. The thin disc samples were backed with 2" x 2" x 3/8" blocks of ATJ graphite to simulate more closely the size of the standard test specimen (2" x 2" x 1/2"). The behavior of the graded CbC - graphite composite material was sufficiently inferior to the graded TaC - graphite, so that no further plasma jet testing was carried out on the CbC material. The TaC - graphite showed only slight reaction, no measurable erosion, and only minor weight loss. This specimen was subjected to five additional 120 second pulses of the 80 N_2 - 20 O_2 plasma jet, which resulted in only a small increase in the specimen erosion depth and weight loss. The appearance of the sample indicated only a moderate surface roughening in the outer ring, where the graphite content was the highest (Figure 51). A second specimen, subjected to a 600 second steady pulse in the N_2 - O_2 plasma, exhibited similar behavior to that of the pulsed testing. The major difference between the two plasma jet tests was the observed increase in surface brightness temperature from 2930°F for the last pulse in the series of five pulses, to 3120°F near the end of the 600 second steady state test. The carbide at

79
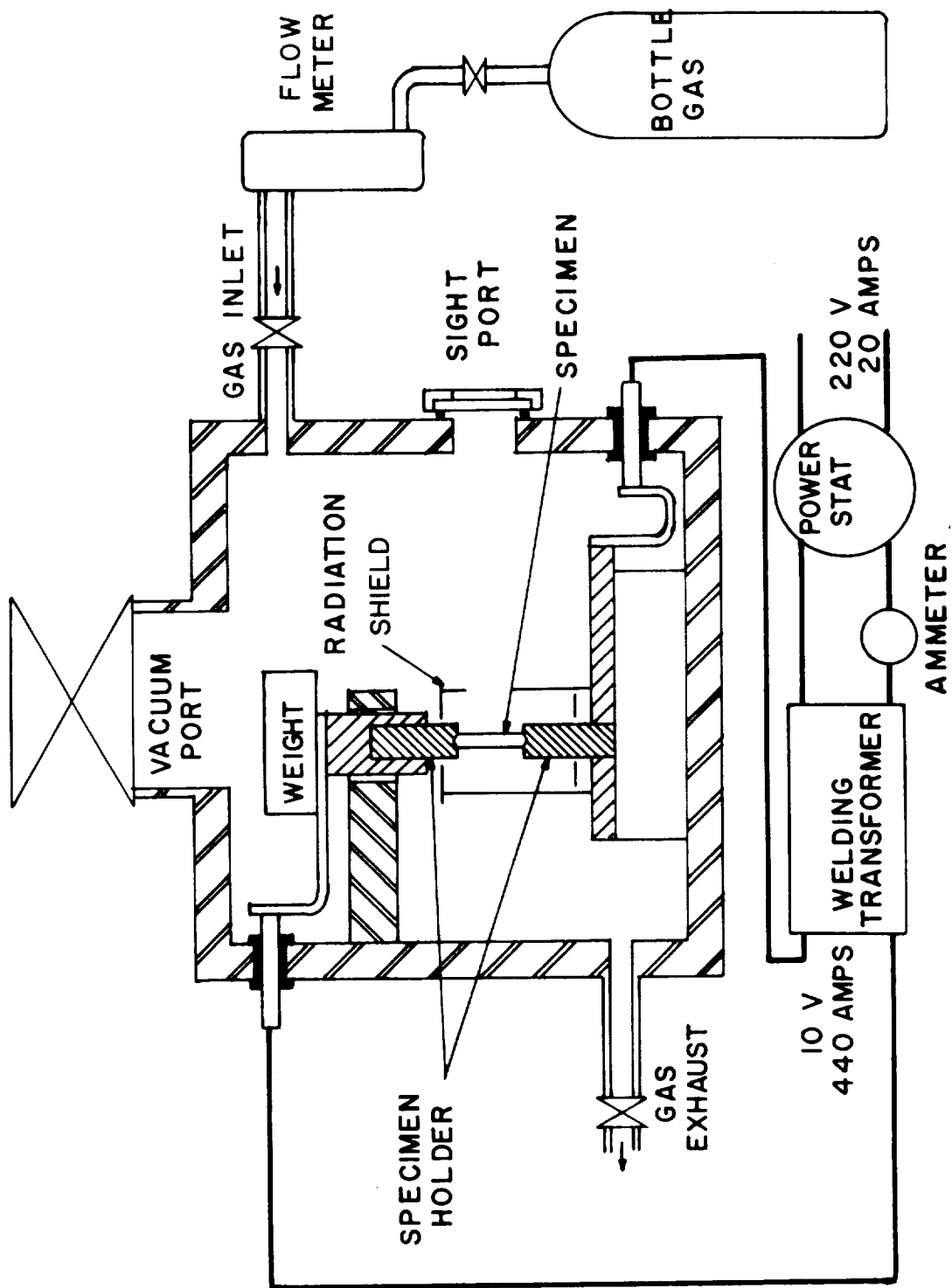
SCHEMATIC DIAGRAM FOR FURNACE FOR COMPATABILITY STUDIES

Figure 49

30 ^{V}/o TaC
70 ^{V}/o Graphite

70 ^{V}/o Tac
30 ^{V}/o Graphite

TaC
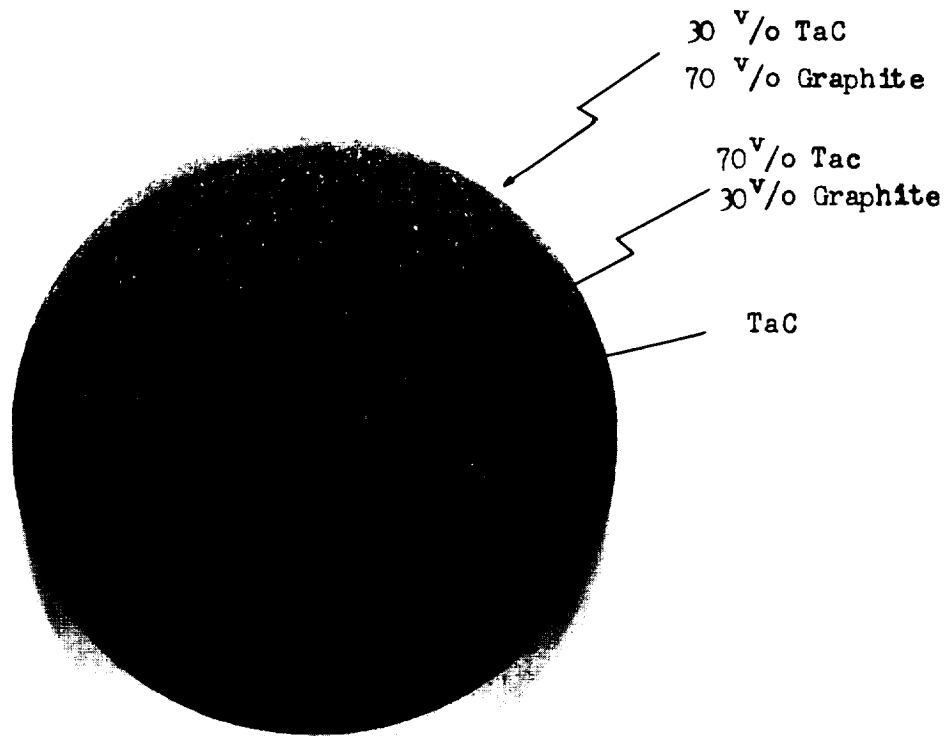
08022   2X

THERMAL SHOCK SPECIMEN - GRADED CARBIDE

A

B

C

0818l
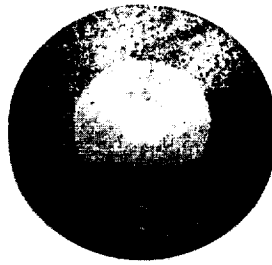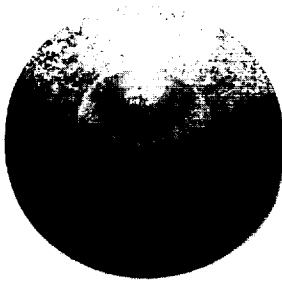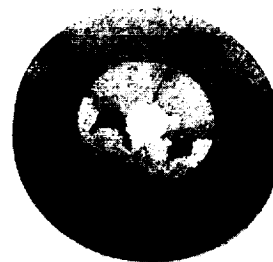
1X

Materials Subjected to a 550 BTU/ft^2-sec Heat Flux (N_2-O_2 Plasma)

A) CbC – Graphite after 120 seconds

B) TaC – Graphite after six-120 second pulses

C) TaC – Graphite after 600 seconds

PLASMA JET TEST SAMPLES – GRADED CARBIDE

Figure 51

the center where the plasma impinged showed no measurable erosion. The center crack in the specimen was produced by the thermal shock test which was performed prior to the plasma jet testing.

A graded TaC-graphite specimen, which had also been tested in thermal shock, was subjected to a 100% N_2 plasma at 1000 BTU/ft^2/sec heat flux for 120 seconds (Figure 52). The specimen reached a surface temperature well in excess of 4000°F, and rapid melting occurred at the point of impingement of the plasma. The relatively good behavior of the TaC-graphite composite at the lower heat flux (3100°F surface temperature), while failing catastrophically at the higher heat flux (4000°F), emphasized the need for further testing to determine both the maximum use-temperature for this material and the oxidation resistance in the temperature range, 3000-4000°F. Studies, using self-resistance heated rods in a CO_2 atmosphere, were planned to determine these properties.

In evaluating the graded carbides, several materials were evaluated to determine their applicability as an ID liner material. These materials were:

Material	Vendor	Processing Method
TaC, CbC, HfC, ZrC	Carborundum	Hot Pressed
SiC Coated Graphite	Texas Instrument	Tikote (Proprietary process, vacuum deposition)
80 Hf - 20 Ta	ITT Research Institute	Arc Melted, rolled

The evaluation method consisted of heating 1/4" diameter x 2" rods by self resistance in the presence of a CO_2 atmosphere (100 mm) and measuring the variation in diameter as produced by a two minute exposure. The experimental apparatus is shown schematically in Figure 49 and was described previously. The test sequence involved the following steps:

(1) Evacuate test chamber to a vacuum of 10^{-2} Torr.

(2) Fill chamber with argon and obtain power setting for desired temperature (determined with two-color pyrometer).

(3) Evacuate chamber and fill with CO_2 at the rate of 5 cfh; maintain a partial pressure of 100 mm in the chamber by balancing vacuum pump valve with CO_2 flow.

(4) Set power settings to obtain desired temperature and maintain settings for 120 seconds.

(5) Remove power and terminate CO_2 flow.

The appearance of the refractory carbide specimens is presented in Figures 53 and 54. At 4500°F, all specimens underwent significant degradation. The oxides formed on the CbC and TaC were molten at 4000°F, and at this temperature the CbC suffered a larger degree of surface regression. Both the ZrC and HfC formed adherent white oxides at the 4000°F reaction temperature which actually resulted in an increase in the diameter of the test specimen. Some question

08184   1X

Material after 120 Seconds in 1000 BTU/ft^2-sec Heat Flux
(N_2- Plasma).

PLASMA JET TEST SAMPLE - GRADED CARBIDE

Figure 52

4000°F

Columbium Carbide (CbC)

4000°F   4500°F

Tantalum Carbide (TaC)

REACTIVITY TEST SPECIMENS - CARBIDES

7802

Figure 53

4000°F   4340°F

Zirconium Carbide (ZrC)

4000°F   4500°F

Hafnium Carbide (HfC)

REACTIVITY TEST SPECIMENS - CARBIDES

Figure 54

exists as to whether this oxide will be retained on the surface of an insert during actual firing conditions. The oxides were removed to evaluate the degree of surface recession which would occur if oxide spalling took place. The ZrC showed a rather thick oxide layer (approximately 0.008 inch), while the HfC had only a relatively thin oxide layer (0.001 inch). On the basis of the reactivity tests and considering the possible spalling of the oxide, the HfC or TaC appear to be the most suitable grades for use in a graded carbide nozzle system.

The results obtained for the silicon carbide-coated graphite are presented in Figure 55. At 3000°F no appreciable reaction took place; at 3250°F a significant degree of reaction was present, and at 3500°F no coating remained on the specimen. In addition, the graphite substrate showed significant cracking after the 3500°F test. A supplementary test was performed at 3500°F in an air environment to determine whether the lower partial pressure of oxygen involved in the CO_2 environment was hindering the formation of a protective coating on the SiC samples. Significant coating degradation also occurred in the air test and the results were consistent with those obtained in the CO_2 tests.

The IIT Research Institute has recently developed an 80 Hf-20Ta alloy which has a melting point approaching 4000°F and which forms a protective coating upon exposure to oxidizing conditions. Oxidation tests were performed on 1/4" diameter rod of this alloy to determine its possible application as a nozzle insert material for liquid propellant environments involving oxidizing conditions. The specimens were preoxidized at 3000°F in air for two minutes prior to testing in order to form the protective oxide.

Tests conducted at 3500°F in 100 mm CO_2 environment indicated no extensive specimen degradation (See Figure 56). A reaction temperature of 3750° produced a relatively thick oxide coating and the specimen fractured, presumably during the cool-down cycle. Testing of the specimen at the 3850°F test temperature was terminated after 105 seconds, and subsequent specimen examination indicated that considerable melting took place.

d. Moldable Graphite Composites

Samples of an experimental molded graphite material, X4110-3, were obtained from Magnesium Aerospace Corporation. The material was composed of graphite particles coated with a 90% SiC - 10% ZrC mixture, and bonded with an organic resin. The material was tested in three conditions: (a) as molded; (b) after mold baking for 24 hours at 1800°F, and (c) after mold sintering for 72 hours at 3000°F. Plasma jet tests of the material in all conditions resulted in erosion of 0.114" to 0.126" after 120 seconds. These rates, being on the order of ablative material, eliminated the molded graphites from further consideration.

e. JT-Composite Materials

Two graphite composite materials developed by Union Carbide (JT-0981 and JT-0992) were evaluated as part of this program. Samples of the experimental JT-graphite alloys were cut from hot pressed slugs, approximately 3" diameter x 3" long. On an atomic basis, the composite materials have the same nominal proportions with hafnium substituted in the JT-0992 for the zirconium on the JT-0981. The compositions by weight of the two composite materials are: JT-0981 - 48% C, 35% Zr and 17% Si; JT-0992 - 33% C, 55% Hf and 12% Si.

3000°F   3250°F   3500°F

REACTIVITY TEST SPECIMENS - SiC COATED GRAPHITE

Figure 55

3000°F 3500°F 3750°F 3850°F

REACTIVITY TEST SPECIMENS - 80 Hf - 20 Ta

Figure 56

Samples of these materials (2" x 2" x 1/2") were subjected to plasma jet tests. Photomacrographs of the JT-0981 are presented in Figures 57 and 58. The JT-0992 had a very similar appearance after testing. For the plasma test with oxygen injection (550 BTU/ft^2/sec) samples were initally subjected to a 120 second heat pulse, cooled to room temperature and evaluated for weight loss and total erosion. These samples were then subjected to additional heat pulses of 120 second duration (four more pulses for the JT-0981, and five more pulses for the JT-0992) with cooling below 1200°F between pulses. The JT-0981 formed an adherent oxide layer in the area of impingement of the plasma arc, which caused an increase in thickness of 0.008", after the first 120 second pulse. Similar behavior was observed for the JT-0992, but the oxide was non-adherent and spalled off before the measurements were made. The two materials must be considered to have very similar behavior under the test conditions used. They demonstrated very good oxidation resistance when compared with the conventional dense grades of graphite.

The JT composite samples when subjected to the N_2 - plasma at the higher heat flux (1000 BTU/ft^2/sec) reached higher surface temperatures at the point of impingement (3800°F vs. 2700°F), and in general the whole sample was hotter after a 120 second pulse than for the 550 BTU/ft^2/sec tests. The total erosion and percent weight loss were considerably greater for the 1000 BTU/ft^2/sec heat flux conditions. Both samples had a gray white oxide on all surfaces, due to the higher overall temperature.

Thermal shock specimens were fabricated from one of the plasma jet test specimens of JT-0981. Two specimens were subjected to a thermal shock test ($\triangle$T = 1900°F) without showing any signs of cracking.

Reactivity rods of JT-0981 and JT-0992 were also tested. Both grades showed extensive reactivity at 4000°F and the JT-0981 graphite exhibited significant degradation at 3500°F. The appearance of the test specimens is shown in Figure 59. The plasma jet tests indicated no significant difference between the two grades but the reactivity tests indicated the JT-0992 grade was superior from an oxidation standpoint.

f. Zirconia

The high melting point and low chemical reactivity of several of the refractory oxides have long made them attractive as potential throat insert materials. However, their extremely low thermal conductivity and susceptibility to thermal shock cracking has prevented their wide usage.

TRW had evaluated various grades of zirconia on previous programs. None of the grades were capable of withstanding a $\triangle$T in the thermal shock test in excess of 1200°F. It appeared that this material shortcoming could be overcome by segmenting the insert into discs and separating the discs with a highly conductive material. This concept would utilize the highly conductive material to transfer heat to the OD of the insert and thus, reduce the thermal gradient across the oxide. With this concept in mind, further thermal shock tests were conducted with zirconia specimens in an effort to determine whether a systematic pattern existed between the number and type of cracks produced and the severity of the thermal pulse. The results were intended to yield data that would indicate the advisability of segmenting the zirconia discs. If a crack structure developed which was a predictable function of the thermal pulse, then appropriate segmenting could be employed to eliminate, or at least minimize, additional cracking during the firing pulse.

90

PLASMA JET TEST SAMPLES - GRAPHITE COMPOSITES

7377

Figure 57

A

B

C

D

0   1   2   3
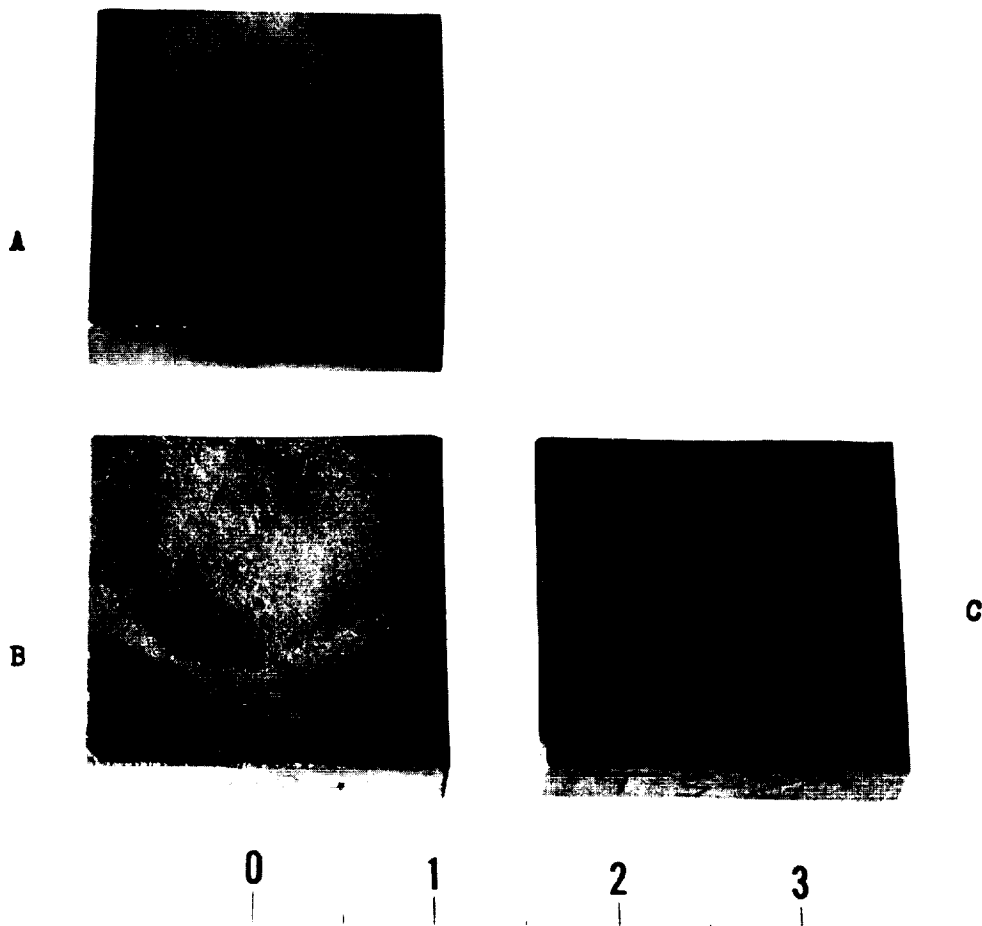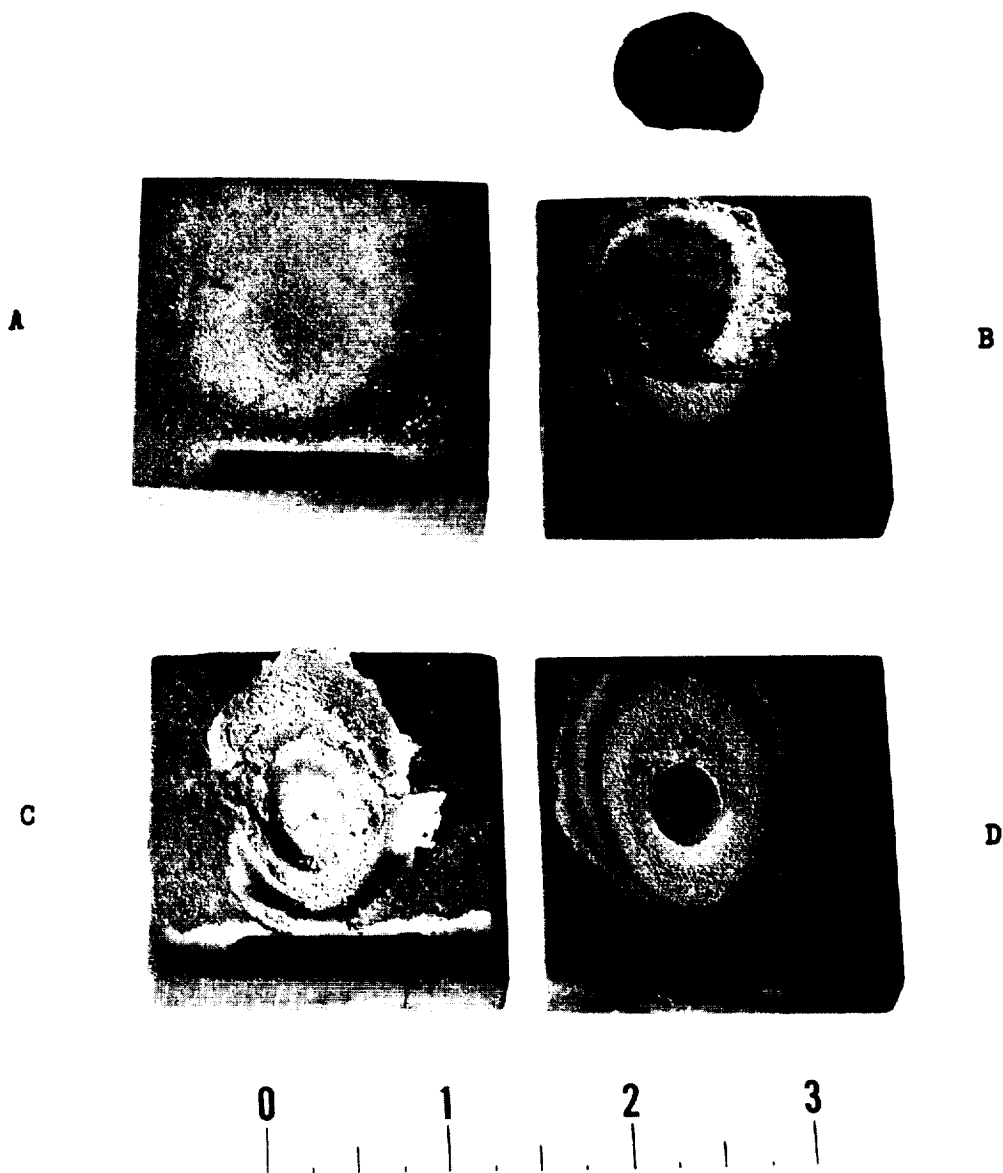
1X

08073-1

PLASMA JET TEST SAMPLES - GRAPHITE COMPOSITES

7378

Figure 58

3250°F 3500°F 4000°F

JT-0981

3000°F 3500°F 4000°F

JT-0992

REACTIVITY TEST SPECIMENS – GRAPHITE COMPOSITES

Figure 59

93

The GTZ zirconia which was used for this investigation is a proprietary product of the Zirconium Corporation of America. It is a partially stabilized zirconia with thermal shock properties reported to be superior to Calcia-stabilized zirconia. The test specimens, fabricated by Zircoa, were received in the form of 1-1/2" diameter discs, 1/4" thick, with an average density of 4.17 g/cc (approximately 73% of theoretical). The thermal shock test apparatus and testing procedures have been previously described.

An initial lot of six specimens were tested at $\triangle$T values ranging from 1000 to 1900°F using an ice-brine quench and a single cycle for each specimen. Specimens were manually flexed after quenching to determine the number of segments produced by the shock test and the results are shown below:

Thermal Shock Data on GTZ Zirconia

Specimen No.	$\triangle$T (°F)	No. of Segments
1	1000	4
2	1200	5
3	1400	4
4	1600	6
5	1800	5
6	1900	6

In no case was any specimen completely fractured during the quench cycle. All specimens had to be subjected to slight manual pressure before actual breakage occurred. Specimens quenched with a $\triangle$T of 1000 and 1200°F had no visible cracks but were broken easily by manual flexing. Those specimens quenched from 1400 thru 1900°F all had one small crack in the center of the specimen approximately 1/2" long. In no case did the crack extend to the outer edge. The specimens are shown in Figure 60 after thermal shock testing and manual flexing.

Additional specimens were drilled with hole sizes of 0.600", 0.800" and 1.200" and thermal shock tested at $\triangle$T values of 1000, 1400, and 1800°F. The data from this series of tests are shown as follows:

Thermal Shock Data on GTZ Zirconia

Hole Dia. (Inches)	$\triangle$T (°F)	No. of Segments
0.600	1000	2
0.800	1000	2
1.200	1000	4
0.600	1400	2
0.800	1400	1
1.200	1400	3
0.600	1800	2
0.800	1800	2
1.200	1800	

Of the 9 pieces tested during this series, only the specimens with the 1.200" ID hole broke during the quench cycle. Most of the specimens with the 0.600 and 0.800 ID holes contained small visible cracks starting on the ID and running radially towards the OD of the specimens.

94
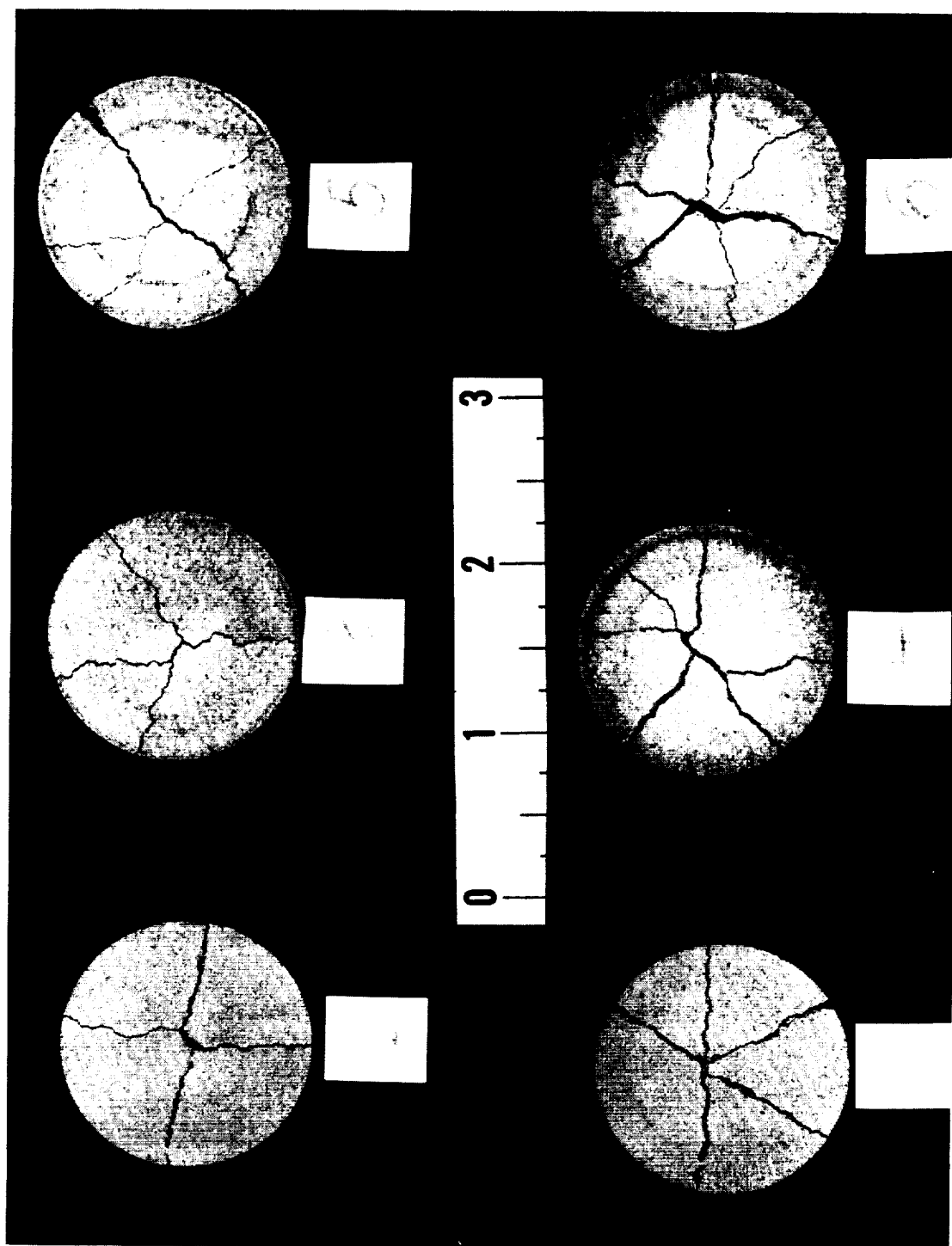
THERMAL SHOCK SPECIMENS - ZIRCONIA

1.-ΔT-1000°F
2.-ΔT-1200°F

3.-ΔT-1400°F
4.-ΔT-1600°F

5.-ΔT-1800°F
6.-ΔT-1900°F

95

Figure 60

The data from the thermal shock tests are shown graphically on Figure 61, which is a plot of specimen hole size versus number of segments resulting from the test. The general indication is that as hole size increases from a solid disc the severity of fracture decreases. However, at some hole size, approximately 0.8 inch diameter for a 1.5 inch disc, the number of segments resulting from thermal shock starts to increase. Figure 61 also indicates that for the throat size under consideration, the oxide discs would crack into two or three segments.

g. Reinforced Oxide

Zirconia discs processed by a variety of methods were evaluated in thermal shock tests. These oxides had comparatively poor thermal shock resistance and were not considered applicable for nozzle inserts. Fiber reinforcement, however, was considered to be a possible method to minimize thermal shock susceptibility in ceramics.

Under an internally funded effort at TRW, a fabrication technique has been developed to produce a tungsten wire reinforced material which produces dense (up to 85% of theoretical), hard, fine pore structures. The specimens consisting of discs with 5 v/o tungsten screen, in layers parallel to the flat surfaces were fabricated. Thermal shock tests conducted on this material system indicated that the reinforcement improved the thermal shock resistance to the point where only moderate cracking of the ceramic matrix occurred and the specimen retained its shape when subjected to a $\triangle T$ value of 1900°F.

Static air tests showed severe oxidation of the tungsten reinforcement at temperatures as low as 2400°F after 20 minutes. Plasma jet tests with a N_2-plasma, 1000 BTU/ft^2/sec. for 120 seconds, and surface temperatures of the order of 3800°F (optical) showed some breakdown of the binder, and oxidation of the layer of tungsten screening nearest the surface, but no oxidation below this surface layer. The zirconia provides sufficiently good insulation, so that only the outermost surface layer of tungsten is subjected to temperatures sufficiently high to cause severe oxidation in the short time interval of the plasma jet test.

Zirconia reinforced with tungsten - 3% rhenium wire (W-3Re) was also evaluated as a potential insert material. The processing parameters involved were:

Consolidation Method	Type of Reinforcement
Phosphate Bonding	W-3Re Screen
Phosphate Bonding	0.003" Chopped W-3Re Wire
Pressed and Sintered	0.003" Chopped W-3Re Wire

Samples of phosphate-bonded zirconia were fabricated for both plasma jet and thermal shock tests. With both the screen and chopped fiber reinforcement optimum adherence between matrix and fiber was obtained by lightly oxidizing the fiber prior to consolidation.

THERMAL SHOCK RESULTS
Hole Size Vs Segments

97

Figure 61
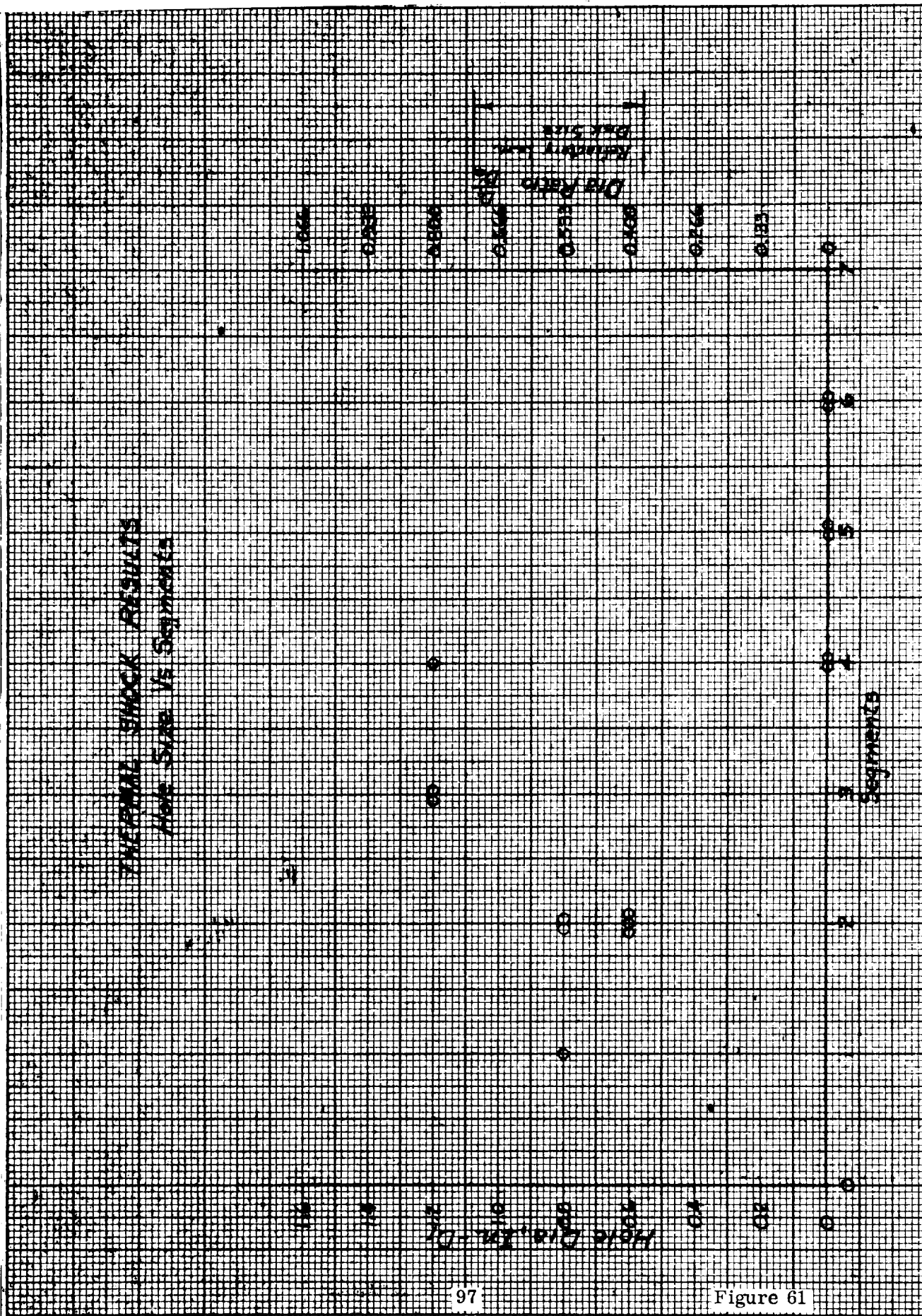
Three specimens, 2-1/4" dia. x 0.300", were fabricated with 5 v/o reinforce-ment (15 mesh screen, 0.010 wire) and tested for varying lengths of time in an oxidizing plasma at 550 BTU/ft^2/sec. Surface temperatures for all tests were 3400-3500°F. The results of the test were as follows:

Specimen Number	Total Change in Thickness (inch)	Length of Test	Comments
1	+ 0.005	2 minutes	Minor surface cracking
2	+ 0.011	6 minutes	Surface upheaval upon cooling
3	+ 0.012	20 minutes	Major surface cracking

Extensive oxidation of more than the surface layer of reinforcement was only noted for specimen No. 3 which experienced the maximum exposure. The W-3Re reinforced material showed substantially better behavior than comparable composite samples using unalloyed tungsten screening.

Samples of non-reinforced phosphate-bonded zirconia were fabricated and tested in the plasma jet to determine a "maximum use temperature" for this matrix material. The results are summarized below:

Summary of Test Results Obtained on Phosphate-Bonded Zirconia

Heat Flux (BTU/ft^2/sec.)	Optical Surface Temperature (°F)	Results
300	2900	No observable effect
400	3180	No observable effect
500	3560	No observable effect
600	3930	Surface glazing
700	4260	Extreme material flow

On the basis of these data, a maximum use temperature for the reinforced phosphate-bonded zirconia system was defined as approximately 3800°F.

Thermal shock tests ($\triangle$ T = 1868°F) were conducted on phosphate-bonded zirconia containing 1, 3, and 5 v/o W-3% Re chopped fibers (1/4" long, .003" diameter) and 5 v/o screen. The zirconia specimens with both the 3 and 5 v/o reinforcement showed no cracking through the reinforced structure (See Fig-ures 62 and 63).

In order to increase the temperature capability of the reinforced oxides, specimens were fabricated of zirconia and W-3 Re chopped wire using a sintering technique. The fabrication process was isostatic compaction at 30,000 psi followed by vacuum sintering for 4 hours at 4000°F or by hot pressing for 30 minutes at 9,000 psi and 2912°F. A summary of the fabrication and thermal shock tests are given in Table VIII.

98

Top View   Side View

Zirconia Reinforced with 1 v/o Chopped W-3Re Wire
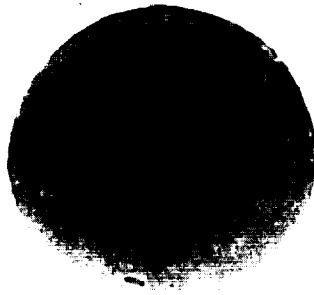
Top View   Side View

Zirconia Reinforced with 3 v/o Chopped W-3Re Wire

THERMAL SHOCK SPECIMENS - REINFORCED OXIDE

Figure 62

7803

99
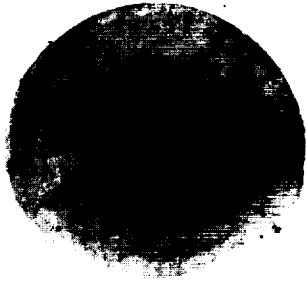
Top View   Side View

Zirconia Reinforced with 5 v/o Chopped W-3Re Wire
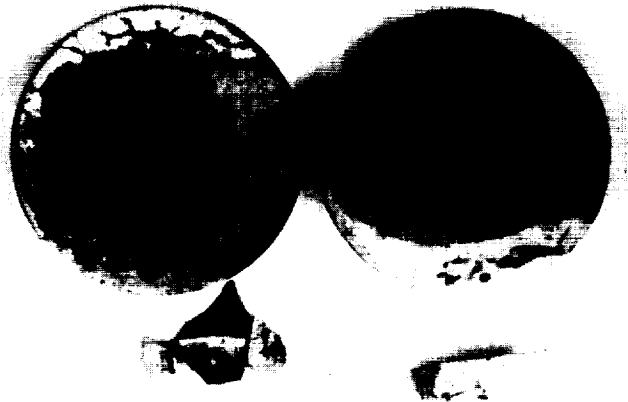
Zirconia Reinforced with 5 v/o W-3Re Screen

THERMAL SHOCK SPECIMENS - REINFORCED OXIDE

7801

Figure 63

SUMMARY OF MICROCRACKING AND THERMAL SHOCK TENDENCIES IN VARIOUS REINFORCED COMPOSITES

Matrix Material	Vol Percent Fiber	Fabrication History	Composite Appearance	Thermal Shock Test Results (1900°F – Ice Brine Quench)
Zircoa F410	10	Press & Sinter	Number of areas where poor bonding and voids existed in clusters of fibers; slight microcracking in the $Zr0_2$ matrix.	Failed after manual flexing
Zircoa F410	5	Press & Sinter	Sound Composite	No Failure
Zircoa B	10	Press & Sinter	Excessive cracking in the composite; many areas of fiber clusters and large voids.	No Failure
Zircoa B	5	Press & Sinter	Moderate degree of cracking	No Failure
Zircoa B Plus W Modified $Zr0_2$	5	Press & Sinter	Sound Composite	No Failure
Zircoa F410	5	Hot Press	Sound Composite	No Failure
Zircoa B	5	Hot Press	Sound Composite	No Failure

Table VIII

Photographs of thermal shock specimens of the various zirconia-matrix pressed and sintered composites are shown in Figure 64 prior to testing. All the reinforced specimens with the exception of Zircoa B + 10 v/o fibers exhibited no thermal shock cracking when quenched from 1900°F into an ice brine solution. The Zircoa B + 10 v/o fibers fractured after quenching when subjected to a slight manual pressure.

Composites containing 10 v/o of chopped fibers and fabricated from either the F 410 or Zircoa B zirconia powders showed some tendency toward cracking during the sintering cycle. The F 410 composites, however, developed much less cracking than the Zircoa B samples. The composite of Zircoa B with 5 v/o fibers showed little cracking, and the F 410 specimen with 5 v/o fibers was particularly sound with no visible fissures. It should be emphasized that, despite the localized cracking which occurred during sintering due to the expansion mismatch between fibers and matrix, the sintered samples did not fail in subsequent thermal shock tests. Representative specimens of thermally-shocked zirconia composites are shown in Figure 65.

Hot pressed composites of Zircoa B and F 410 each containing 5 v/o W-3% Re fibers were also tested. All of the hot pressed specimens survived the thermal shock quench from 1900°F into the ice brine solution without failure.

The modulus of rupture for the hot pressed samples, along with selected pressed and sintered composites, are shown in Table IX. The modulus of rupture obtained on the hot pressed F 410 - 5 v/o fiber composite (14,632 psi), is comparable to the strength of unreinforced zirconia of similar density. The relatively high strength of the composite materials prior to thermal shock testing (see Figure 66) indicates that a sound zirconia matrix supported the load during the bend test and failure occurred abruptly at maximum load in a manner characteristic of brittle materials. This behavior is in contrast to the specimens which had been exposed to a thermal shock cycle and which had significantly lower strengths (approximately 3000 psi). The load deflection curve (Figure 66) for the specimens exposed to thermal shock indicated an "apparent" ductile behavior. This effect can be attributed to the fact that the microcracking which occurs during thermal shock testing results in a lower apparent modulus of elasticity and allows the load to be transmitted to the reinforcing W-Re fiber-zirconia matrix interface. Metallographic examination of the various specimens substantiated the crack-free nature of the as-pressed F 410 composite compared to the matrix in the specimen after thermal shock (see Figure 67).

The bend test data also indicates that porosity and method of fabrication -- press and sinter versus hot pressing -- have little effect on the modulus of rupture after thermal shock testing. It appears that the bonding between the matrix and the fiber represents the critical consideration in the thermally-shocked composites where the fibers must support the load. Metallographic examination indicated that good matrix-to-fiber bonding existed in both the pressed-and-sintered and the hot-pressed specimens. Photomicrographs of composites fabricated by both methods are presented in Figure 68.

Adequate bonding is achieved when fibers are in intimate contact with the matrix material during the high temperature portion of the fabrication cycle. Intimate contact is dependant on a uniform fiber dispersion in the matrix.
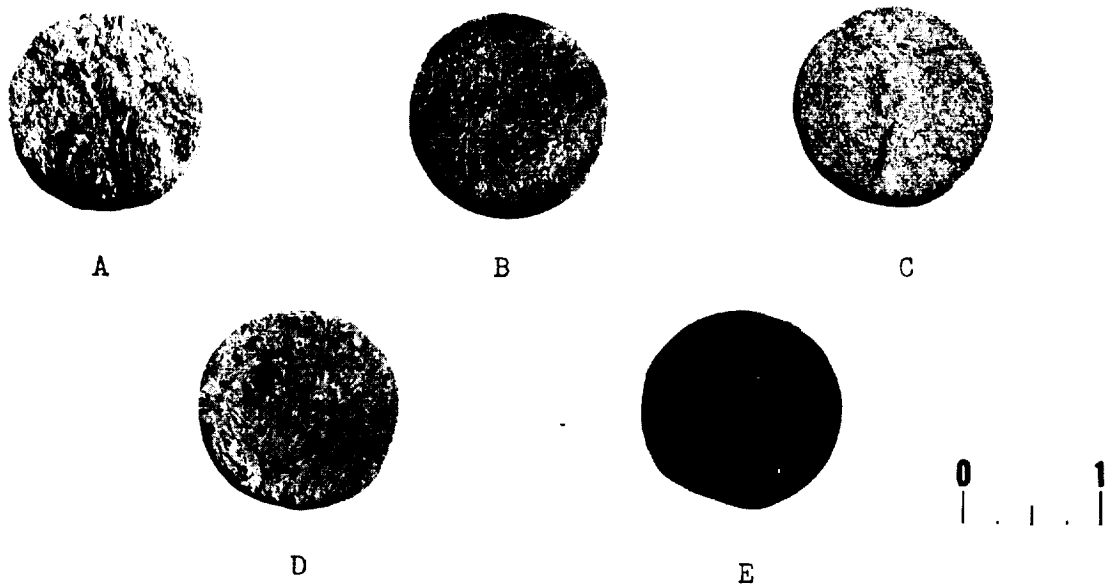
A. Ca Stabilized ZrO_2 + 10 v/o Fibers

B. W Modified ZrO_2 + 5 v/o Fibers

C. Ca Stabilized ZrO_2 + 5 v/o Fibers

D. F410 ZrO_2 + 10 v/o Fibers

E. F410 ZrO_2 + 5 v/o Fibers

THERMAL SHOCK SPECIMENS - REINFORCED OXIDE

9193

103

Figure 64

2X
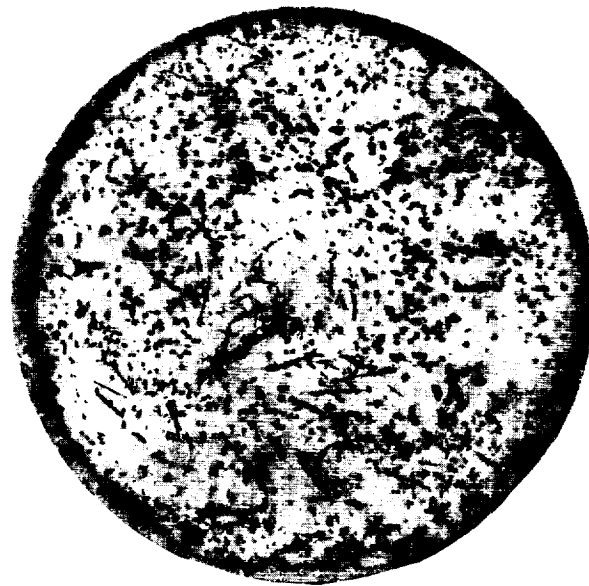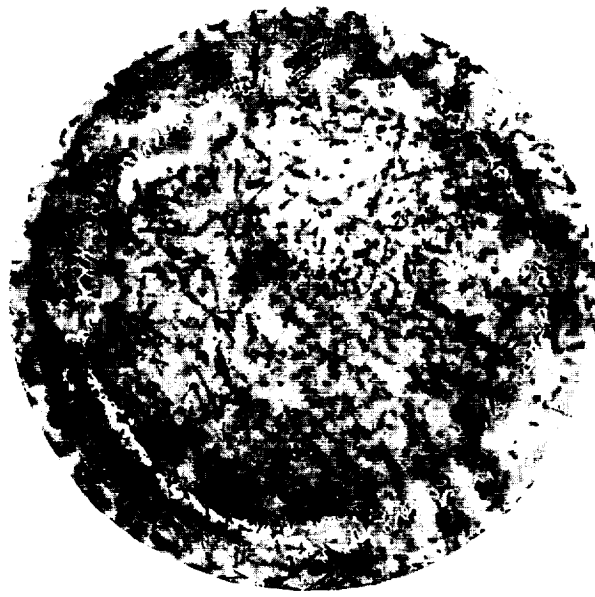
THERMAL SHOCK SPECIMENS - REINFORCED OXIDE

BEND TEST DATA OBTAINED ON REFRACTORY OXIDE COMPOSITES REINFORCED WITH

CHOPPED TUNGSTEN FIBERS (W-3 v/o Re)

Matrix Material	v/o Fiber	Fabrication Procedure	History	Density g/cc	Porosity %	Modulus of Rupture psi
Ca Stabilized	5	Hot Pressed	As-Pressed	5.5	11	3,138
"	5	Hot Pressed	Thermally Shocked	5.5	11	691
F 410	5	Hot Pressed	As-Pressed	6.1	4	14,632
"	5	Hot Pressed	Thermally Shocked	6.1	4	2,481
F 410	5	Isopressed & Sintered	Thermally Shocked	5.6	15	3,119
"	10	Isopressed & Sintered	Thermally Shocked	5.8	20	3,385
"	10	Isopressed & Sintered	Thermally Shocked	5.8	20	2,641

Table IX

105

LOAD DEFLECTION CURVE
Modulus of Rupture
Versus
Deflection
(F410 with 5 v/o Fiber Composite)

(a) As Fabricated

(b) Thermal Shock Tested

Modulus of Rupture - psi

Deflection - Inches X 10^3
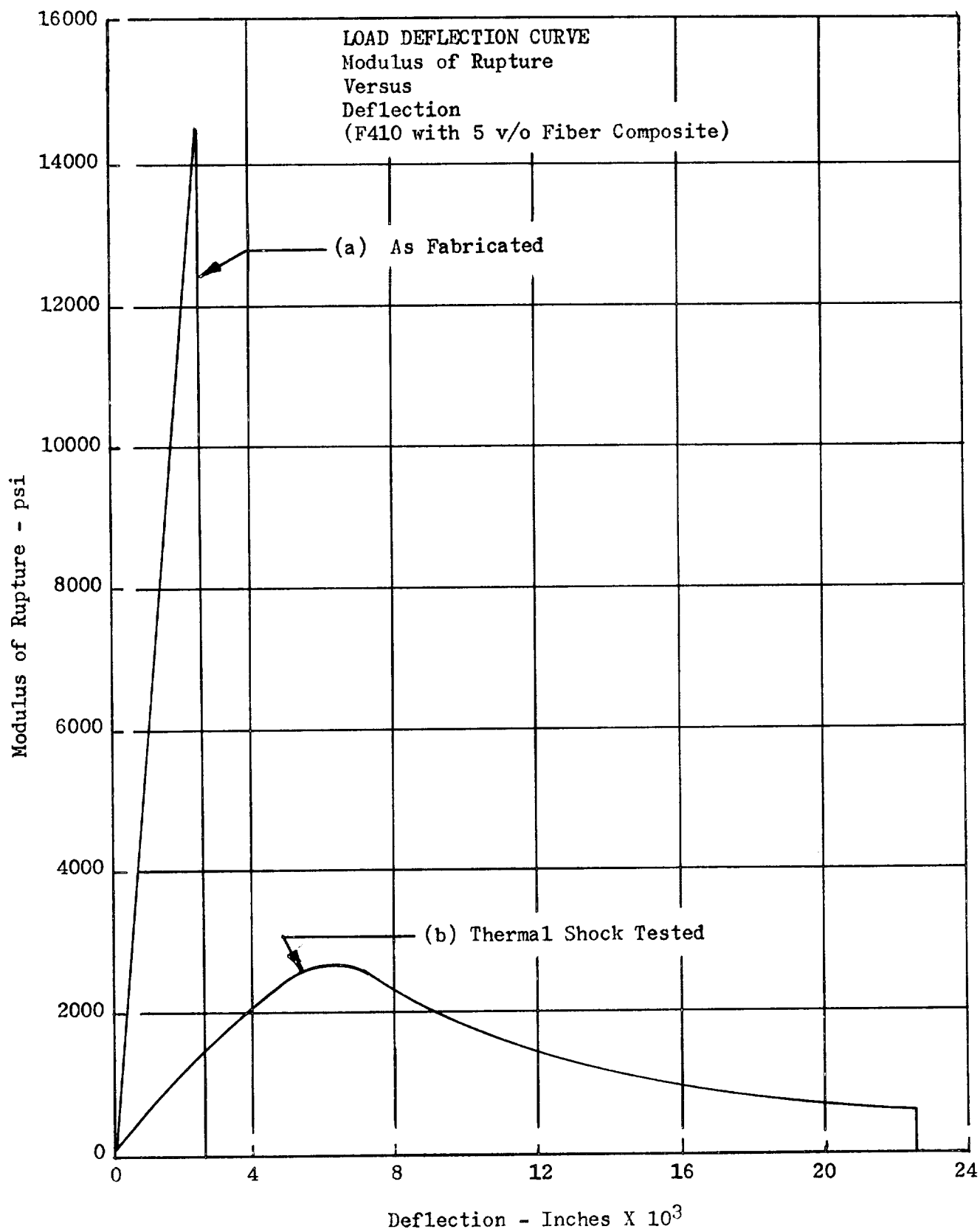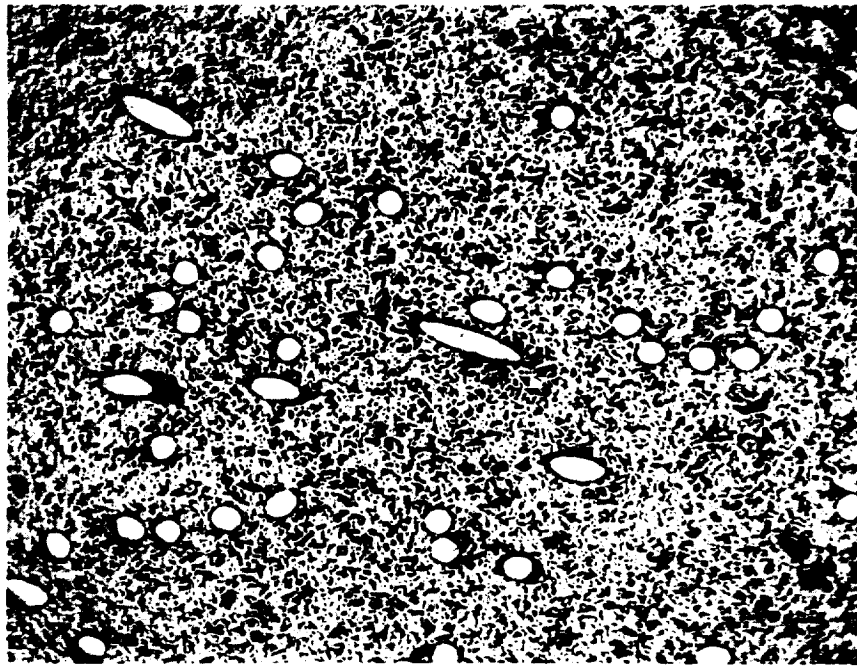
Figure 66

Before Thermal Shock Testing
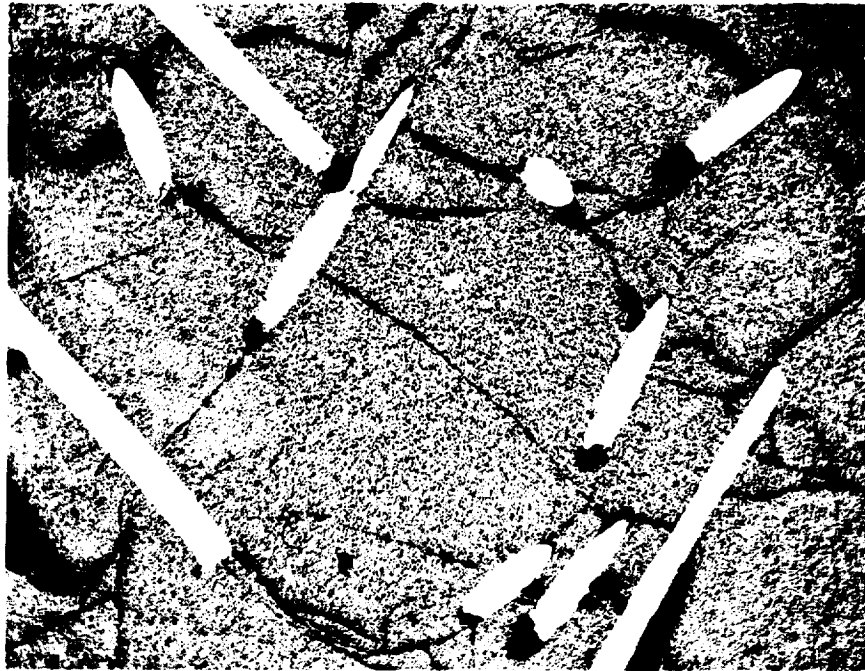
50X

After Thermal Shock Testing

MICROSTRUCTURE PHOTOGRAPHS - REINFORCED OXIDE

Figure 67
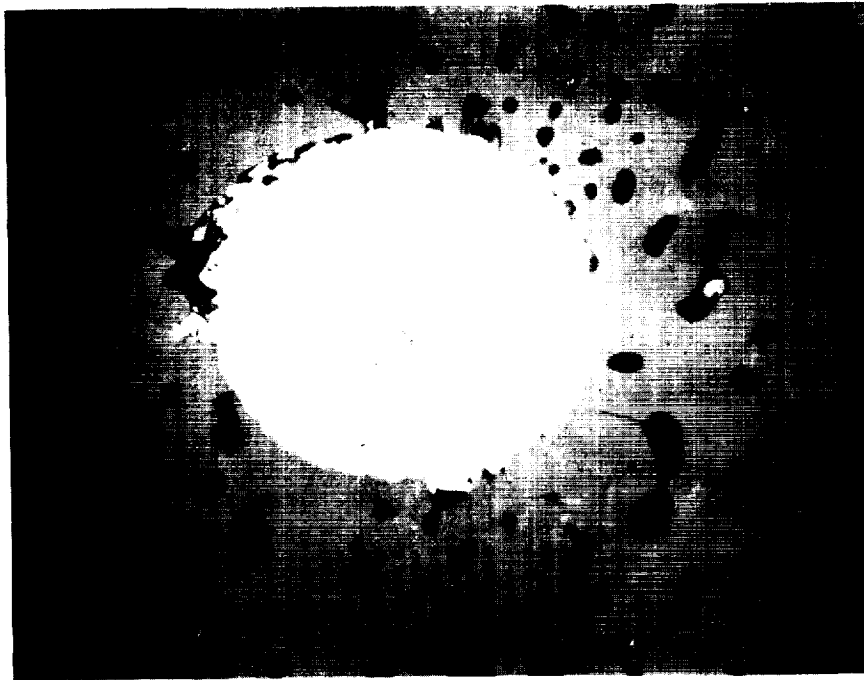
500X

Pressed and Sintered Fiber-Reinforced Zirconia
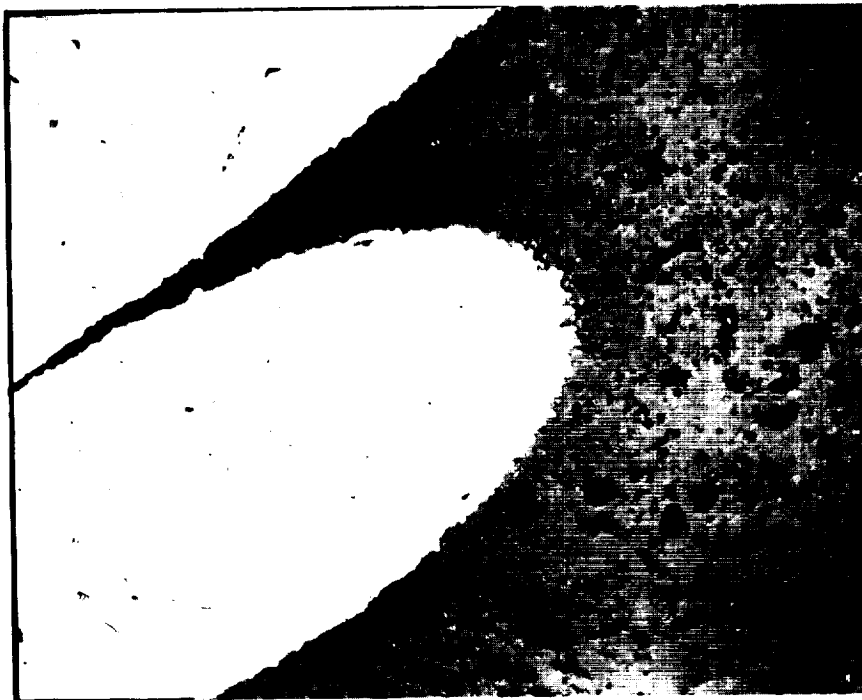
500X

Hot-Pressed Fiber-Reinforced Zirconia

MICROSTRUCTURE PHOTOGRAPHS - REINFORCED OXIDE

Figure 68

108

9192

The difficulty in achieving a uniform dispersion is the probable reason why the 5 v/o fiber reinforced composites are superior to the 10 v/o materials.

On the basis of the processing studies, along with the thermal shock and bend tests, F 410 zirconia + 5 v/o W-3% Re chopped fiber (0.003 dia. x 3/16" long) was selected as the composite material for full-size nozzle fabrication. Both isostatic pressing and sintering, and the hot-pressing procedure appeared to be suitable as a fabrication technique for the material. Because of the simplicity in fabrication method, isostatic pressing and sintering was selected as the primary approach, with hot pressing available as a back-up method.

h. Material Properties

Knowledge of selected mechanical and physical properties of candidate materials is essential for the proper design of nozzle throat inserts for use at very high operating temperatures. Often the necessary properties are available from various sources, including published reports and company data sheets. However, some of the most promising candidate materials are relatively unexplored and some means was required to obtain the necessary properties. Some of the necessary properties were estimated from known data on similar materials, but experimental measurements were required for other necessary properties to provide a more secure basis for design.

Graded Carbides

A graded carbide structure was a promising candidate material for the temperature range under consideration. A search of the literature and consultation with the producer, Carborundum Corporation, uncovered most of the necessary design properties for the pure carbides of hafnium, tantalum, and zirconium. HfC was the leading candidate material for the pure carbide surface. Of the necessary properties, only modulus of elasticity as a function of temperature was not presently available for the HfC material.

Carborundum had investigated the properties of the carbide-graphite materials and had supplied thermal expansion, modulus of elasticity, and thermal conductivity data for many of their carbides and graphite composites. Carborundum's data, in combination with properties already obtained from the literature for carbides, provided sufficient information to initiate an improved design for a graded carbide-graphite throat insert.

The temperature dependence of Young's Modulus of Elasticity for HFC was estimated from data on cast, hypereutectic HfC + C material from "Bureau of Mines Metallurgical Progress Report Number 26", March 1965. A room temperature modulus value for HfC of 51×10^6 psi is reported in "Refractory Ceramics of Interest in Aerospace Structural Applications - A Materials Selection Handbook". This value was obtained for material of 94 percent theoretical density, which would closely approximate the density of the pressed carbide on the inner surface of the layered carbide throat insert. The following estimate was made of the temperature dependence of the elastic modulus of HfC:

Material	Modulus of Elasticity, psi		
	R.T.	2000°F	2850°F
Cast, hypereutectic HfC + C	48×10^6	30×10^6	14.5×10^6

Material	Modulus of Elasticity, psi		
	R. T.	2000°F	2850°F
HfC, Pressed & Sintered	51×10^6	32×10^6*	15.5×10^6*

* Estimated

For design computational purposes, the estimated modulus of elasticity values were extrapolated to 3800°F, yielding a value of 7.5×10^6 psi.

Based on thermal expansion data, TaC + graphite appeared to be the best choice for backing up the pure layer of HfC. A three layer backup structure of TaC + 10% G, TaC + 40% G and TaC + 70% G offered the best combination of thermal shock resistance and thermal expansion match, both in the axial and radial directions. No thermal expansion data was available for the TaC + 70% G mixture, but interpolation between the data for TaC + 40% G and TaC + 90% G indicated a better thermal expansion match for the TaC + 70% G in the axial direction than for a CbC + graphite mixture -- for which there is thermal expansion data.

Reinforced Oxide

The W-3% Re reinforced oxide was a newly developed composite material, and as such, had no previous measurements of physical and mechanical properties. The composite materials which were ultimately chosen for throat insert fabrication were selected on the basis of thermal shock tests and ability to be fabricated without cracks. Materials selected were zirconia (F 410) powder and 5 volume percent W-3% Re wire. Bend strength, modulus of elasticity, and thermal expansion properties were measured on the composite material. All other necessary property values were estimated from data reported in the literature for partially stabilized zirconia and tungsten - 3% rhenium wire.

Because the percentage of W-3% Re wire in the composite is relatively small, (5 volume percent) reasonably good estimates for thermal conductivity and specific heat could be made based on oxide and W-3% Re properties. Thermal conductivity estimates were made based on the ratios of volume percent wires and oxide, while the specific heat estimates were made using weight percent ratios. The following values were defined for the design calculations:

Thermal Conductivity

Temperature	BTU-ft/ft^2-hr-°F
70°F	4.66
2500°F	4.33
5000°F	3.93

Specific Heat

Temperature	BTU/lb/°F
70°F	0.1062
2500°F	0.1537
5000°F	0.1587

Modulus of elasticity measurements for the reinforced composite were made by sonic means and also calculated from the load deflection curves obtained from bend tests. The sonic modulus of elasticity of the composite was determined to be in the 18.0×10^6 psi range. Modulus values measured from the slopes of the load deflection curves were 11×10^6 psi for the "as fabricated" specimens and 0.95×10^6 psi for the thermally shocked specimens. Because the bend test fixtures were not completely rigid, the measured values are considerably lower than the true modulus. A value of 21×10^6 psi for the modulus of partially stabilized zirconia was obtained from the literature. The "as fabricated" modulus value was compared to the literature value, and the resulting ratio used to calculate the modulus for the thermally shocked material. A value of 1.85×10^6 psi was obtained, and this value was used for the design calculations.

Neither the expansion characteristics nor the composition of Zircoa F 410 were available from the vendor (considered proprietary). Without the expansion characteristics of the principal component of the reinforced oxide composite, it was impossible to make a reasonable appraisal of thermal expansion behavior of the composite for use in design analysis and stress calculations. Thus, an experimental determination of the expansion characteristics was made.

A thermal expansion specimen was machined from a pressed and sintered composite of Zircoa F 410 and 5 volume percent W-3% Re wires. Thermal expansion measurements were made in a Leitz dilatometer between room temperature and 1700°F. Total expansion of the composite specimen was recorded directly on photographic paper, and this trace is reproduced in Figure 69. Total expansion measured from the trace was then divided by the temperature interval to obtain the coefficients of thermal expansion. Added to the experimentally determined coefficients was a correction term of 0.3μ - inch/inch/°F to account for the expansion of the quartz specimen holders. The coefficients of thermal expansion for the W-3% Re fiber reinforced F 410 zirconia composites are illustrated in Figure 70, where the coefficients (correction term included) are plotted versus temperature.

Because of equipment limitations, it was possible to measure thermal expansion only up to 1700°F. Values for the thermal expansion were extrapolated from 1700°F to 4000°F on the basis that the stable structure was the tetragonal phase. The expansion characteristics of the tetragonal phase were measured between 1200 and 1700°F and then extrapolated, as indicated by the dashed line in Figure 69. The extrapolated values are indicated on Figure 70. Although it is recognized that rapid heat-up rates, as would be present in a throat insert, could possible affect the kinetics of the phase change, and thus affect the thermal expansion, there is no data to indicate the magnitude of this effect. In the worst possible case, the phase change could be completely suppressed and the expansion rate would be estimated at a maximum of 1.94×10^{-6} in/in/°F up to 4000°F.

The unusually low expansion values measured must be attributed to the proprietary Zircoa F 410 matrix. Furthermore, from the thermal expansion curve, it is evident that a phase change is initiated (on heat-up) at approximately 1000°F, and this change is completed by 1700°F. As with other partially stabilized zirconia systems, there is considerable hysteresis in the phase change when cooling down and this hysteresis is reflected in the thermal expansion curve because of the difference in volumes between the monoclinic and tetragonal phases.

THERMAL EXPANSION

Change in Length
Versus
Temperature
Reinforced Zirconia
(W-3% Re, 5v/o)

112   Figure 69

COEFFICIENT OF THERMAL EXPANSION OF
W 3% Re WIRE REINFORCED ZrO₂ (F-410)

ACTUAL DATA POINTS —○
EXTRAPOLATED DATA POINTS —●

113

Figure 70

The thermal expansion of a fiber reinforced zirconia composite is principally influenced by the oxide matrix because the fiber reinforcement accounts for only 5 volume percent of the composite. Expansion properties of the zirconia matrix are related to the degree of stabilization of the oxide. Pure zirconia -- unstabilized-- exhibits a phase change (a change in crystal structure from monoclinic to tetragonal) upon heating above approximately 1800°F. With this phase change, there is a significant volumetric contraction of the zirconia; and this contraction has a marked influence on the thermal expansion behavior. Since the tetragonal structure is more compact than the low temperature monoclinic structure, upon heating through the phase change region the zirconia contracts. When cooling down through the phase change region at non-equilibrium rate; i.e., 200°F per hour or faster, there is a considerable hysteresis in the phase change which, in turn, causes hysteresis in the thermal expansion behavior.

B. TASK II - FINAL DESIGN

Upon approval of the preliminary designs, the design analysis was initiated. The four designs selected for final design and fabrication were the prestressed design, the reinforced oxide design, the graded carbide design, and the refractory laminate design. The analyses were prepared in report form and are included herein as the subsequent sections. Design sketches of the as-tested units are included at the beginning of each design report.

1. Design Analysis - Prestressed Insert Design

a. Design Requirements

The structural and materials aspects of the design requirements for a rocket engine nozzle are deceptively simple -- maintain the original dimensions throughout the firing. While heretofore we have concentrated on implementation of these requirements in the throat area only, a new aspect of this requirement has been emphasized by the results of the firing at NASA/LEWIS of an SIVB attitude control unit furnished by TRW. Not only the throat area must be maintained, but also the configuration of the inlet section upstream from the throat.

The most likely modes of failure to be anticipated are as follows:

1. Loss of fragments of the insert either through the propagation of cracks that initiate on the back face from thermal shock or through spalling of the throat surface.

2. Erosion of either the throat or the inlet surface due to oxidation, other chemical reaction, or melting.

Means to satisfy the requirements of design against these modes of failure are restricted to the choice of materials and their configuration for the throat insert and backup and for the inlet ring. On this project, the injector characteristics and other engine variables are fixed, and some knowledge of them was gained from the SIVB firing.

To design against loss of fragments through cracking, thermal stresses in the insert must be minimized. To reduce tension on the back face, we have employed the prestressing concept; and to make the prestressed insert function properly throughout the duty cycle, there are three secondary requirements.

a) Minimize $\triangle$T across the insert to minimize thermal stresses.

b) Control the differential expansion of insert and prestressing hoop throughout the duty cycle to maintain enough hoop compression on the insert to prevent tensile fracture.

c) Control the temperature rise of the prestressing ring (as well as the stresses arising from differential expansion of insert and ring) to prevent plastic flow of the ring and subsequent loss of prestress.

Conflicts between these requirements have been resolved with the aid of a carbon liner for the prestressing ring, an annulus of insulating material placed between the insert and the prestressing ring. The results of studies of variations in the thickness and conductivity of the liner was given, and a compromise solution was described.

Design against erosion is a much less quantitative process than design against thermal shock. Because oxidation certainly promotes erosion and may well be a necessary pre-condition for erosion, the prime means for design against erosion are: (a) the choice of oxidation resistant, dense hard refractory material for the insert and inlet pieces, and (b) efforts to minimize surface temperature.

116

This latest design iteration attempts to meet the erosion/oxidation problems revealed in the failure analysis of the SIVB insert, to simplify the geometry of the insert and backup, and to reduce the temperature of the steel shell below 600 F, maximum during duty cycle.

b. Recommended Configuration

At the throat, the best combination of insert and backup materials found is illustrated in Figure 71 . It may be described as follows:

1. Tantalum carbide insert, 0.200 inches thick.

2. Carbon liner, 0.250 inches thick, between the insert and prestressing ring.

3. FS-85 columbium alloy prestressing ring, 0.200 inches thick.

4. Pyrolytic graphite heat sink, 1.35 inches thick installed with the high conductivity (a - b planes) radial.

5. Silica-reinforced phenolic insulator, 0.30 inches thick, which has been added in this latest design iteration to reduce the shell temperature.

6. Steel shell, 0.375 inches thick, standard for all designs.

The TaC insert has been shortened, and the concave back surface has been changed to a conical shape with a four degree taper for easier assembly in the prestressed condition.

Upstream from the throat, the inlet ring has been extended upstream to an area ratio of 3.9 in addition to being lengthened to accommodate the new insert configuration. The inlet ring material is tantalum - 10 percent tungsten, carburized on the exposed surfaces to a depth of approximately 0.015 inches. The JTA graphite ring formerly used was deemed inadequate in the light of the results of the SIVB firing.

c. Recommended Assembly Procedures

The initial prestress required to prevent cracking on the back side of the TaC insert, early in the firing, calls for an initial radial interference of 0.0023 inches on that surface. With a four degree taper, this amount of interference is equivalent to a relative axial motion of the insert and ring of 0.033 inches. The procedure will be to first lap the mating parts together -- insert, carbon liner and prestressing ring -- and note the relative axial position of insert and ring when firmly pressed together. Then machine a support piece for the ring with a stop for the insert that will permit final assembly in a press at the axial position required to achieve the desired interference -- .033 inches, axial. In assembly, the prestressing ring and carbon liner will be warmed to about 700 F to minimize the force required to push the insert in against the stop. Should there be a need to disassemble, a temperature rise of 2000 F is required if the assembly is heated uniformly. This is feasible, although an inert atmosphere would be required.

117

PRESTRESSED INSERT NOZZLE

White Silica (MX 2646)

Tantalum Carbide

Carbon Brick

FS-85

Pyrolytic Graphite

Ta - 10W Ring

JT-0981

Green Silica
(High Silica 184)

White Silica
(MX 2600)

Figure 71
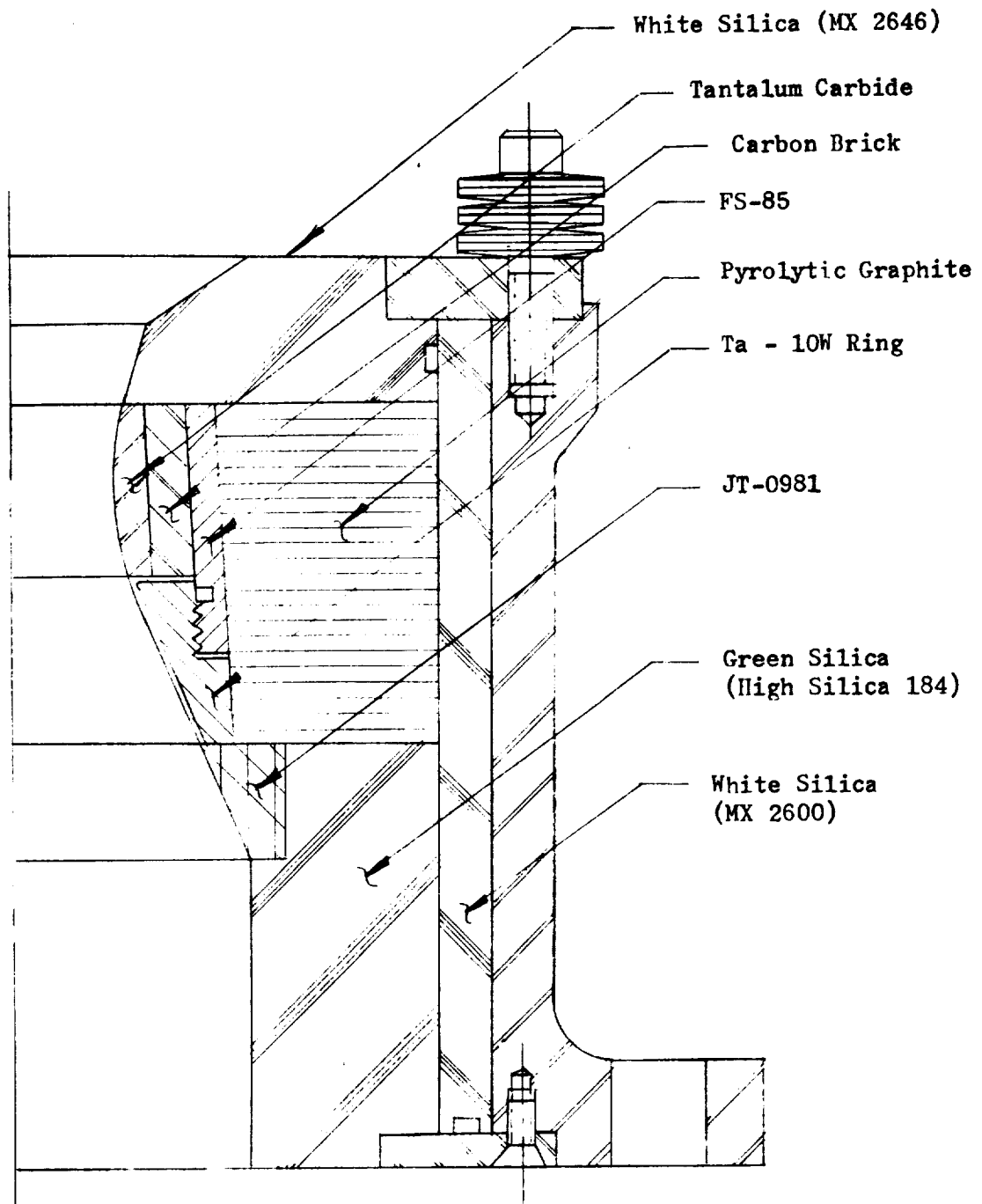
While the most direct check of the establishment of the initial pre-
stress actually obtained would be to check the decrease in throat diameter,
the amount of decrease is only 0.00050 inches. The OD of the prestressing
ring should increase 0.0036 inches (diametral expansion) and this will be
easier to measure accurately. The remainder of the 0.0046 inch diametral
interference is taken up in the carbon liner.

The next step in assembly is to trim the prestressed insert subassembly
to its final length. At the downstream end, the prestressing ring and carbon
liner are to be trimmed flush with the insert. At the upstream end, the
insert itself must be trimmed to match the diameter of the inlet ring at the
interface. This procedure is recommended to avoid the risks of grinding the
carburized surface of the Ta - 10 W inlet ring and to avoid thinning the
carburized layer. The upstream end of the carbon liner must also be trimmed
to match the insert.

If, for some reason, the inlet ring does not fit tightly against the
insert at all points around the circumference of the joint, it may be de-
sirable to insert a thin piece of pyrolytic graphite in the form of a flat
gasket. It will be clamped in place by the threaded connection of the in-
let ring and the prestressing ring.

Third step in assembly is to fit the pyrolytic graphite heat sink
piece snugly to the four degree taper on the back of the prestressing and
inlet rings and trim it to length. Three pieces of phenolic material --
an upstream piece, a downstream piece and an insulating sleeve -- must
then be finish machined to fit the subassembly, bonded to it, finish machin-
ed to fit the steel shell, and finally bonded into place in the shell. The
interior contour of the phenolic pieces will then be finish machined to the
proper configuration.

d. Results of Thermal Analysis

The calculation of temperatures in the insert and backup materials
along a radius at the latitude of the throat was based on the same assum-
ptions and principles previously described, with three exceptions. The
duty cycle studied was a 300 second steady firing. The effects of short
pulses also can be read from the temperature - time and stress - time
plots, assuming complete cool down between pulses and elastic behavior of
the assembly, which is true. The value of recovery temperature used was
4872 °F, and the value of convective heat transfer coefficient used was
1.20×10^{-3} BTU/in.^{2}, sec., degree F.

Results of the thermal analysis of the 300 second steady firing are
shown in Figure 72. Heavy lines denote the temperatures predicted for
the current configuration -- the one in which 0.3 inches of pyrolytic
graphite heat sink material has been replaced by phenolic insulation in-
side the steel shell. To show the effect of this change, the temper-
atures given for the previous design are shown by the light dashed lines.
Shell temperature was brought down from 1600°F to 360°F. Fortunately,
throat surface temperature at 300 seconds went up only 38 degrees. Maxi-
mum $\triangle$T across the TaC insert was unchanged -- 1163 degrees at 1 second
elapsed time. Temperature of the prestressing ring was raised 220 de-
grees after 300 seconds.

119
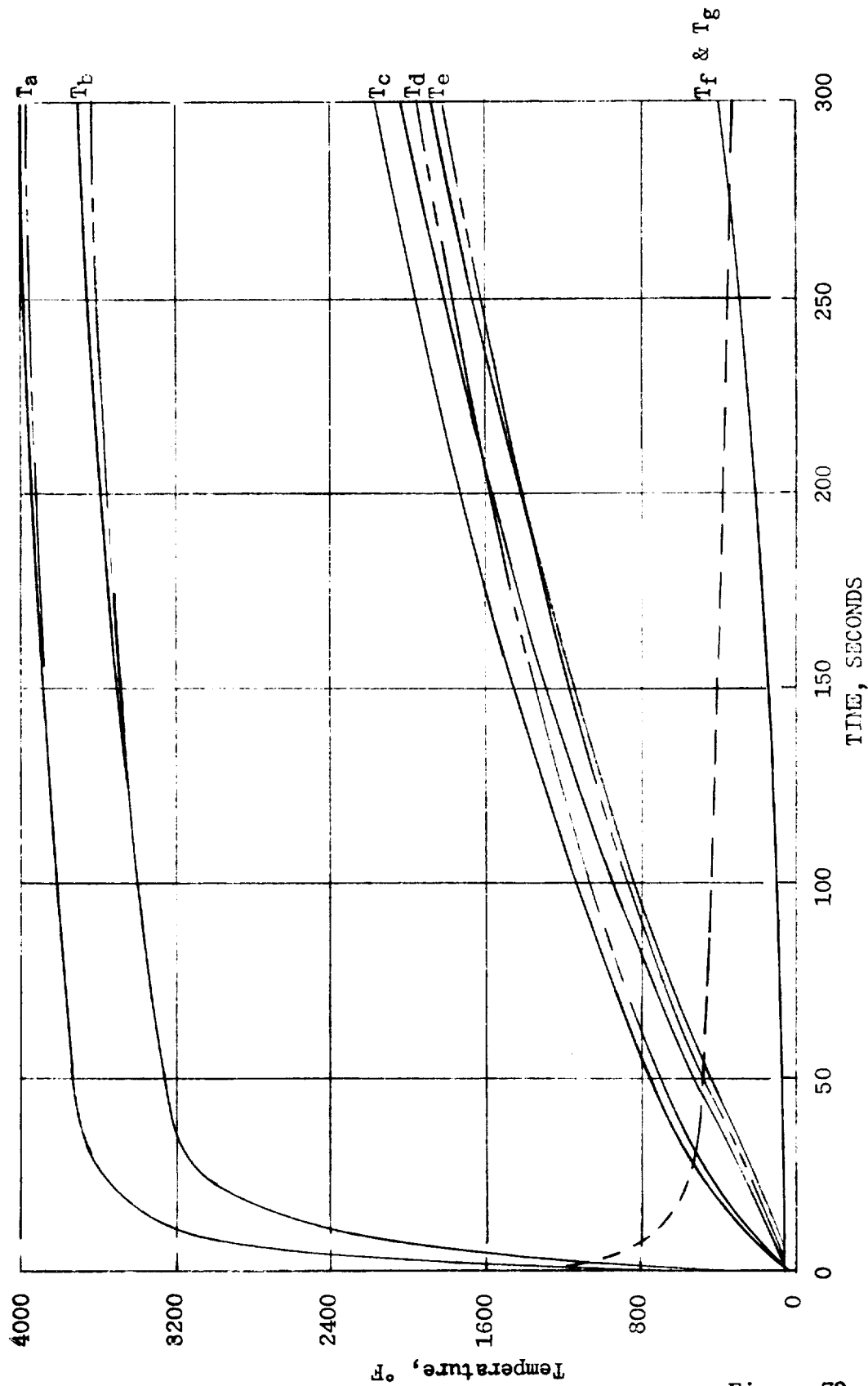
TEMPERATURE AT THROAT, T_a, BACK SIDE OF INSERT, T_b, INNER SURFACES
OF PRESTRESSING RING, T_c, OF PG HEAT SINK, T_d, OF PHENOLIC INSULATOR,
T_e, OF STEEL SHELL, T_f, AND OUTER SURFACES OF STEEL SHELL, T_g.
(Dashed lines are for case with no phenolic insulator)

Figure 72

120

The temperatures developed during the first 30 seconds of the firing are shown to an enlarged time scale in Figure 73. Figure 74 shows the radial temperature gradients at various times.

e. Stress Analysis

To simplify the stress analysis, the carbon liner was assumed to be a thin, segmented ring with no hoop stresses acting and with the same radial pressure acting on its inner and outer surfaces. Unlike the earlier situation, in which the heat flux was much less than that now contemplated, the maximum thermal stress now occurs early in the firing. There follows the additional problem of maintaining the proper amount of interference between the insert and the prestressing ring throughout the 300 second firing. Development of the interference resulting from differential expansion is described in Figure 75.

The effect of the interference stresses in reducing tension on the back side of the insert is plotted in Figure 76. The maximum tensile stress is reduced from 70 ksi at 3 seconds to 39 ksi at 1 second and to 26 ksi at 3 seconds. The accompanying temperature is less than 1300°F. The strength property data pertinent to this situation are meager. Published bend strength values at room temperature range from 30 to 40 ksi. Thus, if the heat flux is as high as we have assumed, and if it is established instantaneously as we have assumed -- say, in 0.1 second approximately -- the design is marginal in so far as thermal shock cracking is concerned. The reason for not going further in efforts to reduce the tensile stress lie in the other requirements of the design.

Compressive stresses on the throat surface of the insert are increased somewhat by the hoop compression induced by the prestressing ring, as shown in Figure 77. Allowable stress values in compression for this material are simply not available, even at room temperature, but an estimate of 200 ksi seems reasonable, based on tests of similar materials.

Stresses at the ID of the FS-85 prestressing ring, given in Figure 78 are in terms of the maximum shear stress $\tau_{max} = .5 (\sigma_\Theta - \sigma_r)$; because σ_r, the pressure of the carbon annulus on the ring, is quite significant. The yield strength in shear, taken as 0.6 of the tensile yield strength, drops off steadily with temperature, but the interference stress due to differential expansion (see Figure 75) also drops. At the maximum temperature -- 2165°F, attained at 300 seconds -- the governing material property should really be the short-time creep strength. Lacking such data, there exists some doubt about maintaining prestress at the end of a long firing. If this happened, performance probably would not be affected at that time; but during a subsequent pulse, the loss of prestress might be detrimental.
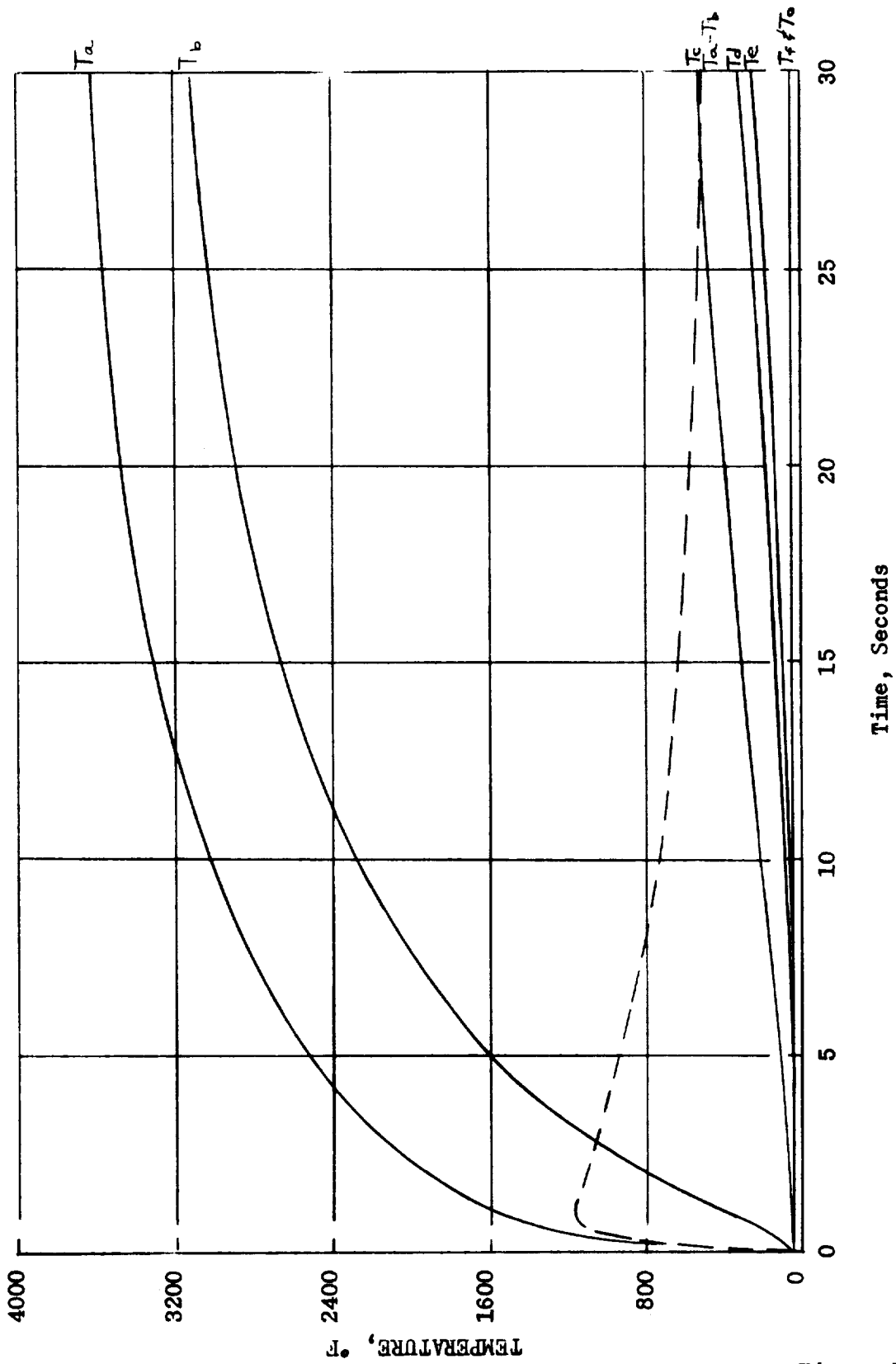
REPLOT OF THE FIRST 30 SECONDS OF THE RUN PLOTTED IN FIGURE 72

122
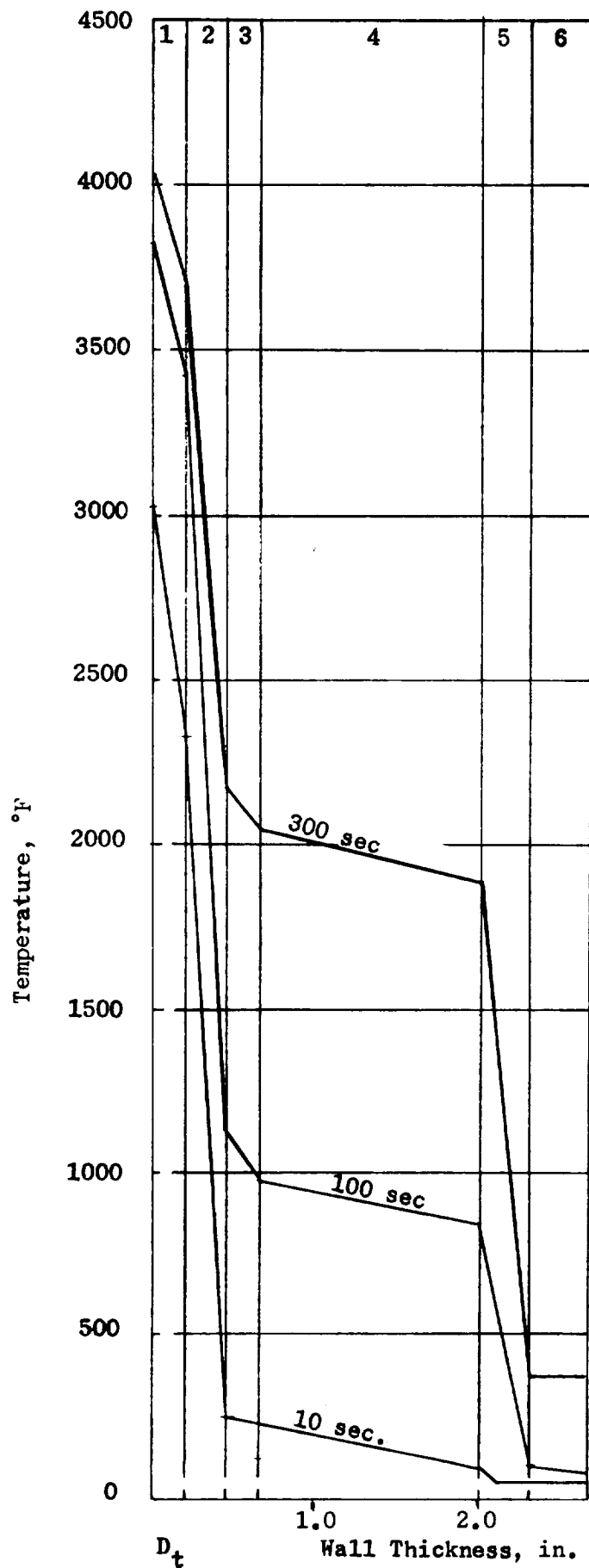
Figure 73

RADIAL TEMPERATURE
DISTRIBUTIONS AT
VARIOUS TIMES

1 - TaC
2 - Carbon Brick
3 - FS-85
4 - PG
5 - Silica Phenolic
6 - Steel

Figure 74

DIFFERENTIAL EXPANSION OF INSERT COMPONENTS

Figure 75

124
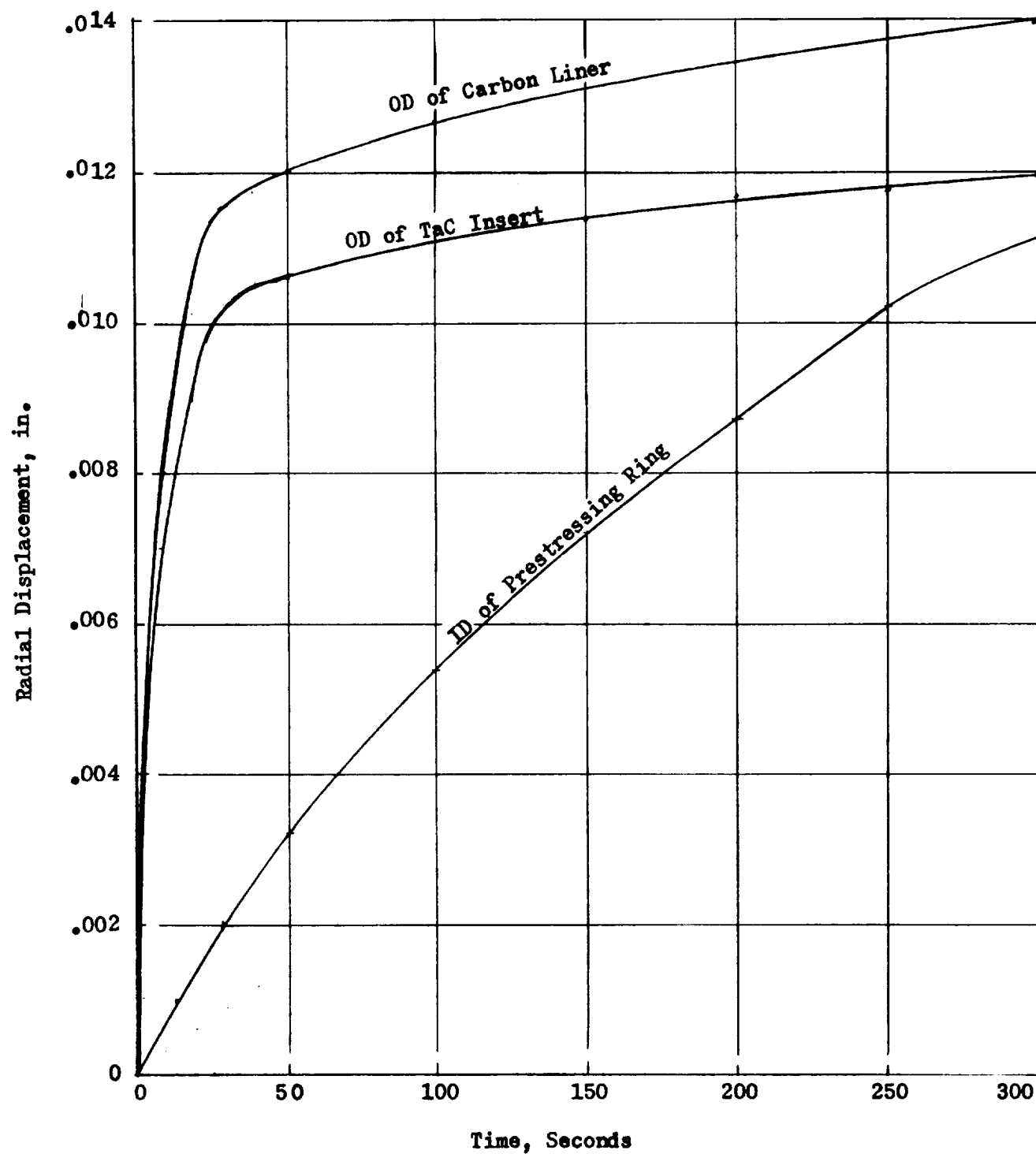
STRESSES AND TEMPERATURE AT
BACKSIDE OF THROAT   (TaC)

Figure 76

125
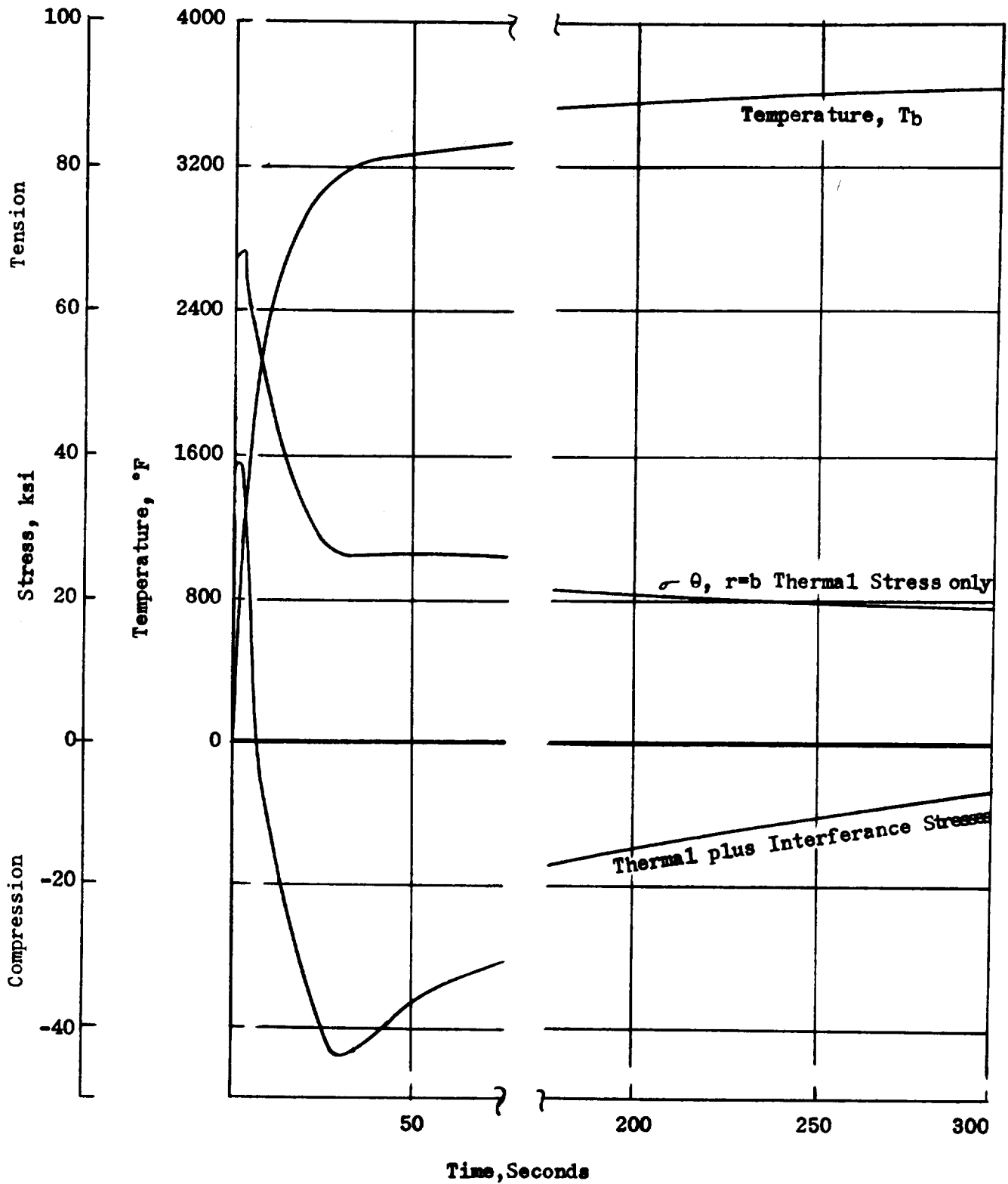
STRESSES AND TEMPERATURE AT THROAT (TaC)

Figure 77

126
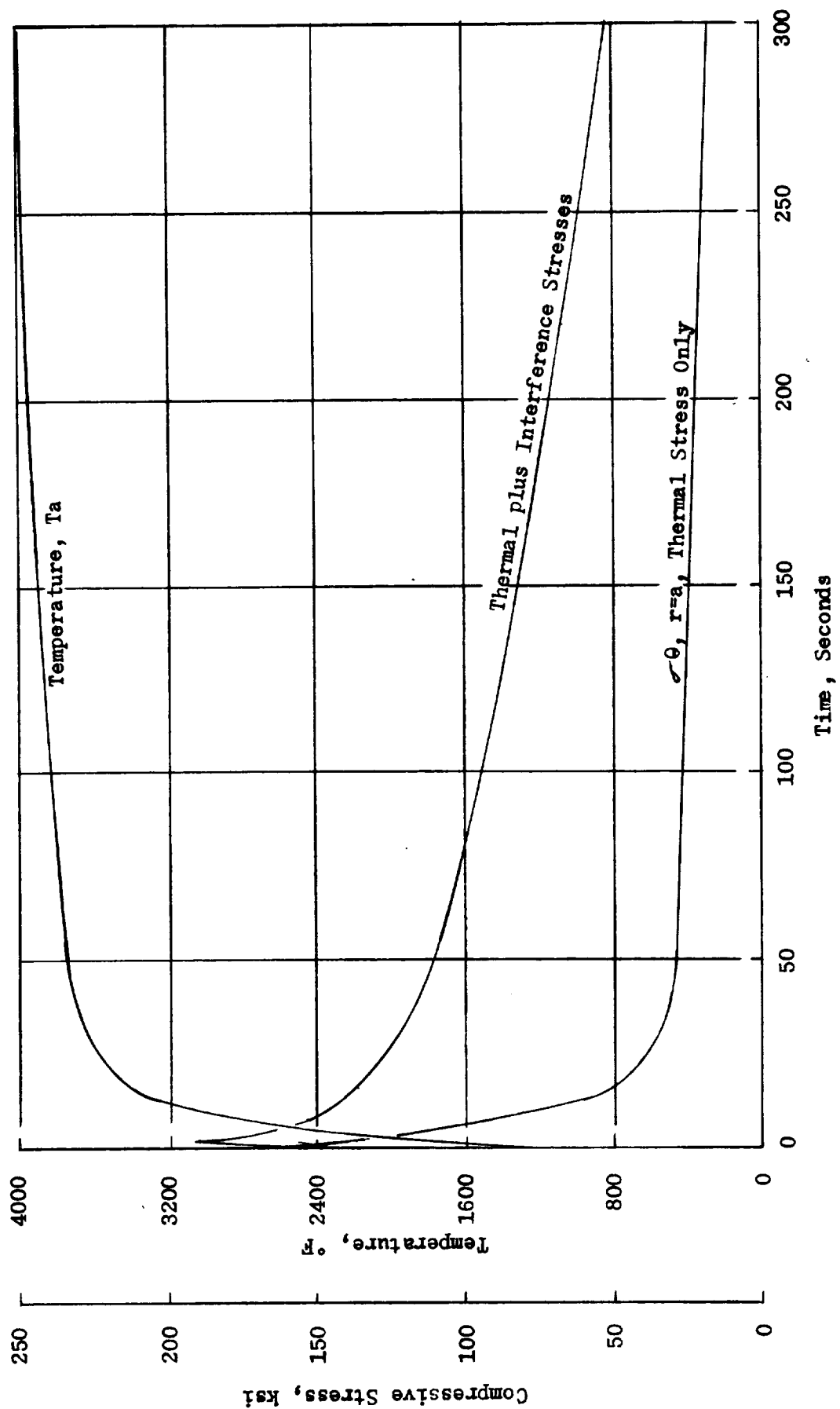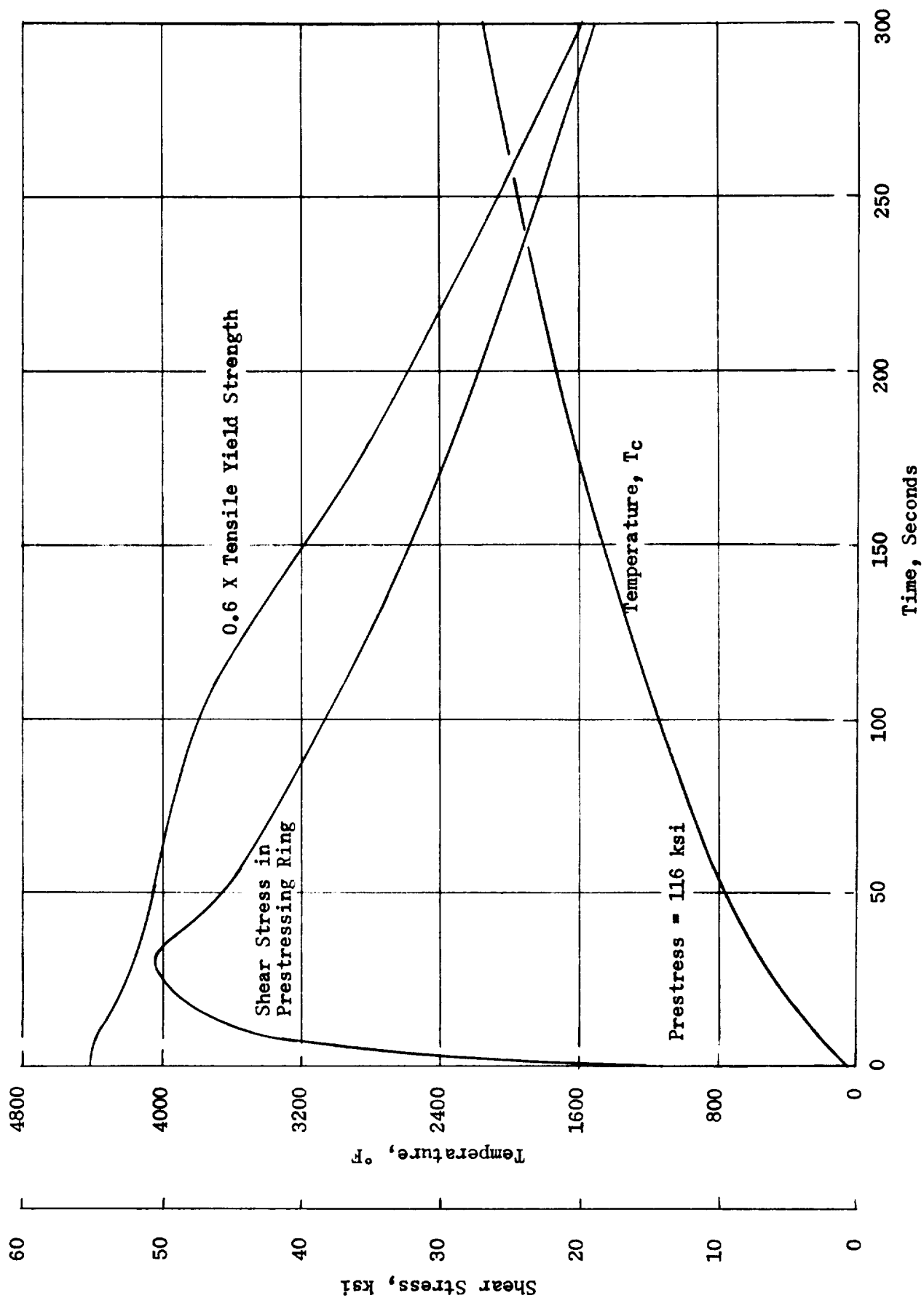
STRESSES AND TEMPERATURES IN FS-85 PRESTRESSING RING

Figure 78

127

f. Reasons For The Choice Of The Recommended Configuration

Tantalum carbide was chosen for the insert, because it has a combination of desirable properties: high melting point, fairly good oxidation resistance and relatively high thermal conductivity. The latter not only acts to reduce the throat surface temperature but also to minimize $\triangle$T across the insert. Hafnium carbide was ruled out because its conductivity is lower. Zirconium carbide is a close competitor. Thermal analyses showed negligible differences between ZrC and TaC. If the ZrO_2 scale that presumably will form during firing adhered to the throat surface, ZrC would be a very desirable insert material. Without some development work in this area, however, it seemed best to pick TaC. The thickness (0.200 inches) was made as small as could be fabricated readily. The edges are only 0.10 inches, with the new conical back surface, and anything less would be likely to chip in handling.

The columbium alloy, FS-85, was chosen for the prestressing ring instead of molybdenum or tungsten alloys, because it has a higher coefficient of expansion. It also has high strength in the temperature range 1000-2500 F. Even so, it was evident in the discussion of the stress analysis that the thermal expansion of the prestressing ring lagged that of the insert (Figure 75). To avoid overstress at times of about 50 seconds, it was necessary to reduce the initial interference (prestress) as much as possible.

In earlier designs, the pyrolytic graphite backup material between the prestressing ring and steel shell was chosen for its high thermal conductivity, for this was to be a radiatively-cooled design. Now this concept has been ruled out by NASA, and an insulating sleeve of phenolic has been introduced between the pyrolytic graphite and the shell. Fortunately, the pyrolytic graphite functioned so well as a heat sink that over 80 percent of the heat flux accumulated in a 300-second firing was stored in it, and less than 20 percent was radiated from the shell surface. In the new design, therefore, the temperature rise in 300 seconds is moderate. Longer firings obviously would cause more severe increases in the temperature of the throat and of the prestressing ring, with increasing damage from oxidation/erosion of the throat and from loss of prestress.

Pyrolytic graphite (a - b planes radial) still remains a good choice for the backup material. As a heat sink, it has high heat storage capacity in terms of BTU per cubic inch (the critical quantity here, since this design is space limited rather than weight limited). In addition, its exceptional thermal conductivity facilitates storage of the heat throughout its mass and minimizes the temperature of the prestressing ring and insert. Note in Figure 74 how flat the radial temperature gradient is in the pyrolytic graphite at all times.

At 300 seconds, the pyrolytic graphite heat sink piece will have expanded about .050 inches, axially. This is about 0.030 inches more than the prestressing ring, which causes concern that differential expansion might open a gap at the ends of the insert. Probably at the aft end only, because the 4 degree taper would prevent relative forward motion of the pyrolytic graphite. However, there is a compensating differential expansion of the phenolic refrasil piece used for the exit cone.

128

Its hot, inner surface will expand axially at least 0.050 inches more than the material 0.5 inch back from the surface, leaving a gap at that point into which the pyrolytic graphite can expand. There was additional concern that the 0.040 inches differential expansion of the heat sink relative to the steel shell will overstress the cap screws holding the retaining ring. To prevent this, Belleville washers were used under the screw heads.

Silica phenolic was chosen for the insulator inside the steel shell, because it combines good mechanical strength and easy fabricability with low thermal conductivity.

Major emphasis was placed on the choice of material and on the thickness of the liner between the prestressing ring and insert. Because the liner must function as a thermal barrier, its thickness and conductivity are prime considerations. Other characteristics desired were a low coefficient of expansion and low elastic modulus, so the thickness increase of the liner from its own thermal expansion would be offset by its elastic compression. Another requirement was good compressive strength at high temperatures to transmit the radial pressure elastically. Carbon seemed to possess these secondary characteristics to a higher degree than any other material except possibly pyrolytic graphite (c direction radial). However, the thickness of pyrolytic graphite equivalent to 0.25 inches of carbon would be only about .070 inches, which causes some geometric problems in assembly of the prestressed insert to the inlet ring and also presents a handling problem in fabrication.

Justification for the choice of carbon, 0.25 inches thick, for the liner can be made most readily by showing the results of several trial analyses. In Table V , the results for carbon and pyrolytic graphite (c direction radial) are compared on the basis of the effect of the ratio of thickness to conductivity, "t/k", on various design requirements. If no liner were used (t/k = 0 as shown in the first column), the advantages would be: a decrease in throat surface temperature of 300 degrees below that found for the chosen configuration, and greatly reduced interference from thermal expansion. The disadvantages would be: a large increase in the tension on the back side of the insert, and an unacceptable temperature of the prestressing ring after 300 seconds.

On the other hand, the value of t/k can be made too large, as shown in the two columns to the right of that for carbon, 0.25 inches thick. Throat temperature rises to values where oxidation/erosion may be serious, and the interference stresses would yield the prestressing ring. Referring to Figure 77 it is clear that even with the .25 inch carbon liner, the interference builds up more than is needed to keep tensile stresses in the insert low. Yet, as shown in Figure 78 , the temperature of the prestressing ring is so high that the yield strength is dropping rapidly. Ideally, the solution lies in finding materials for insert and prestressing ring with a large difference in coefficient of expansion -- preferably, an insert material with less thermal expansion.

Reasons for the choice of Ta - 10 W with a carburized surface for the inlet ring were as follows. The SIVB firing had revealed an erosion problem upstream from the throat. A second prestressed ceramic piece for the inlet would have performed best, but there were geometric difficulties. Principally, the 25 degree cone angle cannot be used for the back side of the ceramic piece, because friction may not be high enough to prevent axial motion with loss of prestress. A reduction in this angle to four degrees would cause an undesirable thickness increase in the lower end of the ceramic piece. Although the carburized Ta - 10 W ring required some study to be sure that the thickness of the carburized layer is going to be the desired amount, there are certain advantages, as follows. From the erosion/oxidation standpoint, the surface material exposed to the gas stream is the same (chemically) in the inlet ring as in the insert. From the thermal shock standpoint, there is no problem, for the Ta - 10W ring is ductile. Spalling is the new mode of failure that possibly will be introduced by the use of the carburized piece. Fortunately, the coefficient of expansion of TaC matches that of Ta - 10 W well -- both are about 3.5×10^{-6} per degree F. The alloy, Ta - 10 W was chosen instead of pure tantalum because the alloy has better high temperature strength and also better machinability, which is important for this threaded part.

2. Design Analysis - Graded Carbide Design

a. Objective

The basis of the NASA Insert program is to provide an insert that will withstand the environment as defined in the program contract and observed in a test of a TRW provided SIVB nozzle. Based on other previous test results and the SIVB test results the primary efforts have been directed toward materials development.

b. Design Review

The graded carbide throat insert was designed to take maximum advantage of the carbides high temperature material properties and yet provide a design coping with associated thermal stress problems. The pure carbides have shown extreme susceptiblity to thermal shock failure. If they are to be utilized as throat inserts some means must be devised to overcome this problem. The most promising method appears to be a layered structure where the inner layer of pure carbide is supported by successive outer layers of carbide with increasing graphite mixtures. Structures of this type have been exposed to thermal shock conditions and have demonstrated excellent thermal shock resistance--that is, the backup layer or layers do not fail by cracking on the outside diameter surface (Ref 1, 2, &3). The type of failure invariably experienced is cracking of the inner layer. Tests have been conducted on a number of throat inserts composed of a pure carbide inner layer and a single backup layer of CbC + 70 volume percent graphite (CbC = 70G). There were no backup layer failures, but all of the pure carbide inner layers failed. Examination of recently generated thermal expansion data shows that CbC + 70G has a very high axial (parallel to direction of pressing) expansion, thus resulting in a large mismatch in expansion between the pure carbide layer and backup material. Radial (perpendicular to the direction of pressing) expansions of the HfC and CbC + 70G are relatively close, but the large mismatch in expansion in the axial direction will result in excessive stresses at the interface. Thus, it is not surprising to find a tendency for the inner layer to separate from the outer layer. In fact, a compilation of available firing data for layered carbide structures (Ref. 3) vividly shows that all mechanical failures observed are directly related to the inner layer. In only one expectional case did failure of the backup layer occur, and this failure was attributed to unsound material.

Another factor affecting the choice of materials was the amount of support each succeeding layer could give to the inner carbide layer. In the throat insert tests referenced in the previous paragraph, there was a great difference in modulus of elasticity values for the layers, i.e., -- pure carbide $\approx$ 50 X 10^6 psi and CbC + 70%G $\approx$ 3 X 10^6 psi. Thus the backup material could strain easily and fail to give adequate support to the inner layer.

c. Material Selection

Hafnium carbide (HfC) was selected as the inside liner material that would be exposed to the gas stream. The selection was based on reactivity tests conducted in CO_2 at 100 mm pressure at elevated temperature. Of the materials tested, only HfC and TaC survived 120 seconds exposure at the maximum test temperature of 4500°F.

At 4000°F both of these materials showed very little erosion, but the HfC has a white, adherent oxide while the TaC has a glassy appearing surface as a result of extensive oxide melting. At 4500°F both materials had significantly more erosion than at 4000°F, with HfC having the greatest erosion and some blistering of the oxide. However, testing these materials in a static atmosphere probably allowed the molten oxide on the TaC to offer some oxidation protection. In the dynamic environment of a throat insert, the exhaust gases would probably blow away the molten oxides, thus exposing a fresh surface to the oxidizing gases. With the protective oxide surface washed away, there is a distinct possibility that high erosion rates would be encountered with TaC. On the other hand, HfC forms a solid oxide scale that appears to be adherent to the substrate. This oxide surface is far more likely to remain in place than the molten oxides formed on TaC. For this reason, HfC was selected as the layer of the throat insert that will be directly exposed to the exhaust gases.

The primary objective of the back-up layers of carbide plus graphite is to give support to the inner layer of pure carbide without causing excessive stresses due to mismatches in thermal expansion. The first backup layer of TaC + 10%G has the best thermal expansion match with HfC, considering both the temperature profile and radial and axial expansions; and also the TaC + 10%G has a relatively high modulus of elasticity, $\sim$ 27 x 10^6 psi at room temperature. The second backup layer of TaC + 40%G serves to match the thermal expansion to the third backup layer, which is TaC + 70%G. This material has excellent thermal shock resistance and provides the required over-all structural support to the throat insert. The final design is shown in Figure 79.

d. Thermal Analysis

The insert design, as stated earlier, was determined by two prime factors; oxidation resistance and thermal stress. The selection of the oxidation resistant material was previously discussed. The selection of the material for the outer layers of the insert material was made on the basis of matching thermal expansion and modulus of elasticity. Matching of thermal expansion and modulus is one method to reduce the effective thermal stress in the insert.

It should be noted at this time that, while considerable materials data was available, the materials were not at that point of development where data was available over the temperature ranges that were anticipated. In addition, data for the carbides with varying amounts of graphite has been extremely difficult to obtain. Much of the data obtained from material suppliers has been for materials which are still in the process of being tested for physical and mechanical properties. A result of this is that many of the material properties are extrapolations from known data. An example of this is shown in Figure 80. The thermal coefficient of expansion for tantalum carbide plus graphite for 10, 40, and 90 percent was available between 1800 and 4500°F. This necessitated extrapolating the curves down to 1000°F and developing a complete curve for TaC + 70%G. A similar method was used in determining the modulus of the insert materials over the required temperature range. Figure 81 shows the modulus of elasticity versus temperature for the insert materials. The modulus for graphite was known, room temperature data points were known, and additional data was available from a Bureau of Mines Report for arc-cast HfC. The curves over the temperature range were developed from these points. It should also be noted here that much of the available data is the result of a single test rather than a series of tests leading to a statistical determination of property values.

132

GRADED CARBIDE INSERT DESIGN

Silica Phenolic

Graded Carbide

CGW Graphite

Carbon Cloth Phenolic

Silica Phenolic

JT-0981 Graphite

Green Silica Phenolic
(High Silica 184)

133   Figure 79
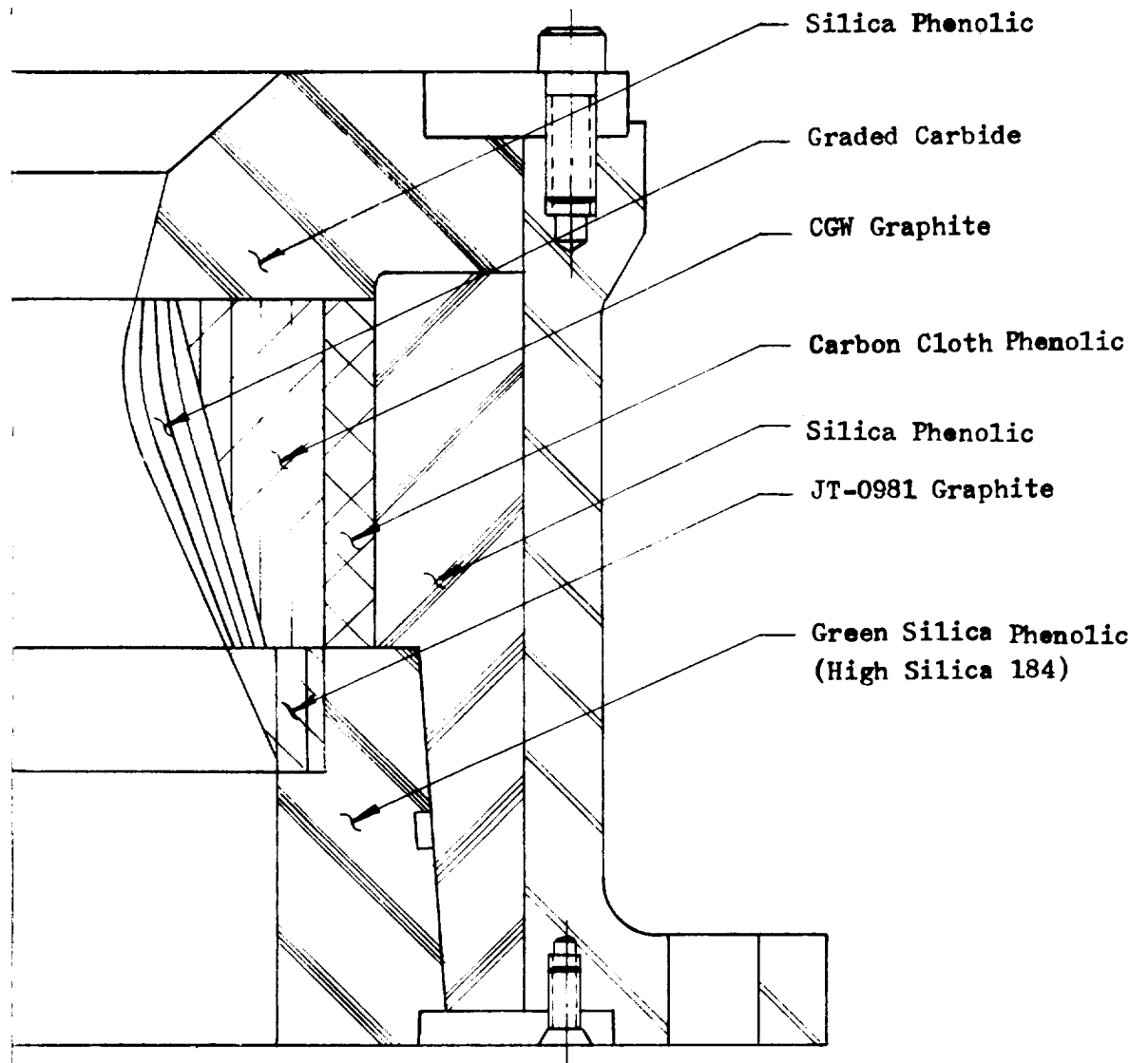
COEFFICIENT OF THERMAL EXPANSION
VS
TEMPERATURE
(Radial Direction)

Figure 80

134

COEFFICIENT OF THERMAL EXPANSION
VS
TEMPERATURE
(Axial Direction)

Figure 80 (continued)

135
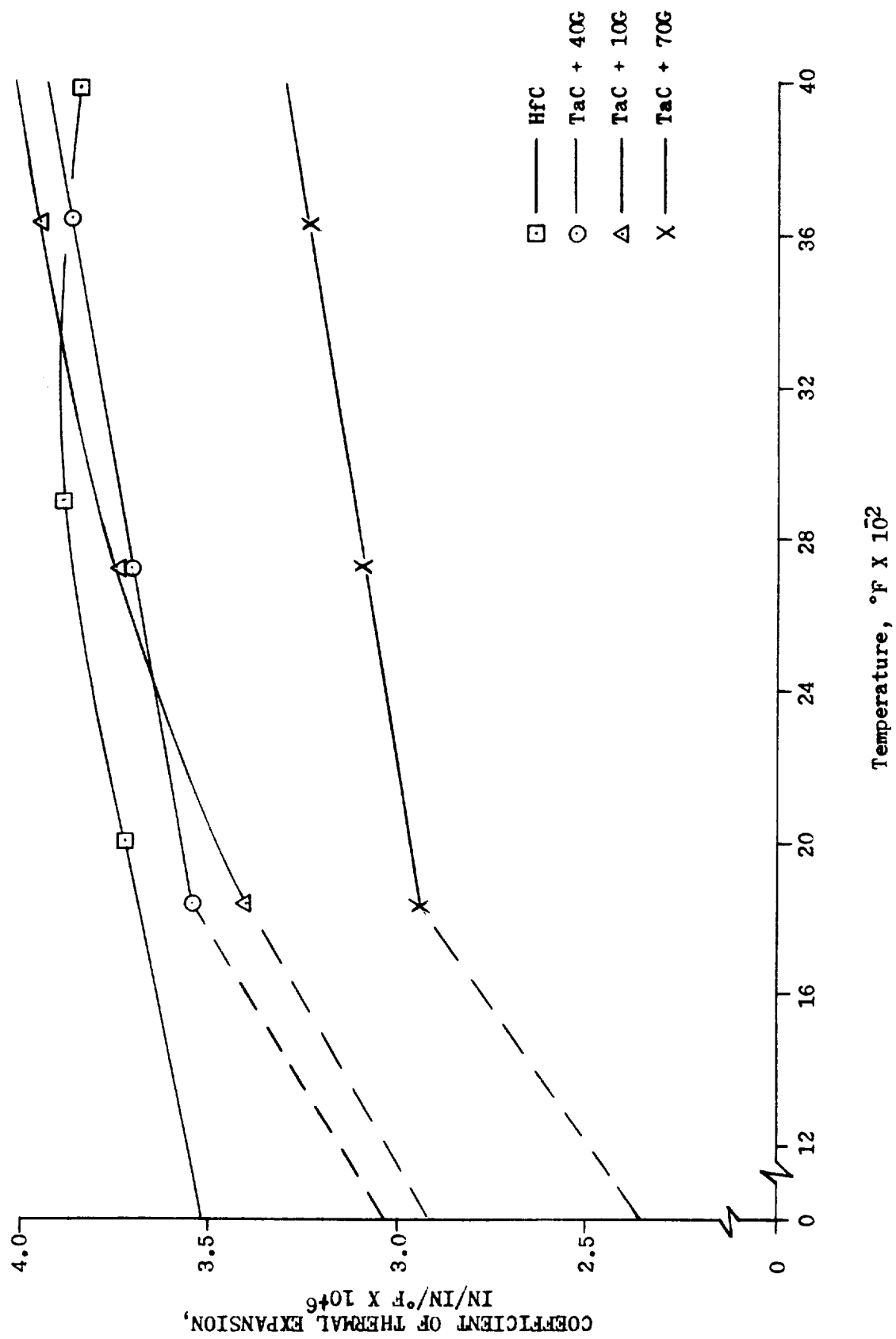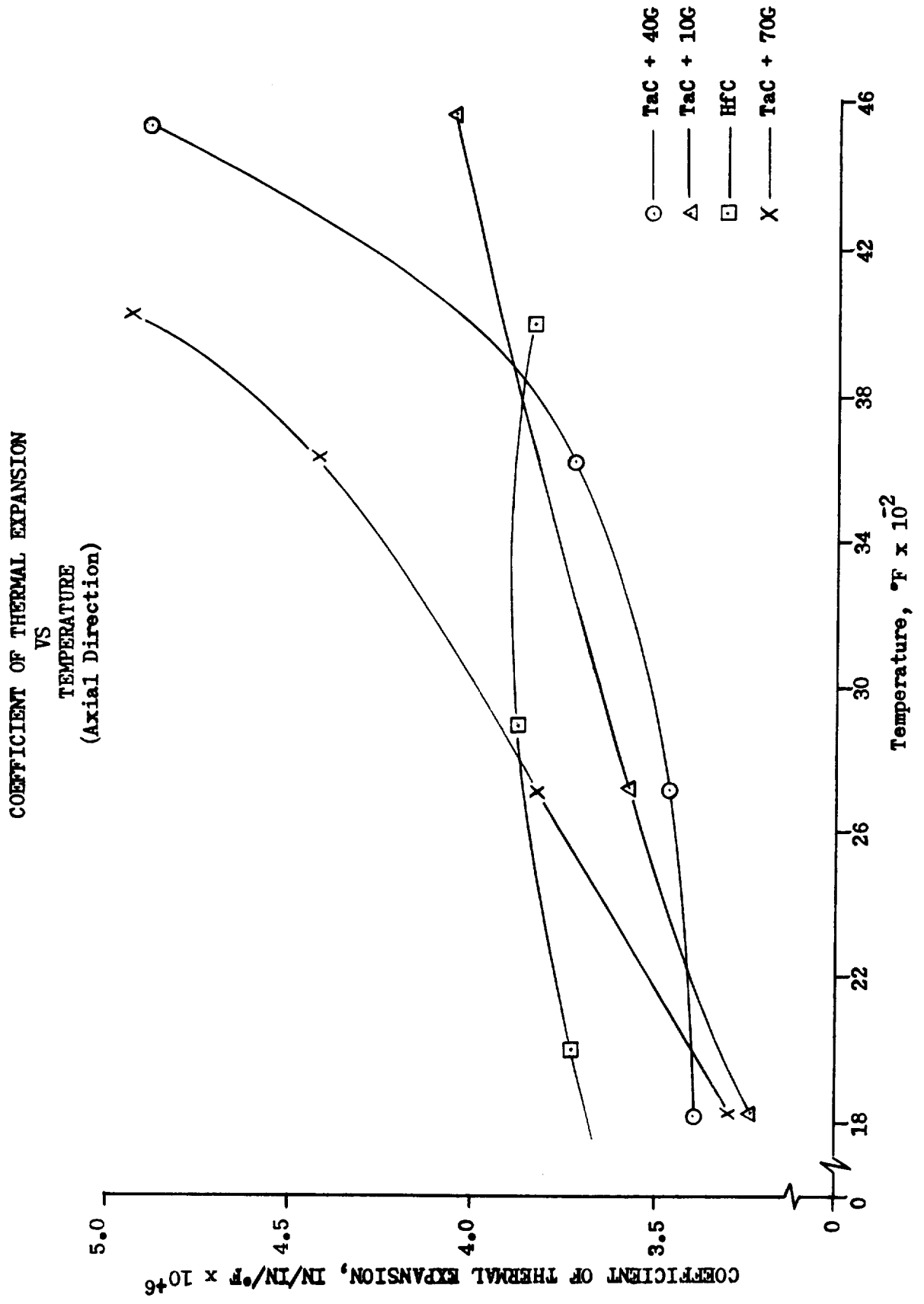
MODULUS OF ELASTICITY
(Estimated)
VS
TEMPERATURE

⊙ Actual Data Point

X Arc Cast HfC
(Bureau of Mines Rpt
26, March 1965)

Figure 81

136
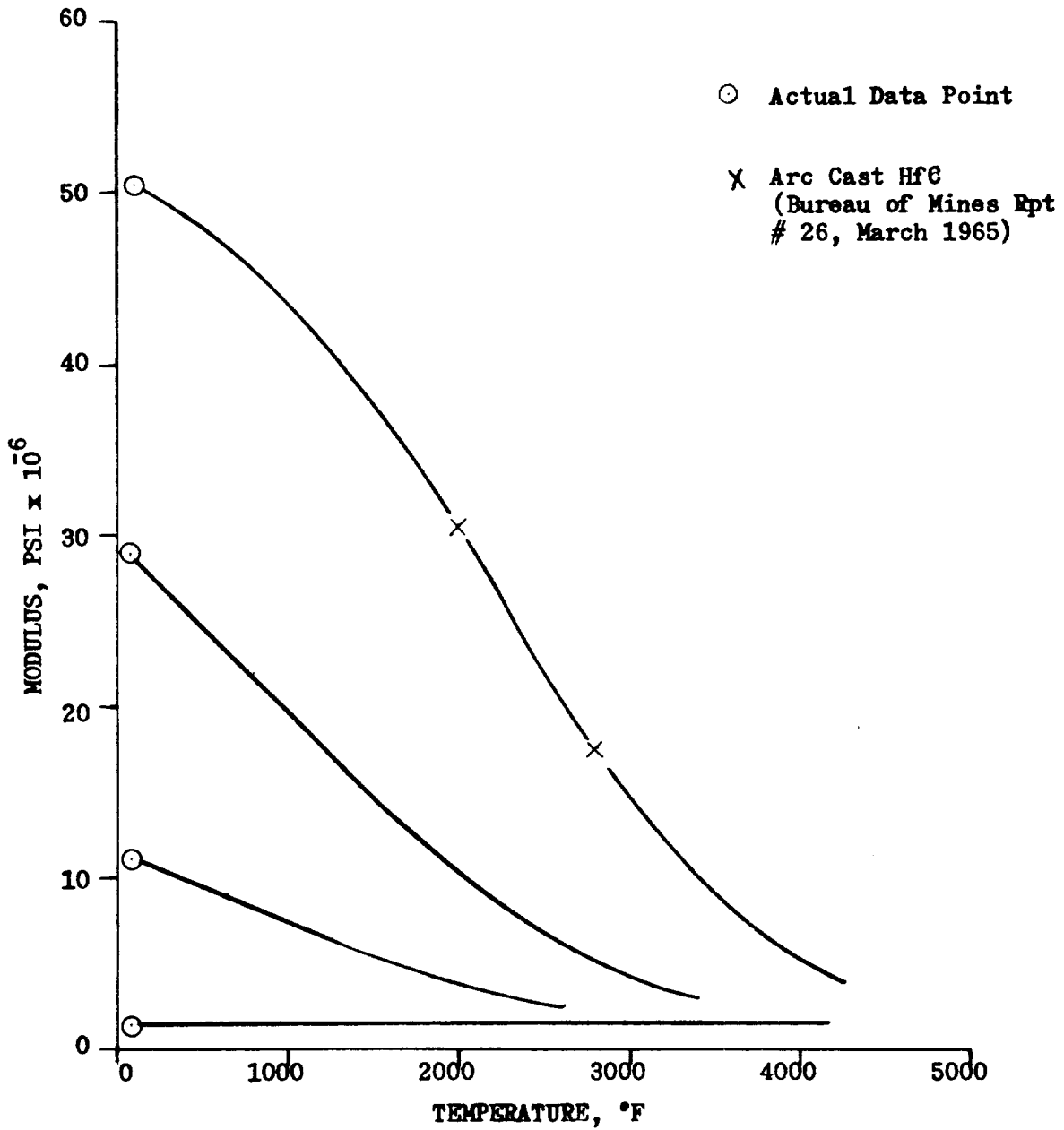
The carbides of columbium, hafnium, zirconium, and tantalum were evaluated as possible backup materials for the HfC liner. The columbium carbides (Figure 82) were rejected because the coefficients of thermal expansion were generally higher than that of the HfC. This would produce a high tensile stress on the outside surface of the HfC caused by the outer layer trying to expand more rapidly than the inner layer. While the carbides with a high volume percentage of graphite were in a usable range, they also possess a very low modulus (Figure 83) which would not permit an adequate support for the inner layer.

Hafnium carbide was rejected for use because of the extreme variation of the thermal expansion over the temperature range (Figure 84) for the carbide plus graphite. Evaluation of the HfC plus graphite did not proceed beyond this point; but it may be noted in Figure 85 that, similar to the other carbides, the modulus decreases with increasing graphite content.

The Zirconium carbide plus graphite did not have the amount of data that generally was available for the other materials. Figure 86 shows the coefficient of thermal expansion over a temperature range from 1800 to 2500°F. While minimum data was available, the zirconium carbide was not pursued further because the available data showed thermal expansion to be considerable higher than HfC.

The tantalum carbides plus graphite all have thermal expansion coefficients less than that of the HfC (Figure 79). This permits the layer external to the HfC to maintain a compressive stress on its inner surface and, in turn to reduce the tensile stresses on the outside surface of the HfC. Figure 87 shows that the modulus decreases for increasing amounts of graphite. The decreasing modulus is undesirable but cannot be avoided if the thermal expansion coefficient is to be varied to permit matching of the $\alpha \Delta T$ values (radial thermal expansions).

After selection of the insert materials, it is necessary to provide back-up support for the insert and insulation for the steel support. Graphite was selected as the throat support material because of its strength and thermal conductivity. For insulation between the graphite and the steel support, the selection was silica phenolic cloth. However, if the graphite was in direct contact with the silica phenolic, the temperatures would be such that reinforcement melting would occur at the interface. To prevent this, carbon phenolic was used between the graphite and silica as an insulator.

Figure 88 shows a temperature profile at the throat for the first sizing of material thickness. The material thickness and location are shown in the following schematic cross-section:

COEFFICIENT OF THERMAL EXPANSION
PERPENDICULAR TO HOT PRESSING DIRECTION (RADIAL)
Graded: GRADED CARBIDES
CARBOROUNDUM

TEMPERATURE, °F X 10^{-2}

IN/IN/°F X 10^{+6}

COEFFICIENT OF THERMAL EXPANSION

138   Figure 82
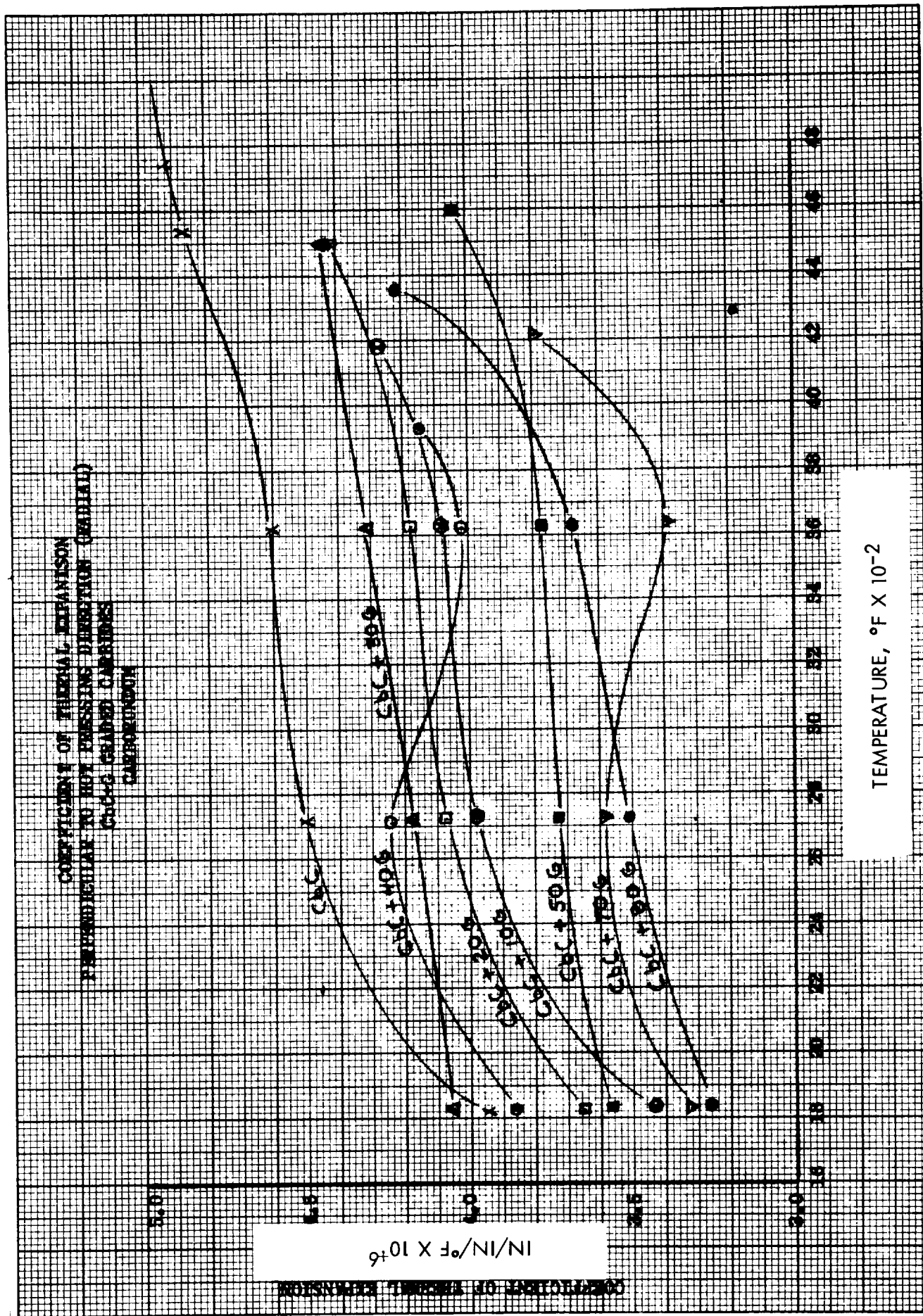
COLUMBIUM CARBIDE
MODULUS OF ELASTICITY
VS
GRAPHITE CONTENT

KEY	Porosity Volume %	Grain Direction
O	5	With Grain
□	5	Across Grain
O	0	With Grain
X	0	Across Grain

Modulus of Elasticity/IP.S.I.

Carbide - 40   50   60   70   80   90
Graphite - 60   50   40   30   20   10
Composition - Volume %

139

Figure 83

COEFFICIENT OF THERMAL EXPANSION
B₄C CLADDED CARBIDE
PARALLEL TO HOT PRESSING DIRECTION

Legend:
▲ B₄C
○ B₄C+20%C
□ B₄C+50%C
✕ B₄C+90%C

TEMPERATURE, °F X 10⁻²

IN/IN/°F X 10⁶

COEFFICIENT OF THERMAL EXPANSION
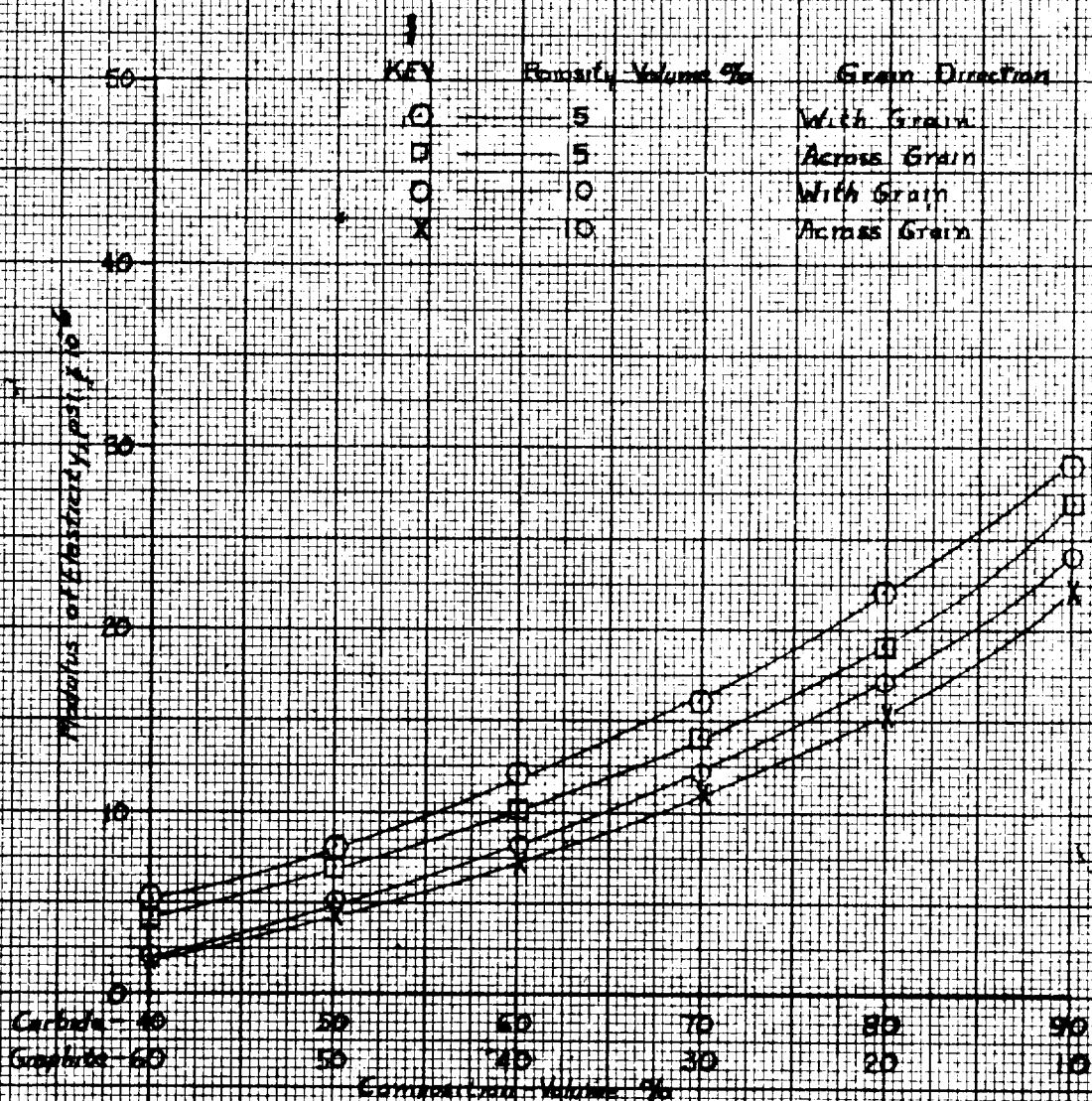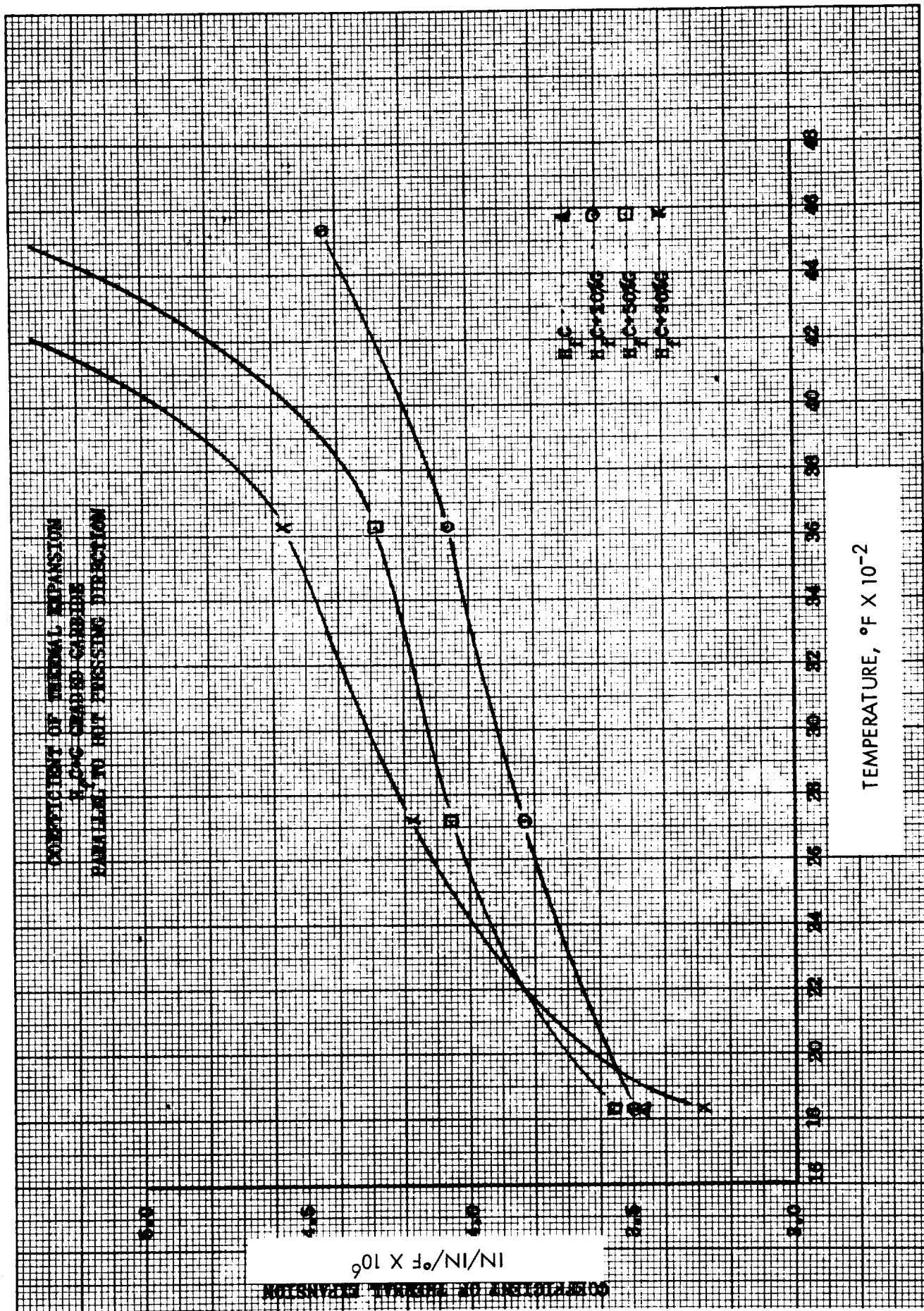
MODULUS OF ELASTICITY
VS
GRAPHITE CONTENT
(Hafnium Carbide)

Key	Porosity - Volume %	Grain Direction
⊙	5	With Grain
⊡	5	Across Grain
○	10	With Grain
X	10	Across Grain

Composition, Volume Percent

COEFFICIENT OF THERMAL EXPANSION
ZrC-C GRADED CARBIDES
CARBORUNDUM

Figure 86

142
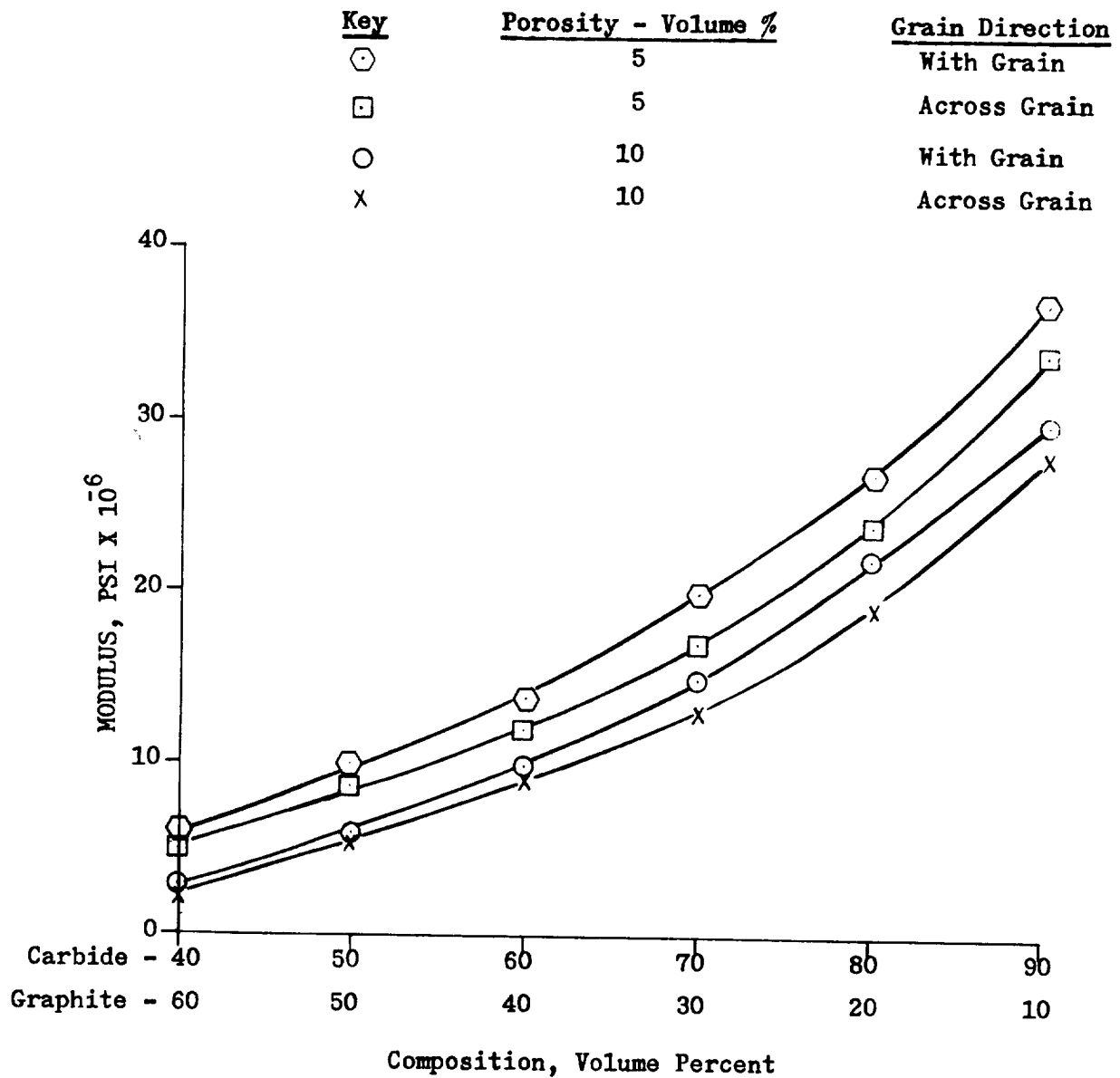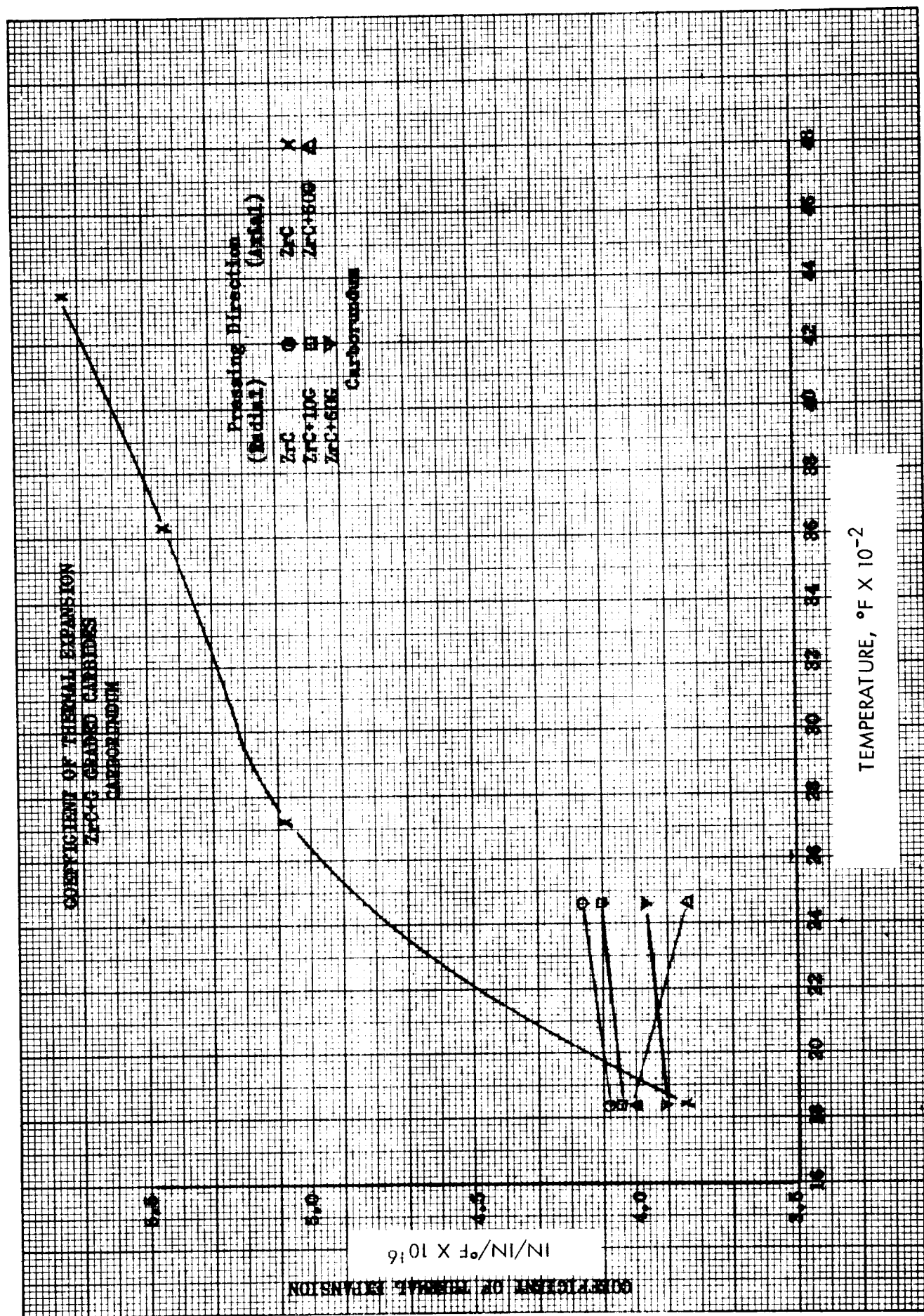
MODULUS OF ELASTICITY
VS
GRAPHITE CONTENT
(Tantalum Carbide)

Key	Porosity – Volume %	Grain Direction
⬡	5	With Grain
☐	5	Across Grain
○	10	With Grain
X	10	Across Grain

143

Figure 87

TEMPERATURE PROFILE
GRADED CARBIDE

Figure 88

	.4	THROAT INSERT
	.5	GRAPHITE
	.25	CARBON PHENOLIC
	1.1	SILICA PHENOLIC
	.4	STEEL
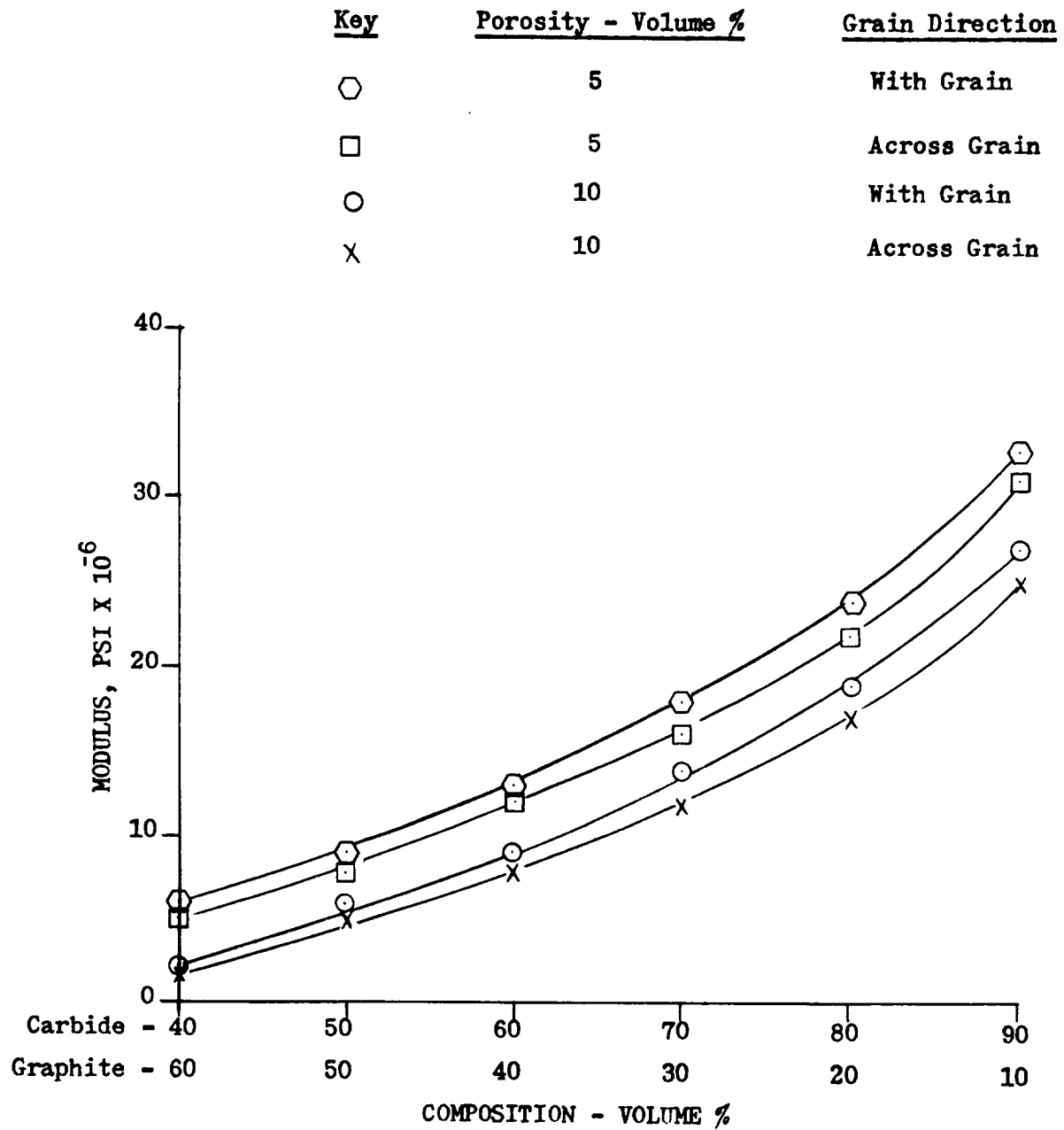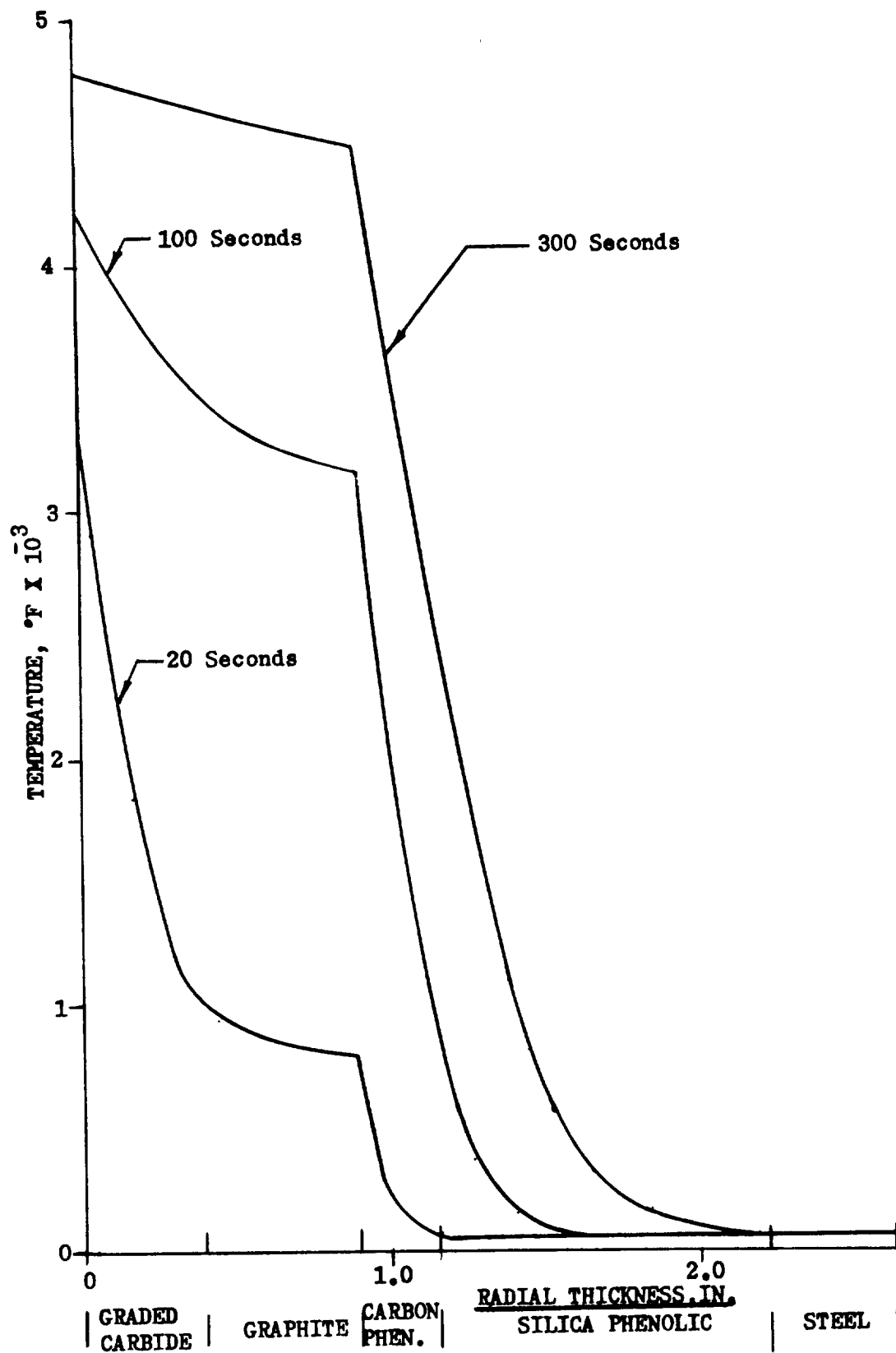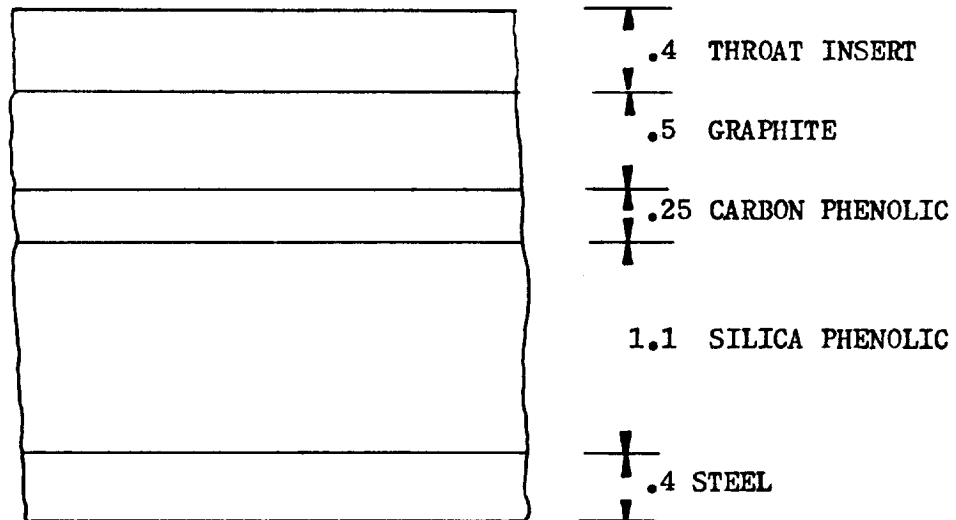
At 300 seconds the temperature profile indicates a temperature of 2600°F at the carbon phenolic-silica phenolic interface. The silica reinforcement melts at approximately 3000°F. To prevent this and to keep the interface at a safe temperature, 2300°F was selected as a maximum temperature. The temperature profile also indicates the silica-steel interface will be at room temperature for a radial thickness of 0.15 inch indicating a degree of over-design in the thickness of the silica.

To reduce the temperature at the carbon phenolic-silica phenolic interface and to take advantage of the overdesign of the silica thickness the design was modified as follows:

	.4	THROAT INSERT
	1.0	GRAPHITE
	.25	CARBON PHENOLIC
	.6	SILICA PHENOLIC
	.4	STEEL
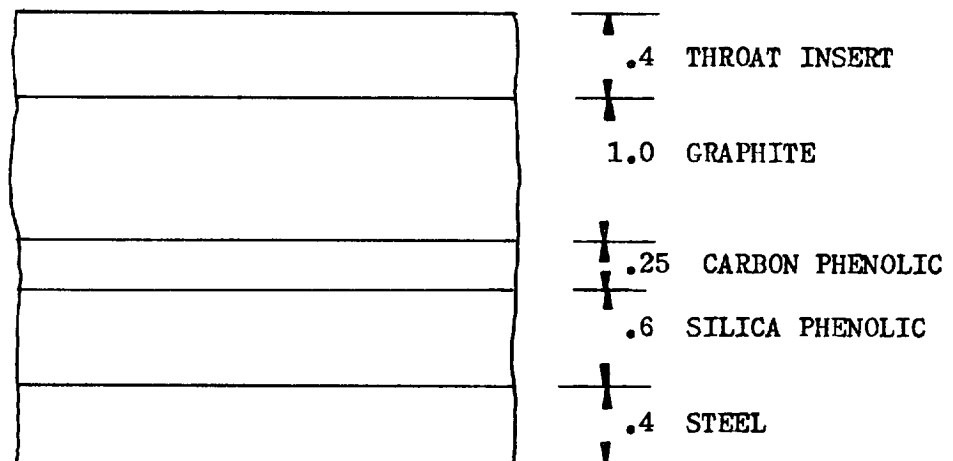
A temperature profile of this design is shown on Figure 89. The temperature at the silica phenolic-carbon phenolic interface was reduced to a safe level of approximately 2100°F, but the silica phenolic steel interface temperature rose to just under 300°F. TRW had established 300°F as a temperature limit for the silica phenolic steel interface, and while this limit had been attained but not exceeded, it appeared desirable to reduce this temperature.

145

TEMPERATURE PROFILE
GRADED CARBIDE

Figure 89

146
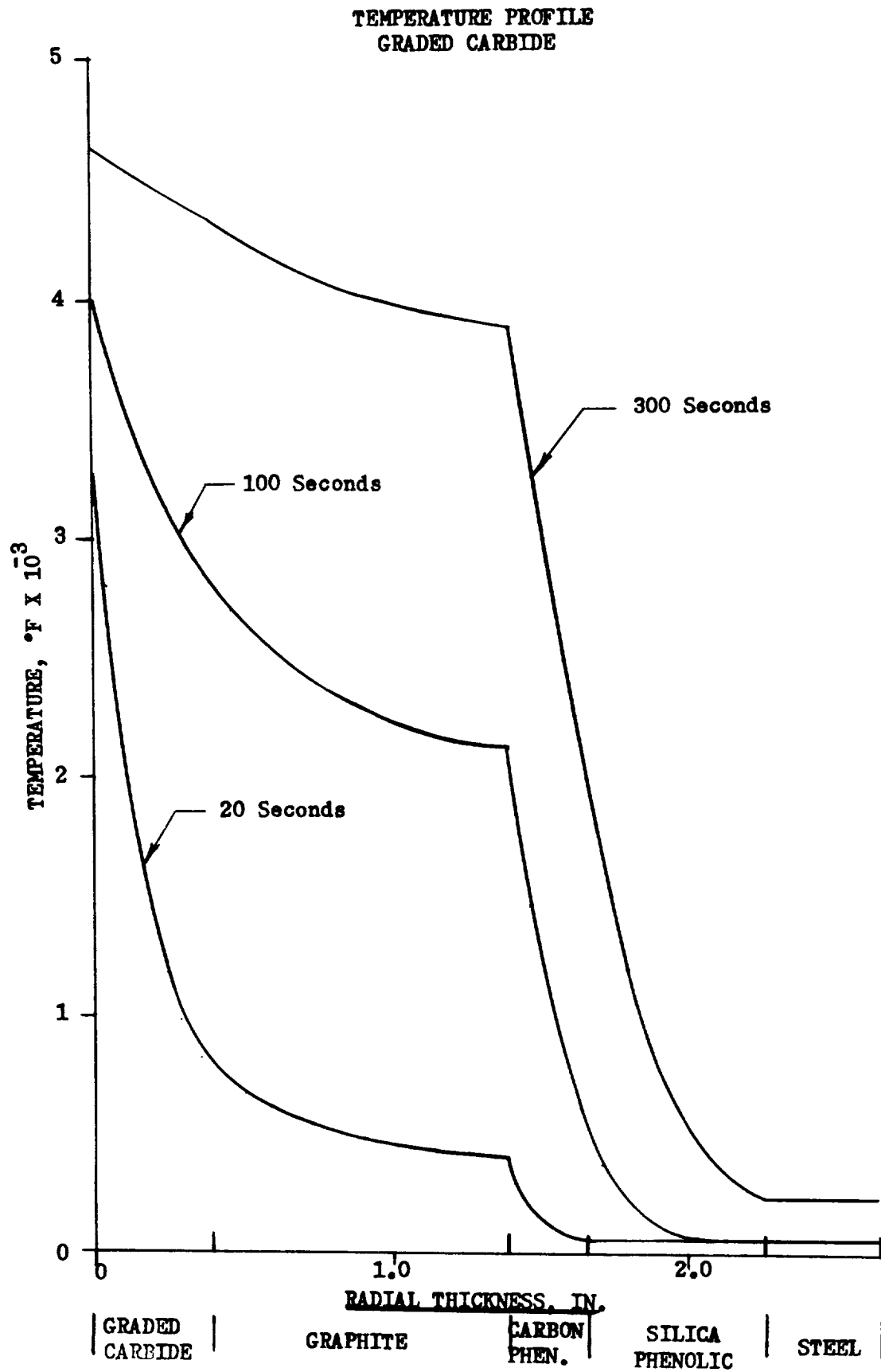
To reduce the silica phenolic-steel interface temperature, the design was modified to use the material thickness as shown below:

.4	THROAT INSERT
.75	GRAPHITE
.25	CARBON PHENOLIC
.85	SILICA PHENOLIC
.4	STEEL
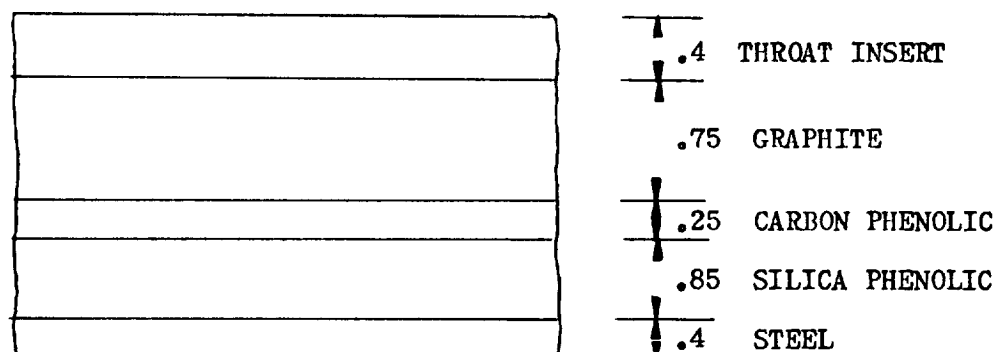
The temperature profile for this design is shown in Figure 90. The silica phenolic - carbon phenolic interface is approximately 2250°F and the silica phenolic-steel interface is 125°F. Both temperature levels are well within acceptable limits and the design, based on temperature limiting properties, was fixed.

e. Stress Analysis

Stresses in the graded carbide design were analyzed by means of an IBM 7070 computer program, which combines thermal and pressure stresses in composite cylinders. The basic equations are those of Timoshenko for long, thick-walled, circular cylinders. The pressure stresses (Ref 4) are calculated for thick-walled, circular cylinders with uniform external and internal pressures. Deformations are symmetrical about the cylindrical axis and do not change along its length. For thermal stresses (Ref 5), the temperature is assumed to be constant along the axis of the cylinder. The cylinders are assumed to be long and axially unrestrained. Compatibility of deflection is enforced at the interfaces between layers, and the resulting elastic stresses are computed.

The input to the stress program includes:

> radial temperature distribution,
> internal and external pressures,
> material properties (Young's Modulus, coefficient of thermal
>   expansion, Poisson's ratio),
> geometry.

As output, the program computes hoop, axial, and radial stresses at each material interface, and the radial displacements at the interfaces.

Radial temperature gradients to be used in the analysis are obtained from a one-dimensional heat transfer computer program. See Figures 88, 89, and 90.

A critical area of the stress analysis is selection of material property values for use in the program. Calculations are made at various times throughout the firing cycle, which means that temperature dependent property values must be

147

TEMPERATURE PROFILE
GRADED CARBIDE

148   Figure 90
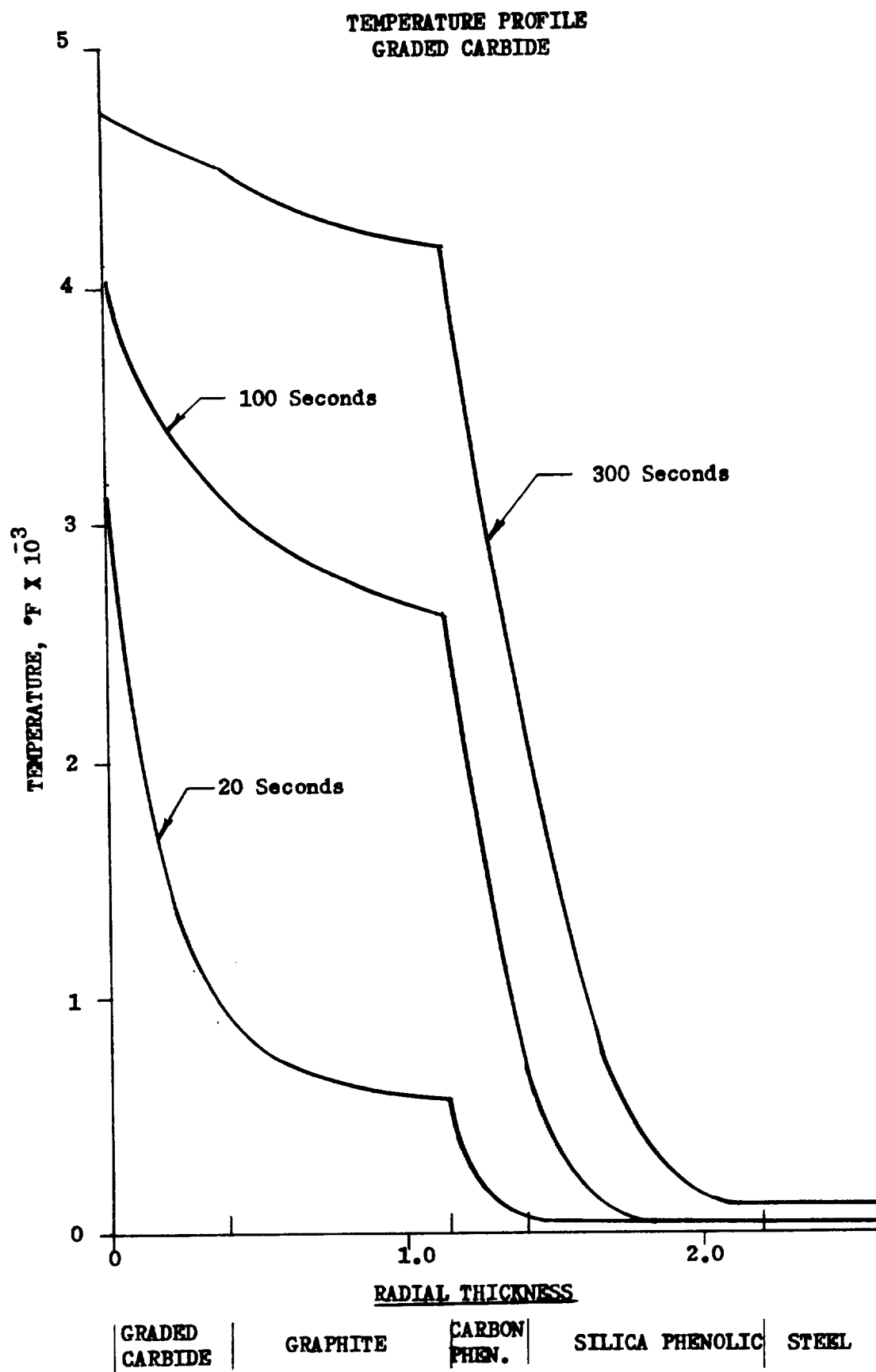
obtained over the range of temperatures experienced by the materials. Since the carbide insert materials are relatively new, the existing property values are less reliable than those for conventional materials and, in fact, some of the required values are not available at all. Material suppliers provided the majority of the property values needed, but some extrapolation of this data was necessary and was done by TRW on the basis of best available information.

The coefficient of thermal expansion for hafnium carbide was obtained from the literature and is shown in Figure 80. This curve was extended for temperatures above 4000°F. No values were needed at 600°F or less.

The coefficients of thermal expansion for the composite tantalum carbide-graphite materials are shown in Figure 91. The extrapolations made can also be seen. Since no values are given from zero to almost 2000°F, the extrapolation of the data was stopped at 1000°F and constant values used on down to zero degrees as shown. This conservative approach was adopted because of the uncertainties that arise in extrapolating that far. No data existed for TaC+70%G. The curve for TaC+70%G was drawn by comparison between given TaC data and that given for various compositions of CbC and graphite which included CbC+70%G.

Figures 85 and 87, respectively, are curves of the data for hafnium carbide and tantalum carbide. This is room temperature data, however, and is not available versus temperature. To estimate Young's Modulus versus temperature, the room temperature value for 100% Hafnium carbide was combined with two other points, obtained from the literature (Ref 6) at 200°F and at 2800°F, to construct the HfC curve of Figure 81.

Room temperature values for TaC+10, 40 and 70 volume percent of graphite were taken from Figure 87. These serve as starting points for the corresponding curves on Figure 81 which have been constructed by reference to the HfC curve of the same figure.

The foregoing extrapolations and interpolations serve as TRW's best estimates on the basis of the available information concerning these materials. While the subject had been discussed briefly in Section d, it was felt that a restatement of the fact was necessary to underline the status of material property data and availability.

Figures 92 through 99 are plots of the hoop and axial stresses in the four insert materials. These stresses were calculated at the external and internal surfaces of the materials by the computer stress program and the curves are labeled accordingly. These calculations were made using pressure and temperature conditions at the throat.

Hoop Stresses

The hoop stresses which have been calculated are due to a combination of internal pressure, thermal gradients, and radial growth of materials. It should be noted, however, that the pressure stresses contribute to a very small part of the total values. Assume, for example, that all the internal pressure is absorbed by the four carbide insert materials. If the internal pressure is 86 psi and the external pressure is 14 psi, the resulting hoop stress will only be:

COEFFICIENT OF THERMAL EXPANSION
VS
TEMPERATURE
(Tantalum Carbide)

TaC
TaC + 10C
TaC + 40C
TaC + 70C
(Dashed lines are extrapolations of abailable data)

⊙ TaC
▣ TaC + 10C
△ TaC + 40C
X TaC + 70C

COEFFICIENT OF THERMAL EXPANSION, IN/IN/°F X 10⁺⁶

TEMPERATURE, °F

150   Figure 91

STRESS PROFILE
GRADED CARBIDE INSERT
HfC LAYER

HOOP STRESS - INTERNAL SURFACE

HOOP STRESS - INTERNAL SURFACE

TIME, SECONDS

151

Figure 92

STRESS PROFILE
GRADED CARBIDE INSERT
$Ta C + 10\% G$ LAYER

152   Figure 93

STRESS PROFILE
TaC + 40% Graphite Layer

Hoop Stress, OD

Hoop Stress, ID

Figure 94

STRESS PROFILE
TaC + 70% Graphite Layer

Figure 95

154

AXIAL STRESSES
GRADED CARBIDE INSERT
H₄C LAYER

STRESS PROFILE
GRADED CARBIDE INSERT
TaC + 10% C LAYER

AXIAL STRESS - EXTERNAL SURFACE

AXIAL STRESS - INTERNAL SURFACE

TIME - SECONDS

STRESS, PSI x 10^3

156

Figure 97

STRESS PROFILE
TaC + 40% Graphite Layer

157

Figure 98

AXIAL STRESSES
TaC + 70% GRAPHITE

AXIAL STRESS
EXTERNAL
SURFACE

AXIAL STRESS
INTERNAL
SURFACE

STRESS - PSI

TIME ~ SECONDS

158
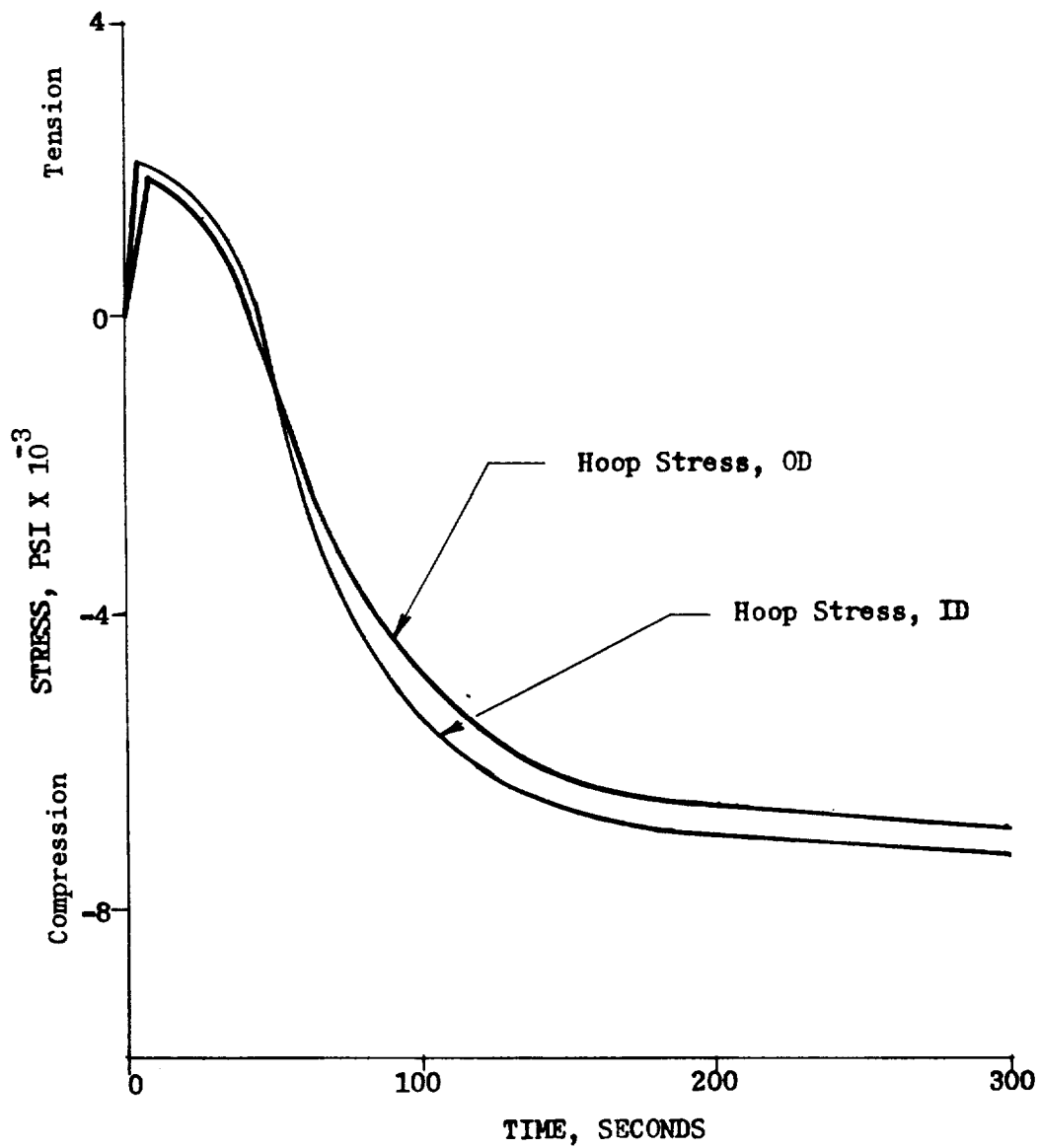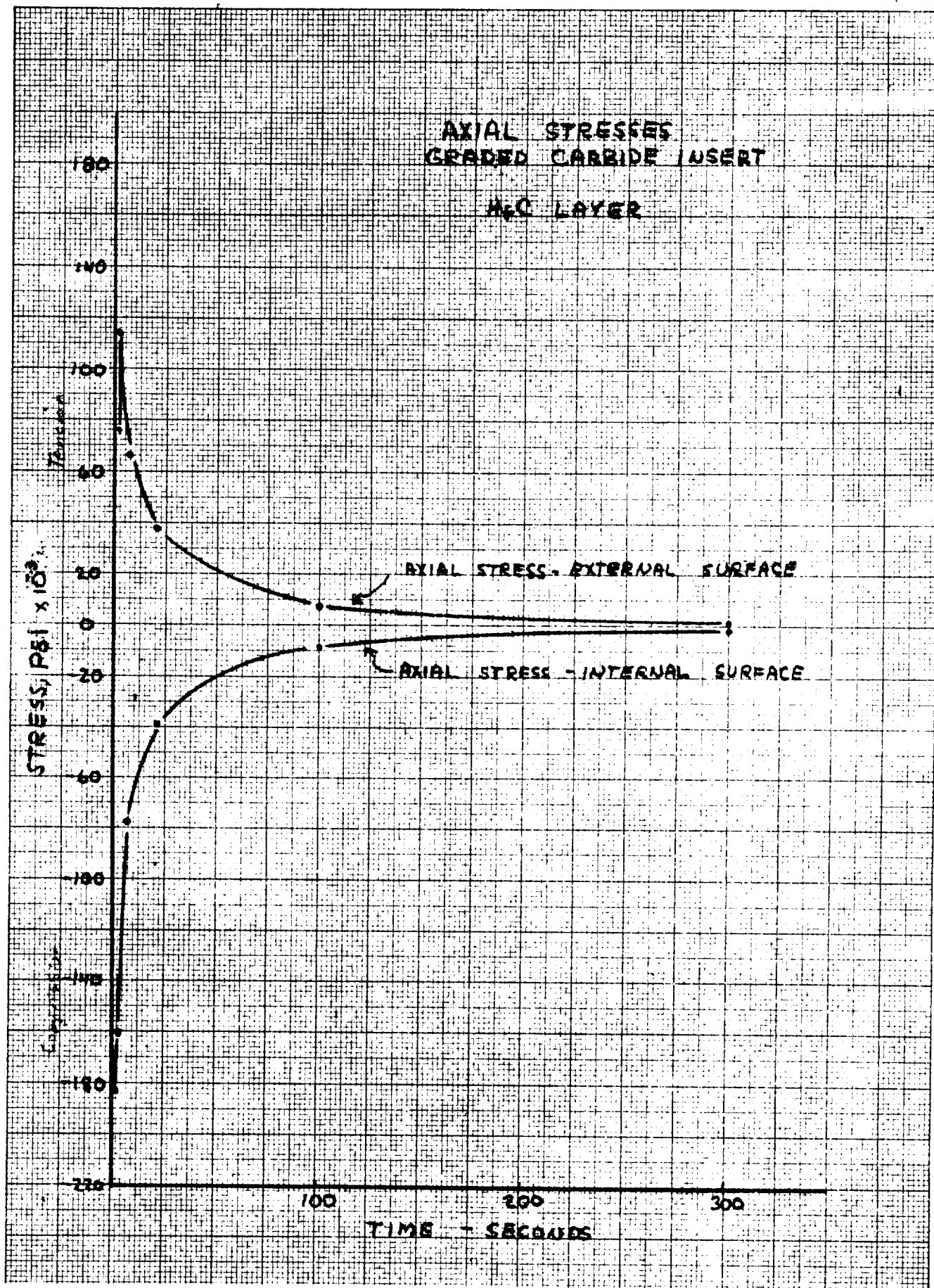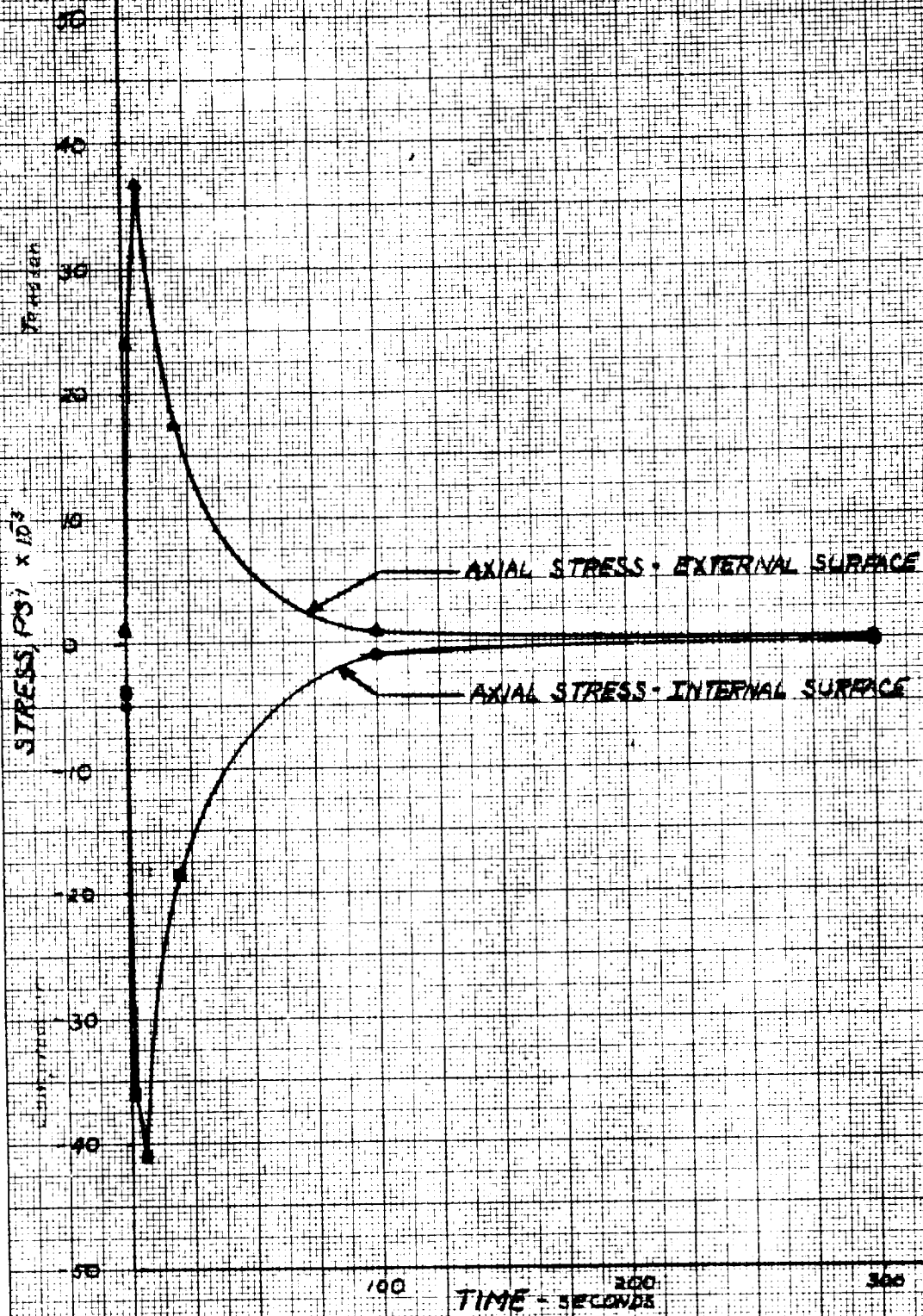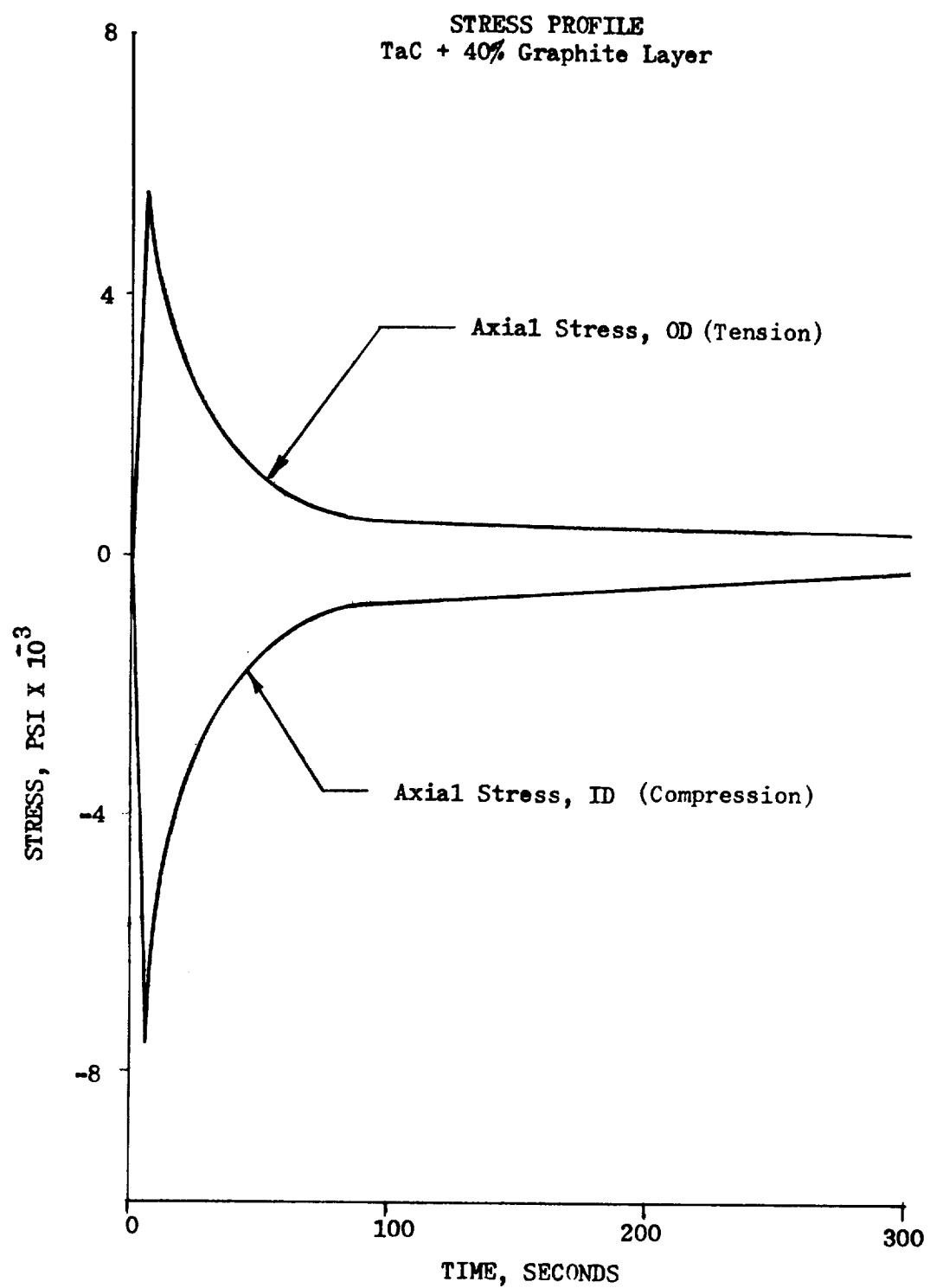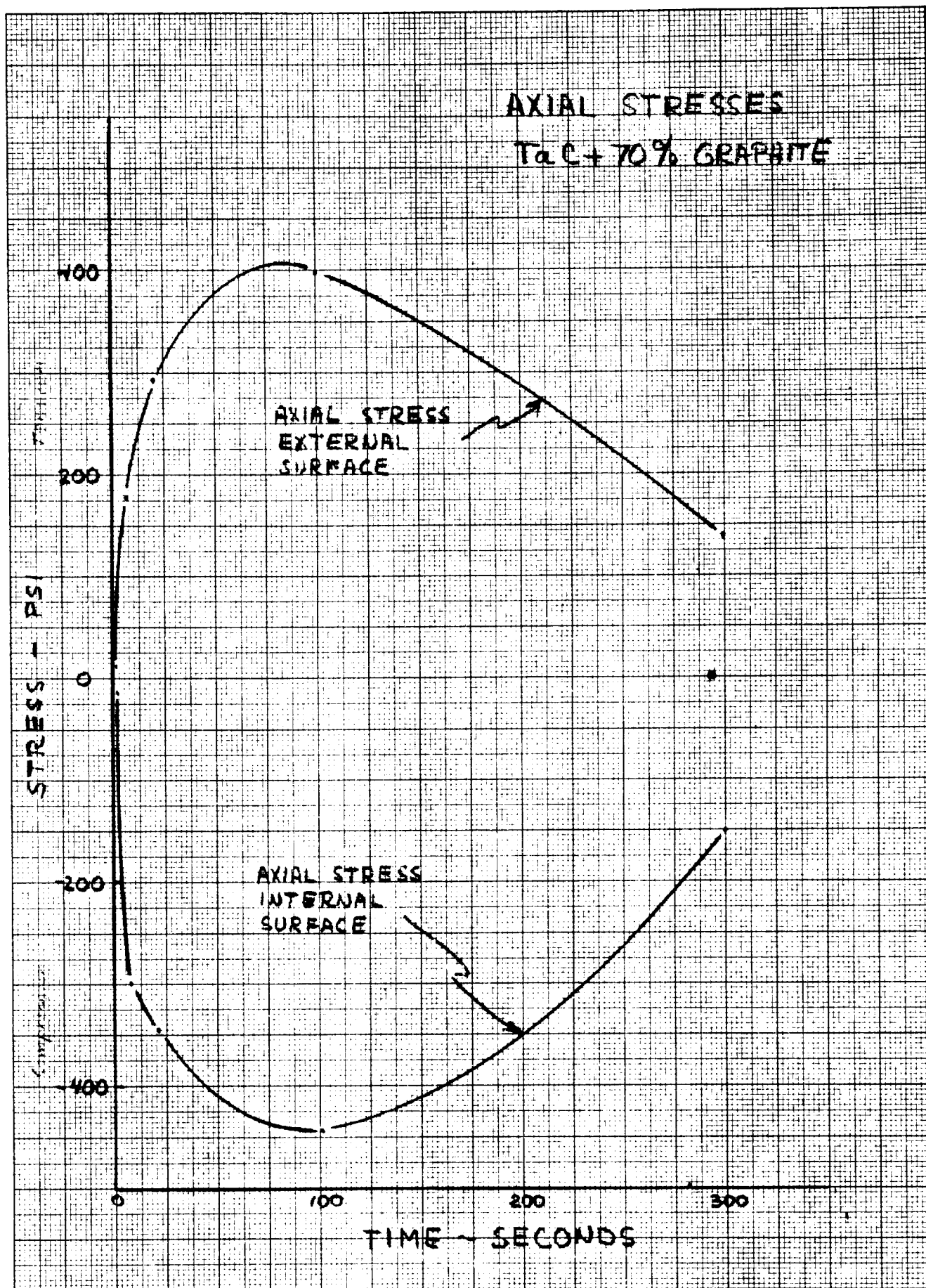
Figure 99

$$\text{hoop} = \frac{PR}{t} = \frac{(72) \ (0.8)}{0.4} = 144 \text{ psi}$$

where R and t are the insert radius and thickness.

By reference to Figures 92, 93, 94, and 95, it can be seen that this value is insignificant. Additionally, this 144 psi is a conservative number since the internal pressure will not be absorbed only by the four insert materials. They will also have some support from the four backup materials. In analyzing the hoop stresses, then, they can be treated as if they are due to thermal effects alone.

Figure 92, hoop stresses in HfC layer, indicates that the hoop stress is initially highly tensile on the external surface and highly compressive on the internal surface. As time increases, the stresses at both surfaces tend to converge as the temperature gradient across the material decreases. This stress pattern is similar to what would be expected for a single cylinder without backup materials, except that in a single material, stresses would be directly proportional to temperature gradient and would also peak early in the firing cycle. The composite effect also tends to make all the stresses on Figure 92 compressive, as the outward growth of the HfC is restricted by the backup materials which experience lower temperatures. This composite effect is pronounced later in the firing cycle when the hafnium carbide is hotter, and in fact, Figure 92 shows both external and internal surfaces to be compressive through most of the cycle.

Figure 93, hoop stresses in the second material, TaC + 10%G, shows both surfaces to be initially tensile. At the first calculation time (0.3 seconds), there is almost no temperature elevation above room temperature in the TaC + 10%G layer. Thus, thermal effects are small and are overcome by internal pressure and by outward growth of the first material (tensile both surfaces). As time increased from zero, the gradient in the TaC + 10%G material increases (maximum at 6.0 sec.) and thermal effects become predominant. The internal surface goes compressive at time $\sim$ 2 seconds. As time increases further, the gradient in the second material decreases and thermal stresses decrease. The absolute temperature of the material is increased, however, and both the first and second materials are now trying to grow outward but are being restricted by the outer materials. Thus, the first two materials are in compression and are being contained by outer materials which are in tension.

This same pattern for hoop stresses continues on through the other two insert materials, Figure 94 and 95. Both of these materials are initially in tension when they are relatively cool, and are helping to contain the inner, expanding materials. Eventually, heat also reaches these outer insert materials. They experience small temperature gradients and, therefore, low thermal stresses. Gradually, as the gradient in each of these materials decreases, the absolute temperature increases and they, in turn, begin to grow outward against the remaining backup materials. Note that TaC + 40%G preceeds TaC + 70%G into compression, and that both eventually become completely compressive.

Reference should be made here to Figure 100, which shows hoop stresses in the steel shell to be always tensile and increasing with time. This is because temperature effects in the steel are small and are always overcome by the expansion of the inner materials.

159

GRADED CARBIDE INSERT
STEEL LAYER

HOOP STRESS - INTERNAL SURFACE

HOOP STRESS - EXTERNAL SURFACE

AXIAL STRESS - EXTERNAL SURFACE

AXIAL STRESS - INTERNAL SURFACE

STRESS, PSI × 10^3
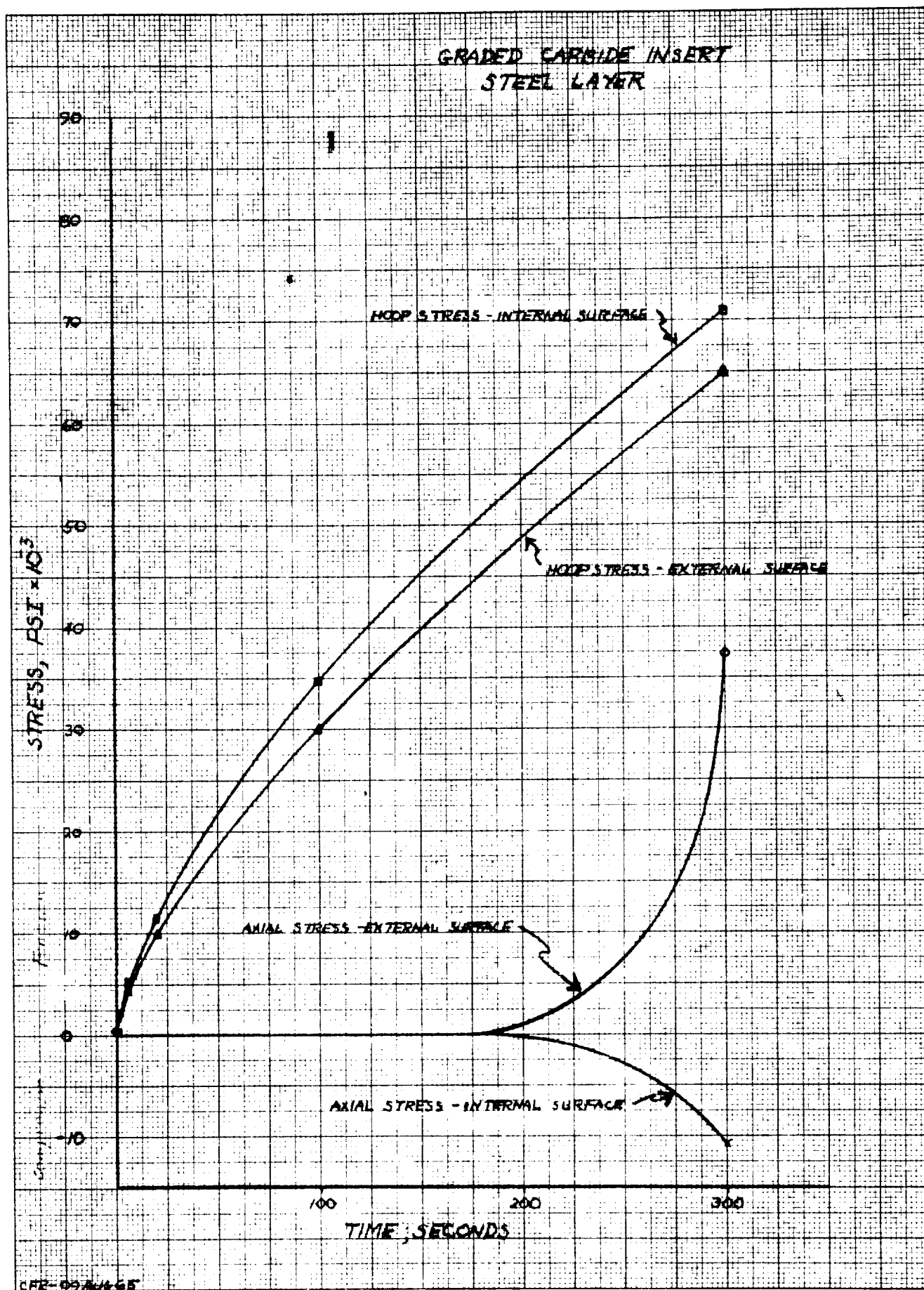
TIME, SECONDS

Early in the firing cycle, a substantial temperature gradient exists across the hafnium carbide layer which produces a tensile hoop stress of 49,000 psi at its outer surface (at time = 0.3 seconds). This tensile stress could be reduced by increasing the restraint on the HfC through use of a higher modulus material as its immediate backup. Since modulus is inversely proportional to graphite content for the carbide-graphite mixtures, this prompted a stress analysis with TaC + 5%G replacing TaC + 10%G as the second material. A computer run was made on this configuration. The results showed that hoop stress at the outer dia-meter of the hafnium carbide was reduced to 44,000 psi, but conditions in the second materials became considerably worse. Maximum tensile stress at the outer surface of the TaC + 5%G increased to 90,000 psi. Previously, with TaC + 10%G, it had been only 61,000 psi. It appears that the original design with TaC + 10%G is the better of the two and the alternate configuration was abandoned.

Axial Stresses

Assumptions required in setting up the stress program make interpretation of the axial results difficult. One problem associated with the axial computa-tions is that the equations are written for infinitely long cylinders. That is, it is assumed that calculations are made far enough away from the ends that, by Saint Venant's Principle, end effects will not distort the results. In reality, the insert is short enough that end effects will influence the stresses ex-perienced by the part.

A second problem that exists with the axial stress data is that interaction between materials is not taken into account. Each material is treated as a separate cylinder. This is untrue in the physical case since the materials are not stressed independently of each other in the axial direction and, in fact, the carbide insert materials are metallurgically bonded together. Neglecting this composite effect causes the program's axial stresses to be extremely con-servative.

With these limitations in mind, the axial stresses calculated by the program have been plotted in Figures 96, 97, 98, and 99 for the insert materials and in Figure 100 for the steel. It can be seen that these stresses are directly pro-portional to the temperature gradients in the materials. Peaks occur progress-ively later in the firing cycle as materials are further removed from the center-line of the nozzle. Also, the stresses "damp out" later in the firing cycle as temperature gradients decrease (steel is an exception since it experiences a slight gradient only toward the end of the cycle).

Some calculations were made to account for the axial interaction between the insert materials, and to bring the computed axial stress values into a more realistic range. This analysis was made at time = 1.5 seconds. The axial stresses reported in Figures 96, 97, 98, and 99 correspond to the theo-retical insert condition shown in Figure 102 which results from treating each material as an independent cylinder. In reality, the insert materials are bonded to each other and cannot expand the total differential amounts shown. Thus, the actual condition of the insert at 1.5 seconds would be closer to the case shown in Figure 103. To account for the descrepancies in the theo-retical insert condition, the hafnium carbide layer will have to be compressed, and the three tantalum carbide plus graphite layers will have to be extended to some intermediate position (h). This change is accomplished by the forces (P) shown in Figure 102 which can be converted to stresses. These compensating

161
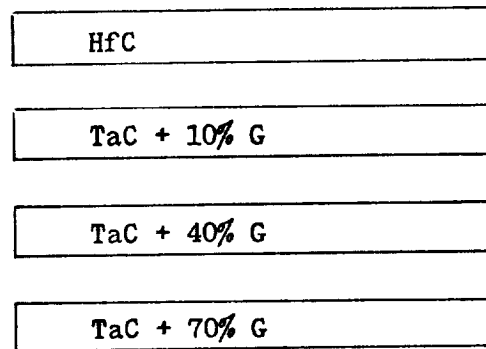
Figure 101 Initial Condition of Insert before Firing
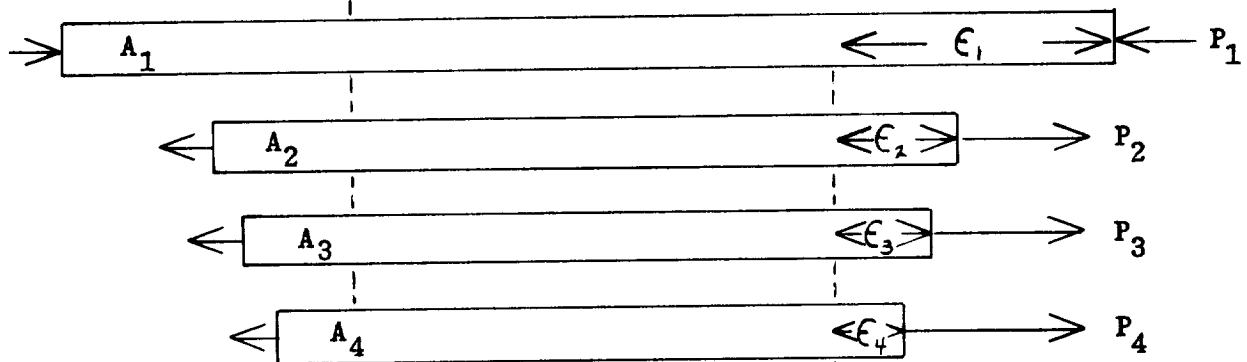
Figure 102 Theoretical Condition of Insert at t = 1.5 sec
According to Assumptions of Computer Stress Program
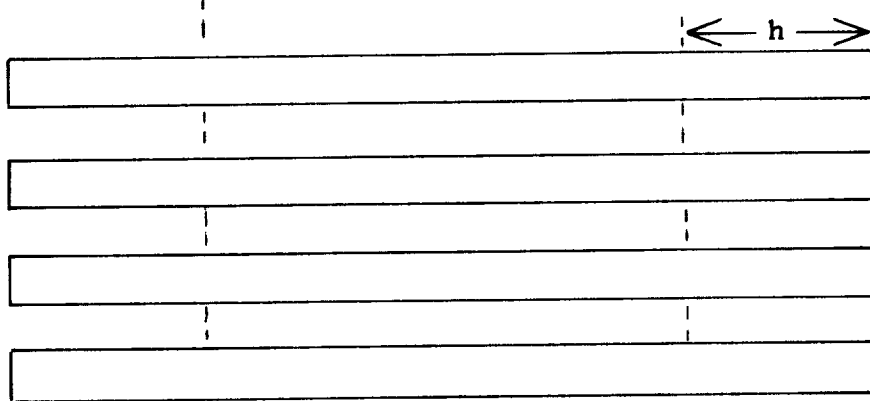
Figure 103 Actual Condition of Insert at t = 1.5 sec.

162

stress values are then superimposed on the computed values which correspond to Figure 102. The resulting stresses correspond to the configuration of Figure 103 which more closely matches the physical condition of the insert at time = 1.5 sec. Calculation of the compensating stresses is accomplished as follows:

In Figure 102, each material has a theoretical strain ϵ_i given by:

(1)
$$\epsilon_i = \alpha_i T_i + \frac{\sigma_{a_i}}{E_i} - \frac{\mu_i \sigma_{h_i}}{E_i}$$

where α = coefficient of thermal expansion

T = temperature

σ_a = axial stress

E = Young's Modulus

μ = Poisson's Ratio

σ_h = hoop stress

i = material layer

All values on the right side of the equation are known so the theoretical strains are known. The intermediate distance (h) is equal to the theoretical strain plus the compensating strain.

(2) $h = \epsilon_i + \dfrac{P_i}{A_i E_i}$

where A is the cross sectional area

Also, it is known that the compensating stresses are internal to the insert and do not come about because of external forces. Hence,

(3) $P_1 + P_2 + P_3 + P_4 = 0$

Equations (2) and (3) yield five equations for the four unknown forces and the distance (h). These forces are then converted to stresses by dividing by the cross sectional area of the cylinders.

The results show that the following values should be superimposed on the theoretical values originating from the computer program.

HfC	-100,000 psi	(compressive)
TaC + 10%G	50,000 psi	(tensile)
TaC + 40%G	28,500 psi	(tensile)
TaC + 70%G	27,000 psi	(tensile)

This is not an exact analysis since the compensating stresses are said to be evenly distributed across each cylinder. Actually, the effects are most pronounced at each material interface and diminish radially away from the inter-

faces. But these calculations do help to explain the mechanism by which the theoretical stresses of the computer program are reduced in the physical case.

To summarize the results of the stress analysis, the most evident point made by the stress curves is that the maximum stress in the insert will occur during the first few seconds of the test. This is the period of maximum thermal gradient and is reflected in the stress values. As noted earlier, the internal gas pressure plays an insignificant role with respect to the stress imposed on the insert. As also noted earlier, the data used for the analysis was limited and in many cases derived from individual tests or, at best, a minimum number of tests. Specifically, the modulus values were obtained by sonic means. While sonic methods have been proven for certain materials, the carbide materials under discussion do not have the data history which would provide a high degree of confidence in the test values. The thermal expansion data is the result of individual tests that establish a range rather than specific values. In addition, the thermal expansion values were extrapolated from 1800 to 1000°F and then estimated as constant down to room temperature. The total effect is to introduce into the stress program a certain degree of uncertainty and conservatism. As in most stress analyses, the results should be interpreted as indicative of trends rather than providing finite values.

The allowable ultimate tensile values were obtained from modulus of rupture values that were determined by sonic means. The allowable tensile strength was assumed equal to the modulus of rupture and as being represent-ative of the maximum tensile stress in the external surface of an equivalent beam. Compressive values of 190,000 psi were obtained from data provided by the material suppliers. However, the reliable data sources report values that range upward to 500,000 psi.

The following table shows the maximum and allowable stress for the insert. The hoop values are taken directly from the stress curves while the axial stresses have been modified to account for the metallurgical bond between the carbide materials. The allowable stress values are those related to the material for the same temperature at which the maximum stress occurs.

		Hoop Stress (psi)	Axial Stress (psi)	Allowable Stress (psi)
HfC	ID	-243,000	-283,000	-196,000
	OD	49,500	15,000	38,000
TaC + 10%G	ID	-17,000	9,000	-102,000
	OD	61,000	86,000	19,000
TaC + 40%G	ID	19,000	21,000	11,000
	OD	26,500	33,500	11,000
TaC + 70%G	ID	-7,000	26,550	7,000
	OD	-7,000	27,400	6,000

164

As noted on the preceeding table, the reported allowable stress is exceeded at some point for every layer of the insert material. However, in view of what has been stated earlier on the interpretation of the stress results, on the lack of available data for the material, the results of similar material tests, and on laboratory tests conducted by TRW, a successful design was anticipated. In addition, the design and the materials used in the design have been reviewed by the materials supplier who has tested inserts of similar materials (Ref 3). They concur that the design approach used is the sound approach to reduce thermal stress and eliminate the mode of failure that has been evident in past tests.

No particular stress problems were encountered in analyzing the support materials -- graphite, carbon phenolic, silica phenolic, and steel. Property values for these materials were more easily obtained.

Maximum tensile stress in the graphite material is calculated as 2100 psi at 700°F. Union Carbide reports the ultimate tensile stress at this temperature as 4,000 psi.

Similarly, the stress levels in the carbon phenolic, silica phenolic, and steel are safe. Maximum tensile stress in the carbon phenolic (MX 4926) is 2,800 psi at 2,000°F. The ultimate tensile strength of the material is 4,000 psi. Silica phenolic (MX 2646) shows a tensile stress of 600 psi and an ultimate tensile strength of 3500 psi. The steel shell (4340 RC 35-40) experiences a maximum tensile stress of 71,000 psi. This material is safe to 150,000 psi.

f. Fabrication

The manufacturing methods used in the fabrication of the nozzle consisted of methods corresponding to those TRW uses in the fabrication of similar nozzles.

The throat support assembly consists of the throat insert support graphite, a carbon phenolic tape overwrap, and a silica phenolic tape overwrap. The processing consisted of wrapping the carbon phenolic tape on the OD surface of the graphite followed by the silica phenolic. The assembly was then cured in a hydroclave at approximately 1000 psi and 310°F. The cured part was machined on the OD and bonded into the steel shell to form the shell and throat support assembly. The assembly was machined on the OD surfaces to the dimensions required to accept the remaining components.

The throat insert was fabricated by a material supplier to TRW specifications and drawings. The entrance insulation was fabricated in a closed die mold from die cut segments of silica phenolic cloth. The segments were packed in the die and cured at approximately 1000 psi and 310°F. The cured part was finish machined on the OD and forward surface to mate with the shell and throat support assembly. The exit cone insulation was fabricated in the form of a flat laminate in a press. The part was cured at approximately 1000 psi and 310°F and machined to assemble with the shell and throat assembly.

After the components were bonded together, the assembly was machined on the ID end surfaces. The assembly was completed by the installation of the end rings.

3. Design Analysis - Reinforced Oxide Design

a. Objective

This discussion provides the analyses and the material data used in the design of the reinforced oxide insert as presented in Figure 104.

b. Design Review

The search for hard throat inserts has invariably led to the refractory oxides. Their high melting point and resistance to chemical reaction has made them a sensible selection. However, past attempts to use these materials have proved unsuccessful because of thermal stress cracking. The factor causing the thermal cracking is primarily low thermal conductivity. As the inner surface of the refractory oxide is rapidly heated to operating temperature, the outer surface remains relatively cool. The low conductivity of the material leads to a high thermal gradient resulting in a compressive stress on the inside surface which is taken out as a high tensile stress on the outside surface. Tensile failure, initiating on the outside surface, leads to the invariable gross failure that has been evident in the past.

TRW, desiring to take advantage of the oxidation resistance and high temperature properties of the refractories, has been investigating for some time a means of producing a refractory composite that would be resistant to thermal stress failures. One of the most promising methods for eliminating thermal stress failure is fiber reinforcement of the oxide matrix. This design is attractive because the oxide matrix of the insert has extreme oxidation resistance while the more ductile fiber reinforcement prevents or limits the size of thermal stress cracks. Cracks that do form in the oxide matrix are arrested by the reinforcement fibers. In addition, the fiber reinforcement will increase the thermal conductivity of the composite, with respect to the pure oxide. Tests on the composite material have also shown the thermal expansion and modulus of elasticity to be considerably lower than anticipated. It is this combination of properties that will combine to overcome the thermal stress failures that have been evident in the refractory oxides.

c. Material Selection

Earlier developments of composite structures involved oxides (primarily zirconia) reinforced with unalloyed tungsten wires. Bonding was accomplished by high temperature sintering (3500-4000°F) and, later, through the use of phosphate bonding techniques. Phosphate bonding offered the advantage of low temperature processing which did not recrystallize the tungsten wires and cause loss of ductility and strength -- as is the case with high temperature sintering. Although sound phosphate bonded composites were produced with satisfactory thermal shock resistance, phosphate bonding breaks down at elevated temperatures (3800°F), and thus limits the usefulness of this approach for producing reinforced oxide throat inserts. Also, unalloyed tungsten, once exposed to high temperatures (above 2500°F) during firing, recrystallizes and looses ductility and strength.

166

REINFORCED OXIDE INSERT DESIGN

- Silica Phenolic
- Reinforced Oxide
- CGW Graphite
- Carbon Phenolic
- JT-0981 Graphite
- Silica Phenolic
- Green Silica Phenolic

Figure 104
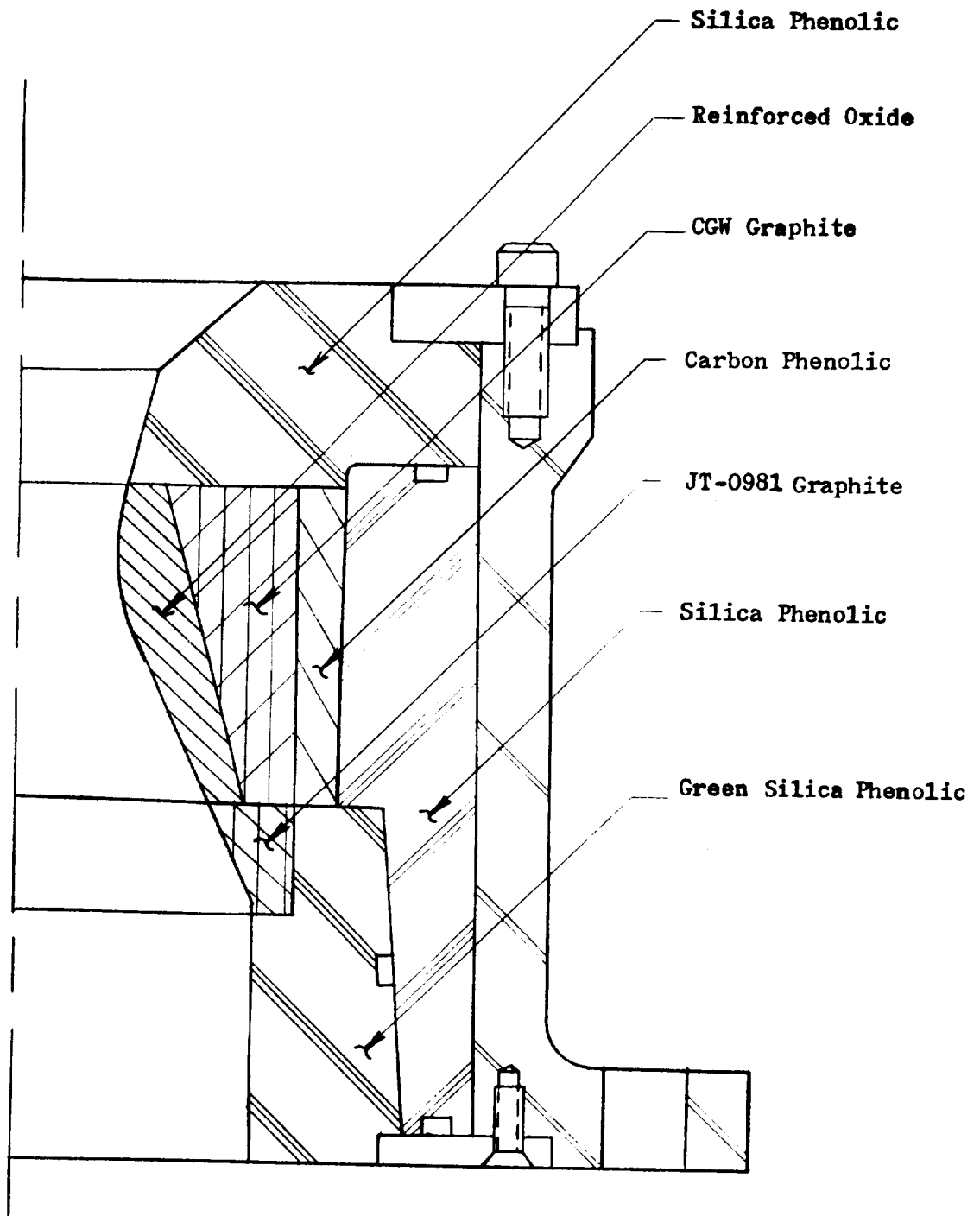
Tungsten alloyed with 3 weight percent rhenium provides ductility and improved strength -- even in the recrystallized condition, and thus is an effective reinforcement fiber for composite structures processed by high temperature sintering and subjected to repeated thermal exposure. Experiments were conducted with W-3% Re wires and oxides of zirconium and thorium to establish pressing and sintering techniques.

Although zirconia is a very satisfactory oxide for performance in rocket motor throat inserts, the optimum oxide from a melting point consideration is thoria -- with a melting point of 5970°F, versus a melting point of 4710°F for zirconia.

From preliminary laboratory tests tungsten-rhenium wire reinforced thoria looked very promising as a throat insert material and would be the apparent logical selection. However, thoria is mildly radioactive so that erosion products in the exhaust gases must be removed from the atmosphere, thus complicating the test firing procedure. Since the problem of capture of radioactive elements is considered impractical, zirconia, which ranks second in order of preference for oxide material in this application, is the alternate choice for the throat insert composite material. Considerable effort has been expended in developing zirconia composites. A number of modified zirconia powders have been fabricated into composites, including fully stabilized Zircoa "B", Zircoa F-410 (a proprietary Zircoa product) and a tungsten-modified zirconia powder. Of the zirconium oxide materials evaluated, Zircoa F-410, with 5 volume percent W-3% Re wire reinforcement, had the least cracking tendencies during fabrication and was also very good in thermal shock tests. Thus, Zircoa F-410 powder was selected for the reinforced composite design utilizing zirconia as the oxide matrix material. Although several other alloyed refractory metal wires have been investigated, they appear to offer no advantage over the W-3% Re alloy in the composite structure. W-3% Re wires were, therefore, selected as the material for reinforcement in the throat insert composite.

Thermal shock tests were performed on pressed and sintered specimens. Specimens with 1 and 3 percent by volume of reinforcing fibers exhibited no processing cracks, but thermal shock tests produced severe thermal cracks. Specimens with 5 percent reinforcing fiber were processed with no cracks and thermal shock tests revealed no separation within the specimens. The specimens with 10 percent reinforcing fiber could not be fabricated without cracking.

Thermal shocked specimens were sectioned and polished for visual examination. Their appearance is similar to that of crazed china with the fracture planes running from fiber to fiber. Other than this, the crazing is non-oriented, but uniform throughout the specimen. This is the apparent method by which the fiber reinforcement prevents the cracking evident in the pure oxide and specimens with less than 5 volume percent of reinforcing fibers. The crazing evident in the thermal shocked specimens is not of sufficient magnitude to separate any continuous fracture planes within the specimen. Several thermal shocked specimens have been sectioned and polished for visual examination. None of the specimens had any evidence of separation or further cracking during the machining operations.

Bend tests were run on beams cut from specimens that had been thermally shocked. The resulting stress-strain curves are shown on Figure 105 (Figure 66 repositioned for convenience). Curve "a" is the stress-strain curve for a pressed and sintered specimen. The curve is typical of that normally evident for a brittle material. Curve "b" is a bend test of a beam from a specimen that has undergone thermal shock. The curve is similar to that of a ductile material. Calculating the modulus of elasticity from this data results in a modulus of 11×10^6 psi for curve "a" and 0.95×10^6 psi for curve "b". The effect seen here is a matrix of irregular, interlocked particles held together by the reinforcing wires. The ductility of the tungsten-rhenium wires along with the interlocking action of the crazed matrix combine to give the composite material an effect observable as a low modulus of elasticity.

The initial stress analyses of the nozzle design used published material properties for zirconia. The stresses, as anticipated, were considerably above the allowable for zirconia. As test data became available, the results were translated into material properties and used in new stress analyses. The modulus of elasticity for zirconia that was used in the stress analyses was 21×10^6 psi. The results of the bend test, as noted earlier, indicated a modulus of 11×10^6 psi for the pressed and sintered material and 0.95×10^6 psi for the thermally shocked material. Assuming experimental error as well as deflection in the test apparatus, the modulus of the non-shocked specimen was equated to that of zirconia. The modulus of the thermal shocked specimen was then assumed to be in a direct ratio and was estimated to be approximately 1.85×10^6 psi. This value was also assumed to remain constant over the temperature range of the analysis rather than drop off with increased temperature as would be expected. The effect on the stress analysis of using a constant modulus is to induce a degree of conservatism into the calculations.

The justification for using the reduced modulus of elasticity is that the initial shock at ignition will cause the insert to craze. The insert will no longer have its original properties but will now possess the low modulus properties of the thermally shocked material. The effect of the low modulus is a reduction of the imposed stresses which is noted and compared in the discussion of the stress analysis.

Neither the expansion characteristics nor the composition of Zircoa F-410 were available from the vendor (considered proprietary). Without the expansion characteristics of the principal component of the reinforced oxide composite, it was impossible to make a reasonable appraisal of thermal expansion behavior of the composite for use in design analysis and stress calculations. Thus, an experimental determination of the expansion characteristics was made.

A thermal expansion specimen was machined from a pressed and sintered composite of Zircoa F-410 and 5 volume percent W-3% Re wires. Thermal expansion measurements were made in a Leitz dilatometer between room temperature and approximately 1700°F. Total expansion of the composite specimen was recorded directly on photographic paper and this trace is reproduced in Figure 106 (Figure 69 repositioned for convenience). Total expansion measured from the trace was then divided by the temperature interval to obtain the coef-

LOAD DEFLECTION CURVE
Modulus of Rupture
Versus
Deflection
(F410 with 5 v/o Fiber Composite)

(a) As Fabricated

(b) Thermal Shock Tested
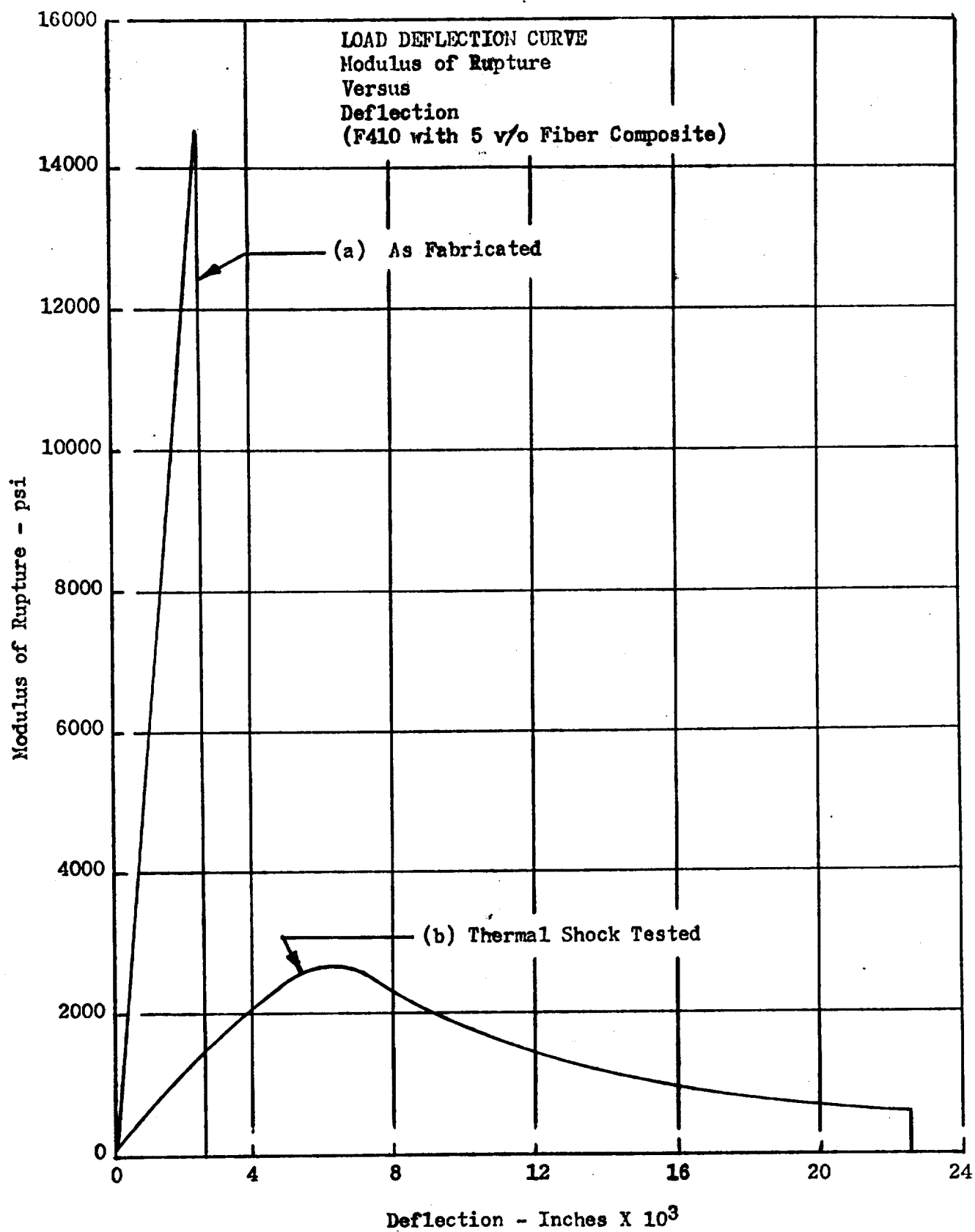
Figure 105

THERMAL EXPANSION

Change in Length
Versus
Temperature
for
W-3% Re Fiber Reinforced L-410
Zirconia Composite
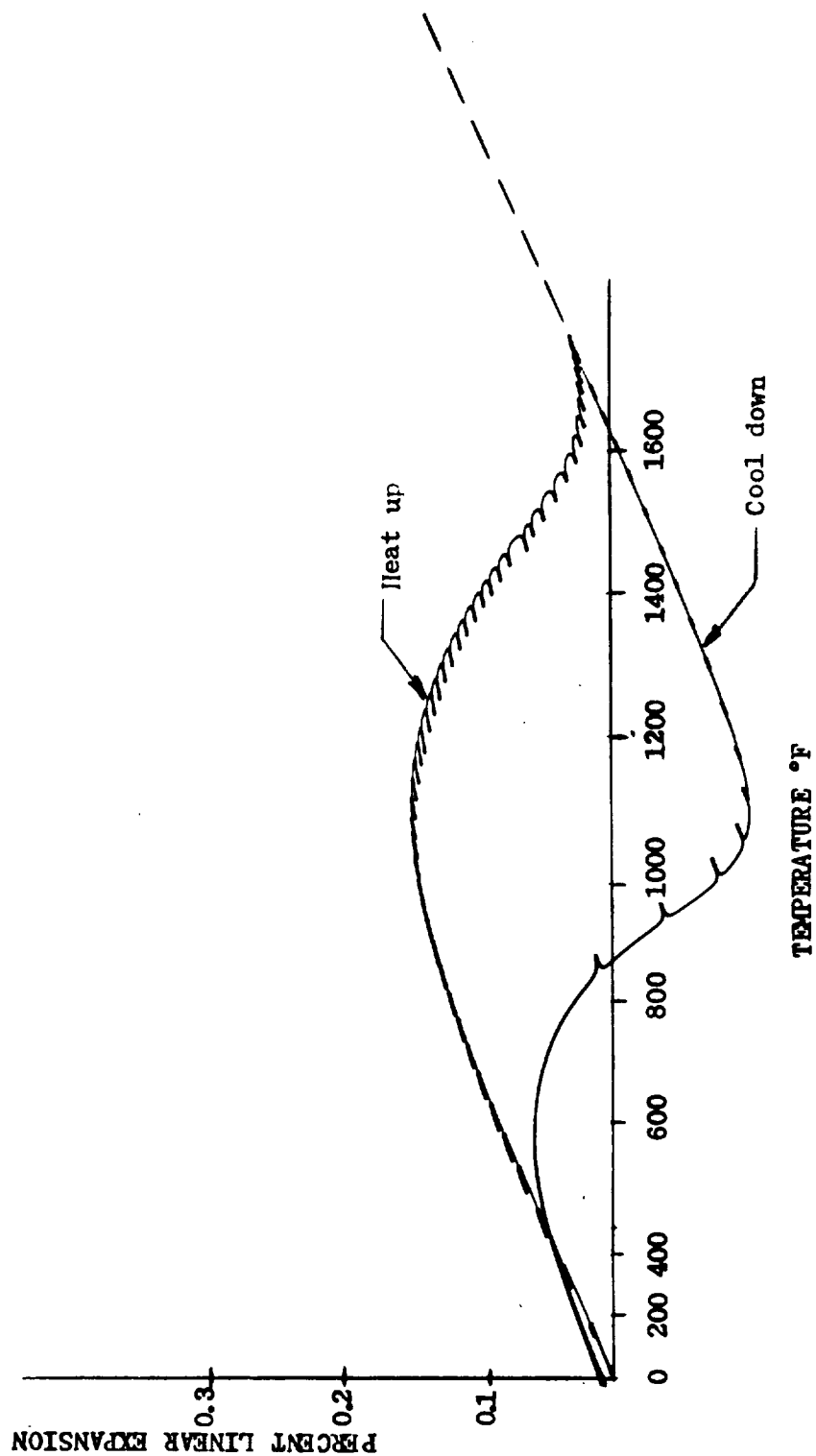
Figure 106

171

ficients of thermal expansion. Added to the experimentally determined coefficients was a correction term of 0.3×10^{-6} inch/inch/°F to account for the expansion of the quartz specimen holders. The coefficients of thermal expansion for the W-3% Re fiber reinforced F-410 zirconia composites are illustrated in Figure 107 (Figure 70 repositioned for convenience), where the coefficients (correction term included) are plotted versus temperature.

The unusually low expansion values measured must be attributed primarily to the proprietary Zircoa F-410 matrix. Furthermore, from the thermal expansion curve, it is evident that a phase change is initiated (on heat-up) at approximately 1000°F, and this change is completed by 1700°F. As with other partially stabilized zirconia systems, there is a considerable hysteresis in the phase change when cooling down and this hysteresis is reflected in the thermal expansion curve because of the difference in volumes between the monoclinic and tetragonal phases.

The thermal expansion of a fiber reinforced zirconia composite is principally influenced by the oxide matrix because the fiber reinforcement accounts for only 5 volume percent of the composite. Expansion properties of the zirconia matrix are related to the degree of stabilization of the oxide. Pure zirconia - unstabilized - exhibits a phase change (a change in crystal structure from monoclinic to tetragonal) upon heating above approximately 1800°F. With this phase change, there is a significant volumetric contraction of the zirconia; and this contraction has a marked influence on the thermal expansion behavior. Since the tetragonal structure is more compact than the low temperature monoclinic structure, upon heating through the phase change region the zirconia contracts, as is illustrated in Figure 108. When cooling down through the phase change region at non-equilibrium rates, i.e., 200°F per hour or faster, there is a considerable hysteresis in the phase change which in turn causes hysteresis in the thermal expansion behavior (forming the loop as shown in Figure 108).

Additions of certain oxides, CaO, MgO, Y_2O_3, etc., modify the crystal structure of zirconia. Small amounts of stabilizing oxides form a mixed structure of monoclinic and cubic at low temperatures while larger additions can stabilize the cubic phase from low temperatures up to the melting point of zirconia. The most common oxide used for stabilizing zirconia is calcia (CaO). The thermal expansion characteristics of a fully stabilized zirconia (Zircoa "B") are shown in Figure 108, along with the expansion characteristics of partially stabilized zirconia (Zircoa "C"). Note that the partially stabilized zirconia exhibits a small hysteresis loop in the thermal expansion curve while the fully stabilized has none.

Some justification for the experimental results is found in the phase diagram for the zirconia-yttria (Y_2O_3) system. The addition of yttria lowers the temperature for the monoclinic to tetragonal phase change to as low as 75°F. Since the phase change initiated at approximately 1000°F in the test specimen, it appears as though Zircoa F-410 may be partially stabilized with yttria. No literature values have been found for the zirconia-yttria system with which to compare the experimental results. Any influence from the W-3% Re reinforcement wire should be small because of the small percentage (5 volume percent) of wire in the composite. In absence of any conflicting data and since the experimental apparatus has in the past proven to be highly reliable, the experimental data is considered representative of the thermal expansion characteristics of a Zircoa F-410 matrix, W-3% Re wire reinforced composite.

172

COEFFICIENT OF THERMAL EXPANSION OF
W 3% Re WIRE REINFORCED ZrO₂ (F-410) 5v/o

ACTUAL DATA POINTS

EXTRAPOLATED DATA POINTS

TEMPERATURE – °F

MEAN COEFFICIENT OF THERMAL EXPANSION – IN/IN/°F X 10⁺⁶

Figure 107
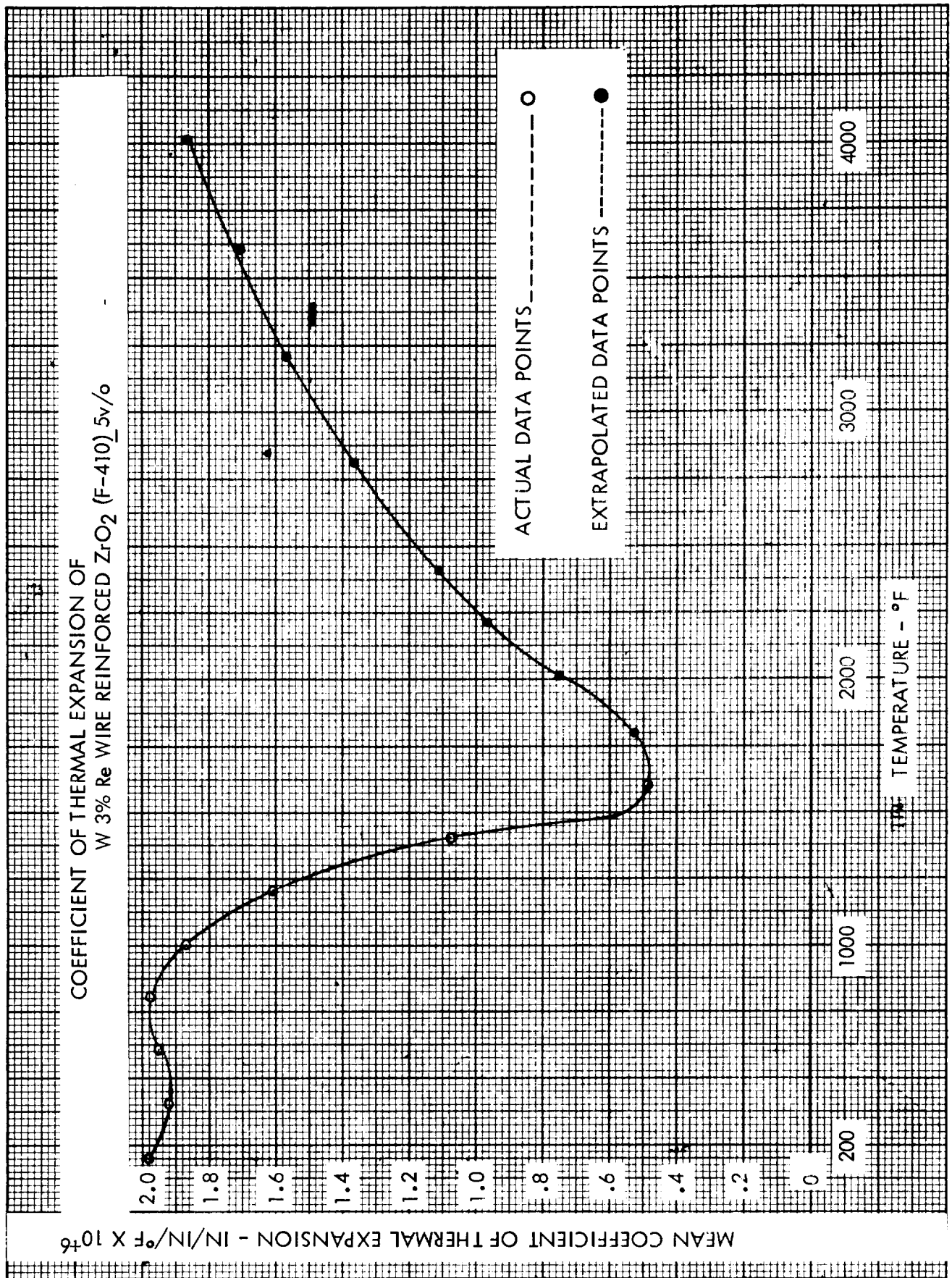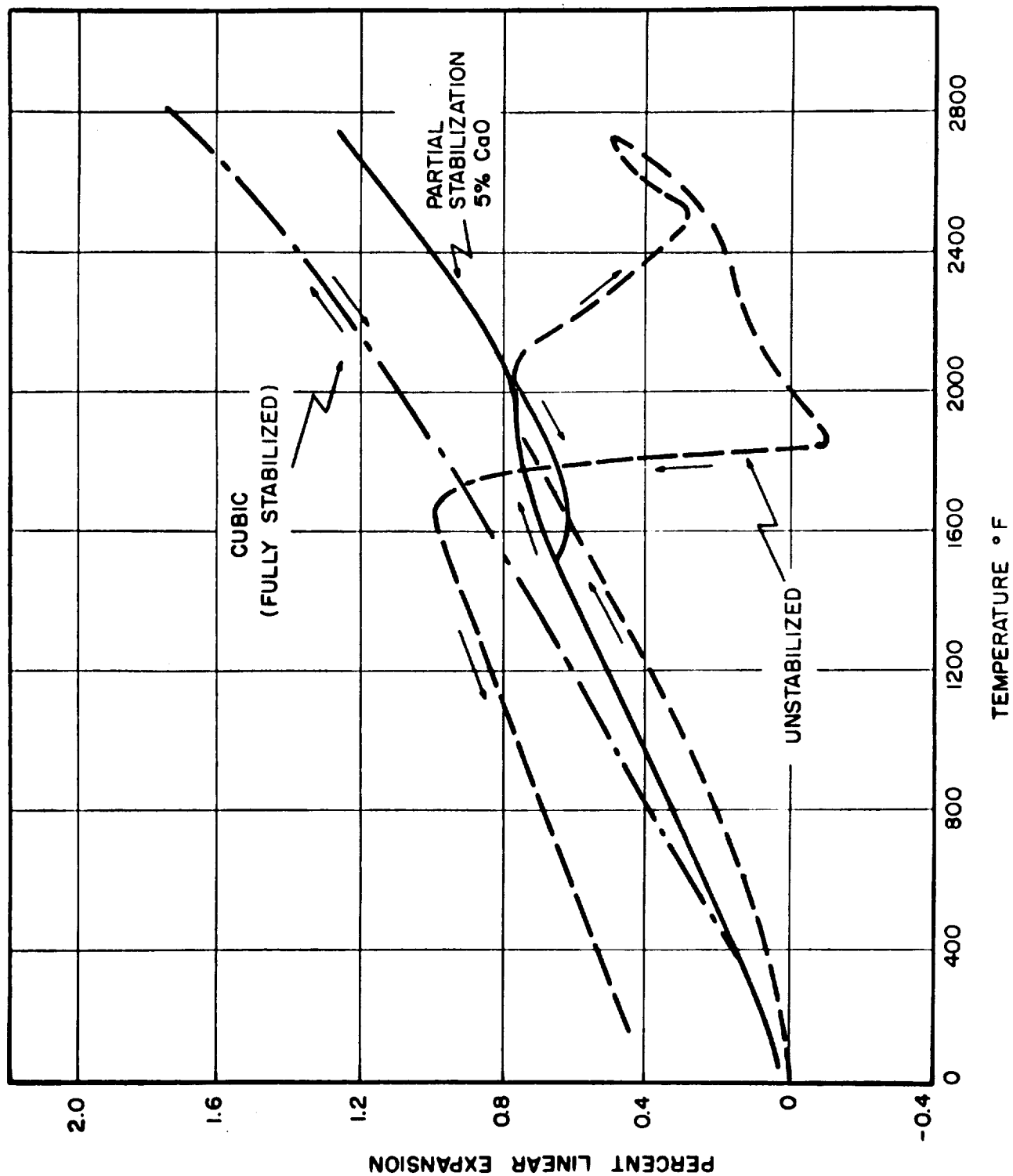
THERMAL EXPANSION OF ZIRCONIA HAVING VARIOUS DEGREES OF STABILIZATION.

174   Figure 108

Because of equipment limitations, it was possible to measure thermal expansion only up to 1700°F. Values for the thermal expansion were extrapolated from 1700°F to 7000°F on the basis that the stable structure was the tetragonal phase. The expansion characteristics of the tetragonal phase were measured between 1200 and 1700°F and then extrapolated, as indicated by the dashed line in Figure 106. The extrapolated values are indicated in Figure 107. Although it is recognized that rapid heat-up rates, as would be present in a throat insert, could possibly affect the kinetics of the phase change, and thus affect the thermal expansion, there is no data to indicate the magnitude of this effect.

d. Thermal Analysis

The initial thermal analyses were made for an insert with 10 volume percent tungsten-rhenium wire. Plots of the data are shown on Figures 109, 110, and 111. Figure 109 represents the thermal gradient through a 0.60 reinforced oxide throat with a backup of 0.55 graphite, 0.25 carbon phenolic, 0.85 silica phenolic, and the 0.40 steel support can. The curves were plotted for 20, 100, and 300 seconds after ignition. All of the temperatures were within established limits (2300°F at the silica phenolic-carbon phenolic interface and 300°F at the silica phenolic-steel interface). However, the gradient across the insert was approximately 3375°F at 20 seconds. In order to reduce this gradient, the insert thickness was reduced to 0.4 and the graphite increased to 0.75 inch. The thermal gradient is shown on Figure 110. Figure 111 is a plot of a similar design, but with the insert thickness changed to 0.30 and the graphite increased to 0.85.

After data became available on the fabrication and thermal shock characteristics of the 10% composite (as discussed in the materials section of this report) new thermal analyses were made on the 5% composite. Figures 112, 113, and 114 are plots of thermal gradients for 0.3, 0.4, and 0.6 inch insert thickness with the variation being accommodated by the graphite. Comparison of the data reflects the variation in reinforcement by the increased thermal gradient across the insert.

e. Stress Analysis

The basic analytical tool in the stress analysis of the reinforced oxide design was the IBM 7070 computer program. A short discussion of the program is included in the design report for the graded carbide configuration.

Heat transfer and stress calculations were made for three insert thicknesses to determine the effect of varying this parameter. In changing the thickness of the insert, a corresponding change was made in the RVD graphite so that the total thickness of the two materials remained constant. The three configurations studied were:

| Insert thickness | 0.30 in. | 0.40 in. | 0.60 in. |
| Graphite thickness | 0.85 in. | 0.75 in. | 0.55 in. |

Initial analyses were carried out on an insert material which consisted of ZrO_2 and ten volume percent W-3% Re reinforcement. The temperature profiles for the three insert thicknesses of this material composition appear in Figures 109, 110, and 111. The corresponding hoop and axial insert stresses for these designs are plotted in Figures 115 through 120. Hoop stresses show high maximum tensile values on the outer surface of the insert in each of these three cases. Figures 121, 122, and 123 show the stresses in the steel shells for these designs to be well within allowable limits.

Temperature Profile
Reinforced Zirconia
(10% W- Re)

0.6 in. thick

Figure 109

Figure 110

177

Figure 111

178

Figure 112

179

Figure 113

180

Figure 114

181

HOOP STRESS EXTERNAL SURFACE OF OXIDE

HOOP STRESS INTERNAL SURFACE OF OXIDE

$$E \begin{cases} 70°F \sim 21.4 \times 10^6 \text{ PSI} \\ 1000°F \sim 19.6 \times 10^6 \text{ PSI} \\ 3000°F \sim 6.6 \times 10^6 \text{ PSI} \end{cases}$$

$$\alpha \begin{cases} 70°F \sim 3.9 \times 10^{-6} \text{ in/in/F} \\ 1000°F \sim 4.4 \times 10^{-6} \\ 3000°F \sim 4.6 \times 10^{-6} \end{cases}$$

HOOP STRESS REINFORCED OXIDE DESIGN. OXIDE THICKNESS = 0.6 IN. 10% W-3Re REINFORCEMENT

STRESS (PSI)

TIME – SECONDS

182   Figure 115

AXIAL STRESS
REINFORCED OXIDE
DESIGN.
OXIDE THICKNESS 0.6 IN.
10% W-3% REINFORCEMENT

183   Figure 116

HOOP STRESS
REINFORCED OXIDE
DESIGN.
OXIDE THICKNESS = 0.4 IN
10% W-3Re REINFORCEMENT

184   Figure 117

AXIAL STRESS
REINFORCED OXIDE
DESIGN.
OXIDE THICKNESS - 0.4 IN.
10% W-3Re REINFORCEMENT

AXIAL STRESS
EXTERNAL
SURFACE OF
OXIDE

AXIAL STRESS
INTERNAL
SURFACE OF
OXIDE

$$E \begin{cases} 70°F - 21.4 \times 10^6 \text{ P.S.I} \\ 1000°F - 17.6 \times 10^6 \text{ P.S.I} \\ 3000°F - 5.6 \times 10^6 \text{ P.S.I} \end{cases}$$

$$\alpha \begin{cases} 70°F - 3.9 \times 10^{-6} \text{ in/in/°F} \\ 1000°F - 4.4 \times 10^{-6} \text{ in/in/°F} \\ 3000°F - 4.6 \times 10^{-6} \text{ in/in/°F} \end{cases}$$

185   Figure 118

Figure 119

AXIAL STRESS
REINFORCED OXIDE
DESIGN.
OXIDE THICKNESS=0.3 IN.
10% W-3R. REINFORCEMENT

Figure 120

Figure 121

HOOP & AXIAL STRESSES
IN STEEL LINER OF
REINFORCED OXIDE
DESIGN
OXIDE THICKNESS = 0.4 ID.
4340 STEEL R_c 35-40

$E = 29 \times 10^6$ psi
$\alpha = 7 \times 10^{-6}$ IN/IN/F°

HOOP STRESS
EXTERNAL & INTERNAL
SURFACES

AXIAL STRESS
EXTERNAL
SURFACE

AXIAL STRESS
INTERNAL
SURFACE

STRESS - PSI

TIME - SECONDS

189   Figure 122

HOOP & AXIAL STRESS
IN STEEL LINER OF
REINFORCED OXIDE
DESIGN
OXIDE THICKNESS = 0.3 IN
4340 STEEL Rc 35-40

$E = 29.0 \times 10^6$ PSI
$\alpha = 7.0 \times 10^{-6}$ IN/IN°F

HOOP STRESS
INTERNAL
SURFACE

HOOP STRESS
EXTERNAL
SURFACE

AXIAL STRESS
EXTERNAL SURFACE

AXIAL STRESS
INTERNAL
SURFACE

STRESS - PSI

TIME - SECONDS

190   Figure 123

Fabrication problems with the 10% reinforced oxide led to the analyses with 5 volume percent reinforcement. The heat transfer data for this insert composition appears in Figures 112, 113, and 114. A stress calculation was made for the 0.4 inch insert design and the results are plotted in Figures 124 and 125. They indicate that the hoop stresses reach a maximum tensile value of 75,000 psi at the outer diameter of the insert. However, the mechanical properties (modulus of elasticity and coefficient of thermal expansion) used in this analysis were for pure zirconium oxide rather than for the reinforced composite material. These pure oxide property values are shown in Figures 126 and 127. The high tensile stresses resulting from this calculation were unrealistic due to the use of the pure oxide property data.

Before further studies were made, experimental data was compiled by TRW on the mechanical properties of the reinforced material. The coefficient of thermal expansion as determined experimentally appears in Figure 107 and the modulus is determined from the stress versus strain curve of Figure 105 for the thermally shocked material. The effective modulus of this material, after it has been thermally shocked, will be representative of the physical condition of the insert during firing as noted earlier in the materials section. A more realistic stress prediction was made possible by using this data for calculations.

Using experimental property data for the reinforced oxide, the stress program was run for each of the three insert thicknesses. The results of these calculations are plotted in Figures 128 through 133.

The maximum tensile hoop stress is of approximately the same magnitude for each of the three insert thicknesses. These maximums are all less than 700 psi. The reduction in the level of predicted stresses is due to the use of the composite material properties. The coefficient of thermal expansion for the reinforced material is approximately half that of the pure oxide. The effective modulus of elasticity used for the composite insert had the greatest influence in reducing the calculated stresses. The value used was 1.85×10^6 psi -- constant for the imposed temperature range. This should be compared to the pure oxide values of Figure 126 which are as high as 21.4×10^6 psi at room temperature. Neglecting the combined effect of the materials on each other, thermal stresses in a single cylinder are proportional to the $E \cdot \alpha$ product. It is understandable, then, that such a great reduction of stresses would result from the use of the modified properties.

Limiting assumptions in the computer program cause the calculated axial stresses to be distorted. The problems involved are outlined in the graded carbide design report. Some of the axial stress curves presented here are of unusual shape. Figures 131 and 133 do not "damp out" with increasing time. This is due to the values of thermal expansion data which change sharply with increasing temperature. The design criteria with respect to stress is, therefore, based on hoop stresses.

A review of the stress analyses indicated that, of the three designs evaluated, none of the inserts had imposed hoop tensile stresses in excess of 700 psi. The data indicate that the preferred design would be the 0.30 inch thick insert, which has the minimum tensile stresses. However, if a 0.30 inch insert is used, the ends become quite thin for a ramp retention insert. One means of incorporating a 0.30 insert would be to decrease the length of the insert. The severe erosion observed on the forward end of the

HOOP STRESS
REINFORCED OXIDE DESIGN
OXIDE THICKNESS = 0.4 IN.
5% W-3Re REINFORCEMENT

HOOP STRESS
EXTERNAL SURFACE
OF OXIDE

HOOP STRESS
INTERNAL SURFACE
OF OXIDE

E - 70°F — 21.4 x 10⁶ psi
E - 1000°F — 13.6 x 10⁶ psi
E - 3000°F — 5.4 x 10⁶ psi

α - 70°F — 3.5 x 10⁻⁶ in/in/°F
α - 1000°F — 4.4 x 10⁻⁶ in/in/°F
α - 3000°F — 4.6 x 10⁻⁶ in/in/°F

STRESS - PSI

TIME - SECONDS

192   Figure 124

AXIAL STRESS
REINFORCED OXIDE DESIGN
OXIDE THICKNESS = 0.4 IN.
5% W-3Re REINFORCEMENT

AXIAL STRESS
EXTERNAL SURFACE
OF OXIDE

AXIAL STRESS
INTERNAL SURFACE
OF OXIDE

$E \begin{cases} 70°F \sim 21.4 \times 10^6 \ PSI \\ 1000°F \sim 19.6 \times 10^6 \ PSI \\ 3000°F \sim 7.6 \times 10^6 \ PSI \end{cases}$

$\alpha \begin{cases} 70°F \sim 8.9 \times 10^{-6} \ IN/IN/F \\ 1000°F \sim 9.1 \times 10^{-6} \ IN/IN/F \\ 3000°F \sim 11.6 \times 10^{-6} \ IN/IN/F \end{cases}$

TIME SECONDS

193   Figure 125

MODULUS OF ELASTICITY FOR ZIRCONIUM OXIDE

194   Figure 126

COEFFICIENT OF THERMAL EXPANSION FOR ZIRCONIUM OXIDE
(ZIRCOA "C" DATA FROM ZIRCOA CORP.)

195   Figure 127

Figure 128

AXIAL STRESS
REINFORCED OXIDE DESIGN
OXIDE THICKNESS - 0.3
5% W-3Re REINFORCEMENT

AXIAL STRESS
EXTERNAL SURFACE
OF OXIDE

AXIAL STRESS
INTERNAL SURFACE
OF OXIDE

$E = 1.85 \times 10^6$ PSI

$\alpha \begin{cases} 70^{\circ}F & \sim 1.90 \times 10^{-6} \text{ in/in/F} \\ 1000^{\circ}F & \sim 1.85 \times 10^{-6} \\ 3000^{\circ}F & \sim 1.95 \times 10^{-6} \end{cases}$

Figure 129

Figure 130

AXIAL STRESS
REINFORCED OXIDE DESIGN
OXIDE THICKNESS = 0.4 IN
5% W-3 Re REINFORCEMENT

AXIAL STRESS
EXTERNAL SURFACE
OF OXIDE

AXIAL STRESS
INTERNAL SURFACE
OF OXIDE

$E = 1.85 \times 10^{6}$ PSI

$\alpha \begin{cases} 70°F \sim 1.95 \times 10^{-6} \text{ IN/IN/F} \\ 1000°F \sim 1.85 \times 10^{-6} \\ 3000°F \sim 1.45 \times 10^{-6} \end{cases}$

STRESS - PSI

TIME - SECONDS

199   Figure 131

Figure 132

AXIAL STRESS
REINFORCED OXIDE DESIGN
OXIDE THICKNESS = 0.6
5% W-3Re REINFORCEMENT

AXIAL STRESS
EXTERNAL SURFACE
OF OXIDE

AXIAL STRESS
INTERNAL SURFACE
OF OXIDE

$E = 1.85 \times 10^6$ PSI

$\alpha \begin{cases} 70°F \sim 1.95 \times 10^{-6} \text{ IN/IN/F} \\ 1000°F \sim 1.85 \times 10^{-6} \text{ IN/IN/F} \\ 3000°F \sim 1.45 \times 10^{-6} \text{ IN/IN/F} \end{cases}$

STRESS - PSI

TIME - SECONDS

SIVB insert tested by NASA dictates that this would not have been a reasonable approach. Therefore, the 0.40 inch thick insert was selected for the design.

The maximum hoop tensile stress imposed on the 0.40 inch insert is 628 psi occurring at 5 seconds. This is well within the value of 3119 psi as obtained by tests on thermally cracked material. The maximum stresses of the insulating materials are well under the allowable limits as noted in the graded carbide design report. The maximum stress in the steel support structure is approximately 80,000 psi which is well within the allowable of 150,000 psi.

The test plan for the reinforced oxide insert nozzle was to fire for 30 seconds, cool down to room temperature, and then fire for 300 seconds. The preimary consideration was the axial expansion of the throat insert and the graphite back up. Thermal analysis indicates that the maximum axial growth of the insert will be on the order of 0.015 inch. This growth will result primarily in the forward direction because of the retention ramp angle. The growth will be accommodated by a nominal 0.015 bond gap between the throat insert and the entrance section. This prevented the increase of present gaps or the occurrence of gaps or cracks that would be detrimental to the nozzle during the 300 second cycle. The expansion of the graphite back up at the completion of the 30 second cycle was approximately 0.004 inch. This was accommodated without problem by the compression of the graphite and in the adjacent bond gaps.

f. Fabrication

The fabrication and assembly procedures defined in the graded carbide design report were used for this nozzle with the exception of the reinforced oxide insert. The insert was processed by isostatically pressing the composite at approximately 30,000 psi and then sintering at 4000°F.

4. Design Analysis - Refractory Laminate Design

a. Objective

This report presents the design analysis and materials data pertaining to the design of a refractory laminate throat insert (see Figure 134). It is the last in a series of four design reports prepared under Contract NAS 3-6280.

b. Design Review

One of the primary objectives of the hard throat insert is to maintain the throat diameter over a predetermined test duration. To attain this objective, the insert material must possess three basic properties. They are resist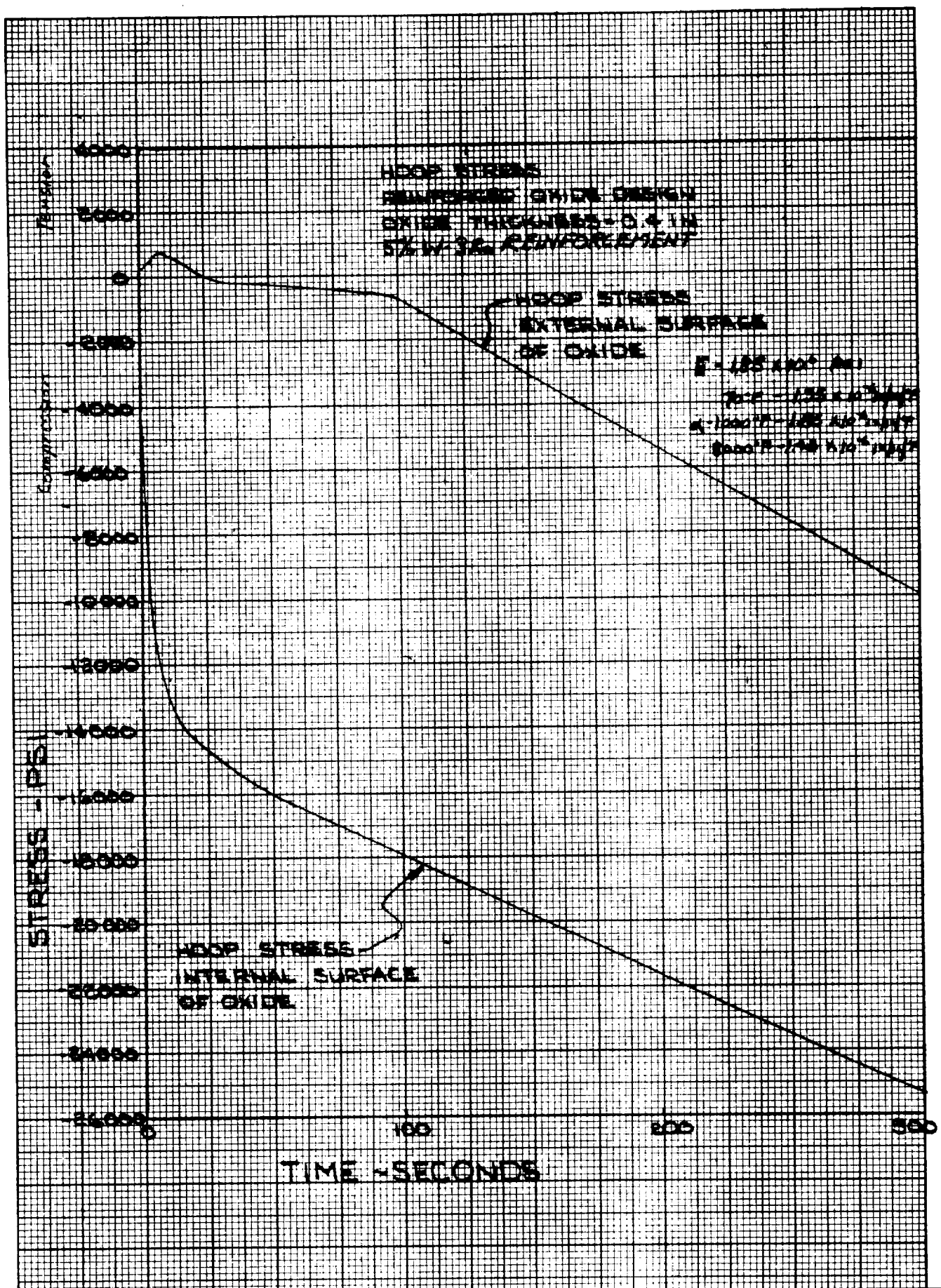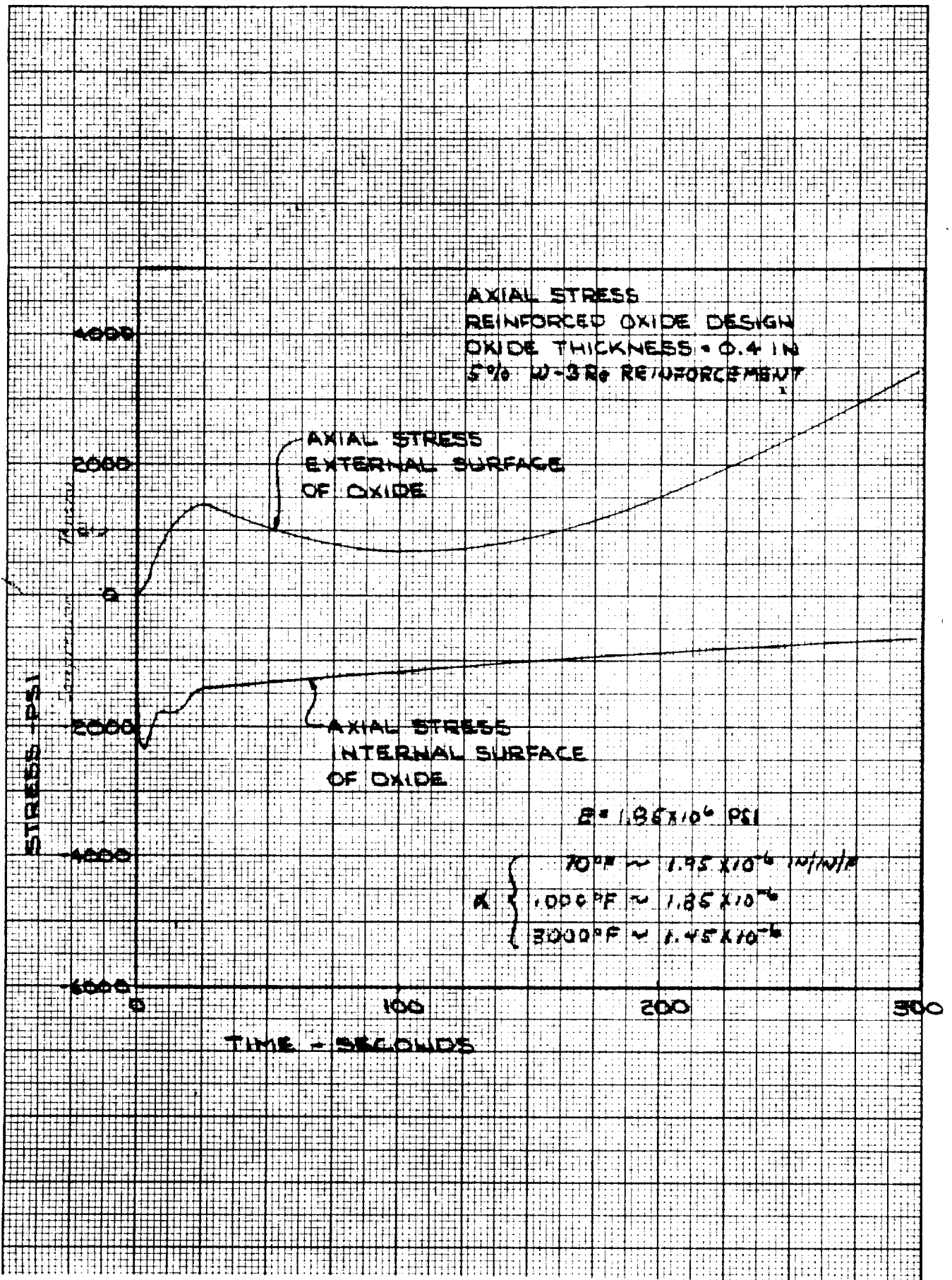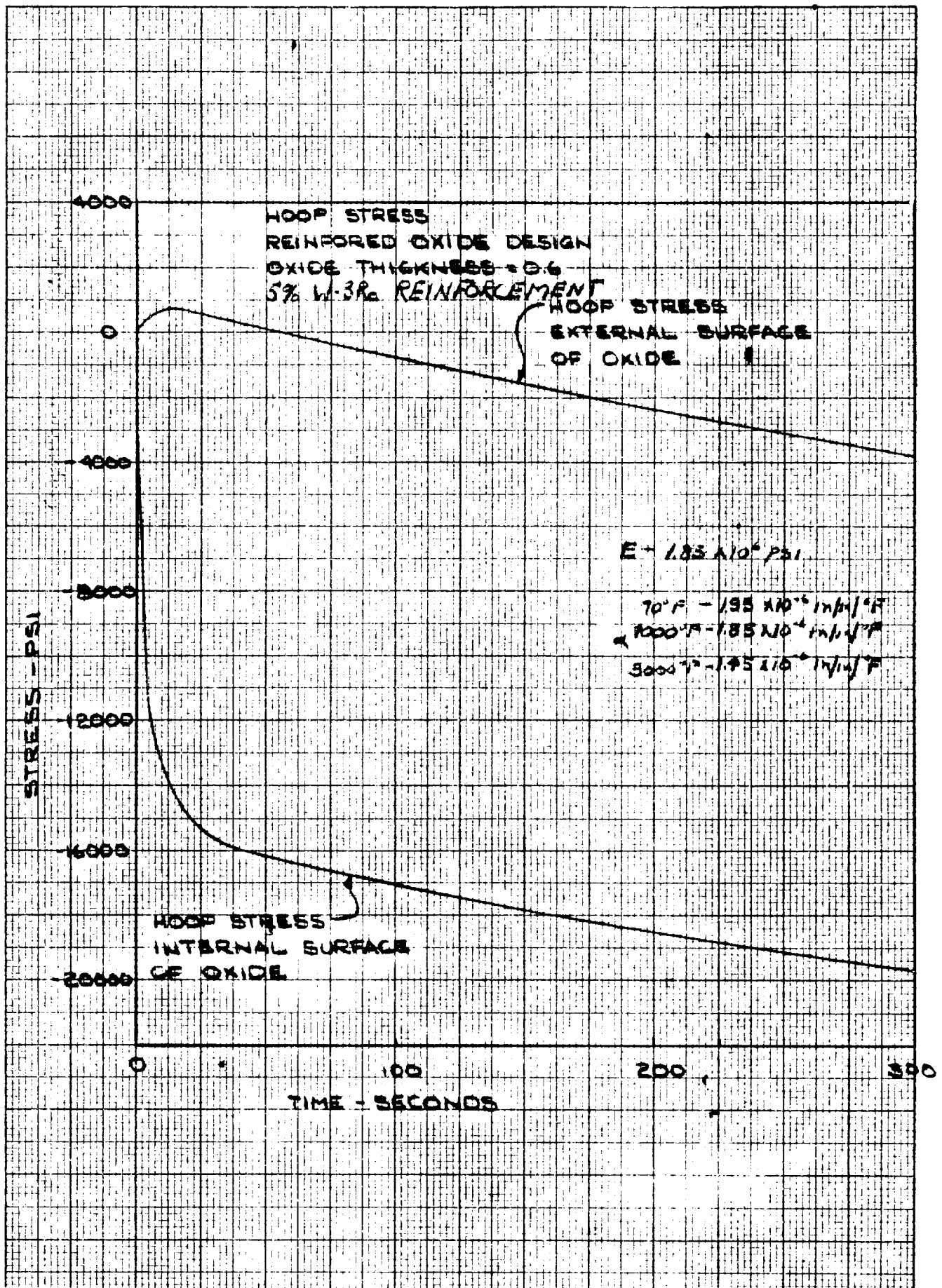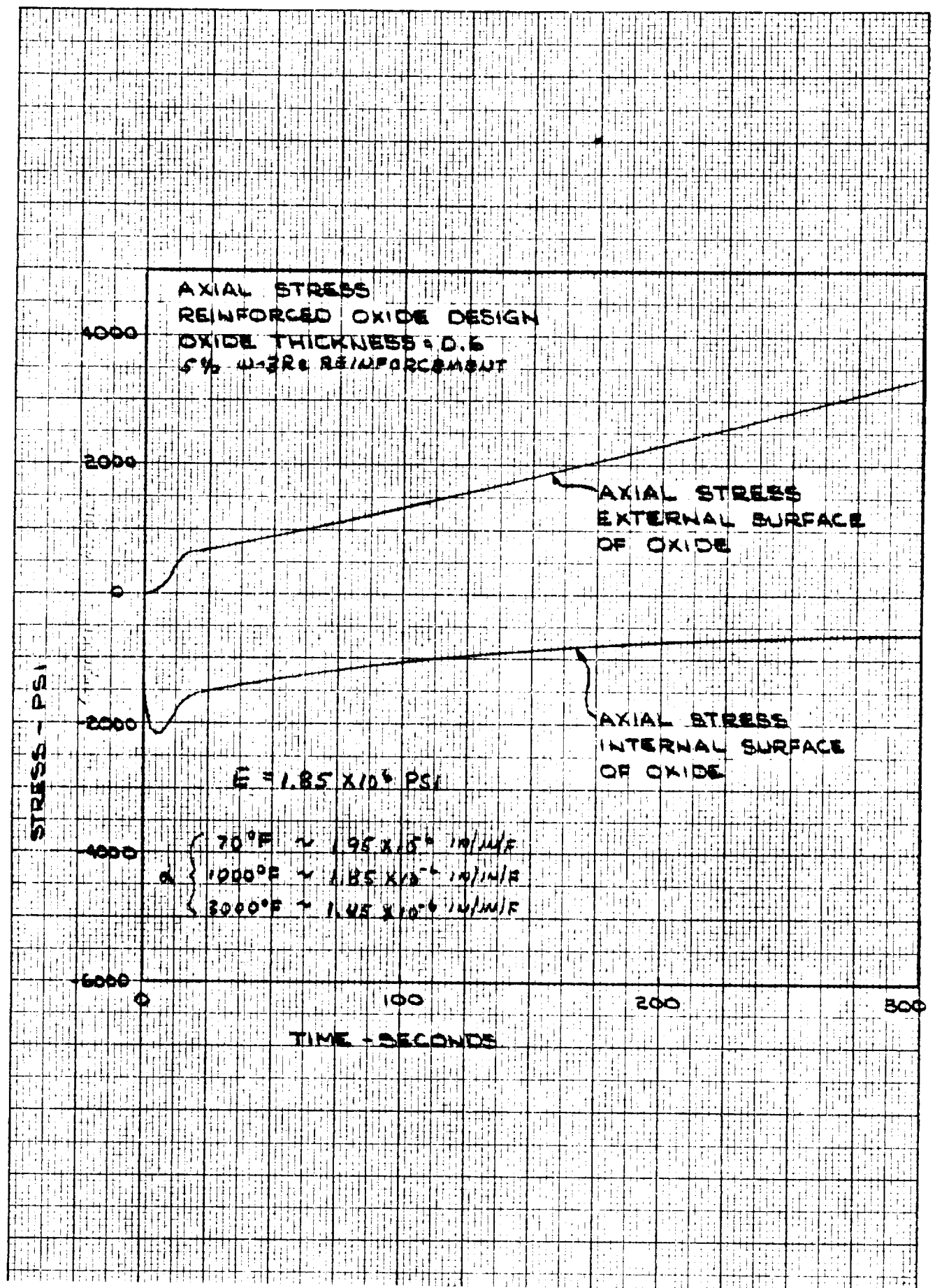ance to oxidiation, a melting temperature beyond that of the nozzle environment, and resistance to thermal stress failures. Several materials may be selected that possess a combination of two of these properties but will be seriously lacking in the third. The proposed design utilizes two materials, each possessing two of the desired properties and so selected as to complement each other in total capability (oxidation resistance and high melting point for oxide, and high melting point and thermal shock resistance for pyrolytic graphite).

Thermal stress failure normally accompanies low thermal conductivity. A typical means of combating thermal stress failure in throat inserts has been to make the insert as thin as possible to reduce the thermal gradient

202

White Silica (MX-2646)

Zirconia

Pyrolytic Graphite

CGW Graphite

Carbon Cloth (MX-4926)

JT-0981 Graphite

White Silica (MX-2600)

Green Silica
(High Silica 184)
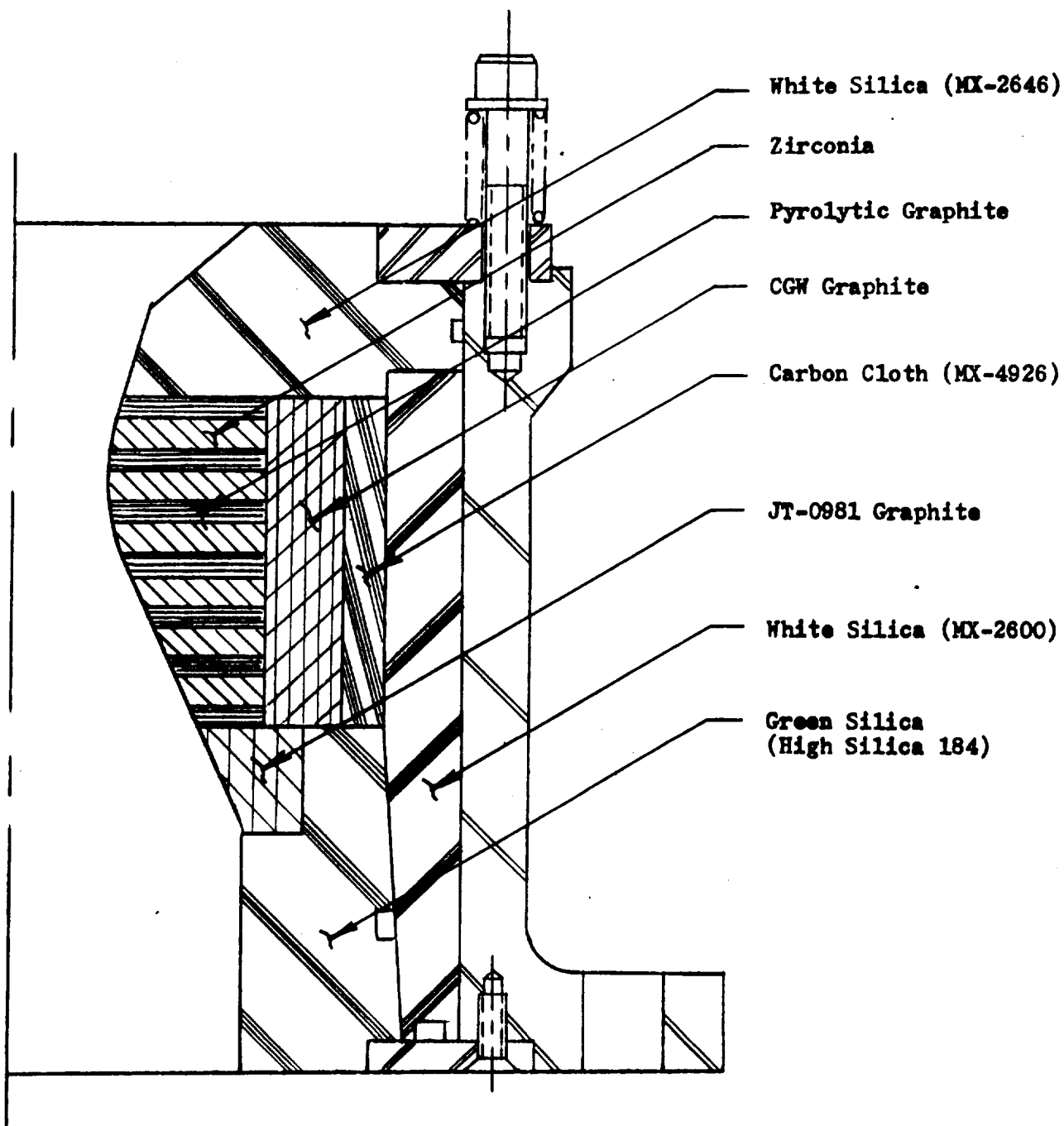
REFRACTORY LAMINATE INSERT DESIGN

and thus, reduce thermal stresses. In general, this method has been unsuccessful for brittle, refractory materials. The low conductivity of the insert material which is normally backed up with a high temperature support material such as graphite, usually produces sufficiently high temperature gradients to cause a thermal stress failure. The mode of such a failure is that the initial high temperature on the inside surface of the insert causes extremely high hoop compressive stresses that are localized on the inside diameter. This compressive stress is then, for the most part, taken out as tensile hoop stresses through the remainder of the insert. Failure, then, is generally by tension and normally originates on the outisde diameter of the insert. In a similar manner, axial stresses imposed by thermal gradients can also lead to failures. It should be noted here that a crack caused by excessive hoop tensile stresses will normally run parallel to the centerline of the insert. A crack caused by axial tensile stresses will normally be circumferential.

A zirconia material, Zircoa modified 1027, was selected for use in this design. This is a proprietary compound from Zirconium Corporation of America. The material was selected for its high oxidztion resistance, high melting point, and its low coefficient of thermal expansion (Figure 135, Figure 127 repeated for convenience) The material displays typical low thermal conductivity and a relatively high modulus of elasticity. The low conductivity results in a large thermal 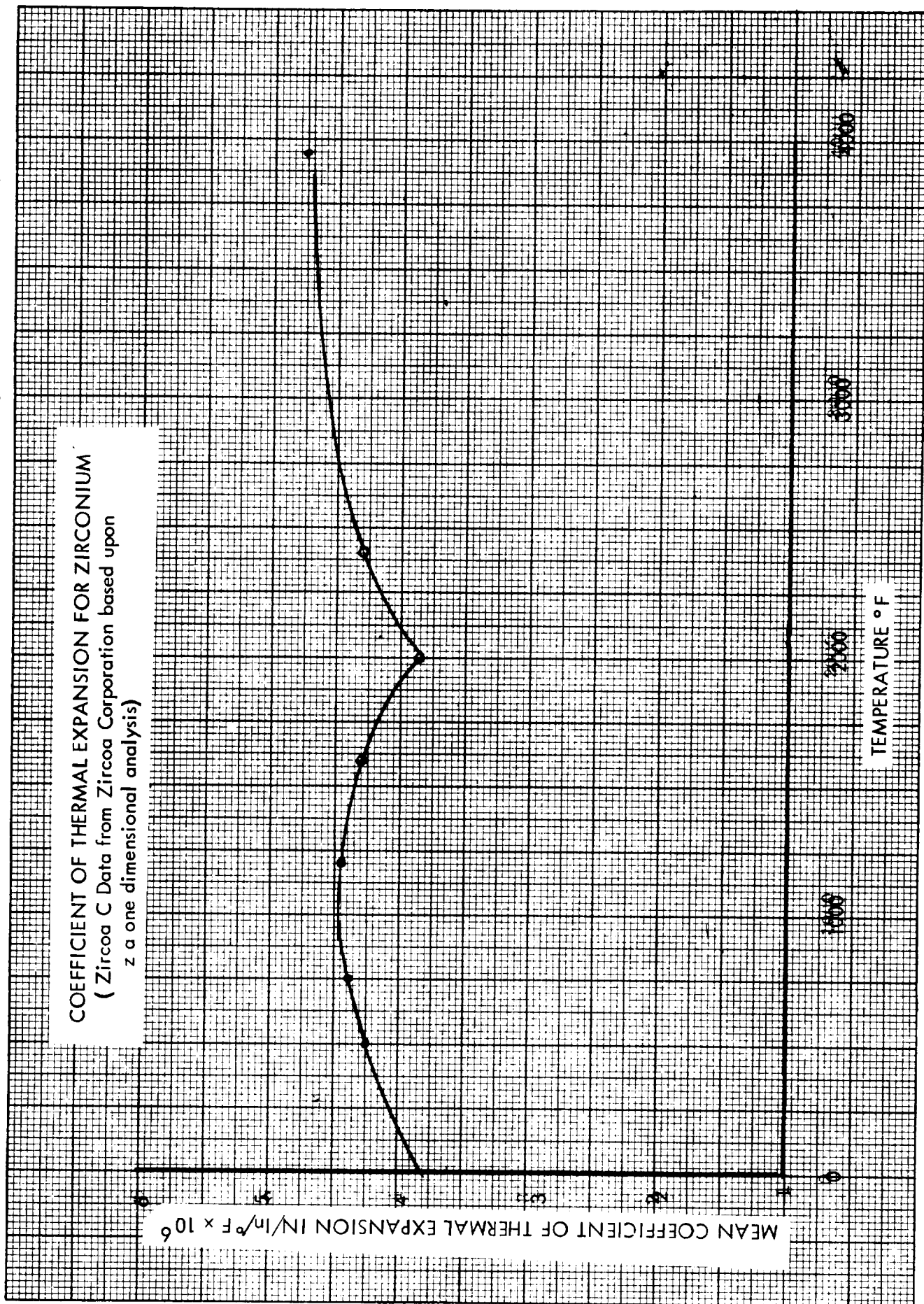gradient as shown in Figure 136. The thermal gradient, produces the high compressive stress on the inside surface as shown in Figures 137 through 142.

The inherent stress problems of the brittle, monolithic, throat insert were noted earlier. The first step in reducing or eliminating continuous axial thermal stress cracks is to segment the insert. The segments are cut in a plane perpendicular to the throat centerline resulting in an insert consisting of a series of disks or washers. This has the effect of precracking (circumferential) to reduce axial stresses and permit controlling the location of the cracks to reduce the possibility of material loss from random cracking.

Isolation and control of the axial stresses through the segmented design was followed by investigation of some means to reduce the hoop tensile stresses which produce axial cracks. As noted before, a common means of accomplishing this has been by reducing the insert thickness to reduce the thermal gradient. However, as also noted, the low thermal conductivity causes a large thermal gradient across the insert during the first few seconds of the test. If the insert is very thin, the tensile force required to overcome the compressive force must be taken out over a very small cross-sectional area. The result is a high hoop tensile stress that causes an axial crack. If the wall thickness is increased, the cross-sectional area available to take out the tensile force is increased and the resultant stress may be decreased dependent on the effect of radial thickness change on the temperature gradient. With increasing thickness, the critical stress period changes from the initial seconds to some later time. Figure 136, which is the result of a one dimensional heat transfer analysis through a one inch thickness of zirconium oxide, shows that the over-all gradient across the oxide has not appreciably changed between 20 and 100 seconds. The major change is in the slope of the curve, as might be expected for an insulating material. This indicates that heat is slowly penetrating the oxide placing more of it in compression and reducing the cross-sectional area available to resist it. A subsequent increase in tensile stress then occurs. By alternating layers of pyrolytic graphite with the oxide (a-b plane perpendicular to the nozzle centerline), maximum heat flow will be to the outside surface of the pyrolytic

204

COEFFICIENT OF THERMAL EXPANSION FOR ZIRCONIUM
(Zircoa C Data from Zircoa Corporation based upon
z a one dimensional analysis)

MEAN COEFFICIENT OF THERMAL EXPANSION IN/In/°F × 10⁶

TEMPERATURE °F

205

Figure 135

TEMPERATURE PROFILE
REFRACTORY LAMINATE DESIGN

HOOP STRESS AND TEMPERATURE
VERSUS THICKNESS
OXIDE THROAT DISC - TIME = 1 SEC.

$\alpha = 1.95 \times 10^{-6}$ in/in °F

$E \begin{cases} 70°F \sim 21.4 \times 10^6 \text{ PSI} \\ 1000°F \sim 19.6 \times 10^6 \text{ PSI} \\ 3000°F \sim 5.6 \times 10^6 \text{ PSI} \end{cases}$

207   Figure 137

HOOP STRESS AND TEMPERATURE VERSUS THICKNESS
OXIDE THROAT DISC   TIME = 5 SEC.

$\alpha = 1.95 \times 10^{-6}$ IN/IN °F

$E \begin{cases} 70°F \sim 21.4 \times 10^6 \text{ PSI} \\ 1000°F \sim 19.6 \times 10^6 \text{ PSI} \\ 3000°F \sim 5.6 \times 10^6 \text{ PSI} \end{cases}$

208   Figure 138

HOOP STRESS AND TEMPERATURE
VERSUS THICKNESS
OXIDE THROAT DISC   TIME = 5 SEC

TENSILE STRENGTH

INSERT HOOP STRESS

$\alpha = 1.95 \times 10^{-6}$ IN/IN °F

$E \begin{cases} 70°F \sim 21.4 \times 10^6 \text{ PSI} \\ 1000°F \sim 19.4 \times 10^6 \text{ PSI} \\ 3000°F \sim 5.6 \times 10^6 \text{ PSI} \end{cases}$

COMPRESSIVE STRENGTH

TEMPERATURE

RADIAL DISTANCE — INCHES

HOOP STRESS AND TEMPERATURE VERSUS THICKNESS — OXIDE THROAT DISC — TIME = 20 SEC

TENSILE STRENGTH

INSERT HOOP STRESS

$\alpha = 1.95 \times 10^{-6}$ in/in°F

$E \begin{cases} 70°F \sim 21.4 \times 10^6 \text{ PSI} \\ 1000°F \sim 19.6 \times 10^6 \text{ PSI} \\ 3000°F \sim 5.6 \times 10^6 \text{ PSI} \end{cases}$

COMPRESSIVE STRENGTH

TEMPERATURE

RADIAL DISTANCE — INCHES

210   Figure 140

HOOP STRESS AND TEMPERATURE
VERSUS THICKNESS
OXIDE THROAT DISC   TIME = 100 SEC

TENSILE STRENGTH

INSERT HOOP STRESS

$\alpha = 1.95 \times 10^{-6}$ in/in°F

$E \begin{cases} 70°F \sim 21.4 \times 10^6 \text{ PSI} \\ 1000°F \sim 19.6 \times 10^6 \text{ PSI} \\ 3000°F \sim 5.6 \times 10^6 \text{ PSI} \end{cases}$

COMPRESSIVE STRENGTH

TEMPERATURE

STRESS ~ KSI

TEMPERATURE ~ °F

RADIAL DISTANCE ~ INCHES

211   Figure 141

HOOP STRESS AND TEMPERATURE
VERSUS THICKNESS
OXIDE THROAT DISC   TIME = 300 SEC

INSERT HOOP STRESS

TEMPERATURE

$\alpha = 1.45 \times 10^{-6}$ IN/IN °F

$E \begin{cases} 70°F \sim 21.4 \times 10^6 \text{ PSI} \\ 1000°F \sim 19.6 \times 10^6 \text{ PSI} \\ 3000°F \sim 5.6 \times 10^6 \text{ PSI} \end{cases}$

TEMPERATURE ~ °F   STRESS ~ KSI

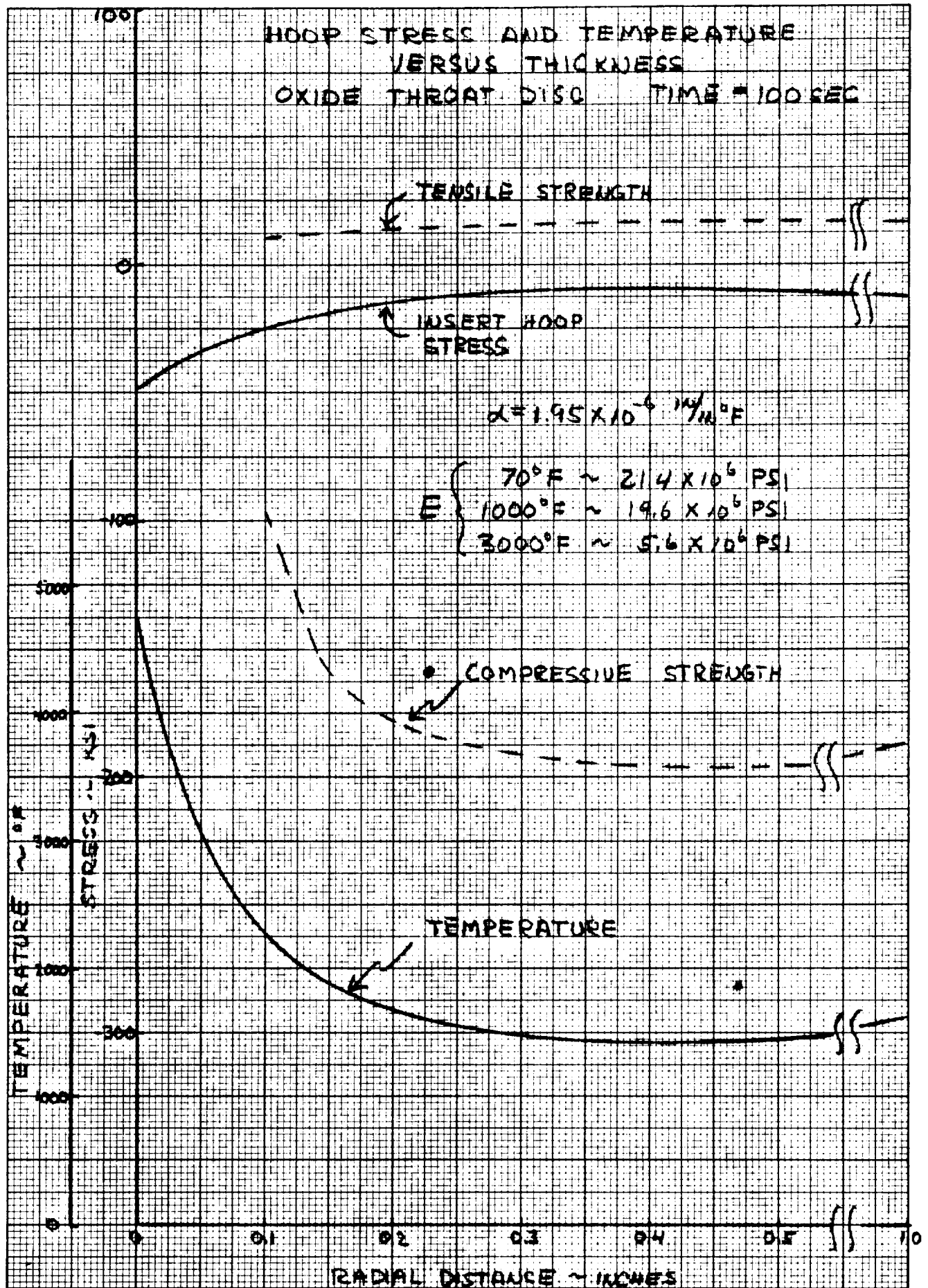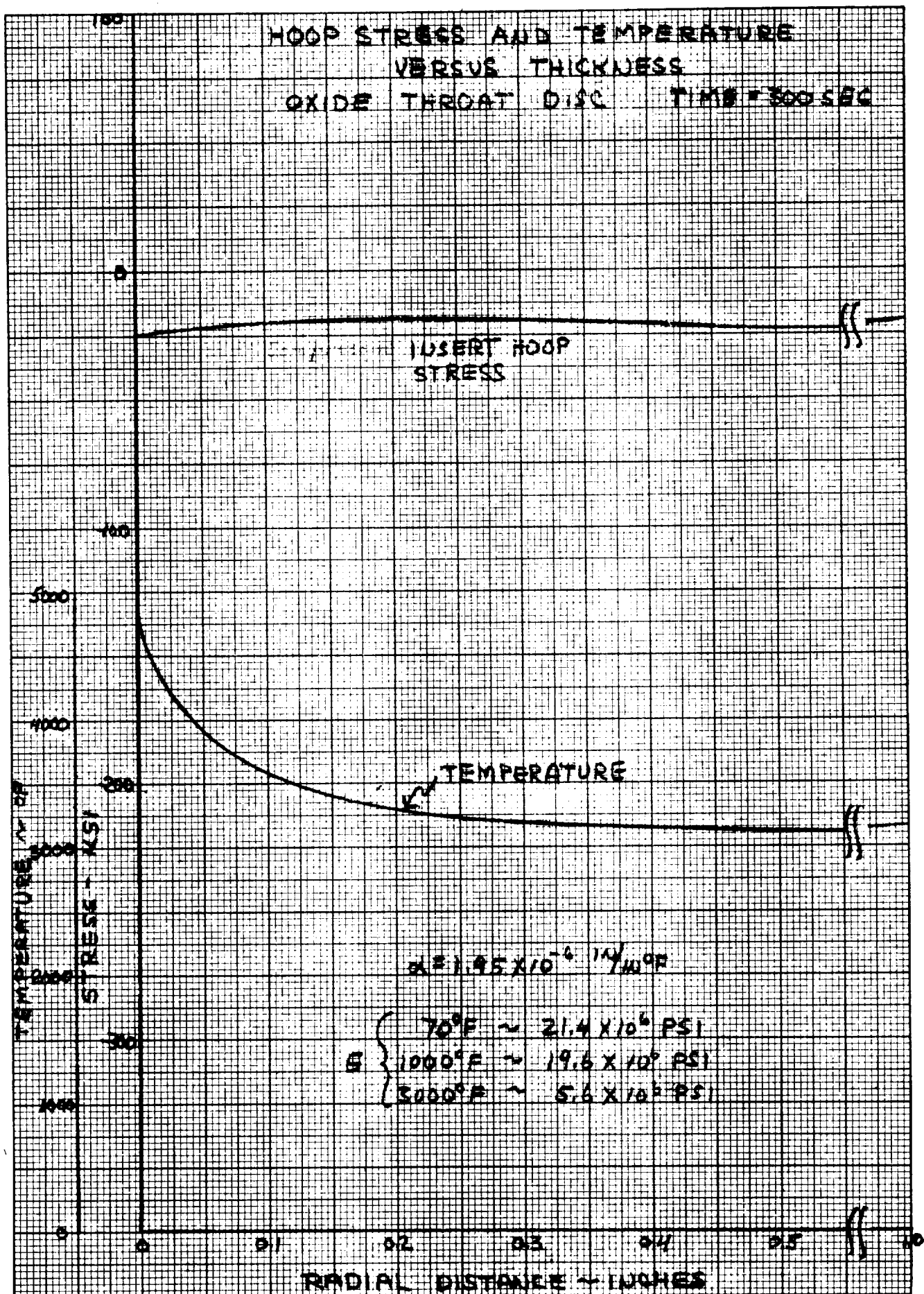RADIAL DISTANCE ~ INCHES

graphite and then be distributed through a graphite sleeve to the outside surface of the oxide disks. The result is graphically evident in Figure 143, which is a plot from a three dimensional heat transfer analysis for a one inch thick oxide wall thickness and may be directly compared with Figure 136.

These figures clearly show the addition of heat to the back side of the oxide disks from the pyrolytic disks. An example of this is illustrated by comparing the data at 100 seconds (referring to Figure 136 and 143). The outside surface which did not allow for heating from the pyrolytic graphite shows a temperature of approximately 125°F. The outside surface of the oxide, when heat is applied from the pyrolytic graphite, indicates approximately 1600°F. The effect on thermal stress of back side heating is shown in Figure 144. This is a plot of maximum tensile stress in the oxide disk for both internal surface heating only (one dimensional heat transfer analysis) and for heating from both the inside and outside surface (three dimensional heat transfer analysis).

Calculations indicate the maximum stress in the oxide ring occurs during the first second of exposure as shown in Figures 137-142. Although the computed value of compressive stress at the surface is in excess of the allowable value of 36,000 psi at 2500°F, several factors combine to make reliable calculations extremely difficult during the highly transient conditions occurring during the initial second of exposure. For the initial microseconds during and immediately after ignition, actual heating rates are indeterminate and can vary both locally and timewise. Also, material values associated with allowable strain rates become more important than mechanical property values.

The analysis used herein divides the insert into 0.20 inch thick concentric cylinders and applies a constant heating rate from time zero. Material properties are then selected for an average temperature across the cylindrical layer being analyzed. The choice of individual cylinder thicknesses for the analysis was based on obtaining a realistic compromise between material property variation with temperature and sufficient section thickness to permit averaging of the computed stress values of each interface. It was determined that the use of very thin sections results in lower than realistic computed stress values because of the relative rapidity in surface heat-up and subsequent large modulus decrease. The minimum time point of 1 second was chosen to minimize transient inputs from ignition effects and thus accommodate more reliable temperature profiles. Shorter time periods were investigated for the thin radial sections; however, and the results verified the importance of using accurate temperature profiles and corresponding mechanical property values. The resulting stress profiles obtained from the concentric cylinder analysis method are shown in Figures 137 through 142.

In summation, the purpose of the design is to maintain constant throat diameter over the duration of the test. The axial stresses are reduced by segmenting the insert into disks -- the oxide disks providing the oxidation resistance and the pyrolytic graphite disks serving to distribute heat to the outside of the oxide and to maintain an axial compressive force through thermal expansion. The heat being added to the oxide disks by the pyrolytic graphite tends to reduce their temperature gradient and hence, reduce both axial and hoop stresses. The insert is encased in a graphite sleeve to support the insert and to unilaterally distribute heat to the oxide disks. A JT-0981 graphite ring has been included in the design just ahead of the insert to reduce the effects of possible high oxidation in that area. A series of coil springs are used to maintain a compressive load on the

Radial Temperature Gradient

Oxide — Throat

Figure 143

215   Figure 144
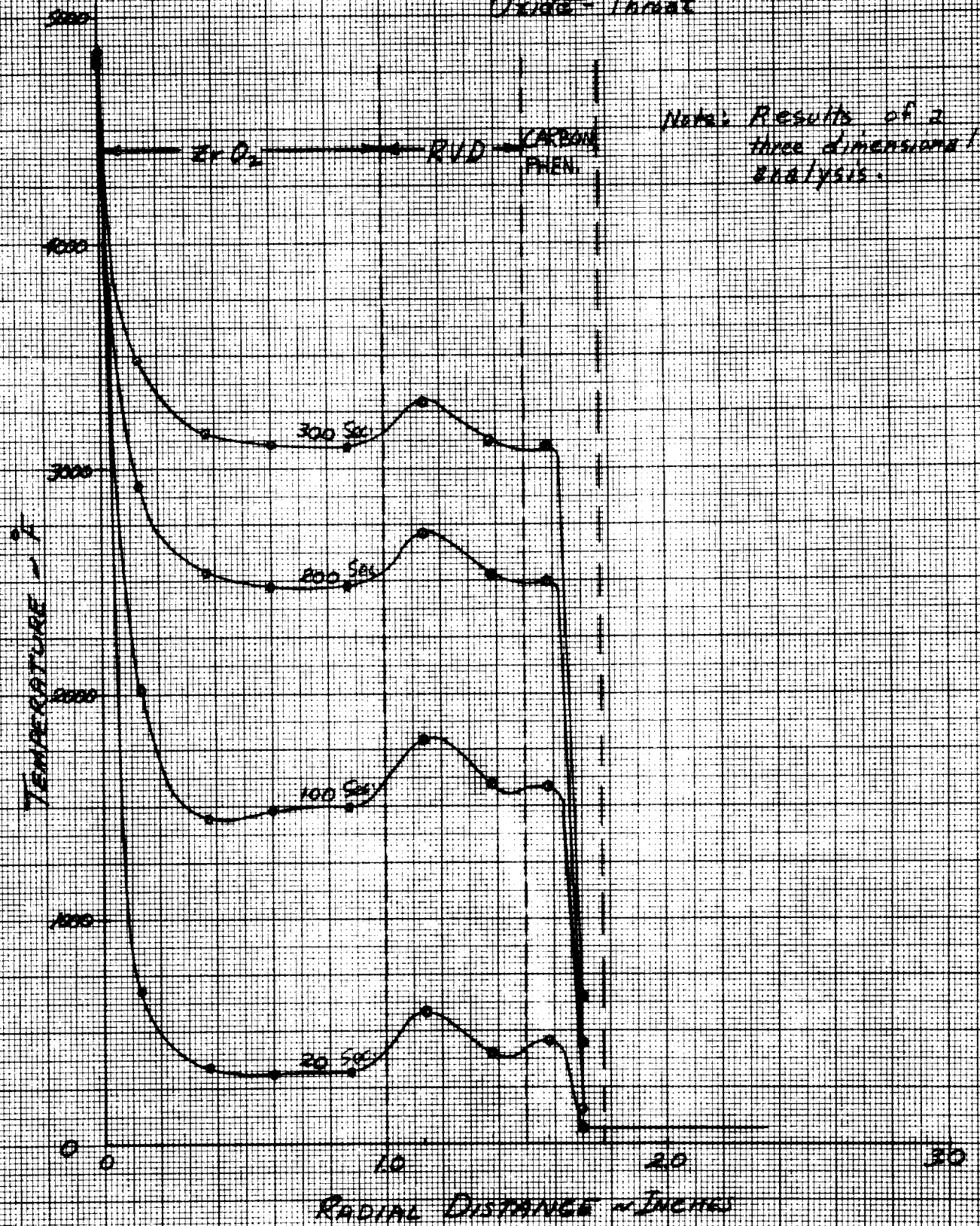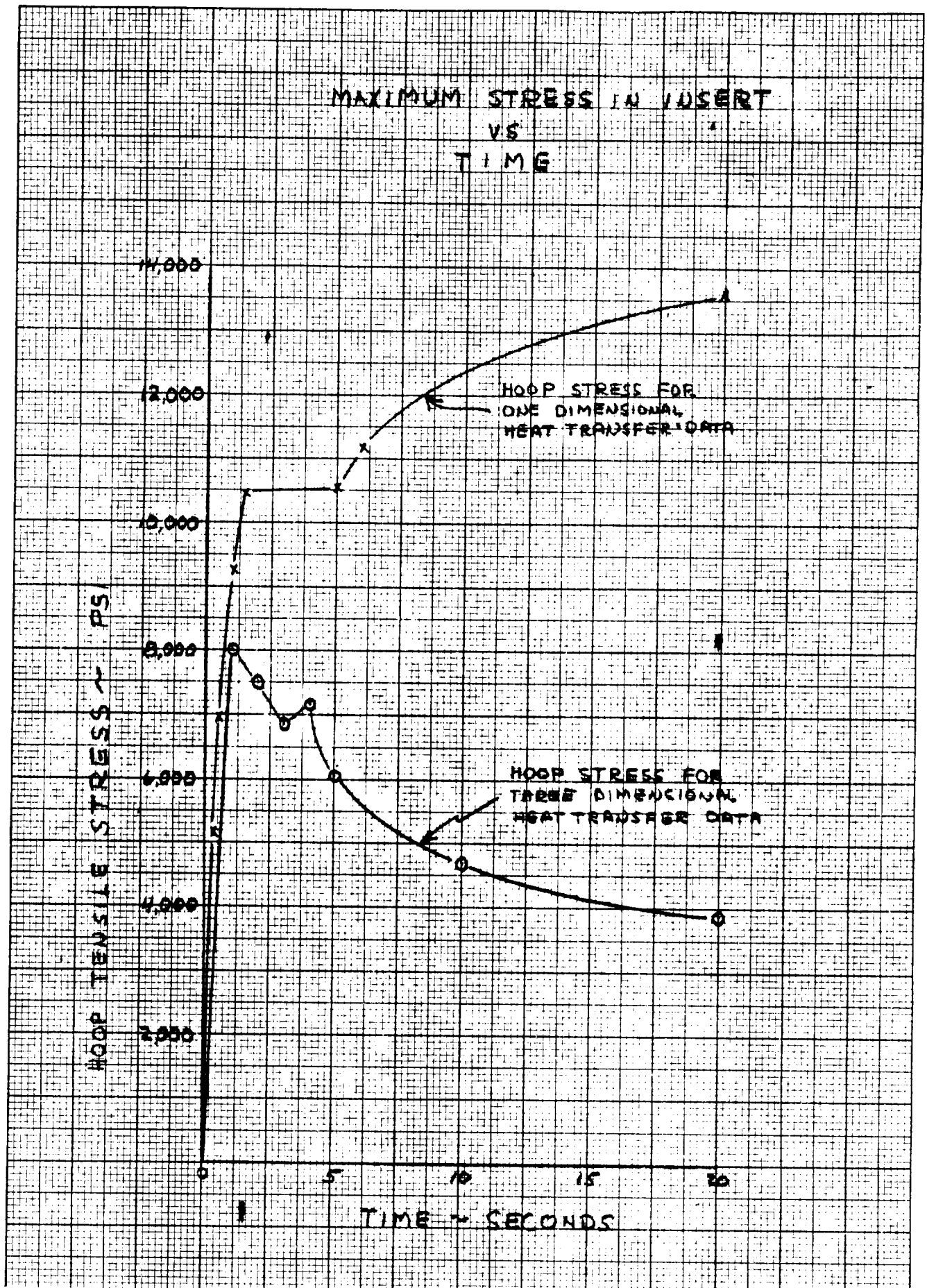
insert, primarily at the start of the 300 second cycle after cool down from the 30 second cycle. The remainder of the design is similar to the three designs already submitted in that carbon and silica phenolic are used as insulators between the throat subassembly and the steel support can.

c. Materials Selection

Oxides have long been considered desirable materials for throat inserts in liquid fueled rocket motors because of their oxidation resistance and relatively high melting points. However, oxides, as a class, are very thermal shock prone and previous attempts to utilize them as throat inserts invariably led to catastrophic thermal shock failure. Selection of material for the washers in the refractory laminate design must, therefore, be based on thermal shock resistance and temperature capability.

Based on melting temperature, the best oxide is thoria -- with a melting point of 5970°F. However, due to the very limited data available on thoria and the problems associated with its radioactive properties, the material was not selected for use at this time. Zirconia, hafnia, and magnesia all have melting points around 5000°F. Oxides with melting points much less than 5000°F cannot be considered because of the anticipated temperature environment. Oxides qualifying from a melting point consideration would then be only zirconia, hafnia, and magnesia.

Thermal shock resistance, which is the second major criteria for selection of the material for the oxide washers, should be optimized to minimize the possibility of thermal shock cracking. Very little is known about the thermal shock properties of hafnia. Designs using hafnia would be based entirely on undetermined properties, thus this material is not attractive. Thermal shock resistance of magnesia and pure zirconia are described as poor. However, a number of modifications of zirconia are commercially available and these modifications have significantly better thermal shock resistance. Evaluation of the thermal shock characteristics of various zirconia materials by TRW's Materials Technology Department, reported in "Thermal Shock Testing of High Temperature Materials" (2), indicates that two of the best modifications of zirconia are Zircoa "C" and Zircoa "1027." These materials have been developed by the Zirconium Corporation of America, Solon, Ohio, (Zircoa). Contact with Zircoa revealed the avaiability of a modified Zircoa "1027" material with reportedly greater thermal shock resistance. Consequently, the modified Zircoa 1027 was recommended for the refractory laminate design.

Material for the support washers must be strong, thermal shock resistant and reasonably resistant to the oxidizing environment. Pyrolytic graphite washers oriented with the "a" planes in the radial direction and the "c" plane in the axial direction are recommended for the support washers because of good high temperature strength and thermal shock resistance. Oxidation resistance of pyrolytic graphite is marginal at high temperatures, with the oxidation rate an exponential function of temperature. With the highly conductive "a" planes oriented radially, the washers will rapidly conduct heat from the inside surface to the supporting graphite block which serves as a heat sink. In this manner, the temperature of the pyrolytic graphite surface exposed to the oxidizing gases will be minimized, and the corrosion losses reduced.

d. Thermal Analysis

Due to the configuration of the refractory laminate insert design, a three dimensional heat transfer analysis was performed in addition to preliminary analyses using one dimensional methods. The three dimensional analysis was able to include the heat flow from the graphite sleeve to the O. D. of the oxide and from the sides of the pyrolytic to the oxide. The one dimensional analysis was not directly capable of evaluating this factor.

A high speed digital computer program was used in determining the transient three dimensional heat transfer through the nozzle wall. A total of 185 node points and 308 resistance points were used. The program was capable of handling variable thermal properties for the materials.

The results of the analysis are shown in graphical form in Figures 143 and 145 through 147. Figure 143 shows the thermal gradient through the oxide disk at the throat, Figure 145 shows the gradient through the pyrolytic washer upstream of the throat oxide disk, and Figure 146 shows lines of constant temperature through the nozzle cross-section at 100 seconds. Figure 141 shows several items of note. The effect of the carbon cloth phenolic as an insulator is most evident. The graphite is shown to be bounded by the 1000 and 2000°F lines indicating its use as a sink to distribute heat into the back side of the oxide. The effect of the graphite may also be seen in the exit cone silica by the fact that the 1000°F isotherm shows a bulge around the aft end of the graphite. Figure 147 is included to show a typical profile through the silica liner in the forward portion of the nozzle.

e. Stress Analysis

Thermal stresses in the zirconia oxide washers of the refractory laminate design were anlyzed by the IBM 7070 computer stress program. The program is based on Timoshenko's theory of thermal stresses in circular cylinders. No analysis was run on the pyrolytic graphite washers since they experience a low temperature gradient due to their high conductivity in the radial direction.

The stress calculations were run at various times through the 300 second firing cycle. Hoop stresses for the oxide washer located at the throat appear in Figures 137 through 142. Hoop stresses for a forward oxide washer are plotted in Figures 148 through 153.

In making this analysis, the throat washer was divided into five layers and the forward washer into three layers. The stress program stress each of these layers as a separate cylinder.

The reason for dividing the insert into layers is to incorporate temperature effects on the mechanical properties used in the analysis. Only a single value for the temperature dependent mechanical properties can be used for each concentric cylinder. Using a layered approach, a different value can be used for each layer as input to the program. Thus, the hotter layers near the inner surface can be analyzed with different property values than the cooler layers near the outer surface of the insert. This is a significant advantage because in the physical case, properties of the oxide material will vary widely in the radial direction due to the extreme temperature variation. Hoop stresses, so computed, are not influenced by the layering approach

RADIAL TEMPERATURE GRADIENT
Pyrolytic Graphite - End of Throat

Figure 145

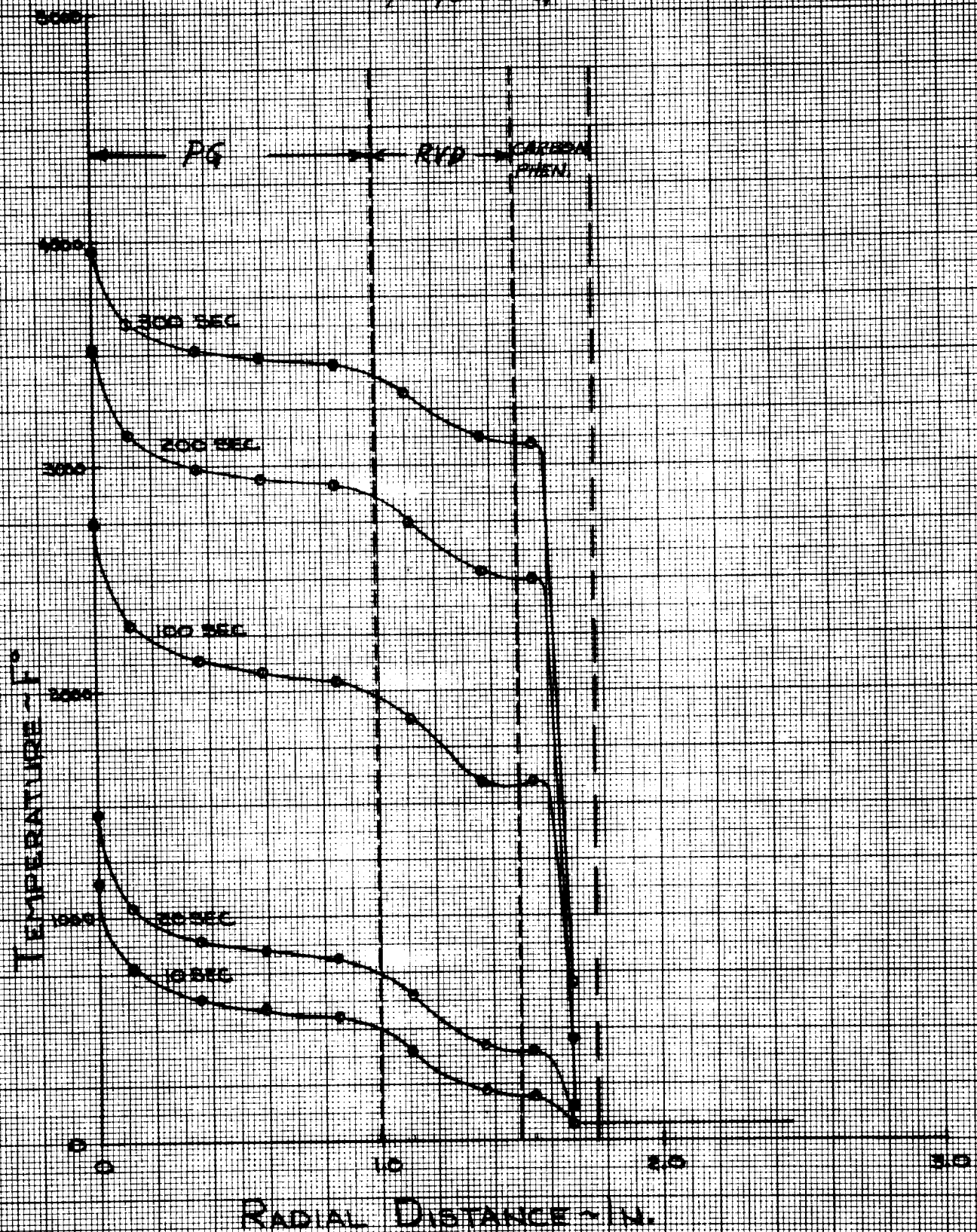Diagram Showing Isotherms Through the Nozzle

Wall at 100 Secs of Simulated Firing
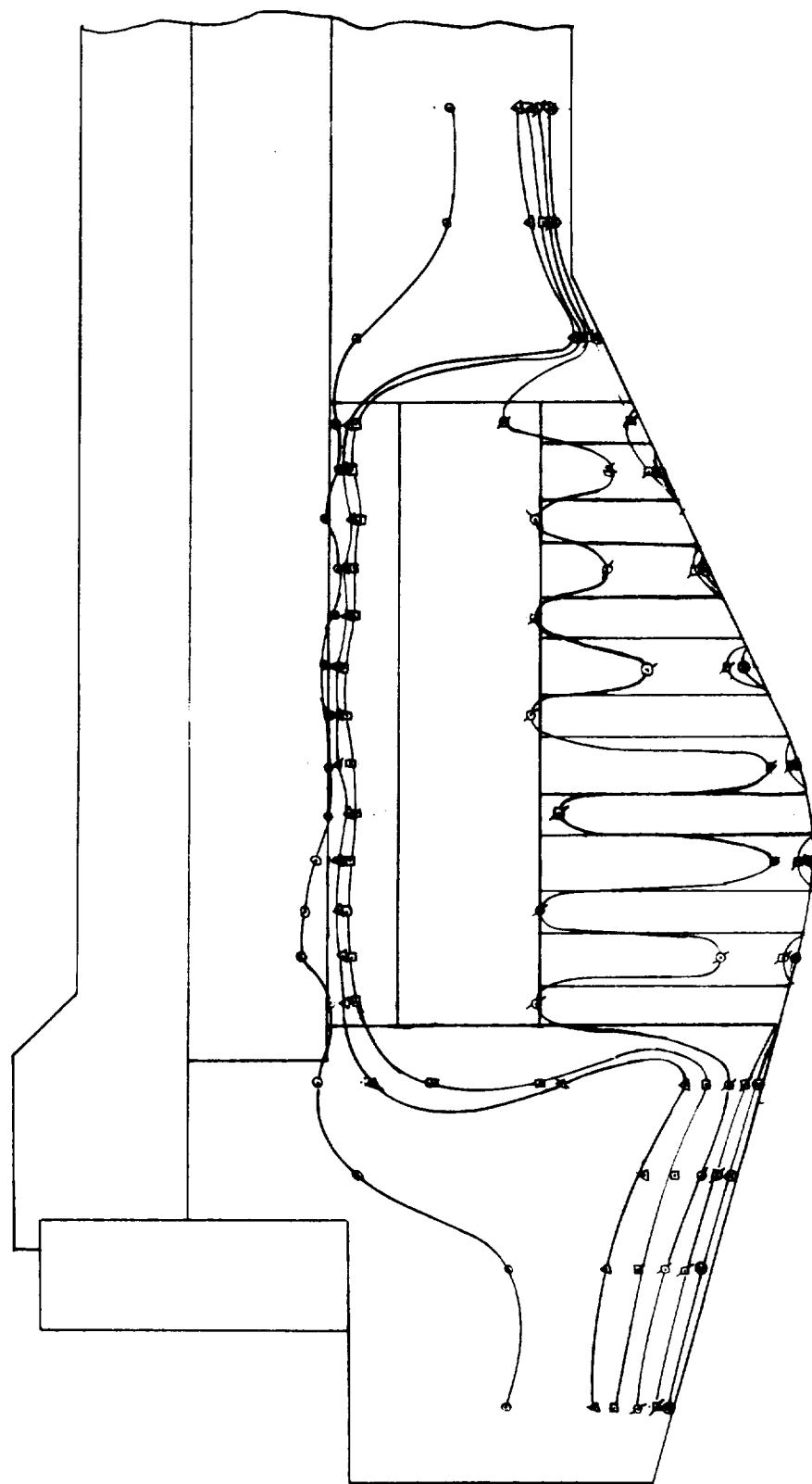
⊙	100°F
◁	500°F
☐	1000°F
◊	2000°F
◢	3000°F
⊗	4000°F

Figure 146

219

TEMPERATURE PROFILE
SILICA
Forward Nozzle Section

Figure 147

220

HOOP STRESS AND TEMPERATURE
VERSUS THICKNESS
OXIDE FORWARD DISC   TIME = 1 SEC

221   Figure 148

HOOP STRESS AND TEMPERATURE
VERSUS THICKNESS
OXIDE FORWARD DISC   TIME = 3 SEC.

TENSILE STRENGTH

INSERT HOOP STRESS

$\alpha = 1.95 \times 10^{-6}$ in/in/°F

$E \begin{cases} 70°F \sim 21.4 \times 10^{6} \text{ PSI} \\ 1000°F \sim 19.6 \times 10^{6} \text{ PSI} \\ 3000°F \sim 5.6 \times 10^{6} \text{ PSI} \end{cases}$

COMPRESSIVE STRENGTH

TEMPERATURE

RADIAL DISTANCE

222   Figure 149

HOOP STRESS AND TEMPERATURE
VERSUS THICKNESS
OXIDE FORWARD DISC   TIME = 5" SEC.

223   Figure 150

HOOP STRESS AND TEMPERATURE
VERSUS THICKNESS
OXIDE FORWARD DISC   TIME = 2.0 SEC

$\alpha = 1.95 \times 10^{-6}$ in/in°F

$E \begin{cases} 70°F \sim 21.4 \times 10^6 \text{ PSI} \\ 1000°F \sim 19.6 \times 10^6 \text{ PSI} \\ 3000°F \sim 5.6 \times 10^6 \text{ PSI} \end{cases}$

TENSILE STRENGTH

INSERT HOOP STRESS

COMPRESSIVE STRENGTH

TEMPERATURE

RADIAL DISTANCE — INCHES

224   Figure 151

HOOP STRESS AND TEMPERATURE
VERSUS THICKNESS
OXIDE FORWARD DISC   TIME = 100 SEC

$\alpha = 1.95 \times 10^{-6} \, IN/IN \, °F$

$E \begin{cases} 70°F \sim 21.4 \times 10^6 \, PSI \\ 1000°F \sim 14.6 \times 10^6 \, PSI \\ 3000°F \sim 6.6 \times 10^4 \, PSI \end{cases}$

225

Figure 152

HOOP STRESS AND TEMPERATURE
VERSUS THICKNESS
OXIDE FORWARD DISC   TIME = 300 SEC

INSERT HOOP STRESS (COMPRESSIVE)

TEMPERATURE

$\alpha = 1.95 \times 10^{-6}$ IN/IN°F

E { 70°F ~ 21.4 × 10^6 PSI
1000°F ~ 19.6 × 10^6 PSI
3000°F ~ 5.6 × 10^6 PSI }

STRESS ~ KSI

TEMPERATURE ~ °F

RADIAL DISTANCE ~ INCHES

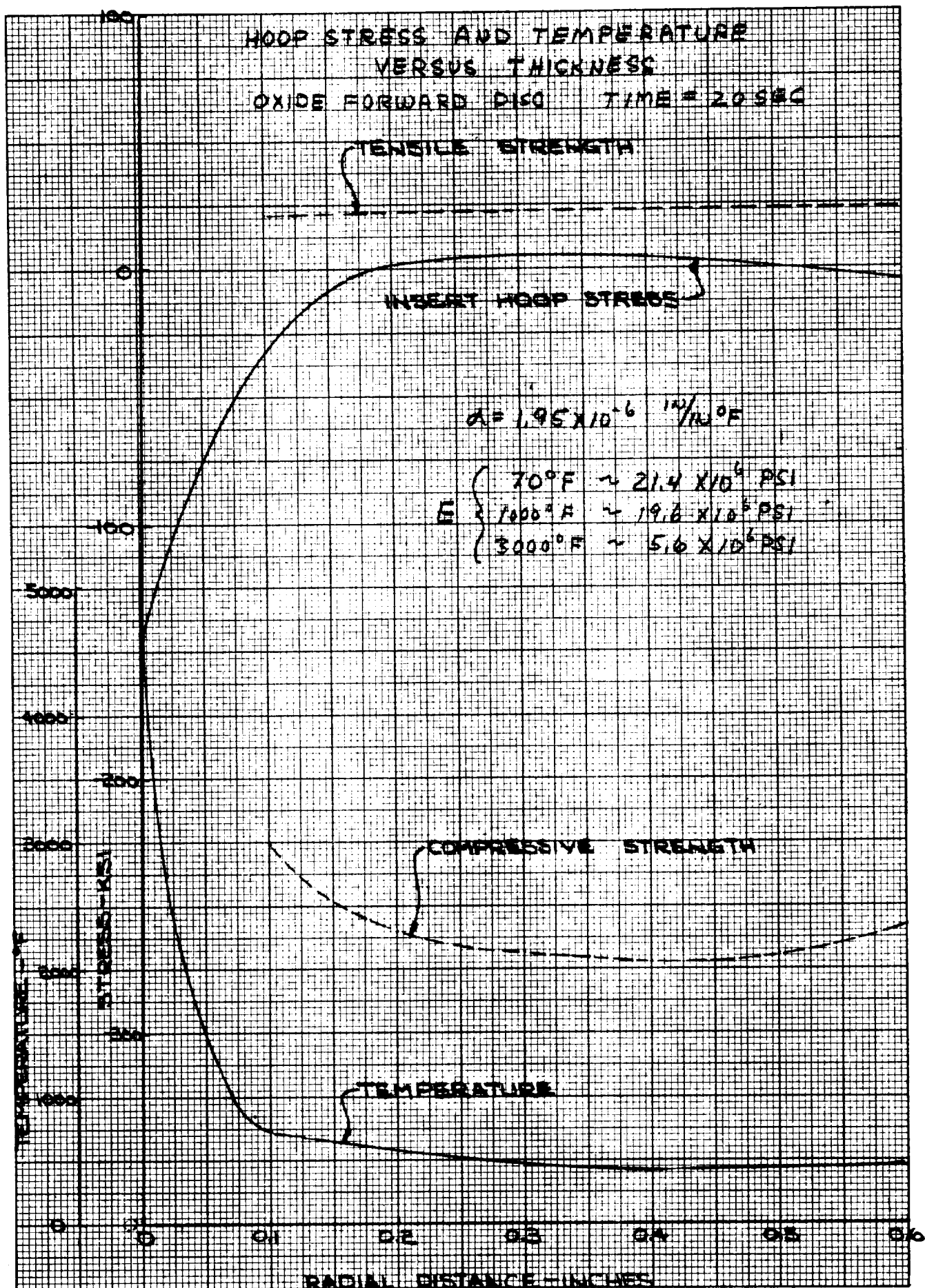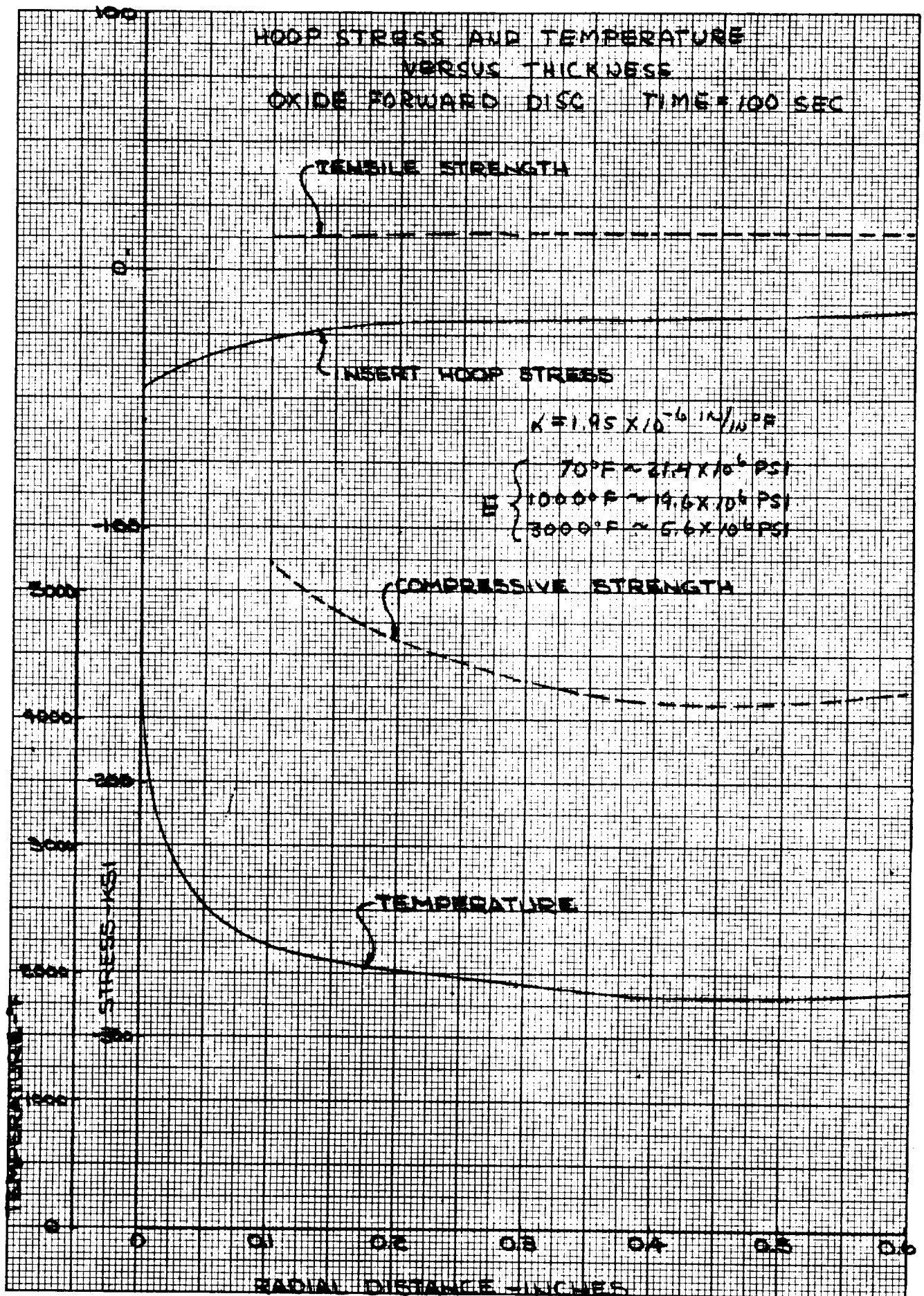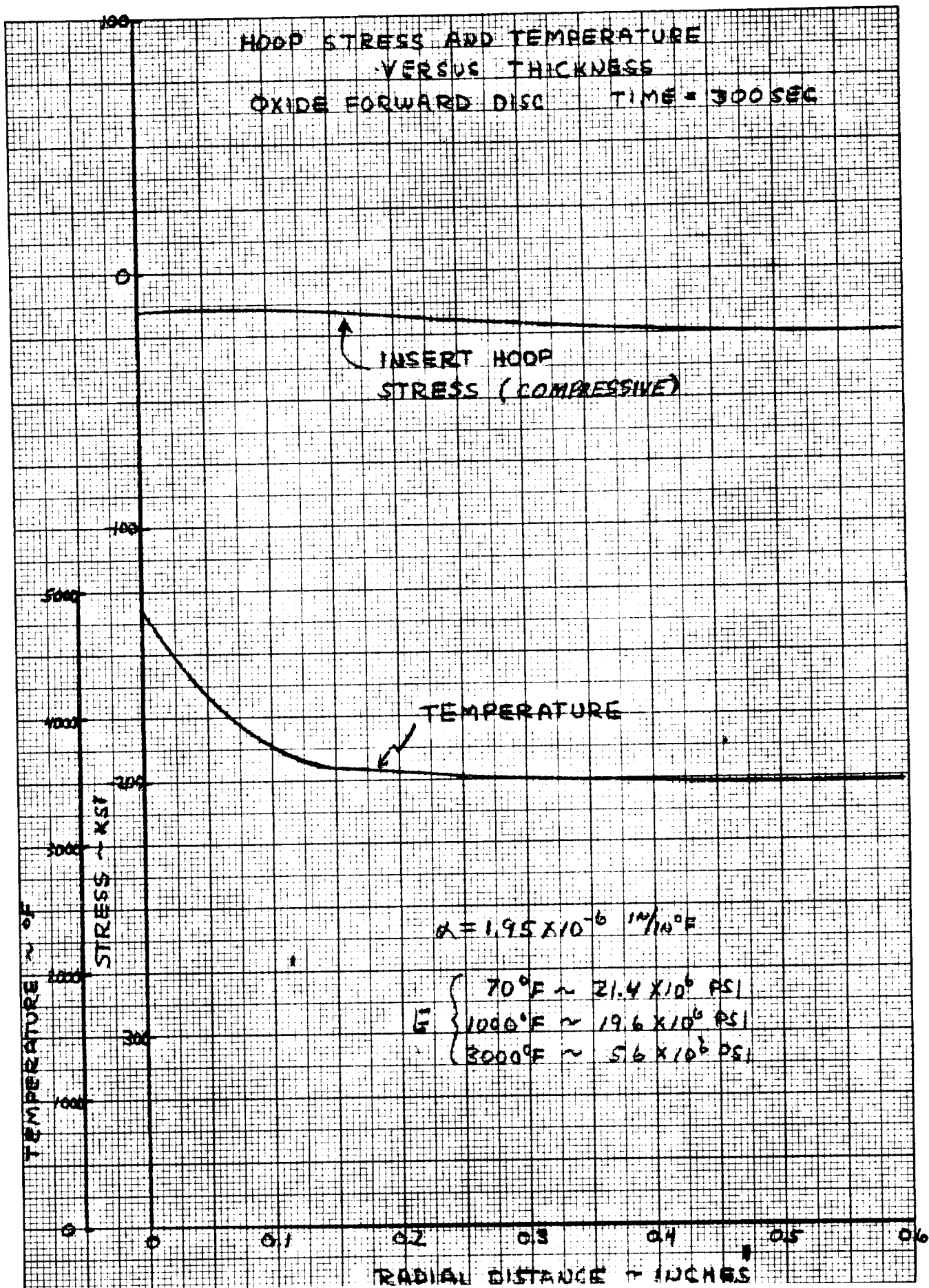226   Figure 153

since the program considers composite effects. Axial stresses cannot be accurately computed by the segmented concentric cylinder approach and hence have not been reported on herein.

Stresses are printed out by the program at the external and internal surfaces of each cylinder. At the interfaces of the layers in the insert, then, there will be two values calculated -- one using the properties of the layer internal to the interface and one using the properties of the layer external to the interface. Thus, there will be two different stress values calculated for one point in the insert. The stresses shown in Figures 137-142 and 148-153 represent the mean values for the two calculated stresses at given radii. These figures also include the temperature profiles, and the compressive and tensile strengths of the oxide which are dependent upon the temperature of the material at the given time. See Figures 154 and 155 for the compressive and tensile strength of the oxide versus temperature.

The stress curves show that the tensile stresses through the insert are low and nowhere exceed the tensile strength of the material at any of the calculation times. Compressive stresses, however, are relatively high during the firing cycle. These high compressive and low tensile values arise because the temperature gradient in the insert is extremely steep early in the firing cycle. That is, the high temperatures at the inner surface drop off so rapidly in the radial direction that only a small inner portion of the insert is experiencing compressive stresses. The remainder of the insert is placed in tnnsion. The physical portion of the insert in tension, being much larger than the compressive portion, does not result in high unit stress levels.

f. Geometry and Mechanical Design

The most noticeable difference between the refractory laminate design and a monolithic throat insert design is the method of throat retention. Monolithic throat inserts are normally retained by means of an angular ramp. This permits a near constant wall thickness of the insert to reduce stress concentrations and permits the use of thin wall inserts to reduce the thermal gradient and thus, thermal stresses. The refractory laminate design approaches the problem of thermal stress with a different solution. As noted earlier, the axial stresses are reduced by segmenting the insert into disks and the hoop stresses are reduced by using alternate pyrolytic graphite disks to heat the oxide from the back. If the ramp retention method was used, the expansion of the pyrolytic graphite in the "c" direction would result in motion of the disks down the ramp in the direction of the nozzle-combustion chamber interface. To accommodate the axial growth in the forward direction, a very complex design is required. Therefore, because axial motion can best be accommodated at the aft end of the nozzle, and because stress analysis indicated that the greater than normal radial thickness of the oxide, when heated from the backside, can withstand the hoop tensile stresses, a cylindrical sleeve was used to support the throat insert.

Considerable thought and discussion was given to the cross-sectional shape of the disks and to whether the disks should be solid or segmented into two or three segments. The major alternative, with respect to cross-sectional shape, was to use a cross-section in the shape of a truncated cone. The outside diameter of the oxide disk would be thicker than the corresponding cross-sectional thickness at the inside diameter. The pyrolytic graphite

COMPRESSIVE STRENGTH vs TEMPERATURE FOR PARTIALLY STABILIZED ZIRCONIA

228

Figure 154

TENSILE STRENGTH VS. TEMPERATURE
FOR PARTIALLY STABILIZED ZIRCONIA

TEMPERATURE °F

TENSILE STRENGTH, KSI

229

Figure 155
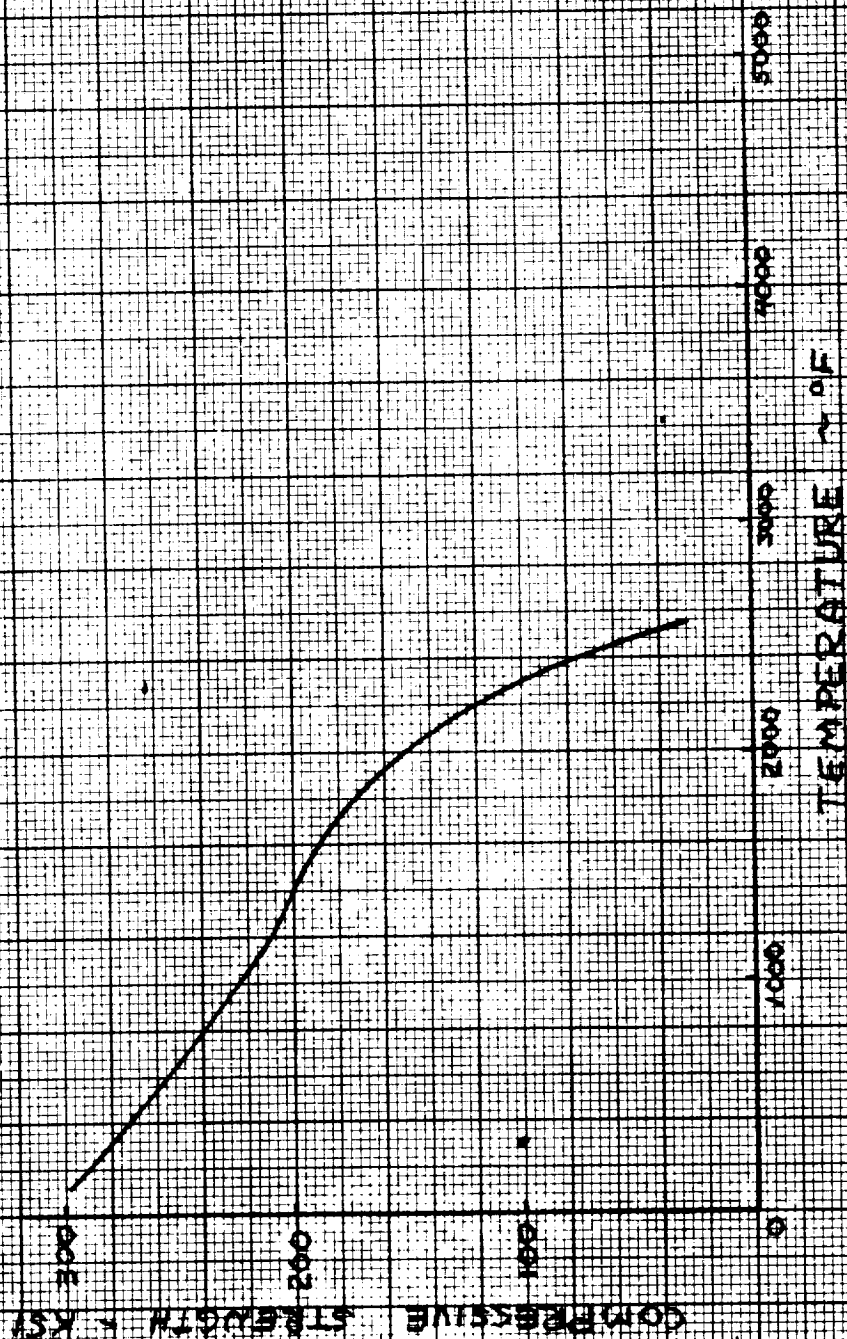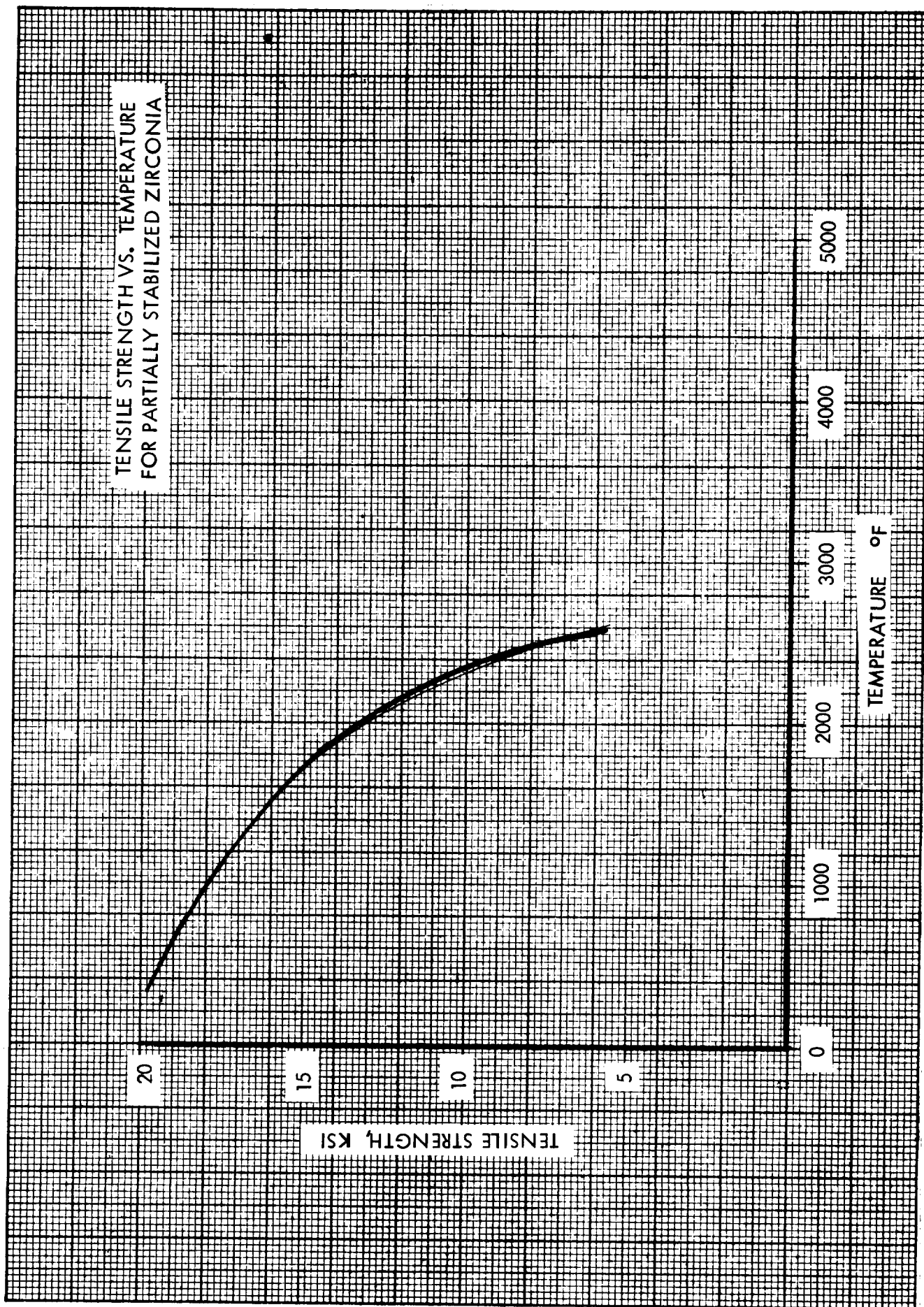
disks would be just the opposite with the inside diameter thicker than the outside diameter. The desired effect would be to lock the thermal stress sensitive oxide disks into position in the event that a thermal crack would occur. However, the resultant forces that lock the oxide into position also tend to lift the pyrolytic graphite away from the graphite sleeve. A gap between the pyrolytic graphite and the graphite sleeve will prevent heat transfer to the graphite and then to the oxide. Since the heat transfer from the pyrolytic graphite to the oxide is the basis for the design, the wedge shape was deemed unacceptable at this time.

Consideration of the concept of segmenting each oxide disk into two or three pie-shaped segments was a result of reviewing the thermal shock test results of various materials. Materials capable of withstanding a thermal shock differential of 1900°F in the form of a solid 1.50 inch diameter disk, will normally withstand test conditions as an insert. It was noted that those materials that will only withstand a low temperature differential normally fail by separating into two nearly symmetrical halves. If the material is subjected to a temperature considerably above that necessary to cause it to fail, the appearance of the tested part is three, pie shaped, symmetrical wedges. Based on this, a material with a low thermal shock resistance was tested. The configuration of the test pieces was changed from a solid disk to a ring with various I. D. to O. D. ratios. However, the results of the tests were inconclusive, and thus the oxide discs were not segmented in this design.

Since the refractory laminate nozzle was subjected to a start-stop-start firing cycle, provision had to be made for the expansion and contraction of the insert materials. If allowance is made for material expansion during the first 30 second firing, gaps will appear on cooldown unless the materials are forced back together. To accomplish this, coil springs were used.

The coefficient of thermal expansion for pyrolytic graphite in the axial direction is shown in Figure 156. There are seven pyrolytic graphite washers, each approximately 0.125 inch in axial width. Using the temperature data for 30 seconds, the linear axial expansion of the graphite washers after 30 seconds can be calculated.

$$\Delta L = L \alpha \Delta T$$

$$= (0.875 \text{ in})(1700°F)(13.3 \times 10^{-6} \frac{\text{in}}{\text{in}°F}) = .0197 \text{ in.}$$

Similarly, the axial expansion for the oxide washers is:

$$\Delta L = L \alpha \Delta T$$

$$= (1.2 \text{ in})(4700°F)(1.95 \times 10^{-6} \frac{\text{in}}{\text{in}°F}) = 0.0109 \text{ in.}$$

Thus, the total insert expansion at 30 seconds is:

$$0.0197 + 0.0109 = 0.036 \text{ in.}$$

This 0.030 inch expansion is a conservative number since the temperatures used were those occuring near the inner surface of the materials. The inner surfaces will expand this amount, but not all of this growth will

Coefficient Of Thermal Expansion Vs Temperature
For Pyrolytic Graphite – "C" Direction

231   Figure 156

have to be absorbed by the springs, since the silica-phenolic will char at its inner surface during the 30 second pulse. Thus, some of the insert growth at the inner surface will be accounted for by the crushing of the charred silica phenolic. There is some expansion of the silica phenolic due to temperature at 30 seconds, but this value is small and will be balanced by compression of the silica phenolic. This effect can be neglected in the spring design.

The springs must be able to overcome friction forces at the various sliding surfaces to force the components back into place. When the first firing pulse is stopped at 30 seconds, these friction forces will be at their maximum values. As the materials become cooler and require repositioning by the springs, the friction forces decrease. In fact, they will approach zero when the materials again reach ambient temperature. In this condition, any small axial force will be sufficient to return them to their original positions.

The possibility exists for a pressure force at the forward face of the silica phenolic if gases are exposed to this interface. From time = 0 to time = 30 seconds, the springs must overcome the gas pressure forces in order to keep the silica phenolic in contact with the insert. The area ratio at the silica phenolic-insert interface is 1.46. The pressure at this ratio is 20 psi since the chamber pressure is 100 psi. Thus, the pressure force at the forward face of the silica at 30 seconds is:

$$(20 \text{ psi}) \quad \left[(2.85)^2 - (.725)^2\right] = 476 \text{ pounds}$$

Spring specifications to overcome this force are:

O.D.	I.D.	Free Length	Load to Deflect 1/8"	Maximum Load
$\frac{1}{2}$"	9/32"	1	28 pounds	80 lbs/.300 Deflection

This spring can deflect 30% of its free length or 0.300 inch. Initial deflection of the spring for the refractory laminate design can then be 0.270 inch, leaving 0.030 inch additional deflection for the insert growth at 30 seconds. The force exerted at the springs' extended position (0.27 inch deflection) is (8 springs)(72 pounds/spring) = 576 pounds.

At 300 seconds, the insert expansion is:

Pyrolytic Graphite: $L = (0.875 \text{ in})(3500°F)(13.3 \times 10^{-6} \frac{in}{in°F}) = 0.041 \text{ in.}$

ZrO_2: $L = (1.2 \text{ in})(4700°F)(1.95 \times 10^{-6} \frac{in}{in°F}) = 0.0109 \text{ in.}$

$$0.041 \text{ inch} + 0.011 \text{ inch} = 0.052 \text{ inch}$$

Of this expansion, 0.030 inch has been absorbed by spring compression. This leaves 0.022 inch to be absorbed by crushing of the charred silica phenolic. The amount of charred material which will have to be crushed is:

$$\frac{0.022 \text{ inch}}{0.625 \text{ inch}} = .0352 \approx 3.5\%$$

The charred silica can easily accommodate this compression since it can be crushed up to 15 to 20% of its volume.

C. FABRICATION

The program was primarily concerned with the design of the throat inserts and supporting structure. As the program evolved, considerable effort, as noted in previous sections, was devoted to material development and, to a lesser degree, to process development for some of the throat materials. Specifically, the materials requiring process development were the reinforced oxides which, prior to this program, had been fabricated in laboratory specimen sizes only and the graded carbide which had never been fabricated in the thin sections required by the design. The remaining materials, both for the inserts and the support structure, were fully defined from a process standpoint but will be reviewed for information purposes.

1. Reinforced Oxide

Considerable processing experience had been gained during the materials evaluation phase of the program in the fabrication of the screening test specimens. However, a full scale insert of the size required had not been fabricated.

The first insert fabricated was a trial piece to determine whether the process used for screening test specimens would produce a satisfactory full scale billet. The initial fabrication attempt produced a high density, uncracked billet but the compaction was greater than predicted. The result was that the axial length of the billet was too short to clean up to the required dimension. The material quantity was adjusted and the second billet was successfully fabricated and used.

The basic materials used in the composite material insert designs fabricated for test firing in this program consisted of Zircoa F-410 partially stabilized zirconia powder (produced by Zirconium Corporation of America, Solon, Ohio) and 0.0035 inch diameter tungsten - 3% rhenium wire (produced by General Electric Company, Lamp Metal and Components Department, Cleveland, Ohio). The F-410 material (stabilizing materials proprietary to Zirconium Corporation of America) was 325 mesh, or finer, particle size. Wire fibers of 3/16" length were thoroughly mixed (random orientation) into the powder by means of a twin-cone blender. A five volume percent mixture of wire to oxide was used.

Materials were cold isostatically pressed, without a binder material, at 30,000 psi pressure. A steel mandrel was used to form the internal contour of the inserts, whereas a rubber membrane material contacted the outer surfaces. Sintering of the compressed insert shapes were performed at 4000°F in a vacuum of approximately one micron. Parts were heated to temperature at the rate of 500°F/hour, held at the 4000°F temperature for 4 hours, and cooled to room temperature at 1000°F/hour (total furnace time of approximately 16 hours).

Finishing of the sintered insert shapes consisted of grinding the end faces to establish squareness and proper axial dimensions. The end facing operations were then followed, respectively, by grinding of the OD and ID surfaces. Final inspection of the finish ground inserts consisted of dimensional, visual (for cracks and other surface discontinuities), radiography, and density determinations.

234

2. Graded Carbide

The graded carbide insert design consisted of four distinct layers of carbide and carbide graphite mixtures selected to produce a composite structure with optimum oxidation/corrosion resistance on its exposed inner surface and improved resistance to cracking due to thermal stressing at the outer (OD) surface. The compositions of the four layers -- selected to provide a uniform transition in thermal coefficients of expansion from a straight carbide inner layer to a thermal shock resistant, high graphite content outer layer -- were, respectively, from inner to outer surfaces: 100% HfC; 90 volume percent (v/o) TaC-10 v/o graphite; 60 v/o TaC-40 v/o graphite; 30 v/o TaC-70 v/o graphite. The compositions were made from mixed powders. Carbide powders (-325 mesh) were all produced by carbon reduction of the respective metal oxides, and the graphite was Union Carbide, Carbon Products Division, Grade BB5 of -270 mesh particle size. Powders were all sized and mixed by conventional ball milling equipment. All processing and machining of the insert was done by The Carborundum Company.

Construction of the insert began with formation of the inner layer, which was followed by successive applications of the outer layers. A layer of HfC, with suitable organic binder, was cold pressed onto a male graphite mandrel and cured at 110° - 120°C (230° - 248°F) to set the binder and provide adequate strength for machining. The HfC was then machined to desired thickness and contour. The OD surface of the HfC layer thus became the mandrel surface for application of the next layer. This sequence of operations was repeated successively for each layer until the final layer (30 v/o TaC - 70 v/o graphite) had been applied. The complete insert blank was hot pressed at a temperature above 3800°F and a pressure above 4000 psia (exact temperature and pressure proprietary to Carborundum). In machining each layer, consideration was given to the changes in dimension and contour that would occur during the final hot pressing operation.

The hot pressed insert was close to specified insert dimensions, so that final finishing (following removal of the graphite mandrel) involved only light diamond grinding. Final inspection consisted of dimensional for over-all size and thicknesses of respective layers, visual examination for cracks or other surface discontinuities, and radiographic for internal contouring and bonding of the various layers. A density determination of the finish machined composite insert was performed for information purposes. This yielded a final density of 8.19 g/cc, which was 91-92% of the theoretical calculated density.

3. Refractory Laminate

The zirconia disks for the refractory laminate design were fabricated from a modified zirconia (Zircoa 1027, modified by Zirconium Corporation of America). The material is made up of two types of zirconia materials -- approximately 75% of a coarse particle fused grog of closely controlled particle size (28 mesh and slightly finer), and the balance an unsintered reaction grade zirconia of particle size less than 5 microns. Both material components are partially stabilized to produce a crystalline structure approximately 20% monoclinic, with the balance cubic. The stabilizing ingredients are proprietary to Zircoa, but are the same for both components

making their chemical compositions identical. The fine zirconia material serves to bind the coarse fused particles together to produce a material with improved resistance to thermal shock cracking.

Discs were "cold" die pressed at approximately 10,000 psi pressure and air dried for 24 hours to remove all uncombined moisture. Following drying, the discs were sintered at 3250°F for 3 hours. The discs were subjected to slow heat-up and cool-down during sintering, involving a total cycle time of approximately 56 hours.

Sintered discs were surface ground on both sides, then ground on the OD to finished dimensions. Diamond wheels were used for the grinding operations.

Final inspection consisted of: dimensional; visual for cracking and other surface defects; radiography for internal discontinuities (high and low density indications); and density determinations (dimensional-weight method). An ultraviolet light exposure test was also used to check qualitatively for amount of monoclinic phase content (monoclinic structure retains some fluorescence when subsequently exposed to white light; cubic does not).

4. Prestressed Insert

The throat insert used in the prestressed configuration was tantalum carbide and was hot pressed by the TRW Systems Group. The raw material (TaC) was obtained from the Cerac Corporation. The particle size was 3-6 microns with a typical analysis of 6.28% total carbon of which 0.06% was free carbon. 0.05% iron powder was added to the TaC and homogenized prior to blending.

The material was pressed in an ATJ graphite die. The compact was sintered at 2180°C under 3000 psi axial pressure for 45 minutes and allowed to cool under pressure. Final density of the insert was 94.5% of theoretical.

5. Plastic Components

There were three major plastic components used in the nozzle assemblies. They were the entrance section, the exit section, and the support and insulator section. The inlet and exit sections, having an oriented ply, were die molded from cut segments. The support and insulator were fabricated by overwrapping a graphite billet, where required, with carbon cloth phenolic and silica cloth phenolic tape. The composite billet was autoclave cured. All parts were X-rayed and tag ends were inspected for density and degree of polymerization.

6. Assembly

The initial operation in the assembly of the nozzles was the machining of the OD of the plastic components. The support and insulator section was bonded into the steel housing using Epon 919. After the adhesive had cured the ID of the support structure was machined to accept the inlet, throat, and exit sections. These were all assembled and bonded into position with Armstrong C-2 adhesive. At the completion of the adhesive cure cycle the inside contour and the end surfaces were finish machined. The final steps

in the assembly procedure consisted of a final diemsnional inspection, assembly of the end retention rings, and assembly of the thermocouples.

D. TEST RESULTS

The four nozzle insert designs were fabricated and delivered to NASA. The test plan for the nozzles was to make a 300 second run, allow the unit to cool to room temperature, five 20 second bursts with approximately one-half hour between bursts, and a final 300 second burst.

The prestressed insert nozzle was tested first for 125 seconds. The test was stopped at that time because of indicated throat erosion as noted by the increased propellant requirements to maintain a constant 100 psi chamber pressure. Because of the relatively minimal throat increase, it was agreed to test the nozzle again. The second run was for 100 seconds and it too was stopped because of increased propellant requirements. Post firing examination showed that the insert had eroded through in one quadrant.

The second unit to be tested was the graded carbide insert nozzle. The test was stopped at 38 seconds because of throat erosion. Post firing inspection of the insert showed the insert to be cracked, both axially and circumferentially. The inner carbide layer had experienced severe erosion in the throat plane.

The reinforced oxide insert nozzle was successfully tested for a total of 720 seconds. The duty cycle consisted of a 310 second run, five 20 second bursts, and a second 310 second run. There was no change in throat diameter but very shallow striations were evident on the ID surface.

The refractory laminate insert nozzle was tested for 214 seconds at which time there was a sudden increase in propellant requirements to maintain chamber pressure. Post firing inspection indicated the pyrolytic graphite discs had oxidized on the ID surface. This permitted the oxide discs to be unsupported at the ID and significant material loss occurred.

Based on the test results, a second unit of both the reinforced oxide and refractory laminate design was built. The reinforced oxide was modified to increase the tungsten wire content from 5 v/o to 7 v/o. The refractory laminate insert consisted entirely of zirconia discs. The reinforced oxide insert nozzle was tested for a total of 1250 seconds which consisted of a 180 second burst, a 300 second burst, five 20 second pulses with 20 minute cool down periods between pulses, and a 300 second burst, and a final 370 second burst.

The refractory laminate insert nozzle was tested for a total of 700 seconds which consisted of a 300 second test, five 20 second pulse, interspersed with 20 minute cool down intervals, and another 300 second test.

1. Prestressed Insert

The prestressed insert nozzle was tested for a total of approximately 225 seconds. The first test ran for 125 seconds and the second for 100 seconds. Both tests were stopped because of an increase in the propellant flow requirement to maintain a 100 psi chamber pressure. This was caused by an increase in the effective throat area. Subsequent examination of the test data as well as actual measurement of the throat diameter verified this increase. The test data was used to calculate throat radius during the test as follows:

$$R = \frac{W_p \; C*}{P_c \; g \; \pi}$$

where W_p = Average propellant flow rate

$C*$ = Actual characteristic velocity

P_c = Average chamber pressure

g = 32.174 ft/sec^2

π = 3.1416

The calculated radii during both tests are shown on Figure 157 Based on this data, throat erosion began much more rapidly on the second test than on the first.

Nozzle temperatures were recorded throughout both tests at selected points. Figure 158 shows the location of the thermocouples. The temperatures for those thermocouples that recorded over a 100° increase were plotted. Figure 159 shows the temperature behind the throat insert T/C(15) and behind the JT-0981 entrance ring T/C(13) for the first test. Figure 160 shows the temperatures at the same location for the second test. The temperatures behind the JT-0981 ring are generally about 400°F lower during the second test.

Figure 161 shows temperature behind the threads of the prestressing ring (7,8), at the OD of the pyrolytic graphite in the same plane (9), and at the OD of the silica insulator in the same general area (2). Figure 162 shows temperatures for the second run are in agreement with those of the first run except for thermocouple 9 during the second test. The drop in temperature after 80 seconds is probably a result of the thermocouple junction being removed from the heated surface by vibration or other mechanical action.
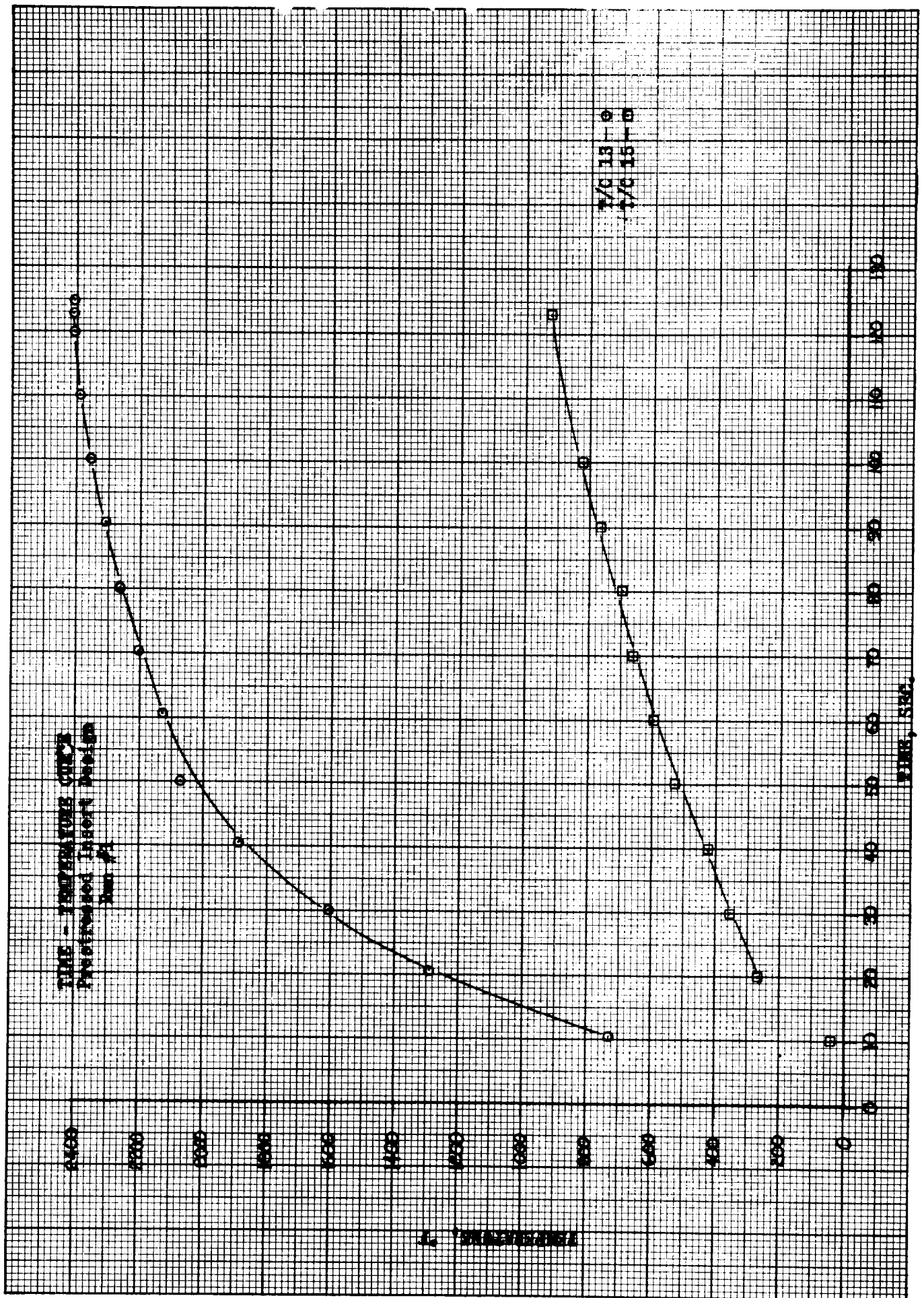
Visual inspection of the prestressed unit after the second test revealed that the insert was eroded through in an area immediately aft of the throat plane. In addition, there was a circumferential groove in the throat plane extending for a full 360° around the ID. The carbon brick was exposed where the throat insert had eroded and had erosion pockets for approximately one-half to three-quarters of its thickness. The Ta-10W ring and the JT-0981 had a very good appearance with no cracks or erosion grooves. All components had a similar appearance after both tests except for the throat insert erosion. The post-firing evalu-
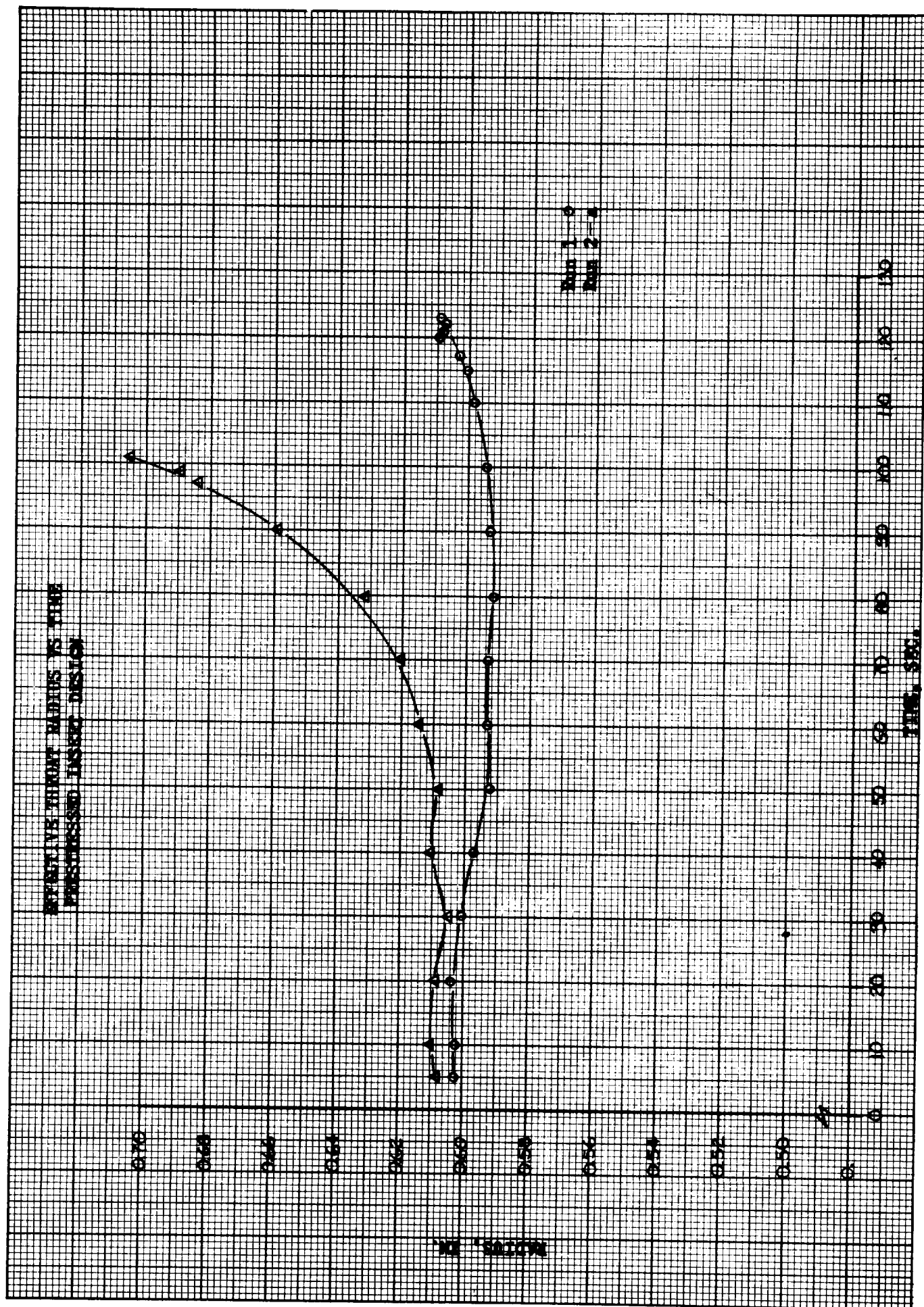
EFFECTIVE THROAT RADIUS VS TIME
PRESCRIBED TAPERED DESIGN

Figure 157

239

THERMOCOUPLE LOCATION

Figure 158

TIME - TEMPERATURE CURVE
Pretreated Insert Design
Run #1

t/c 13 — ⊙
t/c 15 — ▢

TIME, SEC.

T, TEMPERATURE

241

Figure 159

TIME – TEMPERATURE CURVE
Prestressed Insert Design
Run #2

T/C 12 — □
T/C 13 — ▲
T/C 15 — ⊖

Time, Seconds

Temperature, °F

Figure 160

TIME — TEMPERATURE CURVES
Prestressed Insert Design
Run #1
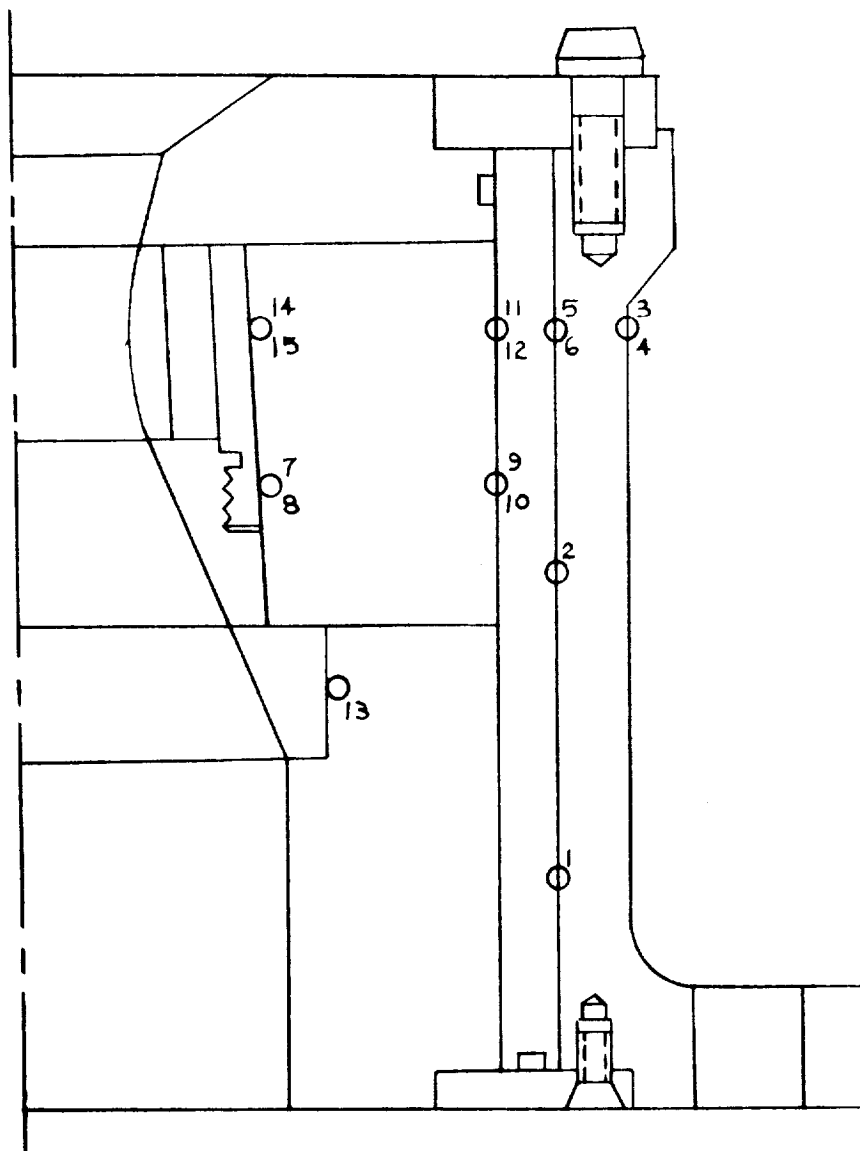
Figure 161

TIME - TEMPERATURE CURVE
Prestressed Insert Design
Run #2

Figure 162

244
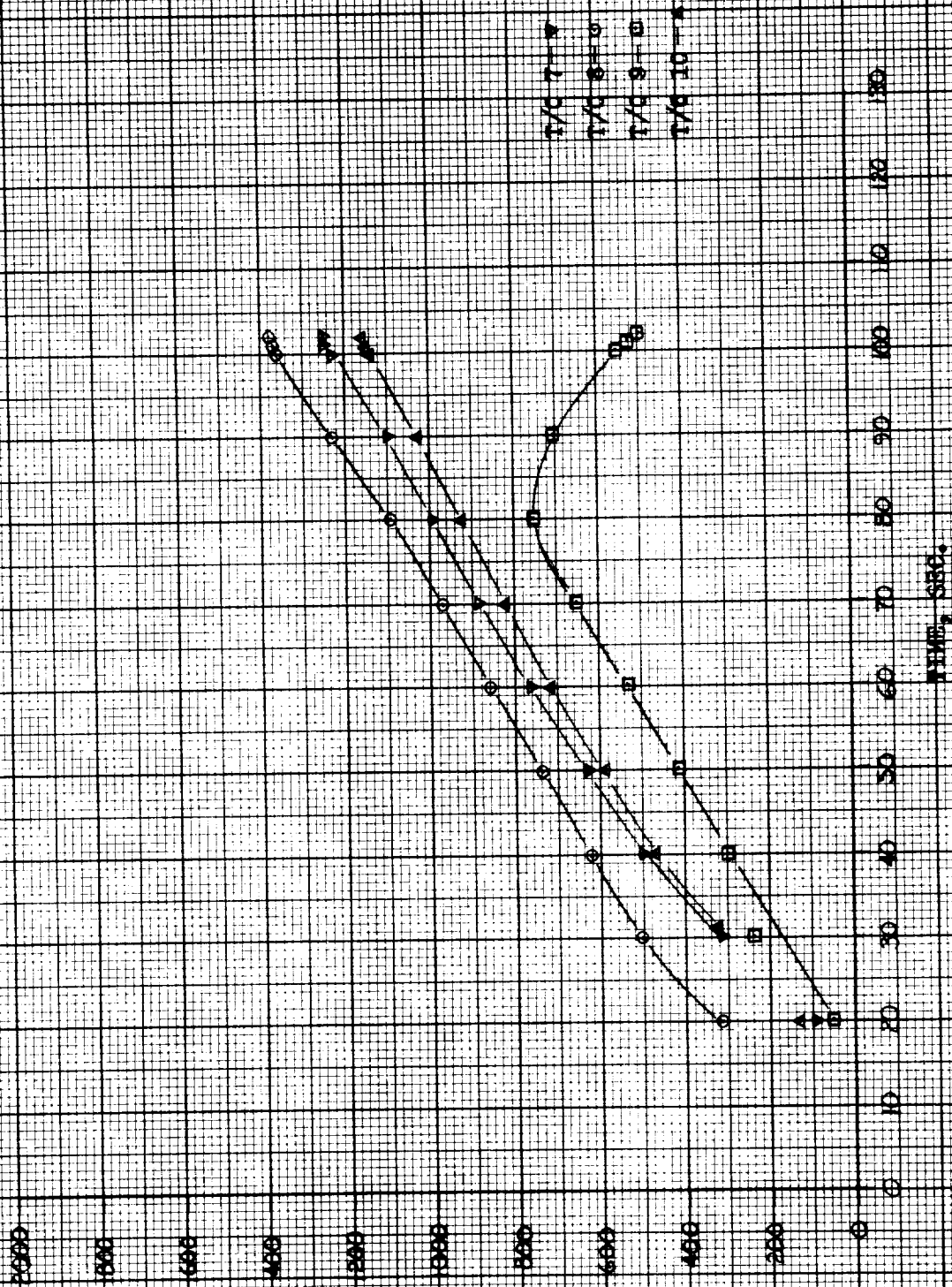
ation of the FS-85 prestressing ring showed no plastic deformation at the inlet end. However, the aft end shows a diameter increase of 0.002 inch. Figure 163 shows the insert after being removed from the nozzle.

In conjunction with the evidence indicating the lack of erosion resistance of the tantalum carbide, one area of the test data is not understood. Figure 158 shows a calculated effective throat radius over the duration of both tests, indicates that on run #1 there was a reduction in radius that apparently stabilized at approximately 50 seconds. At about 90 seconds the radius starts to increase and continues until the test was stopped. Test films, which show a portion of the throat during the test, tend to verify the data in that visible molten flow was evident earlier in the second test than in the first. As noted earlier the thermocouple data does not indicate significantly higher temperatures in the second run than in the first. The oxide (Ta_2O_5) has a melting temperature of 3450°F and there is no apparent explanation currently evident in the data that would explain this situation.

2. Graded Carbide Insert

The graded carbide nozzle was tested for approximately 38 seconds. The test was stopped because of the increase in propellant requirements.

The throat insert consisted of an inner layer of hafnium carbide, a second layer of tantalum carbide plus 10% graphite, a third layer of tantalum carbide plus 40% graphite, and an outer layer of tantalum carbide plus 70% graphite. The design intent was that the inner layer of hafnium carbide would provide oxidation resistance and by matching the coefficient of thermal expansion the outer layers would provide the support to prevent thermal stress cracking.

The test data indicated that significant throat erosion began at approximately 15 seconds. The effective throat radius over the duration of the test is shown on Figure 164. The slope of the curve after 15 seconds indicates the radius is increasing by approximately 1.6 mils per second.

The post-firing appearance of the insert showed two complete circumferential cracks through the entire thickness of the insert. The circumferential cracks were approximately 5/8" apart and generally centered about the throat plane. In addition, there were longitudinal cracks running from both end planes of the insert to the circumferential cracks and between the circumferential cracks. A section view of the post-fired nozzle is shown on Figure 165. The remaining components of the nozzle assembly had no cracks or other unusual features.
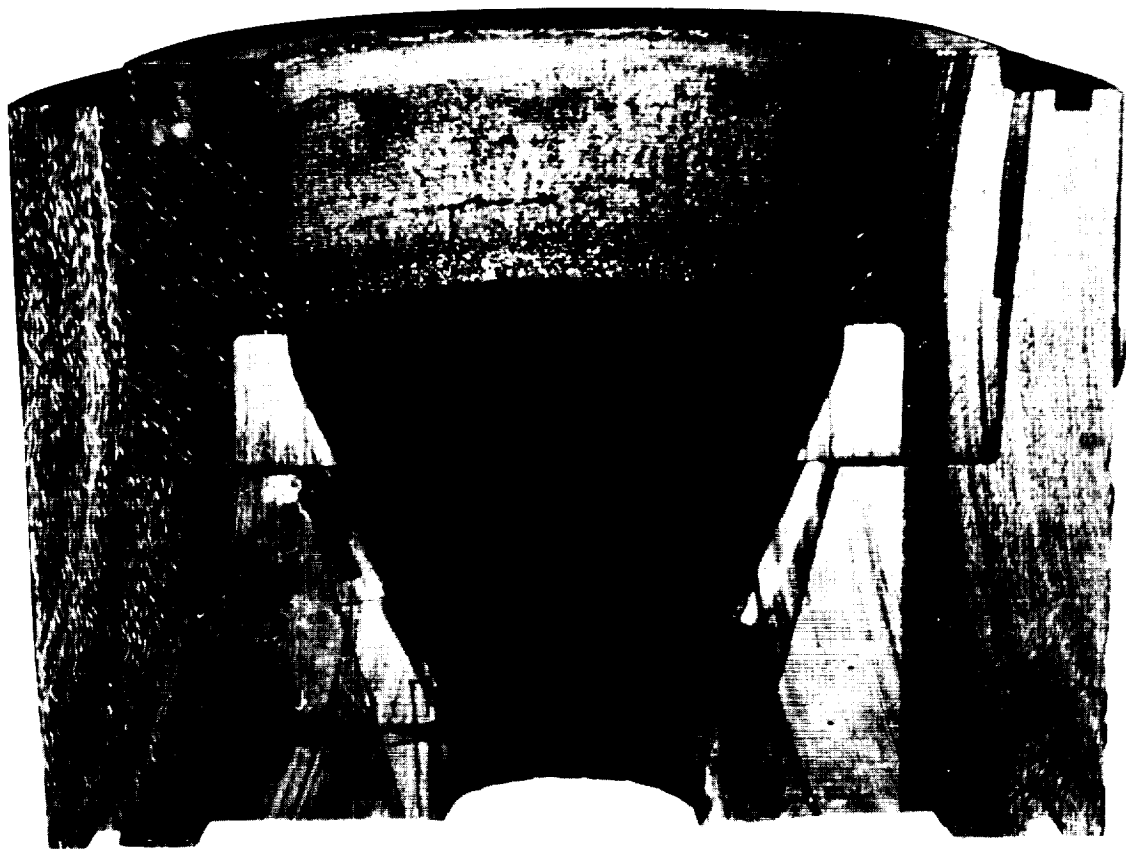
Thermocouples were installed in the nozzle to record temperatures at various locations during the test. The location of the thermocouples is shown on Figure 166.
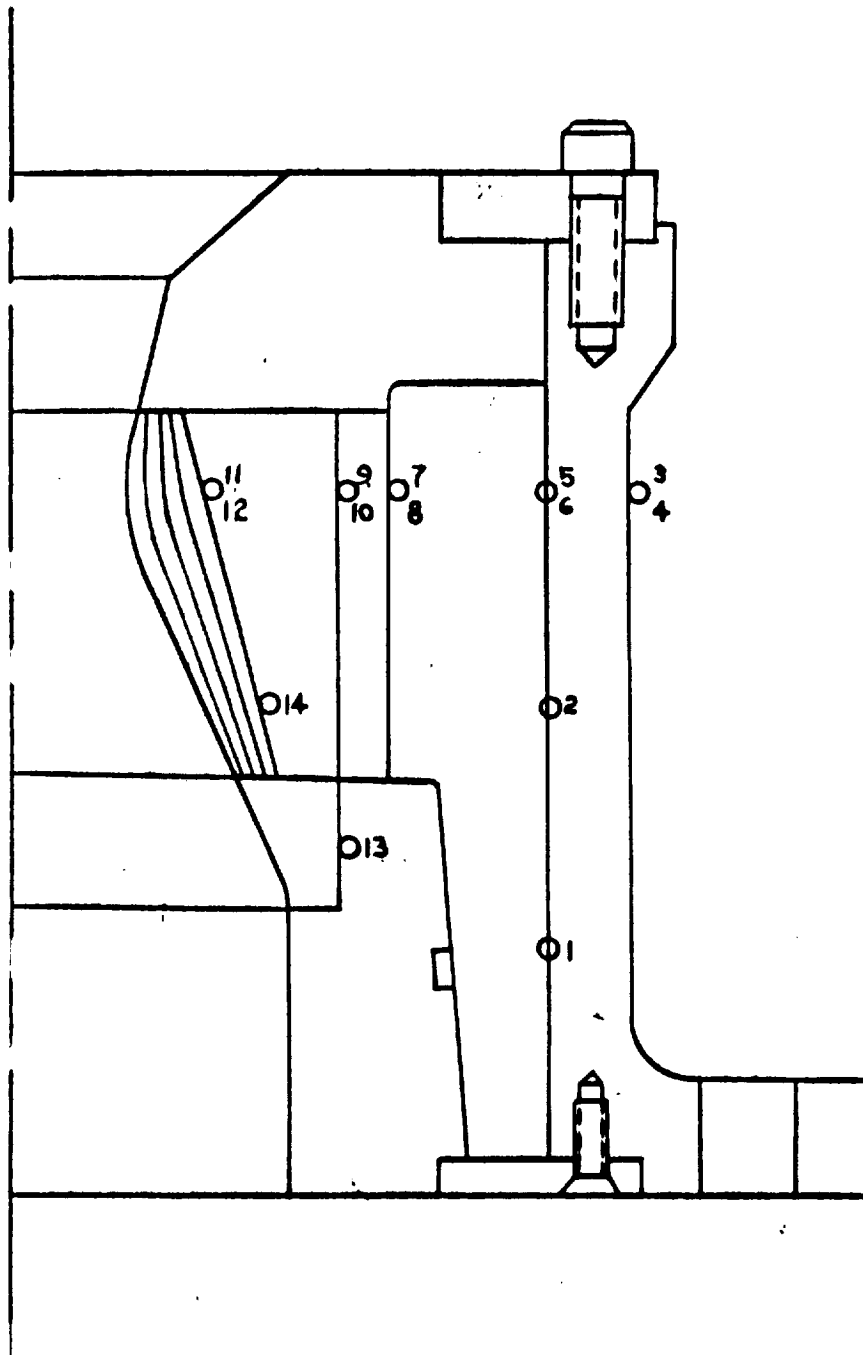
PRESTRESSED INSERT--POST TEST VIEW

Figure 163

EFFECTIVE THROAT RADIUS VS TIME
Graded Carbide Insert

247   Figure 164
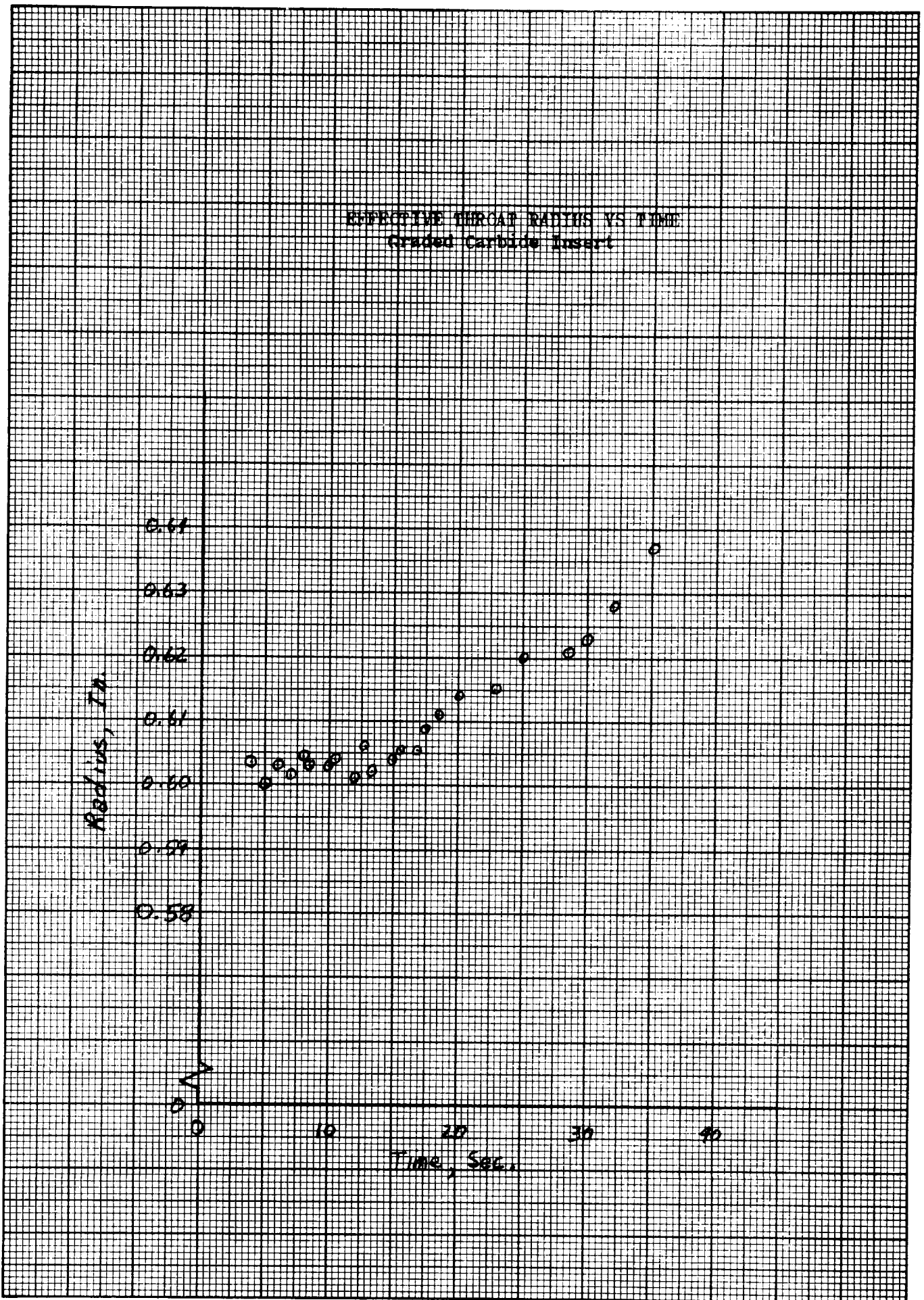
GRADED CARBIDE NOZZLE - POST TEST VIEW

Figure 165

16430

GRADED CARBIDE INSERT DESIGN
THERMOCOUPLE LOCATION

Figure 166

Figure 167 is a plot of the temperature versus time for the five thermocouples that recorded temperature increases in excess of 50°F. Thermocouples 11 and 12 were located in the throat plane and against the OD surface of the throat insert. Thermocouple 9 was located in the same plane but on the OD of the graphite support. The temperature gradient across the graphite is in the range indicated by the design calculations. Thermocouple 14 was located on the OD of the throat insert but near the upstream edge of the insert. The indicated temperature was nearly identical to that recorded in the throat plane. Thermocouple 13 was located on the OD of the JT-0981 inlet ring. The data indicates a rapid temperature increase to approximately 1000°F in 10 seconds with a sudden reversal which is followed by another temperature increase which more closely approximates the expected rate of temperature increase.

While the apparent thermal cracking was most evident, this was not the cause of the indicated erosion during the test and shown in the data. The insert, while severely cracked, was firmly locked in position after the test. It was also evident that none of the fragements had been ejected during the test. Erosion of the hafnium carbide had occurred at the throat plane as well as on the upstream portion of the insert. This was evident on the sectioned insert where the material loss at the throat plane could be observed.
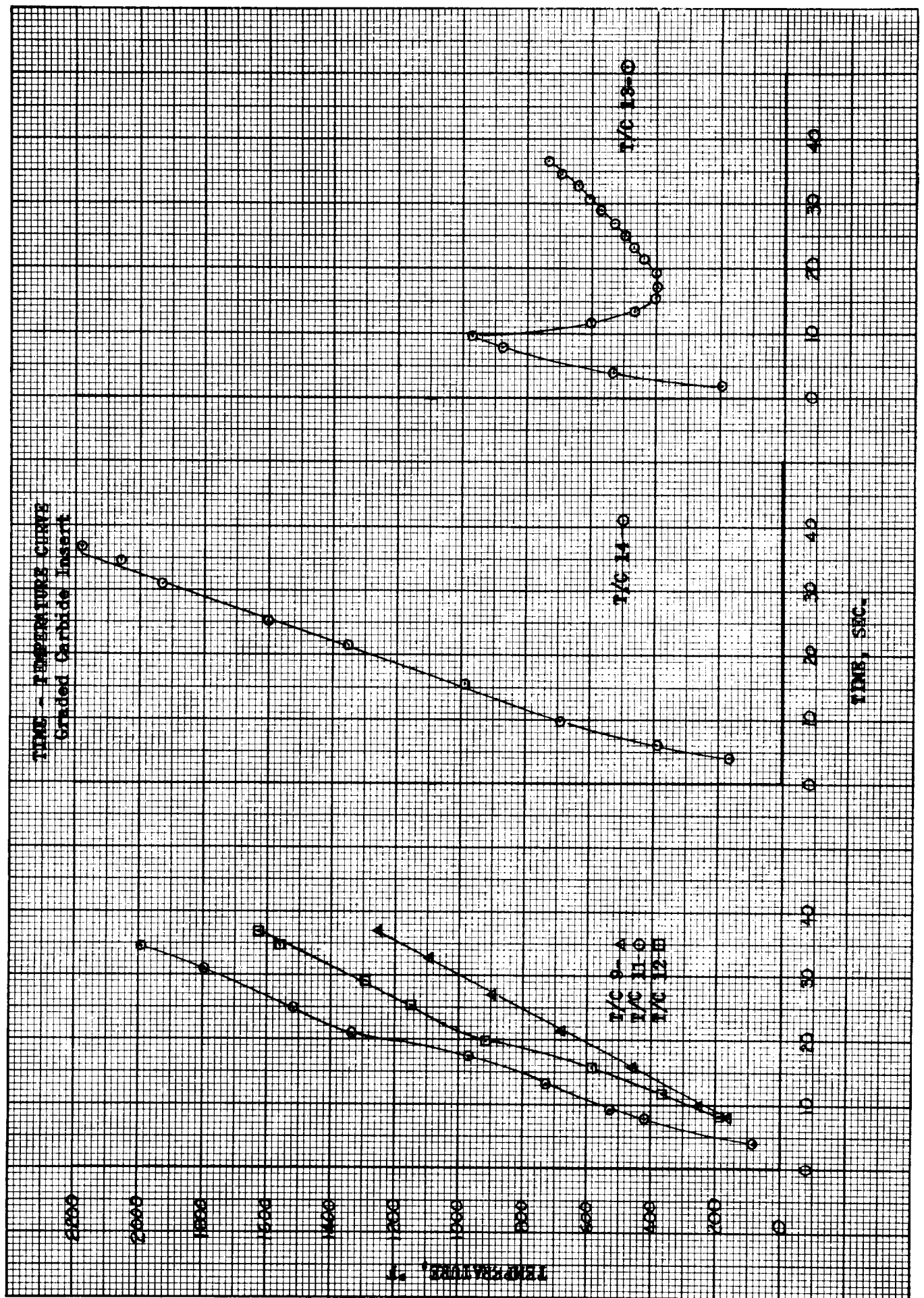
3. Reinforced Oxide

The first reinforced oxide insert nozzle was tested for a total of 720 seconds. The duty cycle consisted of a 310 second pulse followed by a cool down to ambient. This was followed by five 20 second pulses with approximately 30 minute cool down periods between pulses. The final 310 seconds were run after a cool down to ambient.
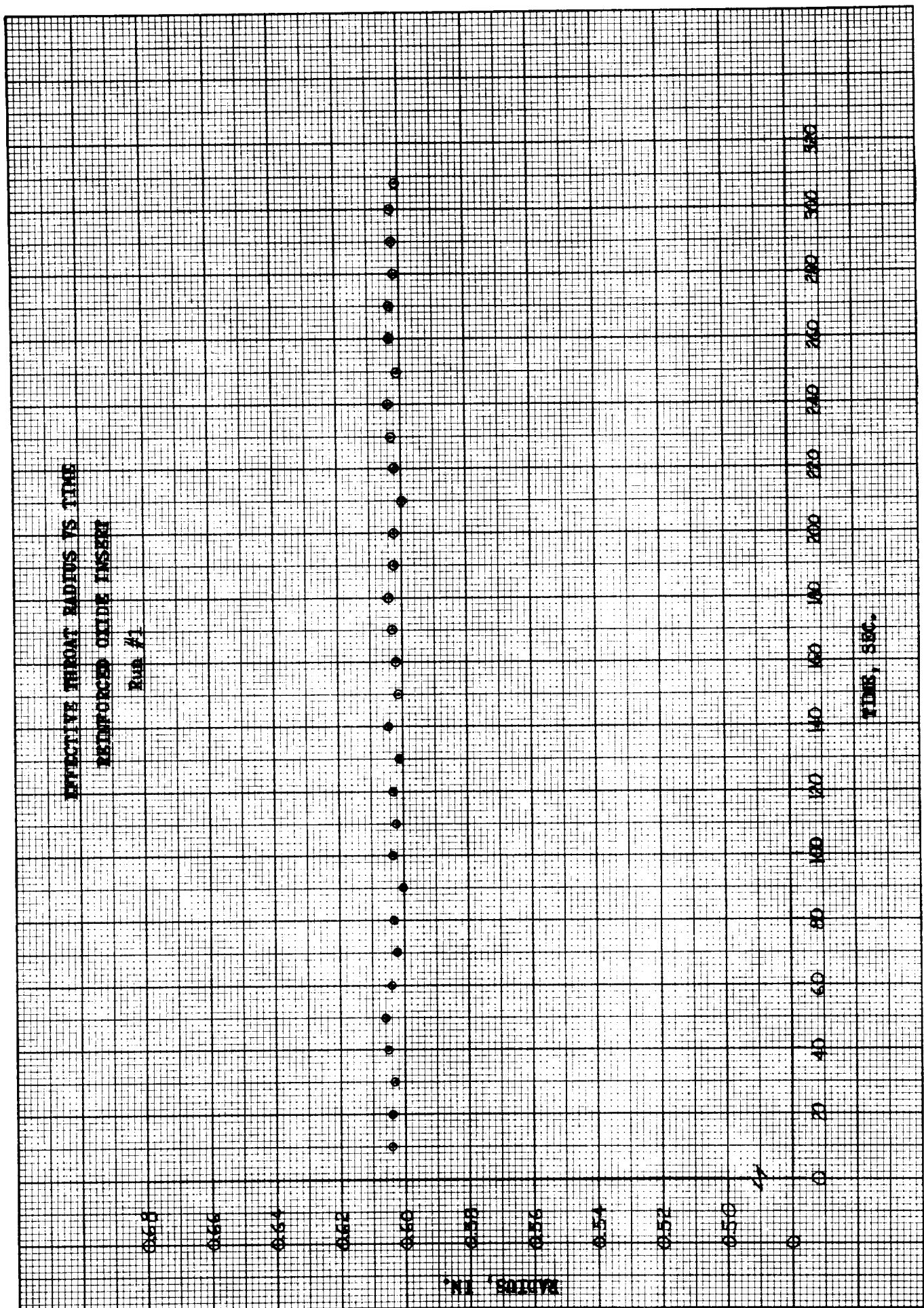
The reinforced oxide insert was fabricated by TRW Equipment Laboratories. The matrix material was a partially stabilized zirconia (F-410). The reinforcing material was tungsten-rhenium wire. The composite contained 5% by volume of reinforcing fibers. The processing consisted of a pressing and sintering operation.

The first test was scheduled for 300 seconds but the run was approximately 310 seconds. The throat radius over the duration of the first test is shown on Figure 168.

The location of thermocouples is shown in Figure 169. Plots of thermocouples 7, 8, 10, and 11 are shown in Figure 170. The other thermocouples that recorded and their change are:

Thermocouple 1 - no change
Thermocouple 2 - 20° rise
Thermocouple 4 - 5° rise
Thermocouple 5 - 30° rise
Thermocouple 6 - 15° rise

TIME - TEMPERATURE CHART
Graded Carbide Insert

251

Figure 167

EFFECTIVE THROAT RADIUS VS TIME

REINFORCED OXIDE INSERT

Run #1

252

Figure 168

Figure 169

TIME TEMPERATURE CURVE
Reinforced Oxide Insert
Run #1

Figure 170

254
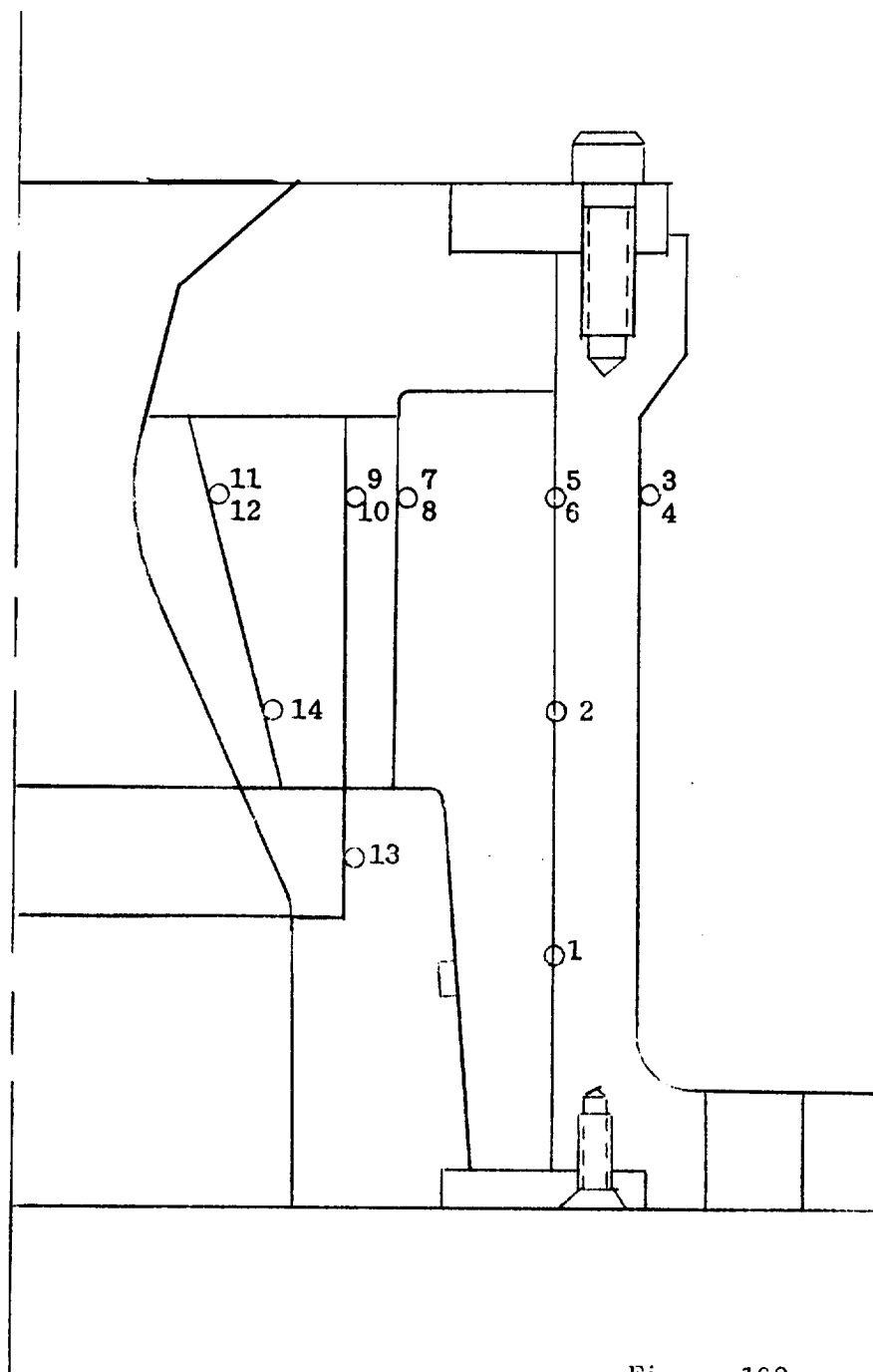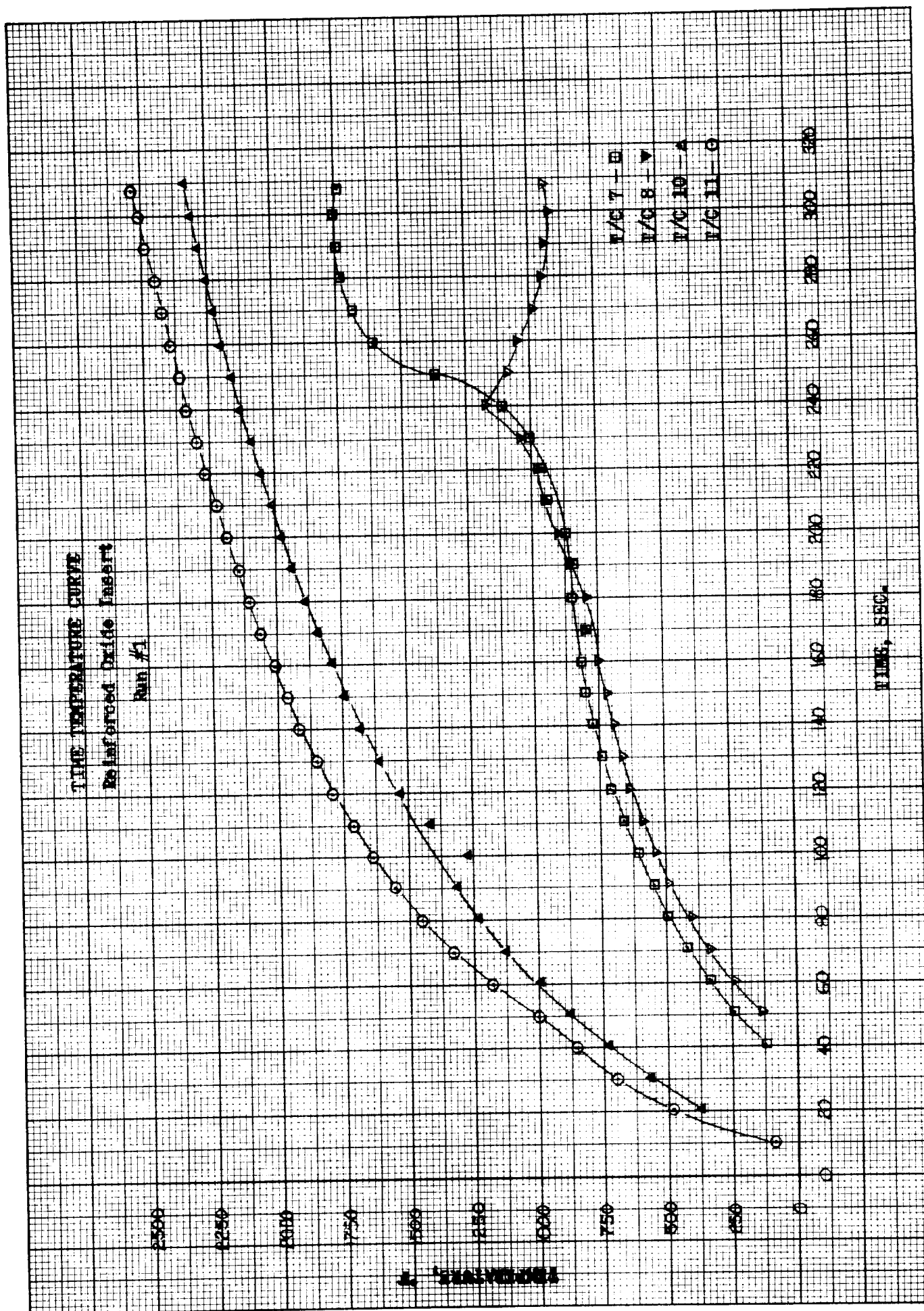
Visual inspection after the first 310 second test run indicated a good general appearance of the insert. They were two visual indications of longitudinal surface cracks approximately 150° apart but there was no indication of gas flow through the apparent cracks. There was no indication that material had spalled from the surface.

Axial X-rays showed several fine radial lines extending from the ID surface. However, the compound curvature at the throat prevented an accurate determination of the nature of the apparent work.

The second test of the reinforced oxide throat consisted of five, 20 second pulses with the nozzle being removed for visual inspection after each pulse. Elapsed time between pulses varied from 30 to 40 minutes. Nozzle thermocouples were not installed in order to facilitate assembly between pulses.

There was no indication by the flow recorders during any of the 20 second pulses of any throat erosion. After the initial pulse, one indication of an axial crack was visible. The crazed surface appearance, as predicted, was more evident after the pulses than after the 310 second test. The general appearance of the insert was good with no evidence of spalling nor was there any indication of flow in the apparent crack.

The third test of the reinforced oxide insert nozzle was also for 310 seconds. Post-firing examination gave no indication of throat erosion or material spalling. The same longitudinal line with the appearance of a crack edge was still evident but, as in the previous tests, there was no evidence of flow along the line.

The temperature curves on Figure 170 show the temperature on the OD of the throat at the throat plane T/C(11) to be 2500°F at 300 seconds. The predicted temperature, based on heat transfer calculations, for 300 seconds was 3250°F. The predicted temperatures were higher than those recorded over the entire test duration with the difference increasing with time.

The fired nozzle was sawed through and one side removed, leaving the throat insert intact. Figure 171 shows two views of the sectioned nozzle prior to removing the insert. The insert was in one solid piece and remained so until sectioned for metallographic examination. Extensive craze cracking was apparent on both the inside and outside surfaces, with some large cracks evident on the outside surface. The inside and outside surfaces were darker in color than typical as-fabricated zirconia, and even material exposed to elevated temperature thermal shock testing, but there was no other significant difference. Material located on the inside surface near the throat plane appeared fused. Above the throat plane in the inlet section, voids were present in the surface where the W-3% Re wires had apparently corroded away. There were no visible wires on the entire inside surface.
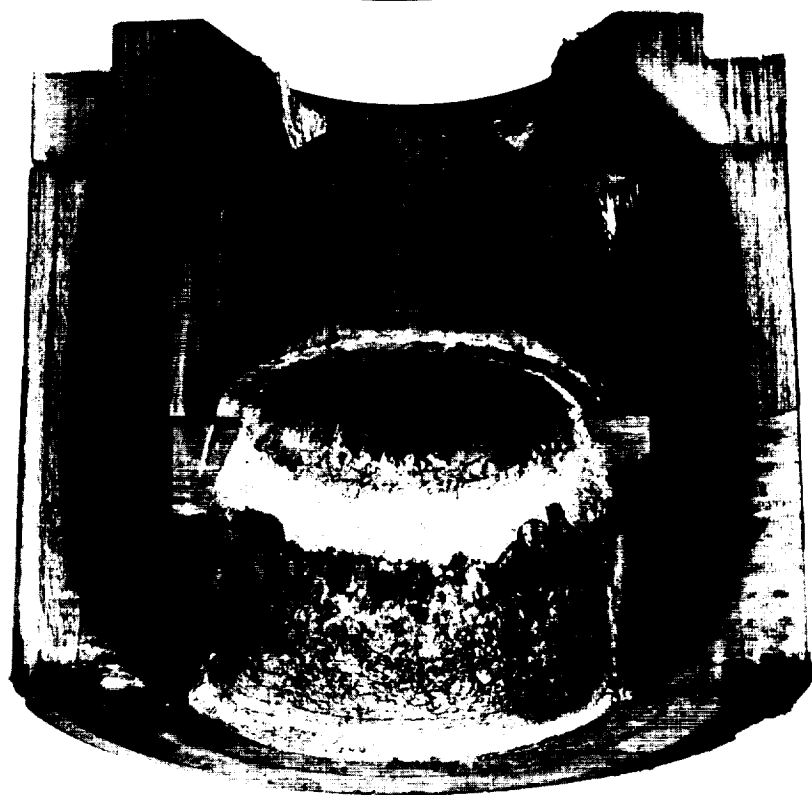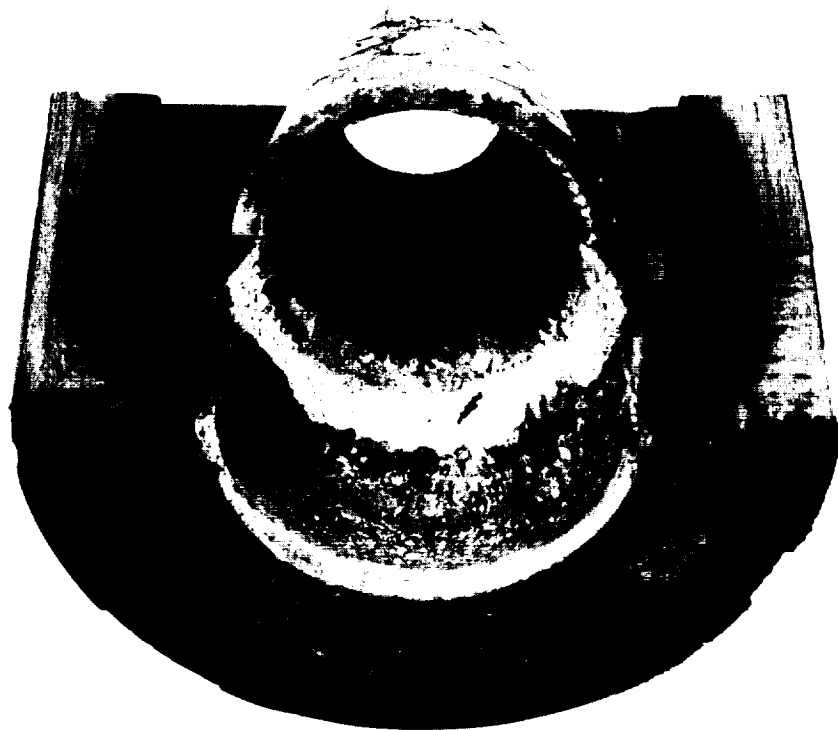
0   1   2   3

POST TEST VIEW - REINFORCED OXIDE INSERT

Figure 171

During the firing, molten material ran from the green silica phenolic combustion chamber over the JT-0981 inlet ring. Also, material, either from the combustion chamber or from the inlet ring, ran over the upper inlet portion of the nozzle throat insert. Past experience has shown that the material from the combustion chamber is silica. No detrimental effects, such as localized erosion or indications of loss of low melting point materials (eutectics) formed by reaction between the nozzle throat insert material and the molten material could be observed visually or by 10X magnification inspection.

An overall view of the axial section reveals that the most numerous and largest cracks occur on the outside diameter and extend inward, even though this area has reinforcement wires that appear unaffected by corrosive attack or reaction during firing. The inside surface, on the other hand, is relatively free from large cracks - even though this area is almost totally void of reinforcement wires. This cracking pattern is in agreement with predictions of cracking from thermal stress, that is, the maximum tensile stresses occur on the outside diameter.

An axial section was cut from the insert, mounted in epoxy, and polished for high magnification examination. At the throat plane, several 50X magnification photomicrographs were taken to show changes of microstructure through the section thickness. Figure 172 (a) represents the material nearest the outside diameter, while Figure 172 (d) represents the material nearest the inside diameter. Figures 172 (b) and 172 (c) are areas between the two.

The microstructure of the insert showed that the reinforcement wires were corroded or reacted away to a considerable depth into the zirconia matrix, with the greatest depth occurring at the throat. At this location, the reinforcing wires were absent to a depth of 1/3 the thickness of the insert. A transitional area occurred, as illustrated in Figure 172 (b), where the reinforcement wires were attacked and appeared deteriorated but not completely removed. Further toward the outside diameter there was no visible evidence of wire corrosion or reaction.

The spongy appearance of the zirconia as seen in the photomicrographs of Figure 172 (c) and 172 (d) is attributed to the diffusion of the W-3% Re alloy into the zirconia and its subsequent oxidation by the combustion gases penetrating into the relatively porous structure. It was noted that a layer of approximately 1/8" thickness following the ID contour of the insert consisted primarily of this spongy-appearing zirconia material. Also, the tungsten-rhenium wire reinforcement was completely removed -- either completely due to diffusion and subsequent oxidation, or partially by direct attack of the oxidizing gases on the wires themselves.

A narrow transition zone between the completely depleted ID layer and the unaffected portion toward the OD contained partially oxidized and/or reacted tungsten-rhenium wires. It was noted, Figure 172 (c), that the zirconia with the spongy appearance tended to surround the individual wires -- further evidence of the high temperature reaction and diffusion of the tungsten alloy into the zirconia. Subsequent oxidation of the tungsten then resulted in the spongy zirconia locally surrounding the tungsten-rhenium wires.
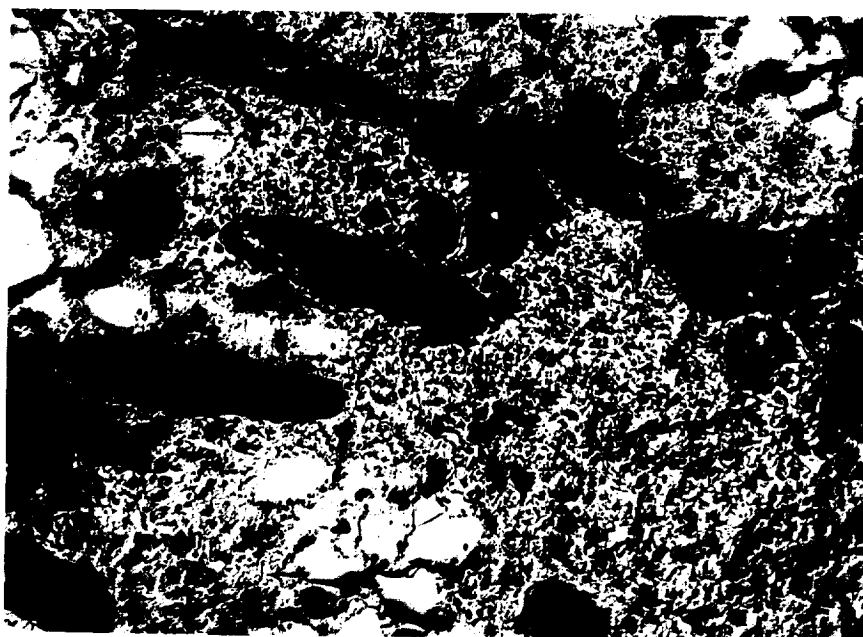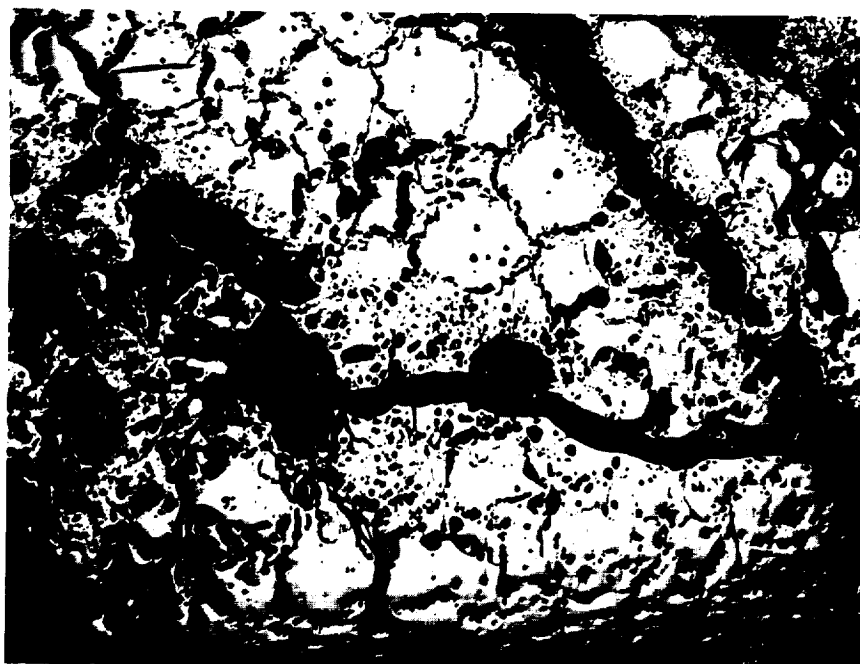
257
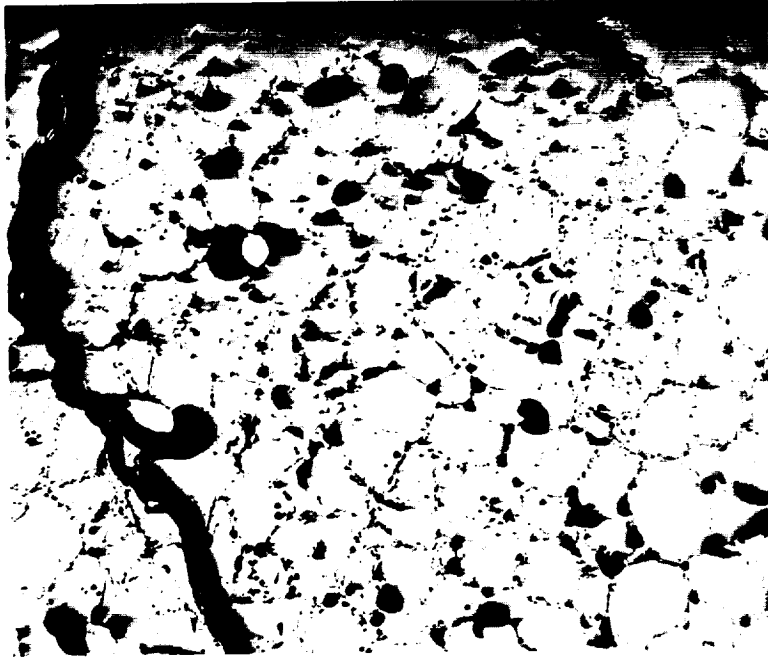
O.D.
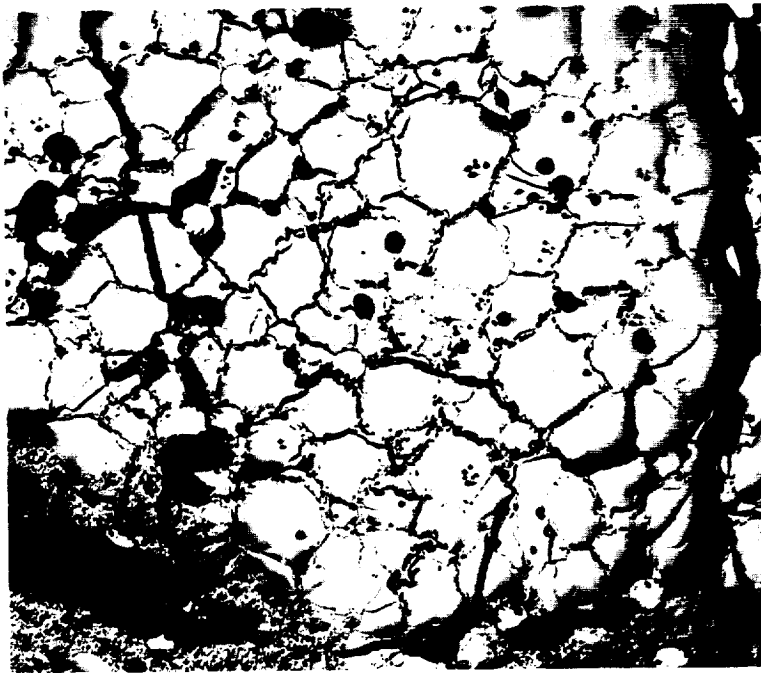
Towards
I.D.

50X Mag.

MICROPHOTOS – REINFORCED OXIDE INSERT

Figure 172

258

Towards O. D.

I. D.

50X Mag.

Figure 172 (con't.)

MICROPHOTOS - REINFORCED OXIDE INSERT (con't.)

Figure 173 shows a photomicrograph of tungsten backed with zirconium oxide after exposure in a non-oxidizing environment for 6-1/2 minutes at 4500° F. This demonstrates the diffusion capability of tungsten into zirconia at high temperatures. Figure 174 shows the metal depleted layer in a zirconia-tungsten (20 w/o) composite after a 30 second exposure to air at 4800°F.

Although they differ in melting point, crystal structure and chemical stability -- most oxides react with tungsten in an identical manner. In the solid-state at high temperatures the oxides absorb tungsten into the lattice. This reaction is typified by a gradual color change of the oxide from white to gray to black, with an accompanying increase in lattice dimensions. For cubic ZrO_2 the lattice parameter increases from a normal 5.07 to 5.12 Å. A final black color represents an oxide lattice saturated with tungsten.

Although the oxide-tungsten reactions in the solid-state are similar in type, rates of reaction vary from oxide to oxide. The rate of reaction, or rate of tungsten diffusion, is primarily a function of the oxide melting point, although crystal structure does have some effect. In general, the higher the melting point and/or the more closely packed the atomic lattice, the slower the diffusion. For example, it was demonstrated that the diffusion, through tetragonal zirconia (M.P. = 4760°F) was faster than through tetragonal hafnia (M.P. = 5080°F). Zirconia in contact with tungsten contained discrete particles of tungsten in its microstructure following a 5000°F exposure for 120 seconds; whereas, hafnia contained no tungsten after similar exposure.

Metallographic examination of the insert at the upper inlet portion, where molten material had run over the surface during firing, revealed no evidence of melting or other detrimental reactions in the material immediately adjacent to the inside surface.

Etching showed the tungsten - 3% rhenium wires to be partially recrystallized, as illustrated in Figure 175. Examination of as-processed tungsten-rhenium reinforced zirconia composites reveals that these wires are also partially recrystallized. Although the wires are purchased in the wrought condition, the sintering treatment introduced during processing of the W - 3% Re wire reinforced zirconia composite is sufficient to initiate recrystallization. Data from the vendor indicates that tungsten - 3% rhenium wires annealed at TRW sintering temperature results in significantly improved room temperature ductility.

Another observation relative to the test-fired insert was its darker-than-normal coloration. Although solution of tungsten into the zirconia matrix could, at least in part, account for the darker coloration of the inside diameter material, temperatures were not sufficiently high on the outside diameter to cause extensive solution of tungsten. Since the insert was backed with a monolithic graphite support ring, the possibility that carbon permeation into the structure caused the darker coloration was considered. Analysis of the material produced the following carbon contents:
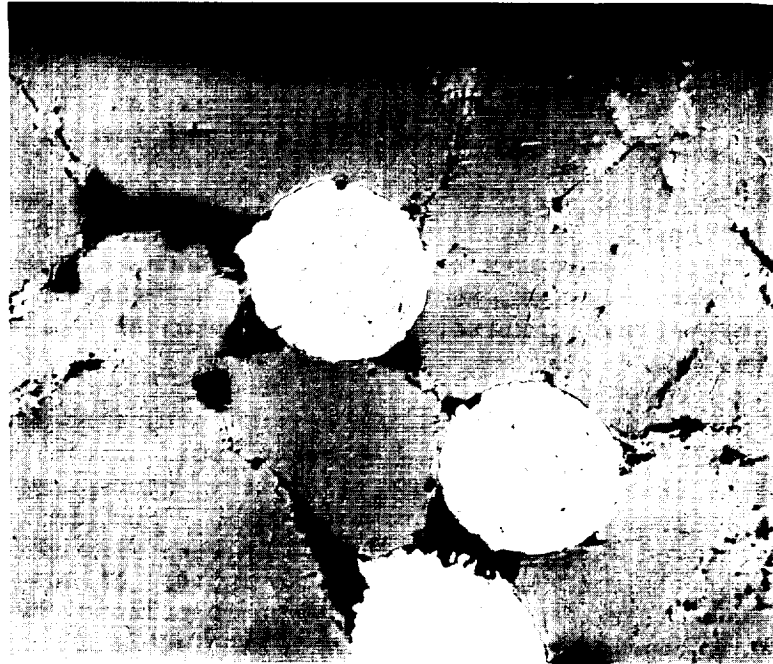
6671   X 250

UNCOATED TUNGSTEN BACKED WITH ZrO_2
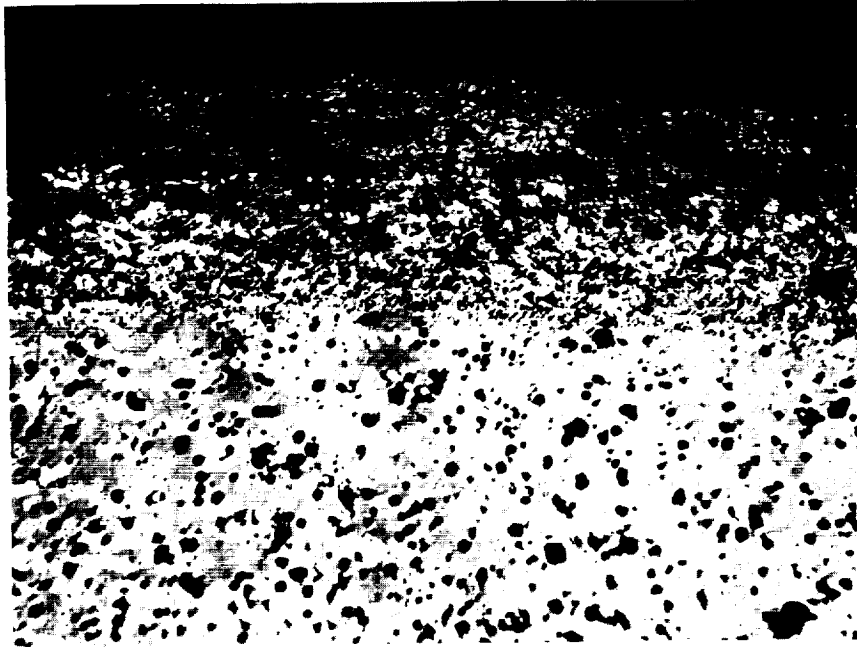
Figure 173

METAL DEPLETED LAYER ON ZrO_2 + 20% W

Figure 174

Refractory Metals Etch   250X Mag.

MICROPHOTO - REINFORCED OXIDE INSERT

12124

Figure 175

263

Material	Carbon, Percent
From Section Near ID	0.03
From Section Near OD	0.05
F-410 Zirconia Powder, As Received	0.01

The carbon content of the insert after firing is significantly higher than the starting material and could logically account for the darker coloration of the zirconia in the test-fired nozzle throat insert.

In order to determine changes which may have occurred in the zirconia structure, X-ray diffraction analyses were performed on an axial section of the tested insert. For purposes of comparison, other materials examined were (a) F-410 zirconia powder, as-received; (b) W-3% Re wire reinforced zirconia, pressed and sintered; and (c) the same as (b), subjected to thermal shock testing.

Unstabilized zirconia has a monoclinic crystal structure at room temperature while fully stabilized zirconia has a cubic crystal structure. In addition, it is believed that the thermal history, specifically the cooling rate, will influence the percentage of cubic structure retained. As the material is heated the unstabilized portion goes through a phase change where the monoclinic structure changes to cubic. If the cooling rate is slow, the cubic structure reverts back to monoclinic, but if the rapid cooling rate is imposed a large portion of the cubic structure is apparently maintained.

The X-ray diffraction analysis indicated a range of values that was much wider than anticipated. In order to establish the validity for such a difference in the structure, a study of the material subjected to various controlled thermal cycles would be required.

4. Refractory Laminate

The refractory laminate throat insert consisted of alternate layers of pyrolytic graphite (PG) and 1027 "modified" zirconia from the Zirconia Corporation of America. The design intent was that the PG, being relatively transparent to heat, would heat the back side of the zirconia and reduce the thermal gradient. This in turn would reduce the tendency of zirconia to crack from the induced thermal stress.
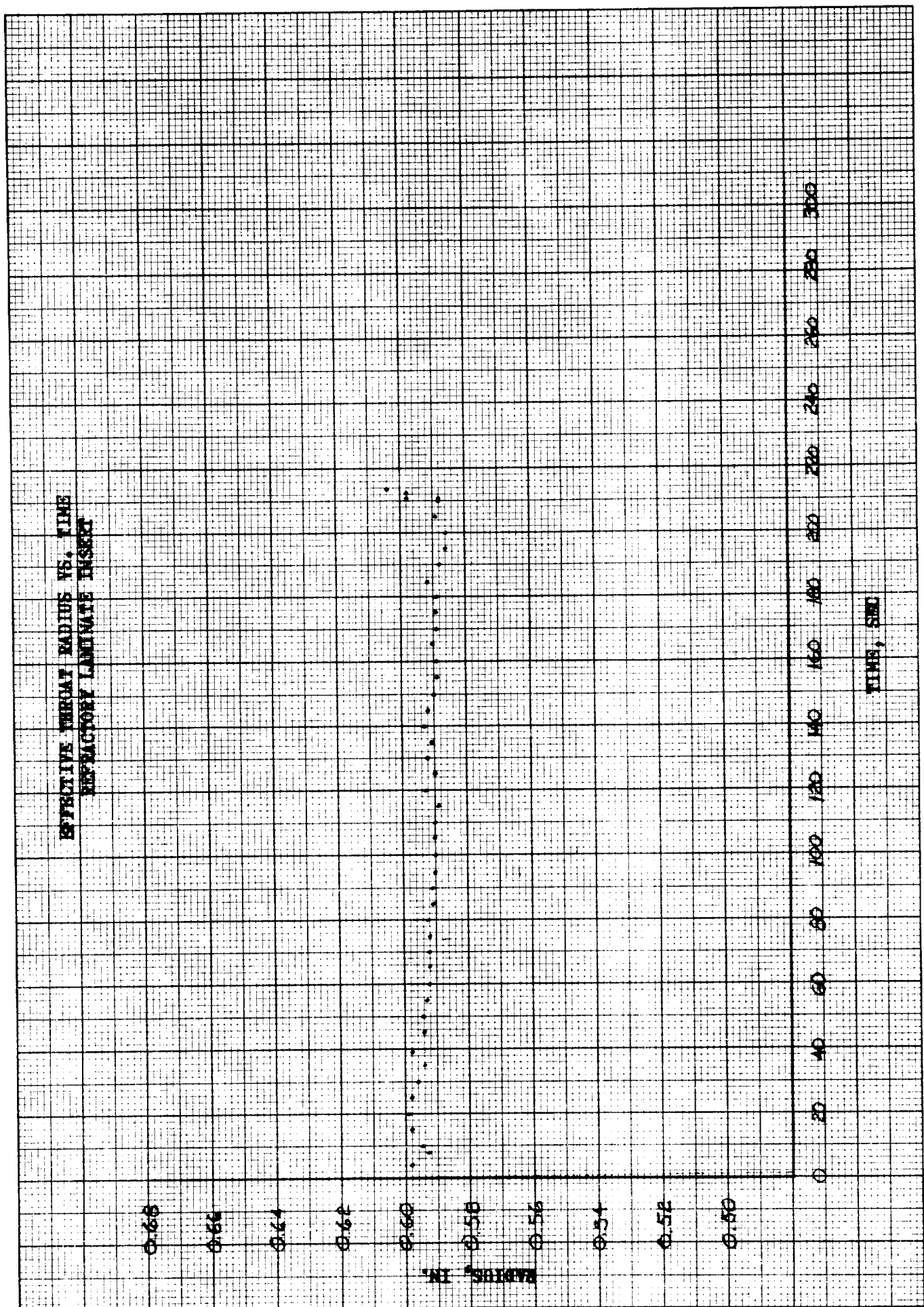
The refractory laminate insert nozzle was tested for approximately 214 seconds. The test was stopped at that time because of increased propellant requirements to maintain a constant 100 psi chamber pressure which indicates an increasing throat diameter. The calculated effective throat radius for the duration of the test is shown on Figure 176. The curve is generally smooth to approximately 211 seconds then the throat size begins to increase. The test was manually stopped at 214 seconds because of the rapid rate of throat erosion.

Post-firing examination of the insert showed that the exposed inside surface of the PG was oxidized 0.030 to 0.060 inch below the surface of the oxide. The oxide disk located at the throat and the adjacent upstream oxide disk were both missing material on the inside surface. The inside edge of these disks gave the appearance of the material having been spalled or mechanically fractured leaving generally sharp and irregular edges.

There was no evidence of flow lines or melting on any of the oxide disks. None of the disks were completely fractured but three of the six oxide disks were cracked. Two of the cracked oxide disks had two cracks, approximately 180° apart with the cracks originating at the inside surface and radiating, from one-half to three-quarters of the way, to the outside surface. The third cracked oxide disk was similar in appearance to the other two with the exception of a third crack that originated on the outside surface and started toward, but did not penetrate, the inside surface. It was also noted that the outside diameter of the oxide disks was reduced approximately 0.020 inch and the thickness was reduced by approximately 0.002 inch. This was attributed to further sintering of the zirconia.

The appearance of the throat insert together with the data indicate that the oxidation of the PG left the inside edge of oxide projecting unsupported into the gas stream. As the PG receded from the inside surface of the throat insert more of the inside edge of the oxide was left unsupported. This event, in conjunction with the low strength at high temperature characteristic of zirconia, appears to have permitted the gas stream forces to fracture the unsupported inside edge of the oxide disk located at the throat centerline and the adjacent upstream oxide disk. Figure 177 shows a cross section of the nozzle prior to removing the disks. Figure 178 shows the disks after removal from the nozzle.
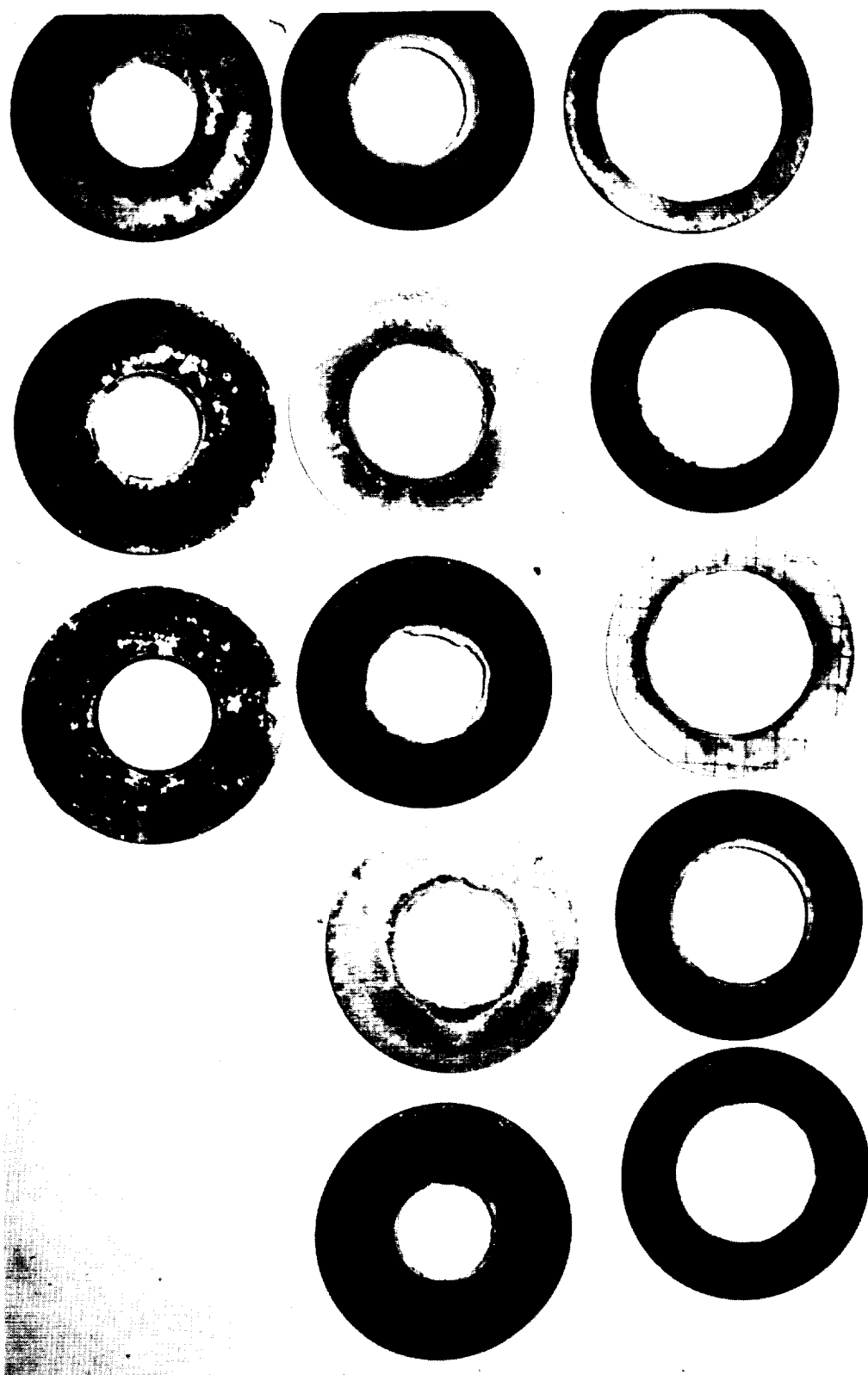
Thermocouples were installed in the nozzle to record temperatures at various locations during the test. The location of the thermocouples is shown on Figure 179. Thermocouples 2, 9, and 13 located between the steel shell and the silica phenolic insulator and thermocouples 3 and 14 located on the outside of the steel shell all recorded temperature increases less than 45°F. Figure 180 is a time-temperature plot of thermocouples 1, 4, and 5. Figure 181 is a time-temperature plot of thermocouples 6 (typical of 6, 7, 10, and 11), and thermocouple 12 (typical of 8 and 12). The data indicates the OD temperature of the insert at 214 seconds was approximately 3000°F. The temperature at the outside of the carbon cloth phenolic was approximately 1800°F indicating the effect of the carbon cloth phenolic as an insulator.
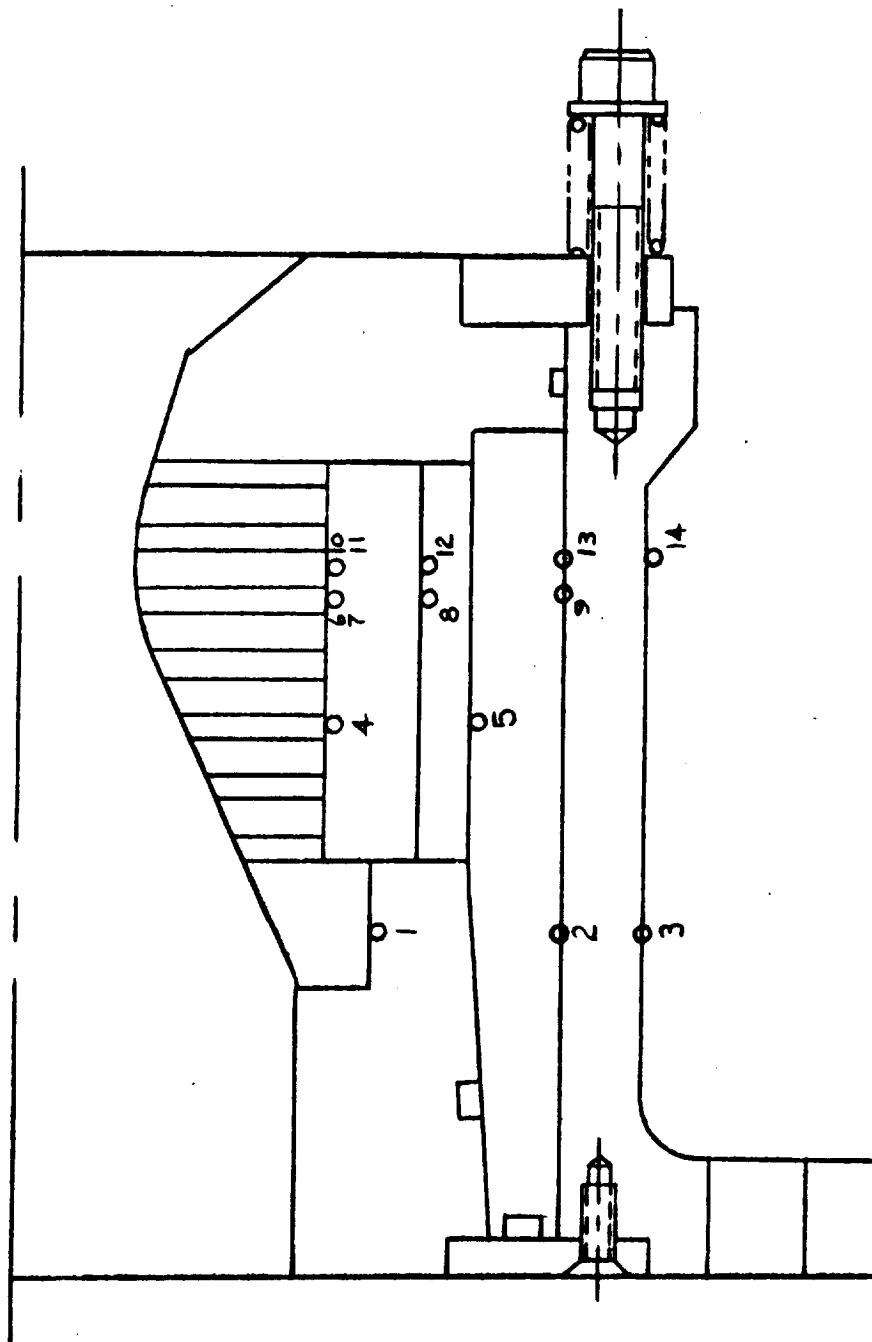
EFFECTIVE THROAT RADIUS VS. TIME
REFRACTORY LAMINATE INSERT

RADIUS, IN.

TIME, SEC

266　　　　　　　　　　　　　　　　　Figure 176

POST TEST VIEW - REFRACTORY LAMINATE INSERT

Figure 177

16400

POST TEST VIEW - REFRACTORY LAMINATE DISKS

Figure 178

THERMOCOUPLE LOCATION

REFRACTORY LAMINATE NOZZLE

Figure 179

TIME — TEMPERATURE CURVES
REFRACTORY LAMINATE INSERT

270   Figure 180

TIME - TEMPERATURE CURVES
DEPOSITION MATERIAL

Figure 181

271
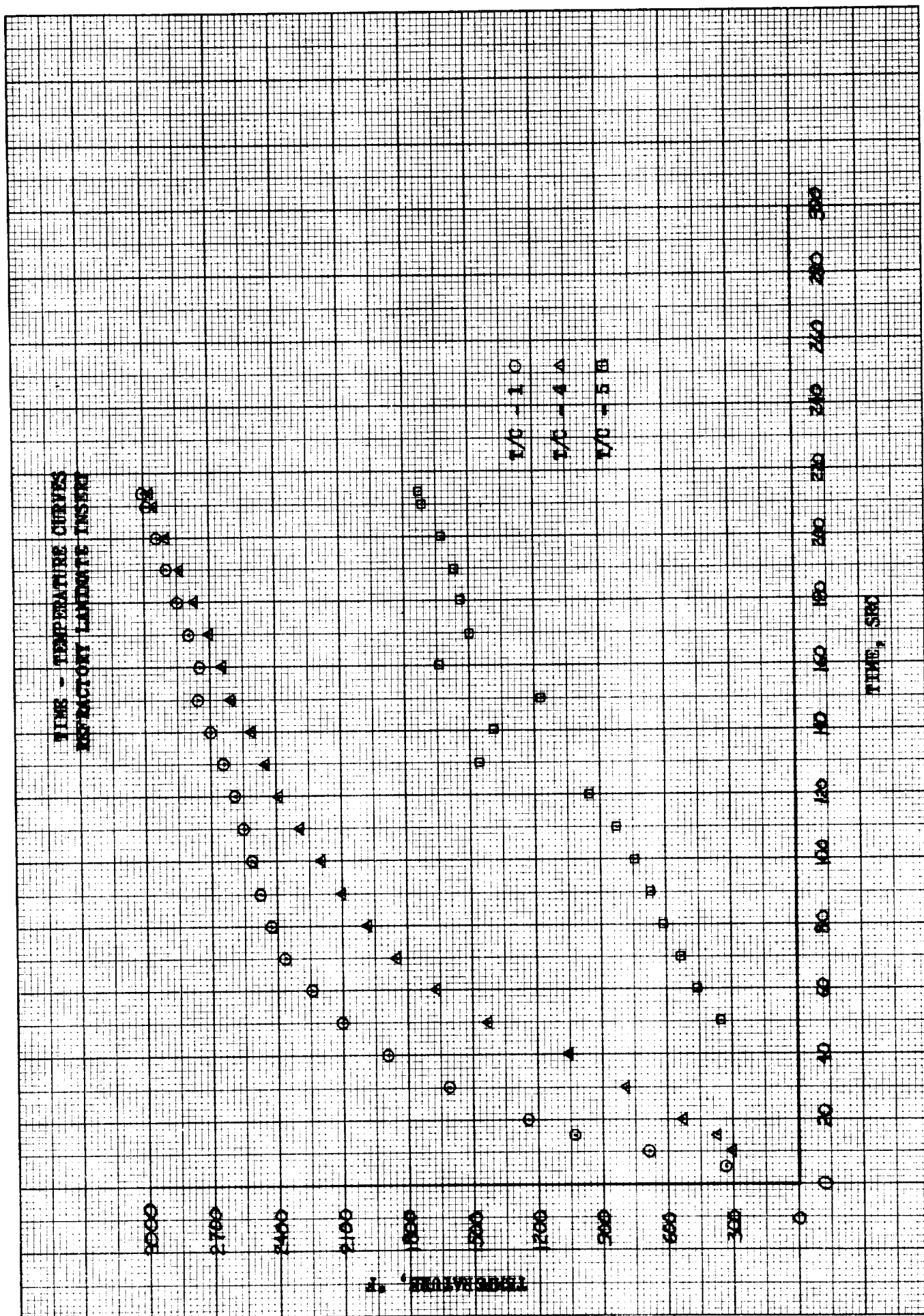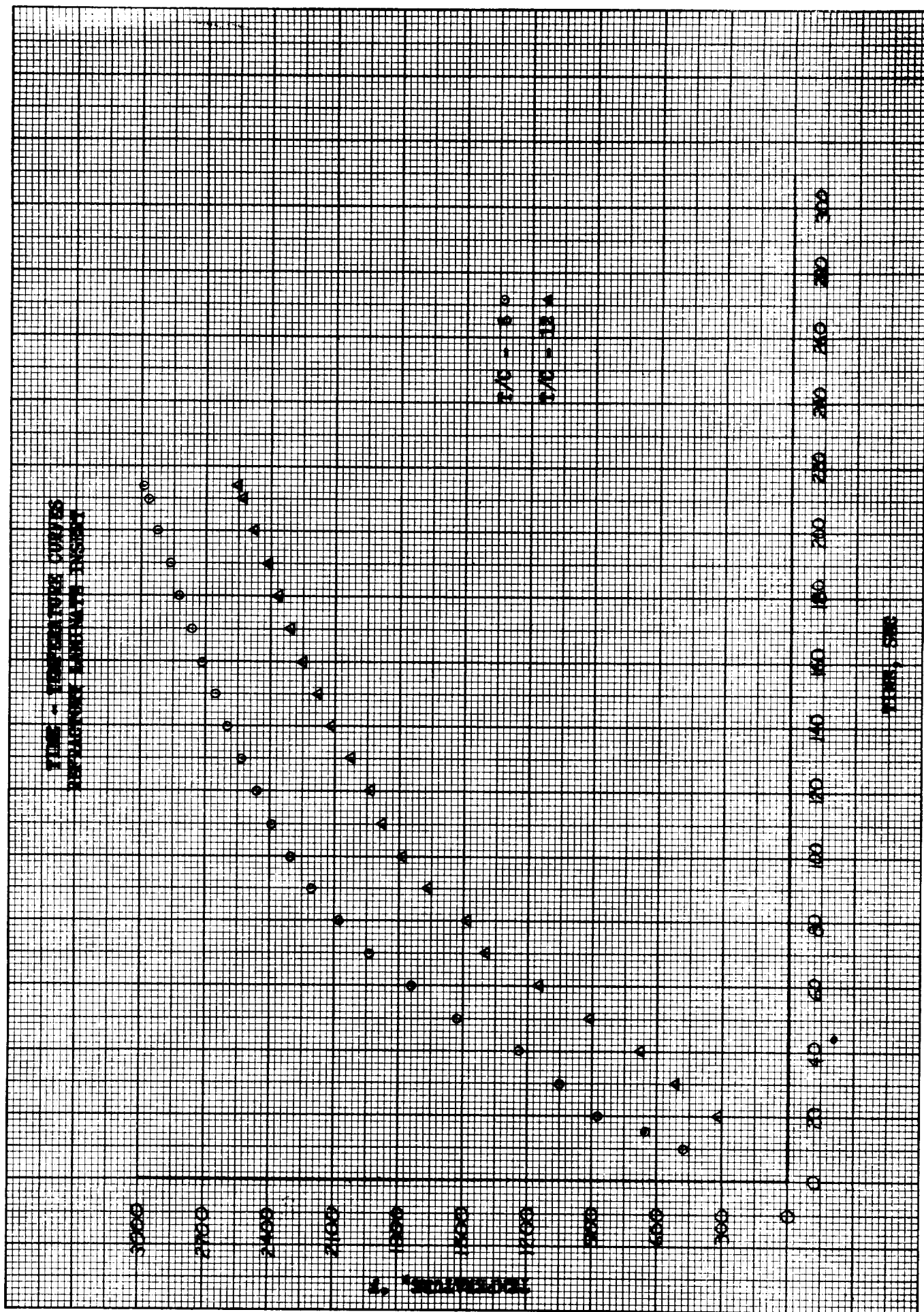
5. Reinforced Oxide (II)

A second reinforced oxide insert nozzle was fabricated to verify the test results of the first unit and to determine the effects of changing the tungsten-rhenium wire content from five volume percent to seven volume percent. The unit was tested for a total of 1253 seconds. The duty cycle consisted of a 180 second burst, a 300 second burst, five 20 second pulses with 20 minute cool down periods between pulses, and a final 300 second burst. Later on, an additional 373 second firing was made. The nozzle was cooled to ambient temperature during the several day interval between tests. There was no evidence of throat erosion observed during any of the tests as indicated by the propellant flow to maintain a constant chamber pressure. Visual examination of the insert both between test cycles and at the completion of the duty cycle indicated no significant difference from the first insert. The crazing effect, as described earlier, was noted as well as one longitudinal crack. The crack would appear on cool down of the insert and was approximately .005 inch wide. When the insert was hot, immediately after a test cycle, only a hairline indication of the crack would be evident. There was never any indication of flow in the line of the crack or any evidence of material loss in or adjacent to the crack.

The insert was fabricated from the same materials (Zircoa F-410 and tungsten-rhenium wire) and by the same process as described in a previous section. The only variation to the insert was an increase in wire content from five volume percent to seven volume percent. At the completion of the sintering process the insert billet appeared identical to the five volume percent billet fabricated for the first nozzle. However, during the machining of the OD surface several cracks, both circumferential and longitudinal, appeared. The cracks were evident only on the outside surface with no indication that they penetrated to the ID surface. The machining of the insert was completed and its general appearance remained the same with the cracks evident only on the OD surface. Figure 182 is a photograph of the finish machined insert. It was agreed to test the insert based on past test results and the characteristic properties of the material.

The nozzle was removed from the test apparatus at the completion of each test cycle. Figure 183 is a view of the nozzle looking downstream. There was no essential difference in appearance between 180 seconds and 1253 seconds with respect to the ID surface of the insert.

There was no change in throat diameter at the completion of the test duty cycle. Figure 184 is a plot of calculated effective radius for the first test cycle.
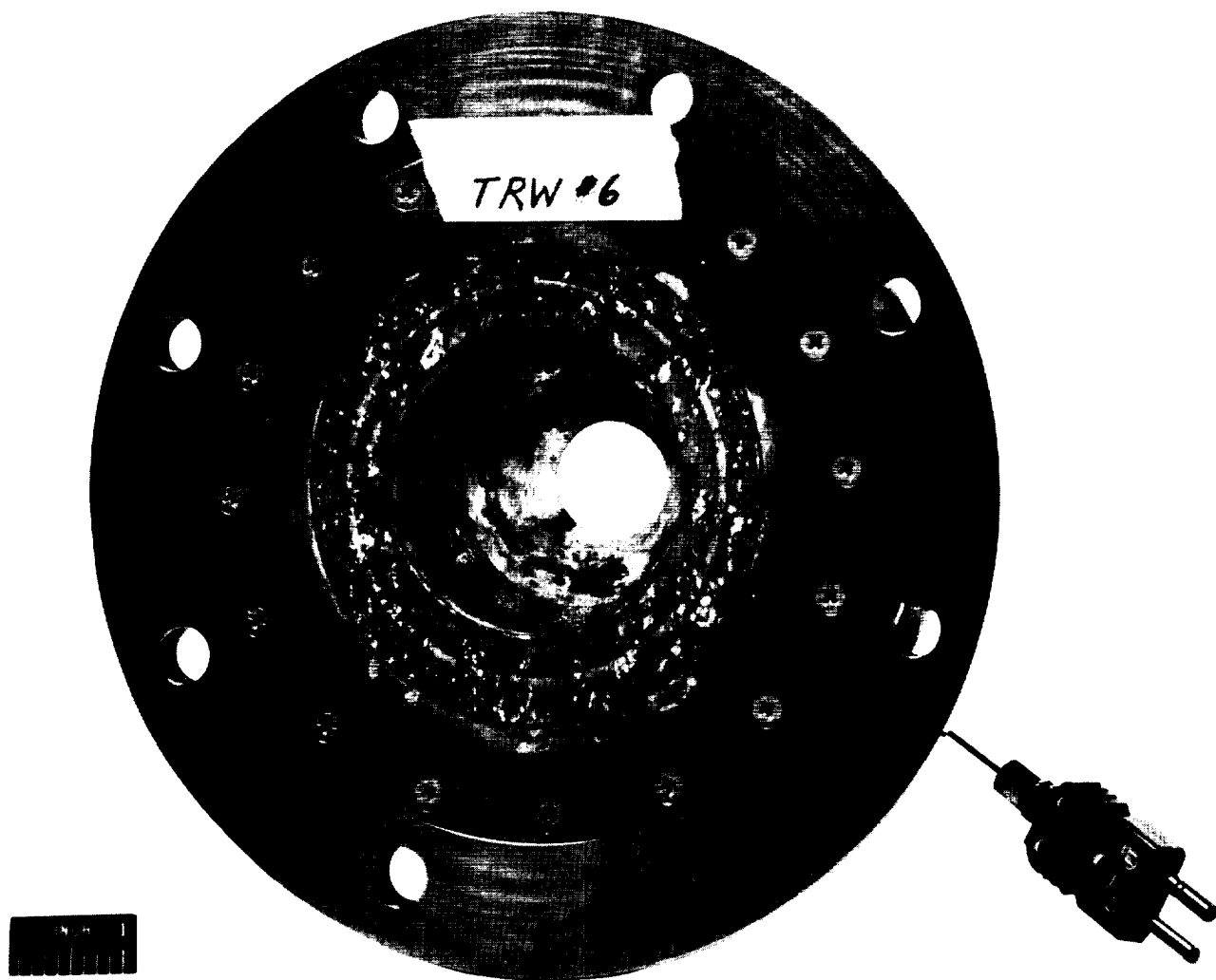
Figure 185 is a temperature plot for the first duty cycle. This may be compared with Figure 170 which is a similar plot for the first insert. Thermocouple location is shown in Figure 186. There was little difference in the recorded temperatures behind the insert or behind the backup graphite. The temperature indicated between the silica phenolic and carbon phenolic is plotted (T/C 1) but the data is unacceptable.

The nozzle was sectioned and is shown in Figure 187. The insert was removed and is shown in Figure 188. The post fire appearance of the insert may be compared with the pre-fire view shown in Figure 182.
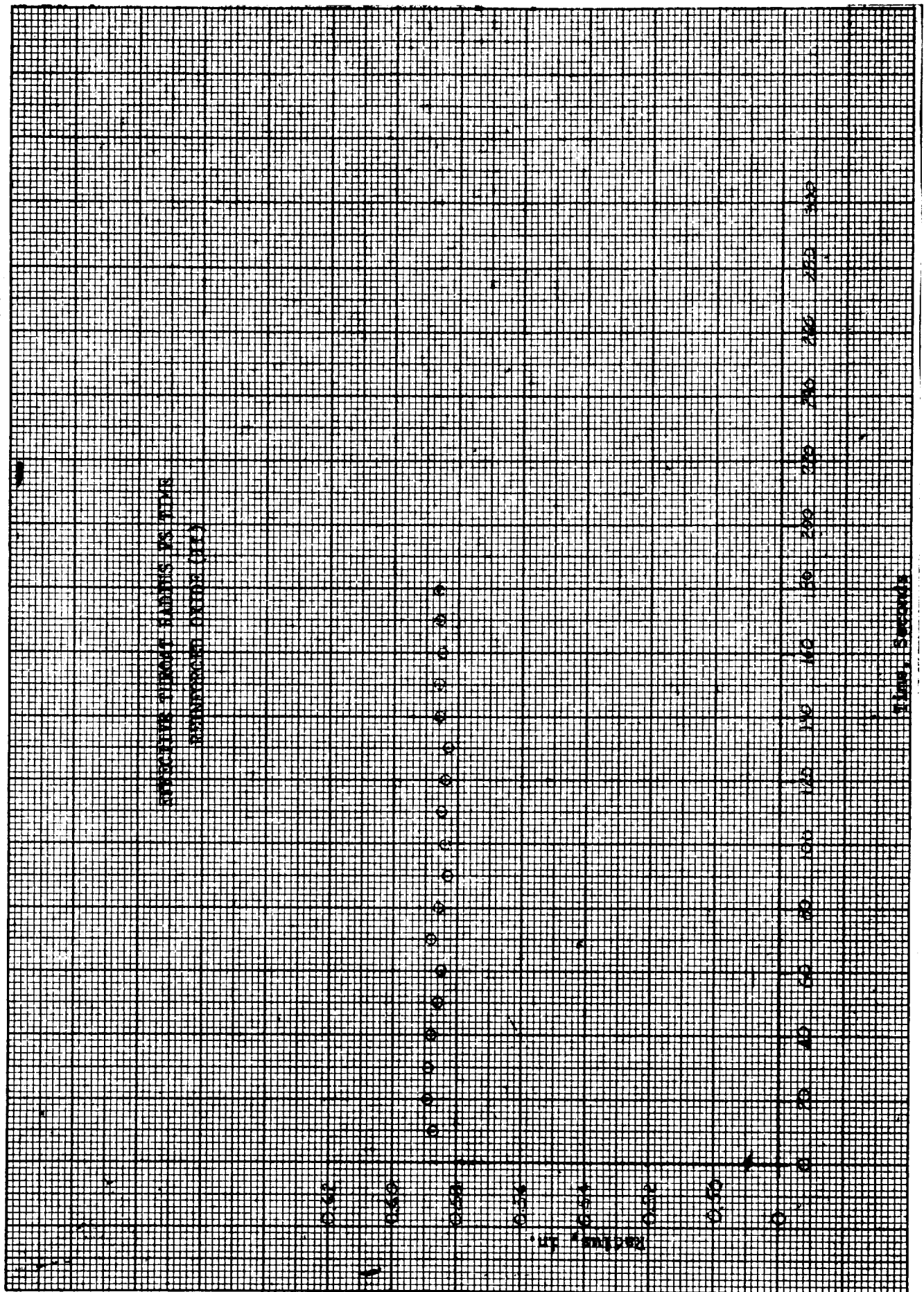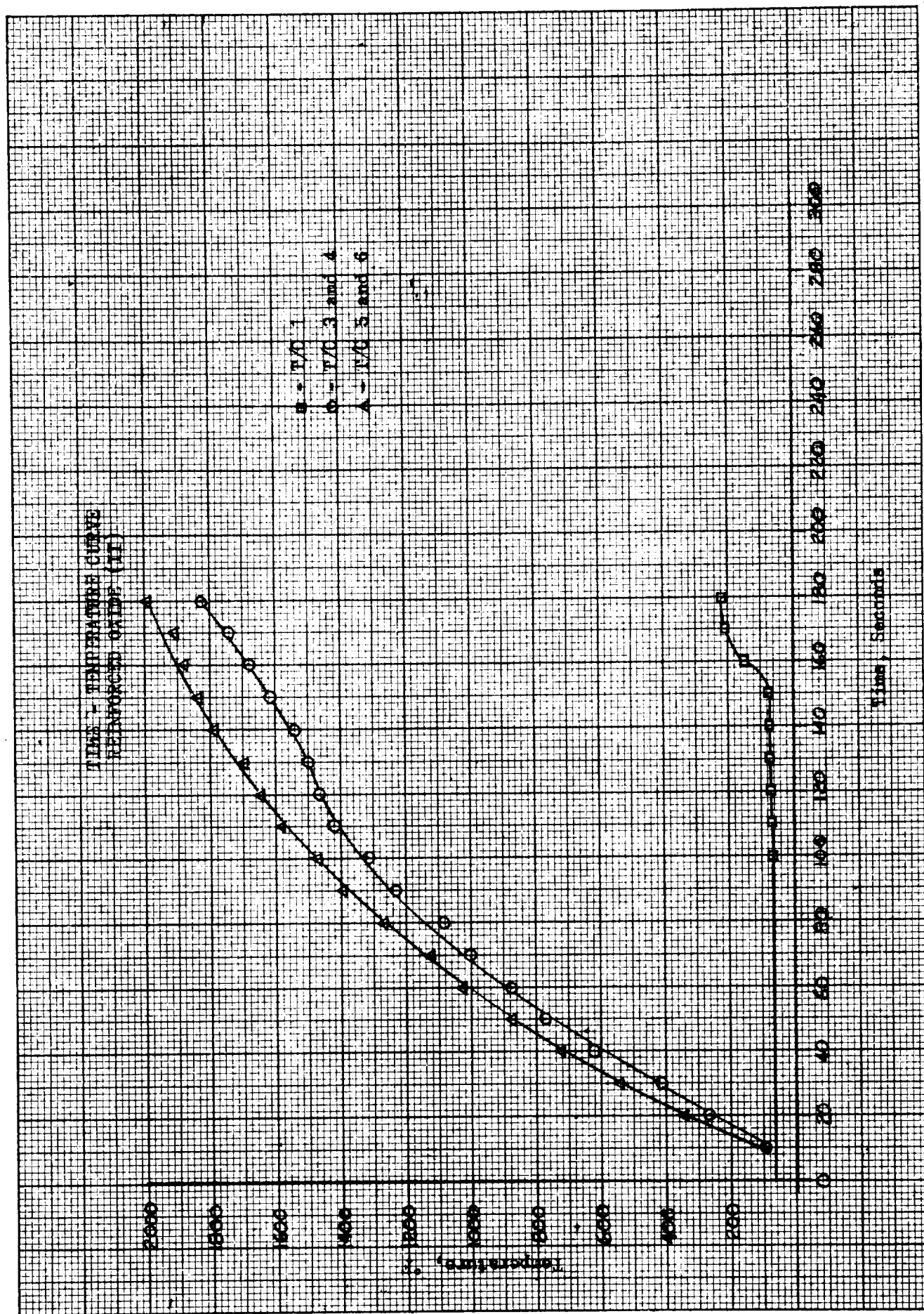
272
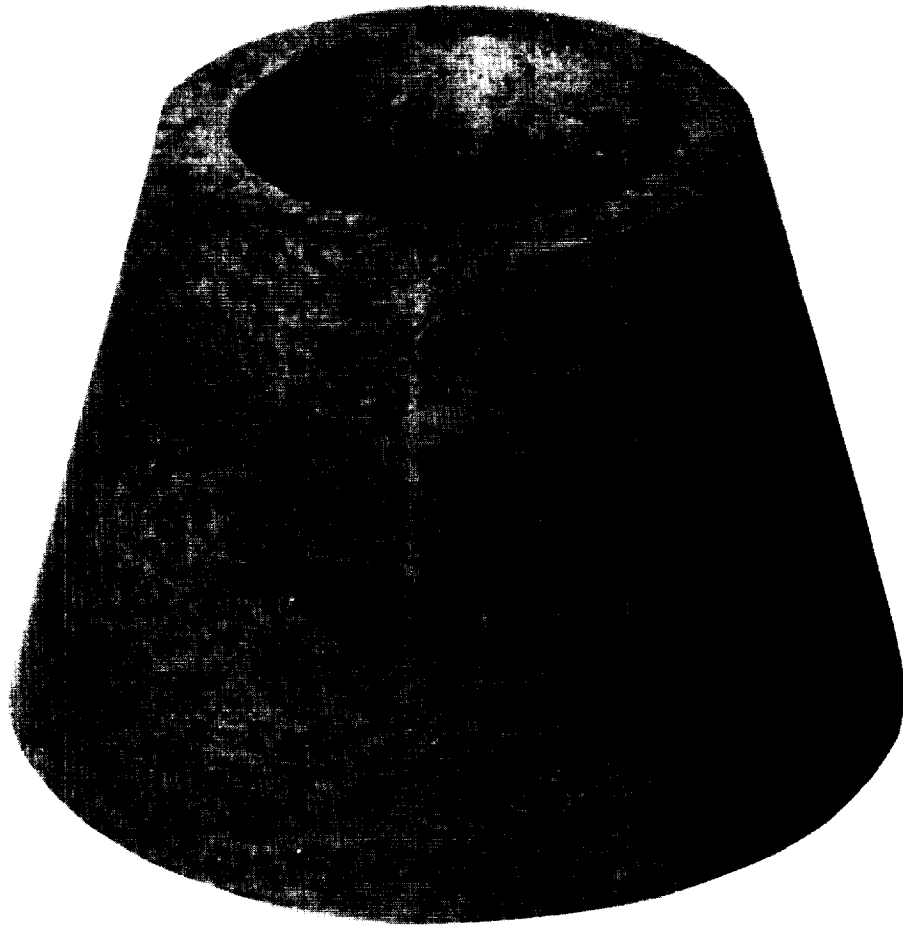
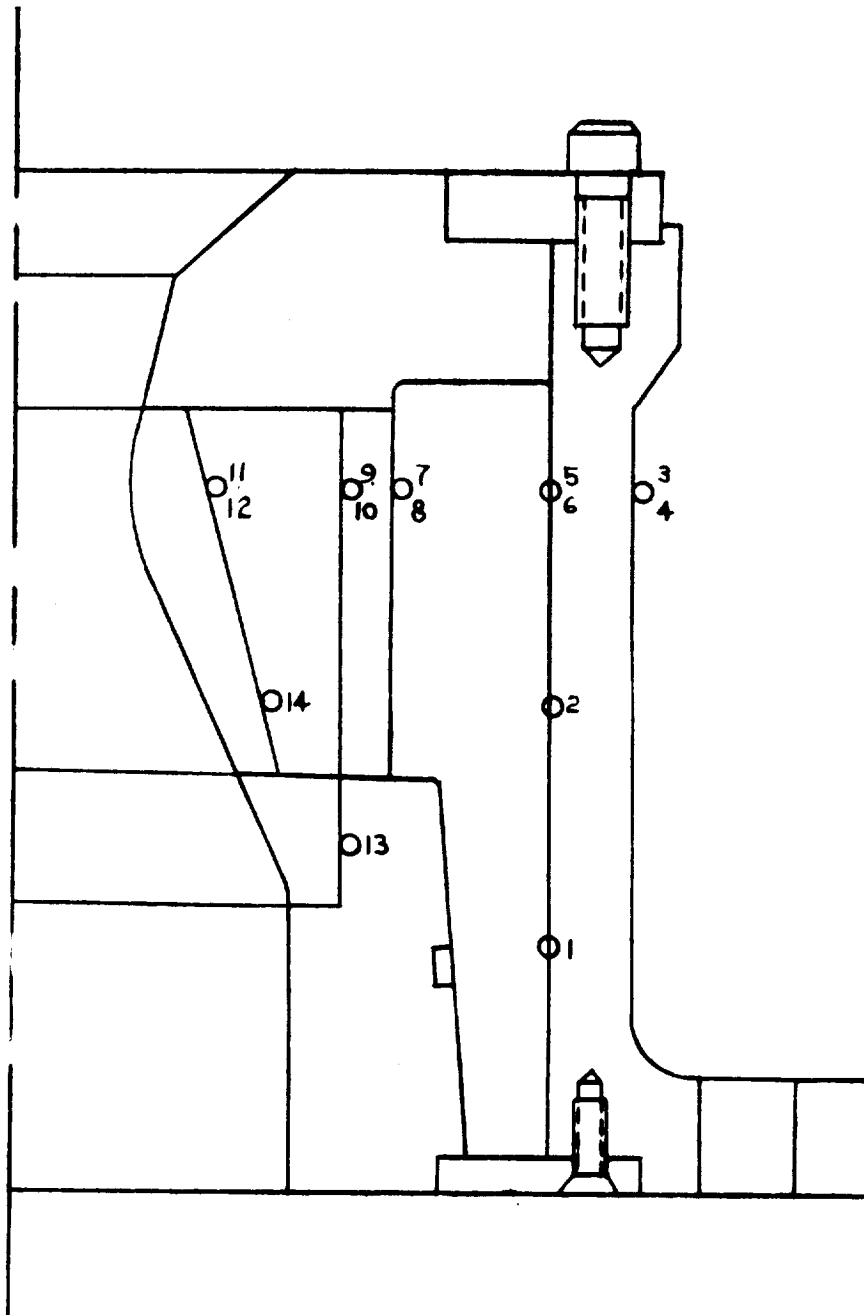PRE-TEST VIEW - REINFORCED OXIDE INSERT (II)

Figure 182

POST TEST VIEW--REINFORCED OXIDE INSERT (II)

Figure 183

275   Figure 184

TIME - TEMPERATURE CURVE
REINFORCED CONCRETE (III)

■ — T/C 1
● — T/C 3 and 4
▲ — T/C 5 and 6

Temperature °F

Time, Seconds

Figure 186

$TRW^\#6$

POST TEST VIEW--REINFORCED OXIDE (II)
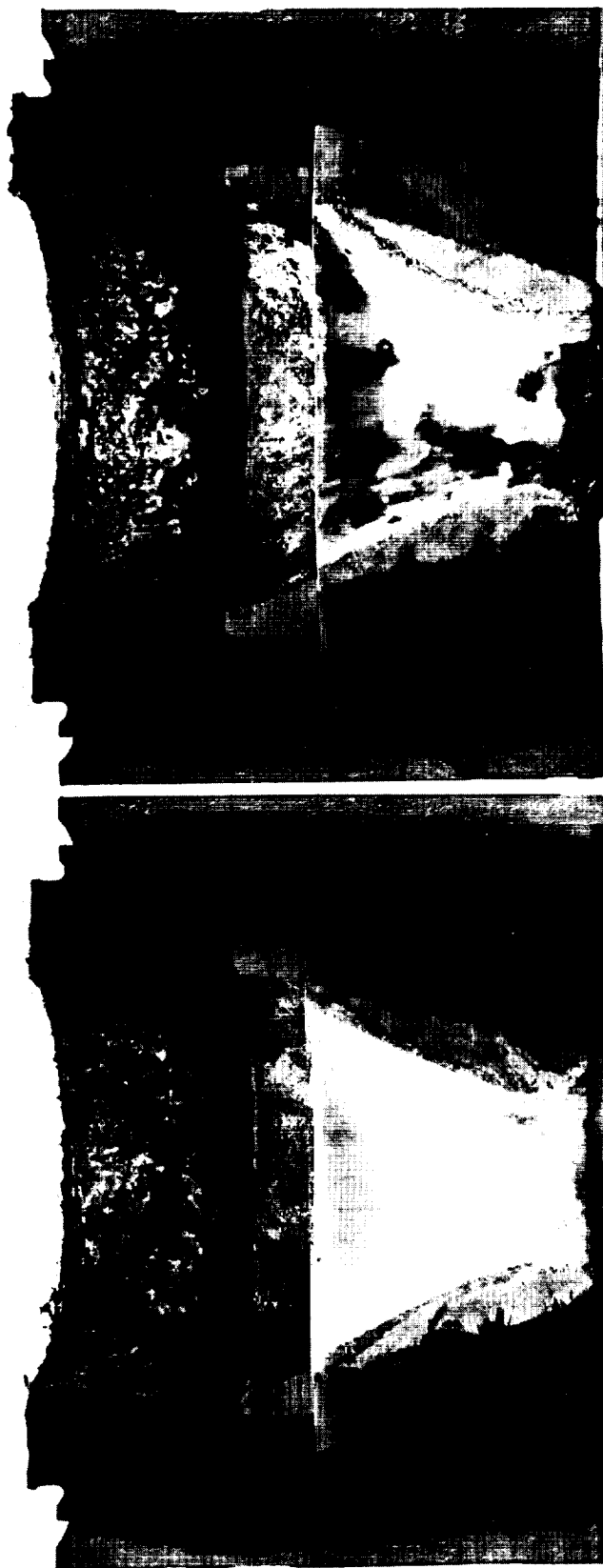
Figure 187

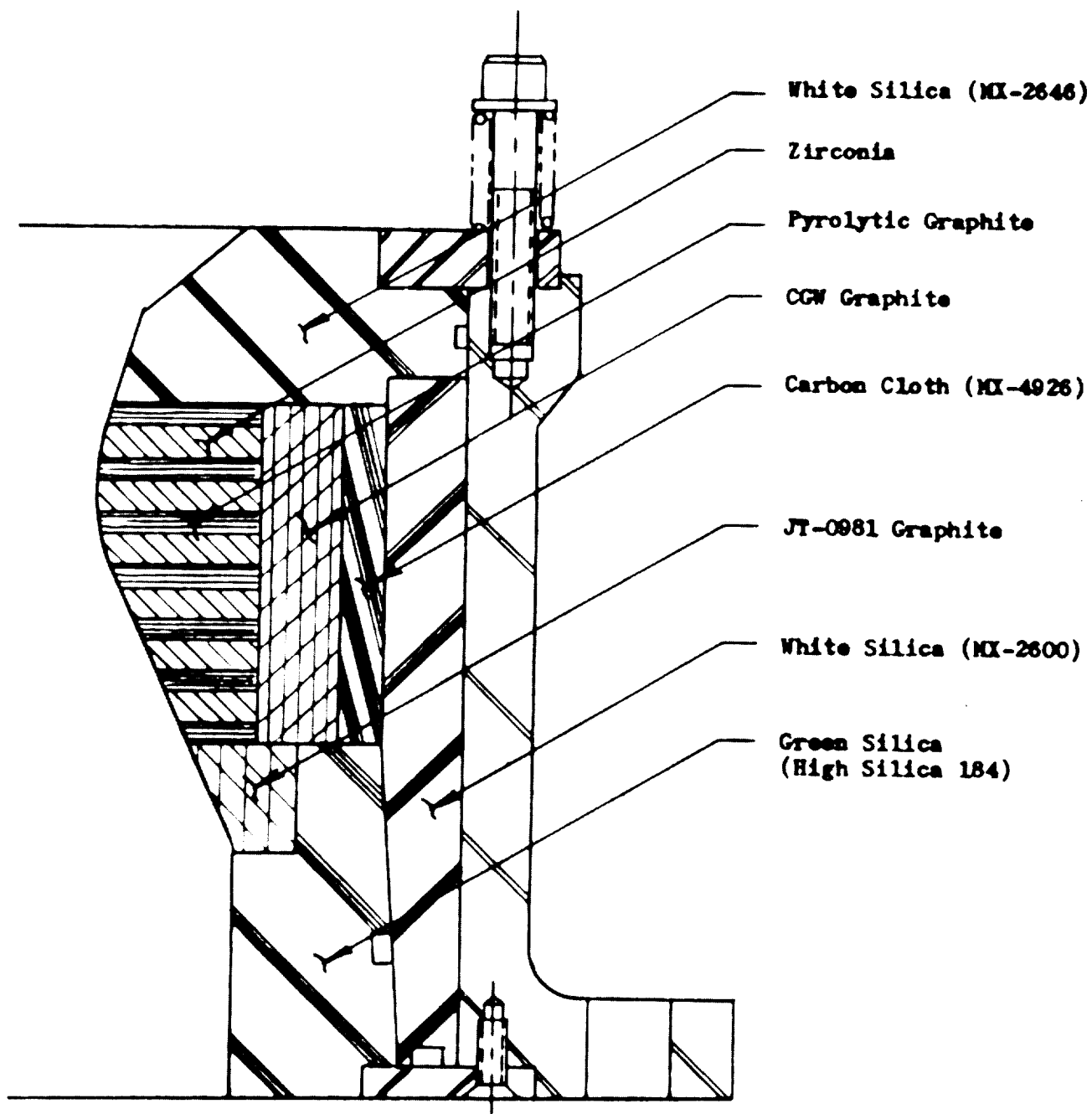POST TEST VIEW--REINFORCED OXIDE INSERT (II)

Figure 188

6. Refractory Laminate (II)

A second refractory laminate insert nozzle was fabricated using the same design concept but deleting the pyrolytic graphite (PG). The test of the first refractory laminate resulted in greater than anticipated oxidation of the PG and subsequent material loss at the ID of the zirconia disks. The only other changes in the design were the increase in thickness of the oxide disks and the deletion of the springs that were used to compensate for the thermal growth of the PG. A design sketch is shown in Figure 189.
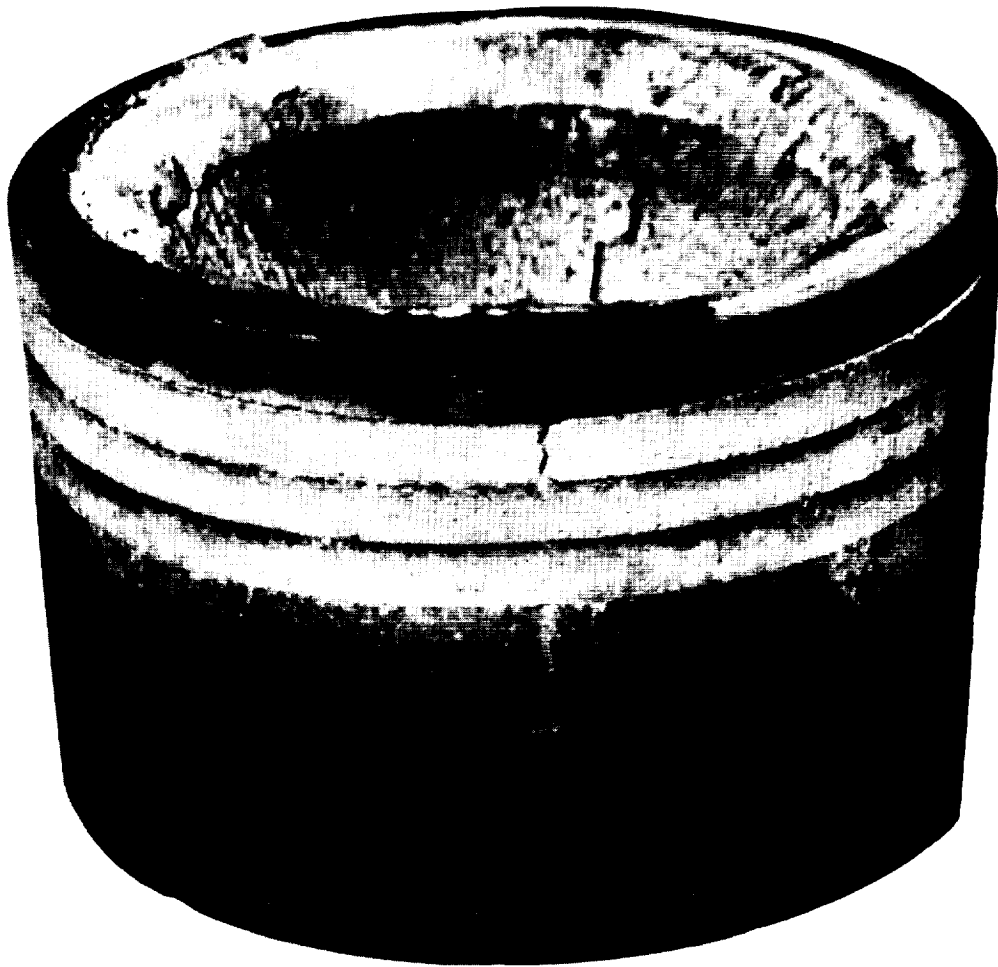
The nozzle was tested for 700 seconds in the duty cycle previously described. There was no throat erosion evidence during the 700 seconds; however, some surface material loss was noted at the completion of the final 300 second burst in an area just upstream of the throat plane. Figure 190 shows the insert as it was removed from the sectioned nozzle. Figure 191 shows the disks disassembled from the throat assembly. It should be noted that the majority of the disks are cracked in three places as could be predicted from the data shown on Figure 61.

While there was surface material loss just ahead of the throat plane, there was no increase in throat diameter as indicated by propellant flow data and noted visually. The calculated throat radius for the first 300 second burst is shown in Figure 192.

Figure 193 is a plot of the temperatures recorded during the first 300 second burst. They are considerably lower than those recorded for the first refractory laminate design, which would be expected. The PG in the first design permitted a rapid heat flow to the OD of the throat insert while the zirconia by itself is a very good insulator. This also indicates that the ID of the throat insert probably reached a higher operating temperature than that of the first design. It was also noted that the JT-0981 ring ahead of the throat underwent considerably more erosion than evident on past tests. No explanation could be made for this effect.

White Silica (MX-2646)

Zirconia

Pyrolytic Graphite

CGW Graphite

Carbon Cloth (MX-4926)

JT-0981 Graphite

White Silica (MX-2600)
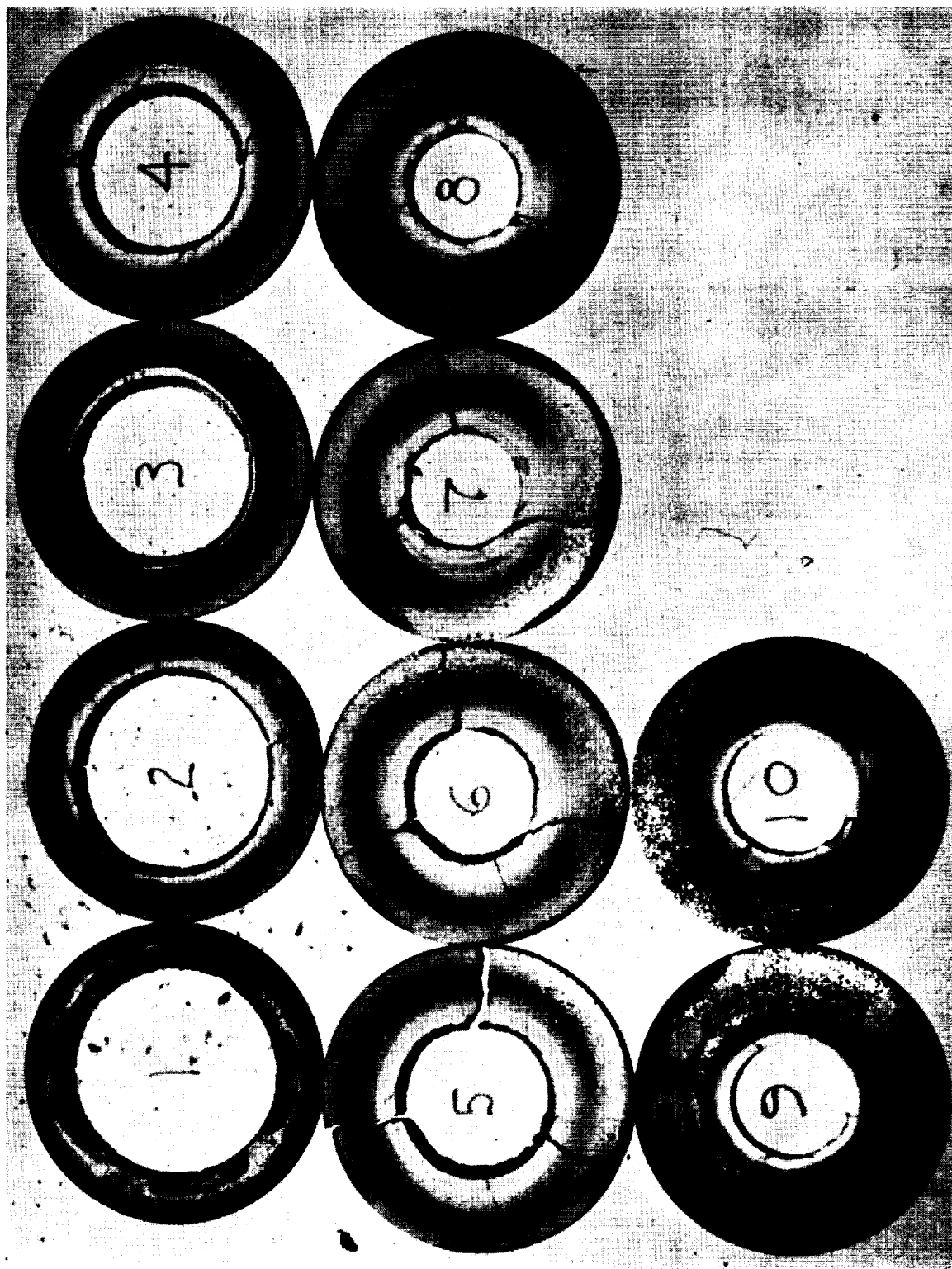
Green Silica
(High Silica 184)

REFRACTORY LAMINATE DESIGN (II)

Figure 189

281

POST TEST VIEW - REFRACTORY LAMINATE (II)

Figure 190

16410

POST TEST VIEW - REFRACTORY LAMINATE (II)

Figure 191

EFFECTIVE THROAT RADIUS vs TIME
PERFORMANCE CALIBRATE (II)

Radius, in.

Time, Seconds

284

Figure 192

TIME – TEMPERATURE CURVES
REFRACTORY LAMINATE (II)

O – T/C 1
□ – T/C 2 and 3
▲ – T/C 4 and 5

Time – Seconds

Figure 193
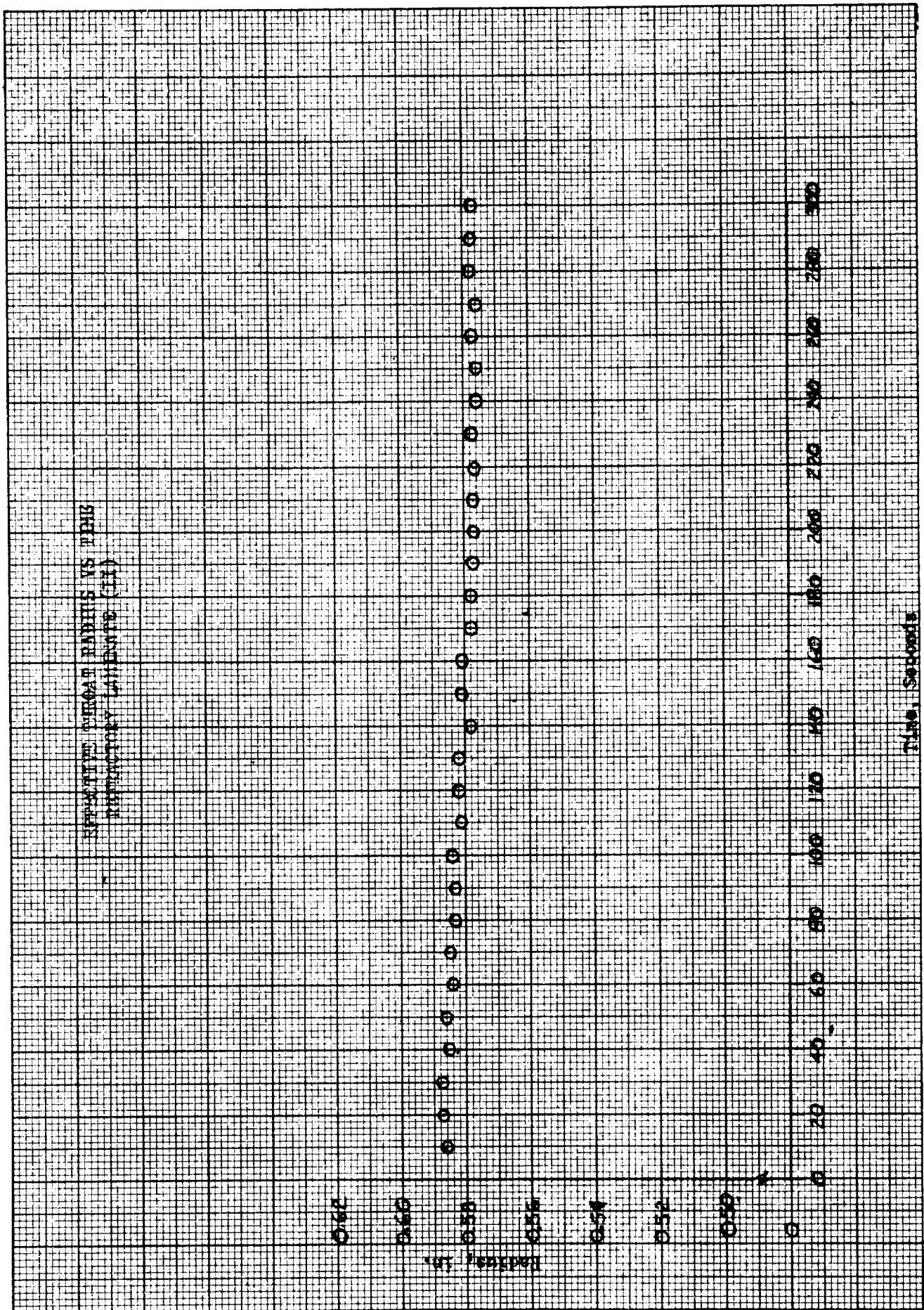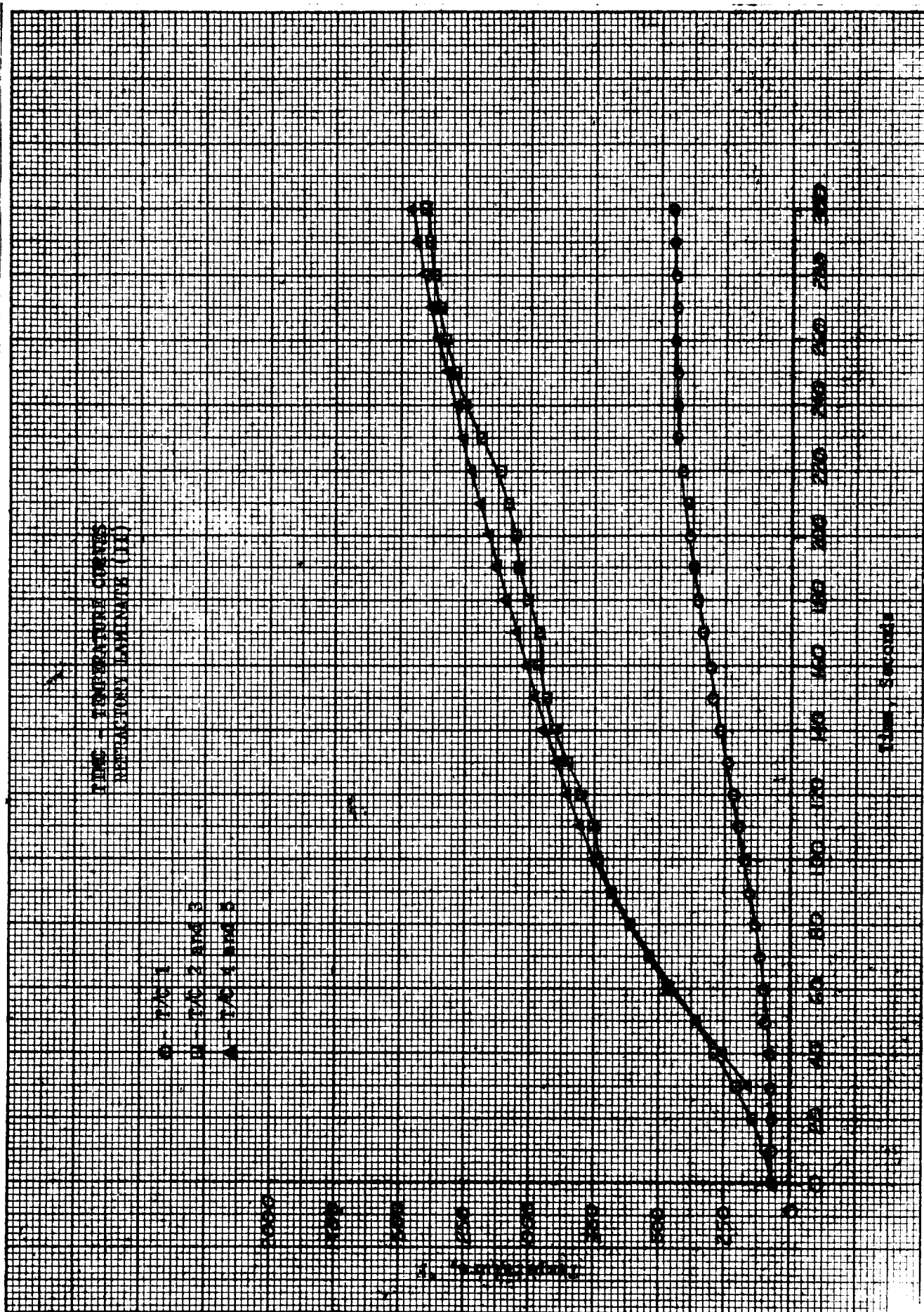
E. The oxide materials such as zirconia, thoria, and hafnia appear
    to have the greatest resistance to oxidation. Compositing
    zirconia with tungsten-rhenium wire for structural considerations
    does not reduce its ability to withstand high temperature en-
    vironments. On a comparative basis, the following ranking of throat
    insert materials in the N_2O_4/aerozine-50 propellant· environment is
    presented in order from best to worst:

    Oxides
    Carbides
    JTO graphite (a composite of silicon and zirconium carbide)
    Tungsten
    Pyrolytic graphite
    High density graphite

    The oxides and the carbides are significantly better than any of
    the subsequent materials listed.

2. Recommendations

    The recommendations for further effort to extend the current state-of-
the-art are presented:

    A. Additional data is required about the performance of these materials
        in more severe operating environments. A program to test these
        design concepts in rocket motors operating with increased chamber
        pressure and firing duration would be of value.

    B. Scale-up considerations of selected throat insert design concepts
        should be examined and flight-weight design characteristics
        examined.

    C. Additional laboratory evaluation is required to provide more pre-
        cise and realistic material control specifications so that more
        accurate and repeatable material properties will be established.

    D. The oxide and carbide materials in a composited form are recommended
        because they are potentially good candidates for high temperature
        service. However, more work is required to further develop fabrication
        techniques for these composite materials.

Conclusions and Recommendations

The superior chemical resistance of the oxides and the carbides in highly oxidizing, high temperature environments of liquid propellant rocket engines has been known for some time. However, application of these materials to throat insert designs has been unsuccessful because of the brittle nature of these materials.

The technical effort of this program has shown how the oxides and the carbides can be used to fabricate throat inserts. This section presents the conclusions of the technical effort. Recommendations for future work are offered.

1. Conclusions

The technical effort was directed towards process development of composite materials and their subsequent evaluation as rocket motor throat inserts. As a result of the effort, the following conclusions are reached:

A. Composites of oxide and reinforcement demonstrated structural reliability and negligible erosion under long duration single pulse and multiple pulse firings. The inherent durability and simplicity of design requirements make this material form attractive. Additional processing development is necessary to improve homogeneity of the composite and to permit reproducibility with respect to composition. Scale-up potential for this design concept is good.

B. Pure oxide discs, with or without alternate discs of a material relatively free from thermal shock sensitivity, provided a relatively simple design concept which demonstrated good over-all performance characteristics although the oxide discs cracked. When utilized, care must be exercised in selecting the thermal shock free material with respect to its compatibility with the propellant exhaust environment. Proper design can anticipate cracking patterns in the oxide discs and provide for retention of the cracked material during firing. Another design approach is to manufacture the oxide discs in circumferential segments (essentially, precracked discs). This latter technique would be attractive for simplifying the fabrication of larger inserts.

C. The concept of a pre-stressed throat insert design is good for use with highly thermal shock sensitive material. However, the concept is difficult to analyze and requires accurate material property design information which is not currently available. Scale-up potential for this design concept appears limited because of the complexity and close dimensional tolerances required.

D. The graded or layered carbide design concept failed structurally during rocket motor test. The structural failure mechanism was a combination of thermal shock and spalling. An extensive design analysis attempted to match thermal expansions and moduli in the layered carbide concept; however, accuracy was limited by the availability of material property information. This concept appears to have limitations similar to those of the pre-stressed design concept.

286

APPENDIX

SCALE-UP ANALYSIS OF REINFORCED OXIDE CONCEPT

Introduction

A cursory analysis of scaling up the reinforced oxide insert approach has been made to establish validity for use in larger sizes. The results of the analysis indicate a moderate stress condition will exist which, when compared to similar analysis for the highly successful 1.2 inch ID size designed and tested, provide a high degree of confidence in providing similar performance in large ($\sim$ 8 - 10 inch ID) sizes.

Discussion

The configuration analyzed is shown in Figure A 1. The insert was proportioned from the 1.2 inch size, although not scaled geometrically. Back-up support materials were selected as the same as those employed for the 1.2 inch design.

A thermal analysis at the throat plane for this configuration is presented on Figure A 2. It is apparent from the figure that for this thickness of insert, the graphite and carbon phenolic material could be greatly reduced in thickness, or eliminated, since the backside temperature of the insert is below the melting temperature of silica and adequate support would probably be maintained. For this study, no attempt has been made to optimize material thicknesses. A thinning of the oxide insert radial thickness might also be accomplished to lighten weight provided OD stresses and protection against forward edge exposure will permit this.

A comparison of the backside temperature of the 0.4 inch radial thickness reinforced zirconia insert (1.2 inch throat diameter) shown on Figure 113, with that for this configuration (1.2 inches radial thickness, 7.8 inches throat diameter), shows little difference for the 20 second duration, but an increasing difference for greater durations. This is predominantly a function of the increased thickness of the insert (good insulative material), although some decrease in heat transfer coefficient due to the large difference in throat diameters ($h_c \sim D_t^{0.2}$) was accounted for in the calculations. The surface temperatures, as would be expected, are almost identical. We would conclude from these analyses that no outstanding thermal difficulties will exist for the larger size unit.

Insert stresses computed for the 7.8 inch throat are shown on Figure A 3. As shown on the figure, the tensile stresses on the OD are moderate and decrease with time as the temperature difference from OD to ID decreases. Property values used to make these calculations were identical to those used for Figure 130, the 0.4 inch thick, 1.2 inch throat diameter insert. A comparison of Figures A 3 and 130 show a similarity in peak values, but with less tendency for increasing compressive stresses with time for the larger throat. This mirrors the relations for heat transfer in that the thicker insert maintains a greater temperature difference, OD-to-ID, than does the thinner one. On the basis of the peak tensile values being almost identical, and tensile failures being the predominant failure mode for brittle materials, it is expected that the larger size insert will perform equally as well as the smaller.
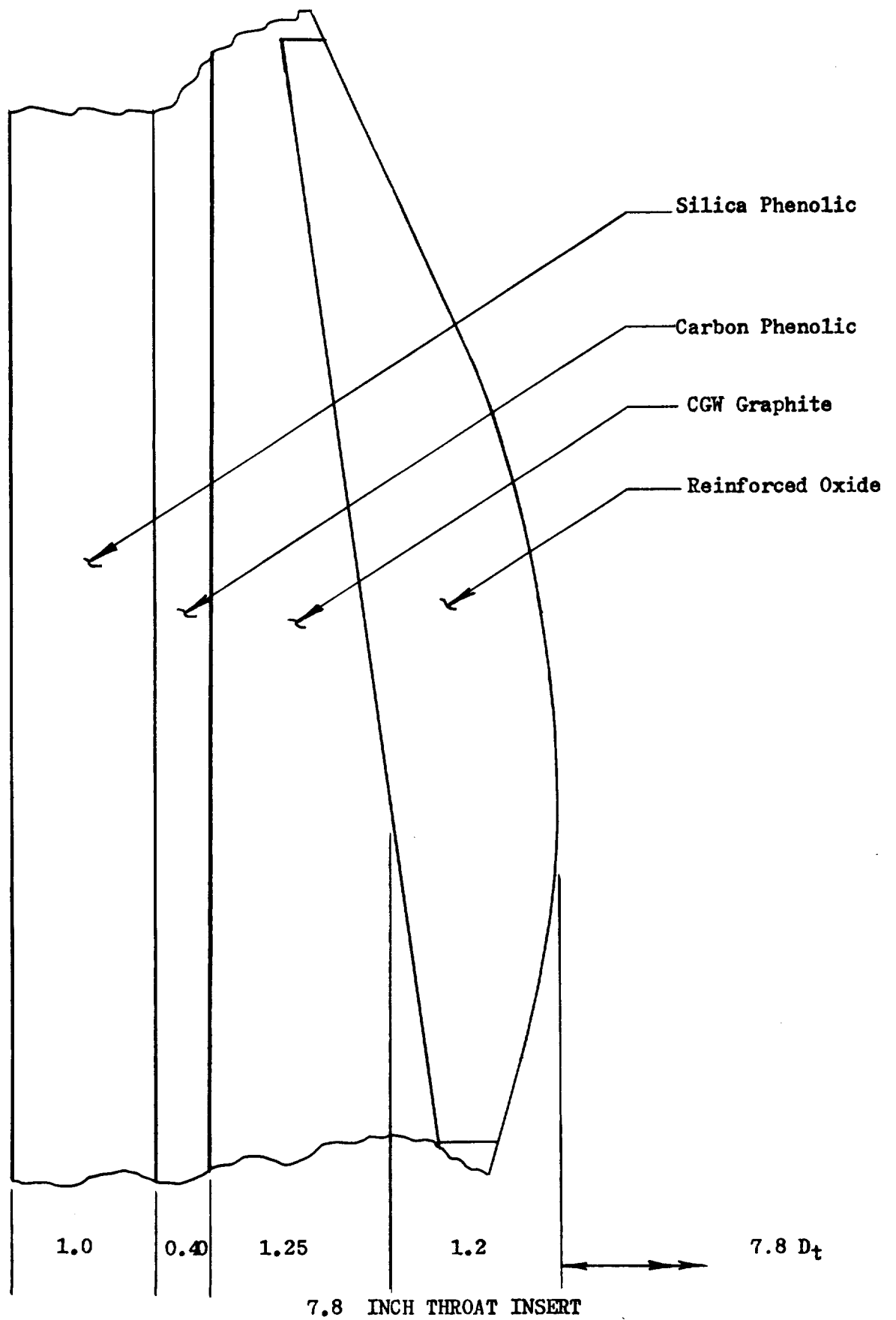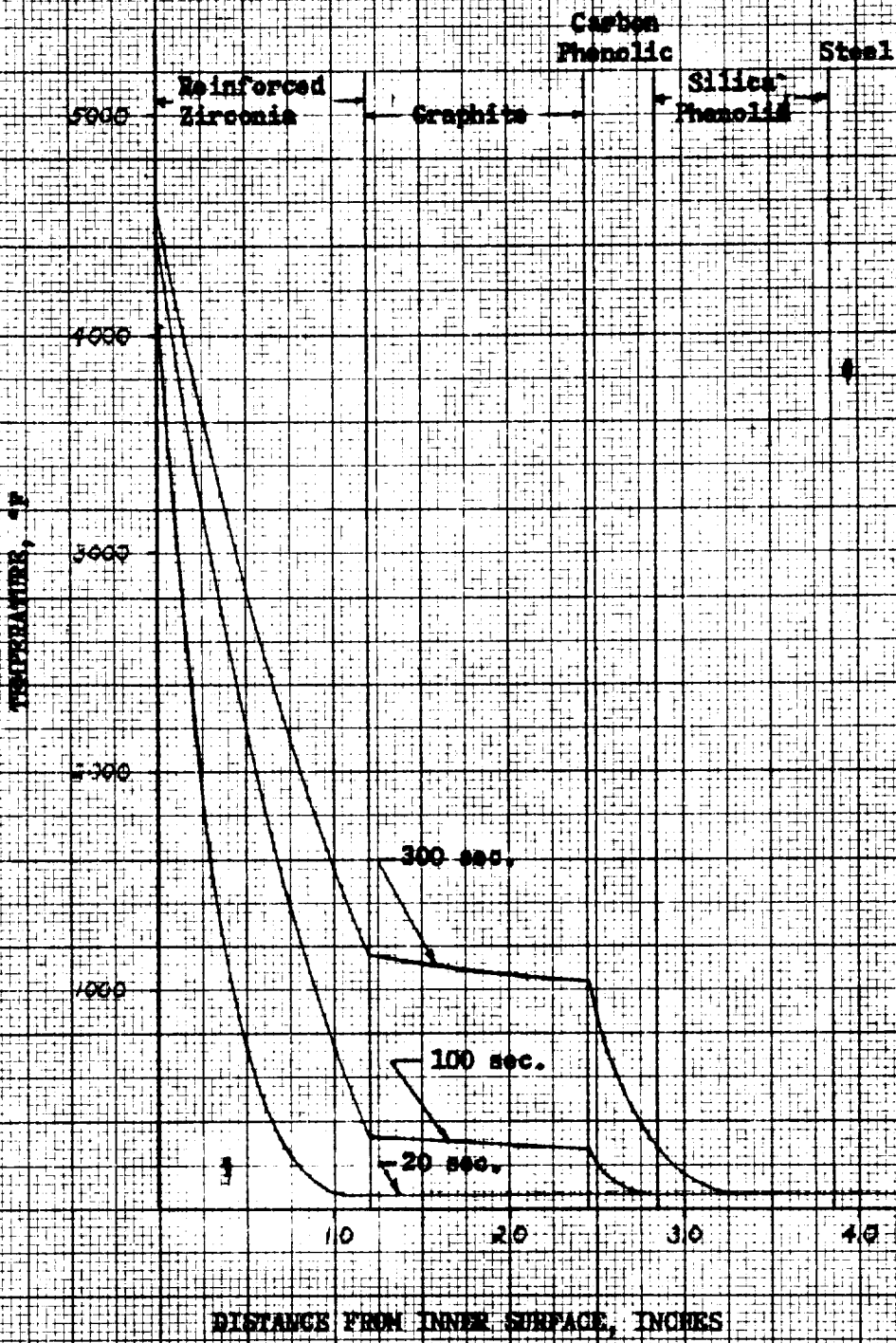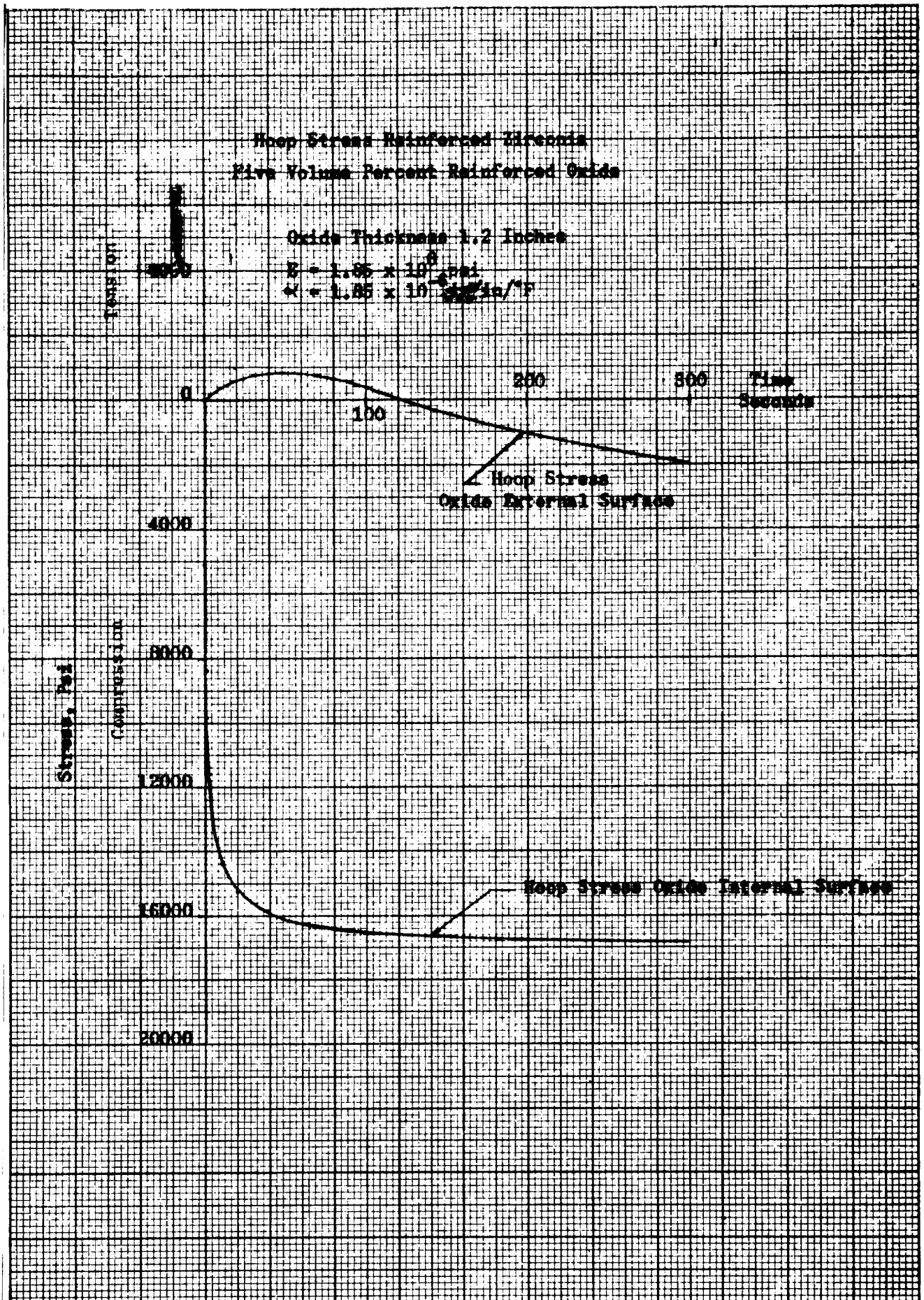
289

FIGURE A 1

290

TEMPERATURE PROFILE
REINFORCED ZIRCONIA
FIVE VOLUME PERCENT
REINFORCED OXIDE

$h = 639$ BTU/Hr Ft^2·°F
$D_t = 7.6$ inches

Figure A2

Hoop Stress Reinforced Zirconia
Five Volume Percent Reinforced Oxide

Oxide Thickness 1.2 Inches
$E = 1.85 \times 10^6$ Psi
$\alpha = 1.85 \times 10^{-6}$ in/in/°F

REFERENCES

(1) Wolfson, M. R. and Thielbar, W. H., "Nozzle Material Testing with Solid Fluorocarbon Propellants," ASM Report No. W-13-1-65, February 1965.

(2) Bohn, J. R., "Thermal Shock Characteristics of Refractory Materials," TRW AF 33(615)-1662, 3rd Quarterly Report, April 1965.

(3) Miccioli, B. R., Julien, H. P., "Refractory Materials Suitable for Use in Guided Missile Propulsion Systems," Carborundum, NOw 64-0412-6, June 1965.

(4) Timoshenko, S., Strength of Materials, Part II Advanced Theory and Problems, Third edition, Van Nostraud, Princeton, New Jersey (1965), P. 208, equation 171.

(5) Timoshenko, S. and J. N. Goodier, Theory of Elasticity, 2nd edition, McGraw-Hill, New York (1551), P. 409, equation 244, 245, 246.

(6) Bureau of Mines, Report #26, March 1965.